Genetic Control of T-Cell Proliferation with Synthetic RNA Regulatory Systems

Thesis by

Yvonne Yu-Hsuan Chen

In Partial Fulfillment of the Requirements

for the Degree of

Doctor of Philosophy

California Institute of Technology

Pasadena, California

2011

(Defended December 10, 2010)

© 2011

Yvonne Yu-Hsuan Chen

All Rights Reserved

Acknowledgments

The following pages tell a tale that has been five years in the making. As much as I would like to claim this work for the countless hours spent pipetting alone in tissue culture rooms, singing to Frank Sinatra and Ella Fitzgerald on Pandora Radio, it is in fact the fruit of many individuals' labors. I only hope that the final product has reciprocated some of the efforts given to it by so many.

First, I would like to thank my tireless thesis advisor, Prof. Christina Smolke, for her unfailing support and infinite patience with my research and myself. Even with her abundant talents, Christina is a model of diligence and commitment. I thank her for the thoughtful care she puts into steering this laboratory and guiding its members. Even amidst my most draining experiments, I always had the comfort of knowing that I did not walk alone on this journey.

I must also thank Dr. Michael Jensen for his boundless energy and excitement about my research, his generosity in providing me with resources and advice, and his interest in my professional development. I could not have completed this work without the help of many friends at City of Hope. I thank Araceli Hamlett and Bessie Meechoovet for initiating me into the art of T-cell culturing, Brenda Aguilar for laboring many hours in the animal facility on my behalf, and Cherrilyn Bautista for being my reliable source of expert knowledge on T cells and beyond. I also thank Dr. Christine Brown, Wen-Chung Chang, Michelle Hunter, Renate Starr, Jamie Wagner, and Winnie Wong for being always ready teach me a technique or lend me a hand. I also must acknowledge Christine Wright for managing the most organized laboratory I have ever seen.

The Smolke Laboratory has been a wonderful home for the past five-and-a-half years. I would like to thank Dr. Chase Beisel and Dr. Stephanie Culler for showing me the ropes in tissue culture and for being so generous with their time and knowledge whenever I had questions or needed advice. I thank Dr. Maun Nyan Win for sharing his expertise on his beloved creation, the ribozyme switch platform. I will always remember Katie Galloway for our stimulating discussions on not-so-scientific subjects, Arwen Brown for sustaining a passion for the humanities in a sea of scientists and engineers, and Leo D'Espaux for his amazing culinary skills and unfettered pursuit of life, even if it leads to a broken bone or two.

Graduate school would not have been nearly as eventful or enjoyable without the many friends I met at Caltech. I thank Arthur Chan, Puneet Chhabra, Claire Farnsworth, and Andrew Metcalf for leading me out of the lab and onto hiking trails. Mike Rubel, Karen Lau, and my cousin Solomon kept me in a semblance of fitness by humoring me on the badminton court. The many hours spent first on transport and thermo problem sets and later on the equally intellectually rigorous game that is Mexican Train with Diana Smirnova, Havala O. T. Pye, and Mary Louie will remain some of my fondest memories of Caltech. Mary, my roommate of three years, kept me sane by being the patient ears for my happy and melancholy ramblings alike. I thank her for showing me a generosity of spirit that I am not sure I knew was possible.

Finally, I would like to thank my most constant supporters—my family. I thank my parents and grandparents for showing me the virtue of perseverance, and for providing a secure and nurturing environment in which to grow. 感謝阿嬤教我謹慎；感謝阿公教我好學；感謝外婆教我努力奮鬥；感謝外公教我在工作之餘不忘生活的

浪漫。爸爸媽媽給我的一切是篇幅再長也述不完的。在這裡只能說聲「實在真多謝。」And last but certainly not least, I would like to thank my sister, Alice, whose path I seemed destined to follow, at least until now. If the road I traveled has been smoother or more colorful, it is because you have blazed the trail and shown me the way.

Abstract

Adoptive T-cell therapy, or the use of autologous T cells to seek and destroy diseased cells, is a promising treatment option for opportunistic diseases, virus-associated malignancies, and cancers. However, the safety and efficacy of adoptive T-cell therapy depend, in part, on the ability to sustain and tightly regulate the proliferation of transferred T cells *in vivo*. The emerging field of synthetic biology provides powerful conceptual and technological tools for the construction of regulatory systems that can interface with and reprogram complex biological processes such as cell growth. Here, we present the development of RNA-based regulatory systems that can control T-cell proliferation in a ligand-dependent manner, and examine the construction of integrated control systems capable of fine-tuned programming of cellular behavior.

We systematically investigate the translation of ribozyme-based regulatory devices from yeast to mammalian cells and identify design parameters critical to the portability of regulatory devices across host organisms. We report the construction of ligand-responsive ribozyme switch systems capable of modulating the transgenic expression of growth-stimulatory cytokines in mammalian lymphocytes. We demonstrate the ability of ribozyme switch systems to regulate T-cell proliferation in primary human central memory T cells and in animal models. We further develop ligand-responsive, miRNA-based devices to regulate the endogenous expression of cytokine receptor chains and the functional output of cytokine signaling pathways, highlighting the ability to construct integrated T-cell proliferation control systems employing various regulatory mechanisms to modulate multiple components in relevant signaling pathways. Finally, we describe efforts in the generation of novel RNA aptamers to clinically suitable

molecules, which can serve as the molecular inputs for ligand-responsive, RNA-based control systems in therapeutic applications.

The regulatory systems developed in this work are designed to be modular and transportable across host organisms and application contexts, thus providing a template for future designs in RNA-based genetic regulation. This work demonstrates the capability of RNA-based regulatory systems to advance next-generation treatment options for critical diseases, and highlights the potential of synthetic biological systems to achieve novel and practical functions in diverse applications.

Table of Contents

List of Tables

List of Figures

Chapter 1

Introduction

Cancer research in the past decades has advanced our mechanistic understanding of the heterogeneity in disease presentation and prognosis observed in patients with similar cancers[1]. These insights have highlighted the importance of tailoring treatment strategies to specific cancer subtypes to increase clinical efficacy[2-4]. However, the identification of effective biomarkers and the development of personalized cancer treatment using protein- or small-molecule-based pharmaceuticals have proved challenging[1]. Furthermore, non-targeted treatment options such as chemotherapy and radiation, which pose significant systemic toxicities due to a lack of target specificity, remain the standard care for cancer patients. Immunotherapy, which seeks to redirect the exquisite specificity of the immune system against otherwise intractable diseases, has been proposed as an alternative approach to addressing the complex challenge of cancer treatment.

Immunotherapy is a broad treatment paradigm that elicits prophylactic or therapeutic responses by modulating the immune system. In particular, cancer immunotherapy focuses on stimulating the immune system to recognize and destroy tumor growth[5, 6]. Several immunotherapeutic strategies, most notably monoclonal antibody-based agents, have achieved adequate safety and efficacy for clinical applications[7, 8]. Provenge™, a dendritic cell-based vaccine against prostate cancer, recently became the first United States Food and Drug Administration (FDA)–approved therapeutic cancer vaccine, providing powerful support for cell-based immunotherapy as a feasible cancer treatment option[9]. Despite these recent advances, the number of conditions curable by immunotherapy remains limited, and alternative strategies such as

the adoptive transfer of tumor-targeting T cells are under active investigation as potentially more versatile treatment options[10-12].

Adoptive T-Cell Therapy: Potentials and Current Limitations

T cells are lymphocytes integral to the adaptive immune response in humans and other higher-level organisms. Several types of T cells—including various helper T cells (T_H cells), regulatory T cells, and cytolytic T cells (CTLs)—patrol the body for the presence of foreign antigens that match specific T-cell receptors (TCRs) expressed on T-cell membranes. T_H cells and CTLs are activated upon antigen recognition and, together with other components of the immune system, initiate signaling cascades to mount a vigorous defense against foreign infection[13]. One of the central events in a coordinated immune response is the clonal expansion of CTLs that recognize the particular foreign antigen present in the body. CTLs form conjugates with their targets via receptor recognition, and target-bound CTLs undergo cytoplasmic rearrangements to align intracellular, electron-dense storage granules with the target cell interface. Pore-forming proteins called perforins and serine proteases called granzymes are then released into the CTL-target cell junction, thus effecting target-specific cell destruction[13, 14] (Figure 1.1).

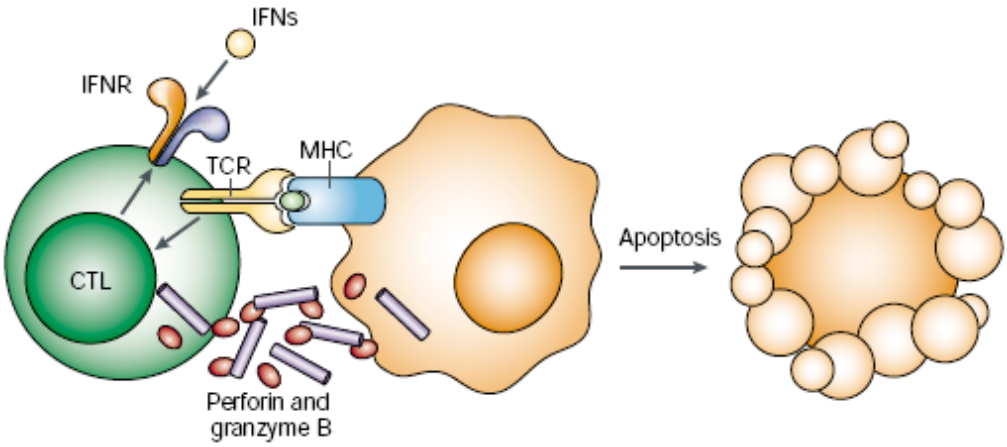

Figure 1.1. Schematic of CTL-mediated cell lysis. Activated T cells form conjugates with target cells via receptor-mediated recognition of antigens presented by major histocompatibility complexes (MHCs). Perforin and granzyme B are released into the cell-cell junction, leading to membrane perforation and eventual apoptosis of the target cell. Ancillary molecules such as interferons (IFNs) promote antigen presentation and T-cell activation. IFNR, interferon receptor. This figure is adopted from Ref. 14.

TCRs dictate the specificity of target recognition and destruction by CTLs. Tumor-infiltrating lymphocytes (TILs) found in select cancer patients are naturally occurring CTLs with tumor-targeting TCRs. Autologous TILs can be isolated from patients, expanded *ex vivo*, and reintroduced into the same patients by adoptive transfer to boost the immune response against cancerous growths[15, 16] (Figure 1.2). However, the isolation and expansion of TILs are time and resource intensive, and not all cancer patients have autologous TILs. As an alternative, the engineering of artificial TCRs provides a mechanism for redirecting CTL activity against otherwise unrecognized targets such as tumor cells[17]. For example, the Jensen Laboratory has engineered T cells to express chimeric receptors that specifically target tumorigenic growth in glioblastoma multiforme[18] and neuroblastoma[19]. In this strategy, CTLs harvested from the patient are genetically modified to express the chimeric receptor, expanded *ex vivo*, and re-administered to the patient to elicit tumor-specific cytolytic activity[20] (Figure 1.2). Pilot studies have demonstrated the safety of engineered T cells as a treatment option[21, 22].

However, sustaining T-cell survival after adoptive transfer remains a major challenge for both natural TILs and engineered T cells, and multiple clinical trials have shown that the efficacy of adoptive T-cell therapy in humans is often limited by the failure of transferred T cells to survive in the host[23-25].

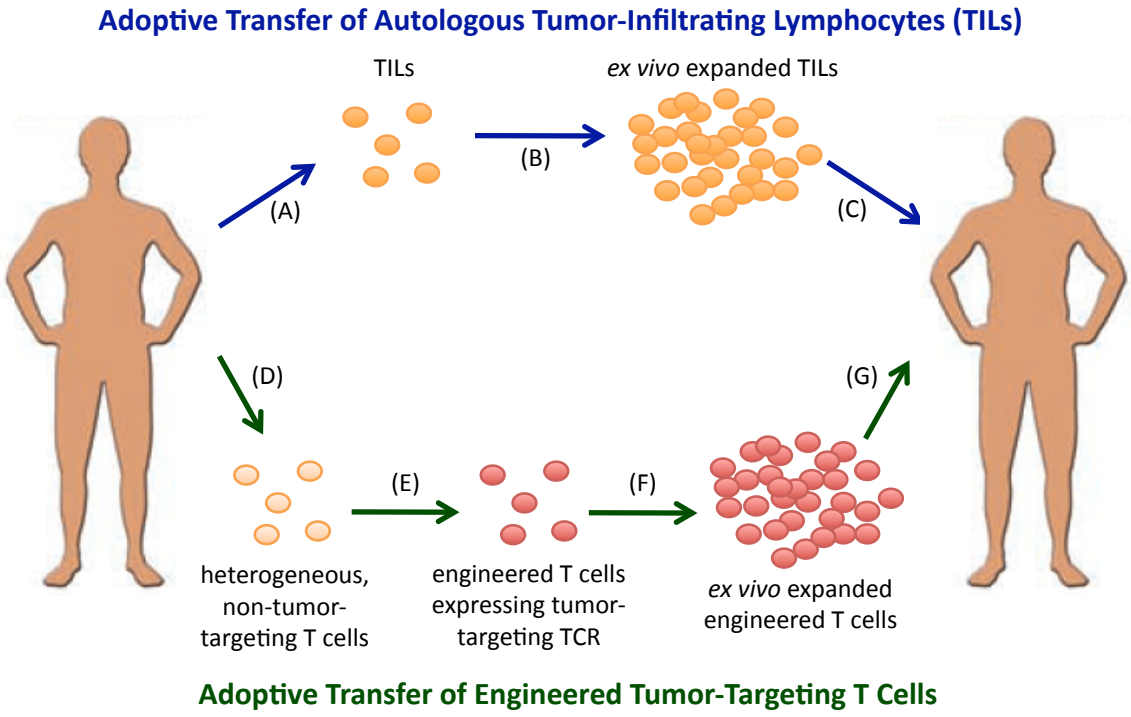

Figure 1.2. Schematic of adoptive T-cell transfer using either autologous TILs or engineered tumor-targeting T cells. (A) Autologous TILs are cultured from resected tumor specimens with exogenous interleukin-2 (IL-2). (B) Isolated TILs are expanded *ex vivo*. (C) Expanded TIL populations are reintroduced into the patient. (D) A heterogeneous population of T cells is harvested from peripheral blood samples of the cancer patient. (E) Isolated T cells are genetically modified to express tumor-targeting receptors. (F) Engineered tumor-targeting T cells are expanded *ex vivo*. (G) Expanded engineered T-cell populations are reintroduced into the patient.

The survival and proliferation of T cells following adoptive transfer is constrained by the limited availability of homeostatic cytokines (interleukin (IL)-15/IL-7) and stimulatory antigen presenting cells. Pre-transfer lymphodepletion, which removes pre-existing cytokine-consuming lymphocytes, combined with post-transfer administration of high-dose IL-2 has been shown to significantly improve the persistence of adoptively

transferred tumor-infiltrating lymphocytes[26]. However, such treatments require that the patients be subjected to total body irradiation/chemotherapy and toxic levels of IL-2. Alternative strategies based on the unregulated expression of growth-related genes have been developed to prolong T-cell survival, including expression of the anti-apoptotic genes *bcl-2* and *bcl-x_L*, overexpression of the human telomerase reverse transcriptase (*hTERT*) gene, and expression of genes encoding the growth factors IL-2 and IL-15[27]. While capable of sustaining T-cell survival, these strategies also pose the risk of uncontrolled lymphoproliferation and leukemic transformation. Therefore, the ability to integrate growth-stimulatory gene expression with tightly controlled genetic regulatory systems could greatly improve the safety and efficacy of adoptive T-cell therapy. The emerging field of synthetic biology provides useful conceptual and technical tools for the construction of such regulatory systems.

Synthetic Biology: Constructing Novel Devices with Biological Parts

The advent of enabling technologies such as rapid and affordable DNA synthesis and sequencing, high-throughput protein screening and characterization, and computational approaches to large-scale bioinformatics has transformed biological research and made possible efforts to not only understand nature, but also adopt, improve, and reprogram natural systems to perform human-defined functions. Accordingly, researchers have begun developing new tools for the manipulation and control of cellular components and their functional outputs, leading to the emergence of synthetic biology as a new discipline in biological research and engineering[28].

The concept that novel biological systems can be constructed by recombining existing biological parts—much as new plant hybrids can be generated by grafting parts of existing species—is not unfamiliar to science. However, the ability to efficiently identify, produce, and recombine biological parts at the genomic level was made possible by relatively recent developments of the aforementioned enabling technologies. The tools of synthetic biology have the potential to construct novel genetic devices with functions that are unknown to or difficult to co-opt from nature. For example, synthetic devices capable of inducing gene expression oscillation[29], performing light-sensitive edge detection[30], and directing bacterial migration in response to the presence of herbicides[31] have been developed in recent years. Synthetic biology techniques have also been applied to the construction of diverse control devices capable of gene expression regulation, thus providing new toolsets for the engineering of biological systems with fine-tuned functions.

RNA as the Design Substrate for Synthetic Control Devices

Biological control devices such as inducible promoter systems have been studied intensively in the past decades, and various protein-based systems capable of information processing have been developed[32-34]. However, the therapeutic use of protein-based regulatory strategies has been constrained by immunogenicity of heterologous protein components, toxicity of the narrow selection of compatible input molecules, and limited ability to tune the regulatory response. Furthermore, the need to stably express multiple heterologous protein components poses a significant challenge in medical applications. Inspired by the diverse functional roles exhibited by regulatory RNAs in natural

systems[35-37] and the relative ease by which RNA can be modeled and designed[38], researchers have begun developing synthetic RNA-based regulatory devices as alternative genetic control strategies[39-41].

RNA is composed of four ribonucleotide bases whose interactions through hydrogen bonding, base stacking, and electrostatic interactions are well understood and aptly modeled by freely available softwares[42, 43]. Furthermore, the ability of compact, non-protein-coding RNAs to perform gene expression regulation through a variety of mechanisms—including transcription termination, translational inhibition, and post-transcriptional modifications such as mRNA cleavage and alternative splicing—renders RNA a versatile substrate for the design and construction of synthetic control devices[41]. The small footprint and non-coding nature of regulatory RNAs avoid the problems of multiple-component integration and immunogenicity associated with protein-based systems, making RNA-based devices particularly well suited for therapeutic applications.

Frameworks for Constructing RNA-Based Control Devices

Although a variety of RNA devices capable of programming biological functions have been developed, most devices can be deconstructed into three functional components: sensors, actuators, and transmitters[41]. The sensor component detects an input signal, which could be a molecular ligand or a change in environmental cues such as temperature, and translates the signal into a downstream regulatory function executed by the actuator component, such as post-transcriptional modification or translation inhibition. The sensor component in most RNA devices designed to date consists of aptamers, which are nucleic acid sequences capable of high-affinity binding to specific

ligands, including small molecules, nucleic acid sequences, proteins, and whole cells[44]. Aptamers to specific ligands of interest can be generated *de novo* using various *in vitro* selection methods[45-48], thus allowing for a large variety of ligands to serve as potential input signals. The actuator component varies widely among RNA devices and consists of one or several functional elements, including but not limited to catalytic RNAs such as self-cleaving hammerhead ribozymes (HHRzs), RNA interference (RNAi) substrates such as microRNAs (miRNAs) and short hairpin RNAs (shRNAs), and RNA sequences containing a ribosome binding site (RBS), which could be obscured or exposed in response to signal detection by the sensor component[41].

RNA devices can be constructed by direct coupling between the sensor and actuator components. In one example, a theophylline-responsive RNA switch is generated by connecting the theophylline RNA aptamer to an shRNA actuator[49]. Theophylline binding to the aptamer inhibits Dicer processing of the shRNA and prevents gene expression knockdown mediated through the RNAi pathway. The device thus serves as an "ON switch," which responds to the presence of molecular input by increasing, or turning on, gene expression. An alternative construction strategy requires a transmitter sequence inserted between the sensor and actuator components for switch function. In one example, the theophylline RNA aptamer is coupled to an RBS sequence preceding the *cheZ* gene via a randomized linker sequence[50]. Utilizing cheZ's role in regulating bacterial cell tumbling and chemotaxis, researchers were able to screen for linker sequences that confer ligand-responsive control over ribosome access to the RBS by measuring cell motility in a plate-based assay, ultimately isolating a theophylline-responsive RNA device capable of regulating phenotypic output in bacteria.

Although several functional RNA devices have been created by the construction methods described above, both architectures pose sequence and structural restrictions that require extensive modifications for each new device and limit the modularity of the device framework. For instance, regulatory activity of the theophylline-responsive shRNA switch is highly sensitive to the distance between the sites of ligand binding and Dicer cleavage, such that single-base-pair changes can abolish device function[49]. In the second device, switch activity depends on sequence base-pairing between the sensor and actuator components despite the presence of a transmitter domain. As a result, both architectures would require complete redesigns for the incorporation of new sensor components, and neither can be easily tuned for regulatory stringency due to the limited number of sequence combinations that can produce functional devices.

As an alternative, RNA devices can include an independent transmitter component that translates signal detection by the sensor to functional output by the actuator. In this architecture, the transmitter component provides structural and functional insulation between the sensor and actuator, thereby allowing greater flexibility in the pairing of sensor and actuator components. An example of this construction method is the ribozyme switch platform previously developed in the Smolke Laboratory[51, 52].

Ligand-Responsive Ribozyme-Based Regulatory Devices

Win and Smolke have reported a platform for the construction of ribozyme switches whose components are modularly coupled and thus adaptable to application-specific requirements[51]. These devices are composed of three functional domains: a sensor component consisting of an RNA aptamer, an actuator component consisting of a

satellite RNA of tobacco ringspot virus (sTRSV) hammerhead ribozyme, and a transmitter component consisting of a rationally designed RNA sequence that links the sensor and actuator components (Figure 1.3A). The sensor component can be systematically altered to accommodate the desired aptamer (and thus the molecular input specificity) without modifications to the remaining device components[51]. The sTRSV hammerhead ribozyme is an RNA sequence capable of self-cleavage under specific conformations[53, 54]. In the ribozyme-based device, the actuator samples at least two different conformations, only one of which allows ribozyme cleavage. Ligand binding by the sensor component changes the relative thermodynamic stability of the different conformations and alters the rate of change from one conformation to the next, thus affecting the ribozyme's cleavage activity. The transmitter component relays ligand-binding information from the sensor to the actuator, encodes competitive hybridization events to specify the signal processing function (ON or OFF switch), and contributes to performance tuning of the device. The ribozyme switch is integrated into the 3' untranslated region (UTR) of the target gene, where ribozyme cleavage results in rapid degradation of the target transcript and downregulation of gene expression. In an ON switch, ligand binding prevents ribozyme cleavage, thereby preserving the target transcript and upregulating gene expression (Figure 1.3B). Conversely, in an OFF switch ligand binding results in the downregulation of gene expression. In addition to single-input switch devices, ribozyme-based devices capable of higher-order computations have been developed, including AND, OR, NOR, and NAND gate devices with functionalities demonstrated in the eukaryotic model organism *Saccharomyces cerevisiae*[52].

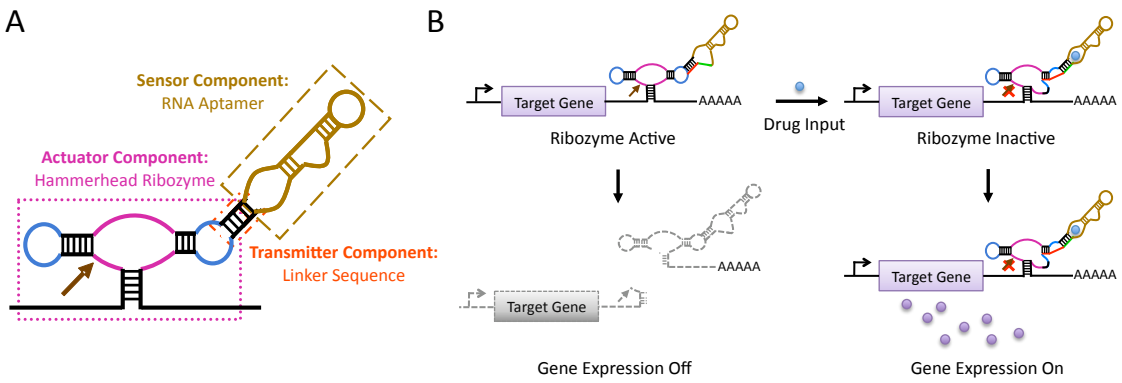

Figure 1.3. Schematic for a ligand-responsive ribozyme-based ON switch. (A) Ribozyme switches are composed of an RNA aptamer (sensor) and a self-cleaving hammerhead ribozyme (actuator) modularly coupled through a rationally designed linker sequence (transmitter). (B) Switches are designed to sample alternative structural conformations. The most thermodynamically stable conformation changes with the availability of the cognate ligand molecule. An ON switch prefers the ribozyme-active conformation in the absence of ligand molecules, a state in which ribozyme cleavage removes the poly-A tail and subjects the transcript to rapid degradation, resulting in gene expression knockdown (OFF state). In contrast, ligand binding to the sensor component stabilizes the ribozyme-inactive conformation, thus preserving the transcript and upregulating gene expression (ON state).

The modularity and tunability of these ribozyme switches as ligand-responsive gene-regulatory devices have been demonstrated in yeast culture[51]. For example, switch functionality is preserved and the input responsiveness appropriately altered when the sensor domain is changed from the theophylline aptamer to the tetracycline aptamer. Furthermore, switches exhibiting various knockdown efficiencies and dynamics have been constructed based on rational design strategies that modify the switches' thermodynamic properties. Specifically, by tuning the sequence of the transmitter component, one can control the absolute stability of each secondary structure and the energetic differences between the ribozyme-active and -inactive conformations of the switch. For example, a ribozyme switch can be designed to have greater knockdown activities by stabilizing the ribozyme-active (i.e., cleavable) conformation relative to the ribozyme-inactive (i.e., non-cleavable) conformation.

In addition to ribozyme-based regulatory designs, the RNAi pathway also holds promise as an RNA-based mechanism for gene expression regulation in diverse organisms. Modularly composed, ligand-responsive switch devices utilizing miRNAs and shRNAs as actuator components have also been developed in the Smolke Laboratory[55, 56].

Ligand-Responsive RNAi-Based Regulatory Devices

RNAi is a gene-silencing pathway first recognized in *Caenorhabditis elegans* as a biological response to exogenous double-stranded RNA (dsRNA)[57]. In this pathway, RNAi substrates including miRNAs and shRNAs are processed by endogenous RNases into 21-23-nt double-stranded RNA sequences. Alternatively, double-stranded short interfering RNAs (siRNAs) can be synthesized and used directly without the need for RNase processing. One of the two RNA strands is selectively incorporated into the RNA-induced silencing complex (RISC), thereby activating the protein complex. Activated RISC recognizes its regulatory target by sequence complementation to the loaded miRNA guide strand, and it silences target gene expression by either direct cleavage or translational inhibition of the target transcript[58].

Due to its ease of use, RNAi has quickly become a standard tool for sequence-specific, post-transcriptional gene silencing in biological systems ranging from plants to mammalian cells[59, 60]. Rationally designed miRNA sequences that resemble naturally occurring miRNAs in structure but carry altered stem sequences targeting specific genes of interest have been shown to inhibit gene expression in human cells[61]. Synthetic shRNAs have also been engineered to achieve targeted gene silencing in mammalian

systems[62, 63]. Since RNAi substrates cause cleavage in *trans*, it is possible to silence both endogenous and transgenic expression through the RNAi pathway[63, 64].

The Smolke Laboratory has developed modular and tunable platforms for the construction of small-molecule-responsive shRNA[55] and miRNA[56] switches. A strand displacement strategy is used to construct shRNA switches, which operate through the interaction of three components: an RNA aptamer (sensor) is coupled to the terminal loop of an shRNA (actuator) by a competing strand (transmitter) (Figure 1.4). The shRNA switch has at least two accessible conformations, in which the shRNA stem is either properly base-paired or disrupted by the competing strand. Only the properly formed shRNA can be processed by the RNase Dicer and proceed through the RNAi pathway. Similar to the ribozyme switches discussed previously, shRNA switches sample alternative conformations based on the relative thermodynamic stability of each accessible conformation. Ligand binding stabilizes one conformation over the others, thus changing the equilibrium distribution of conformations and allowing ligand-responsive gene expression modulation. Characterization studies performed in human embryonic kidney (HEK) 293 cells have demonstrated the modularity and tunability of shRNA switches, which can be rationally designed to respond to various molecular ligand inputs and generate gradient outputs in response to varying input concentrations[55].

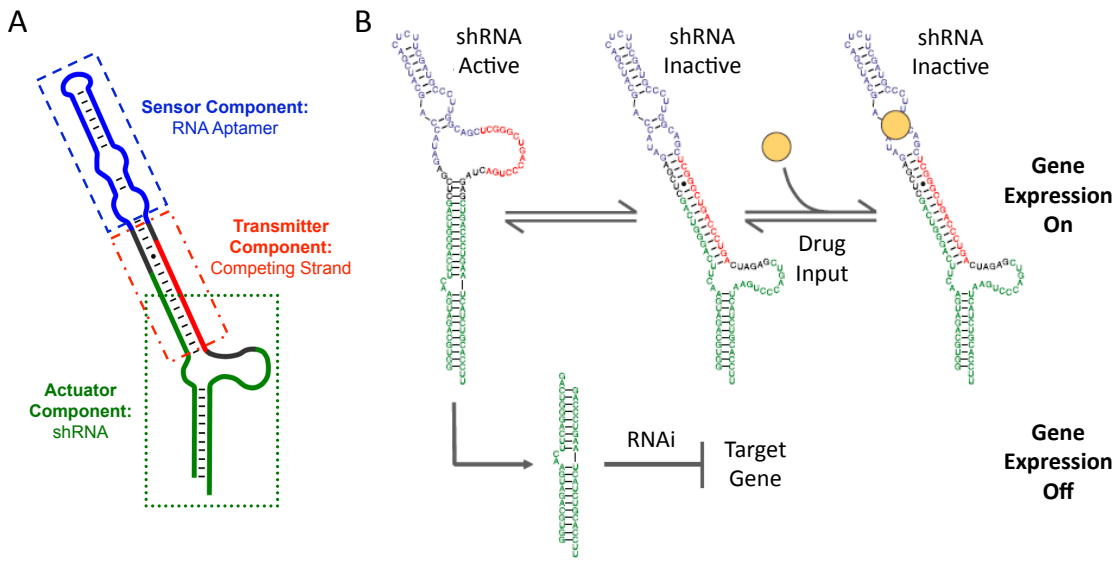

Figure 1.4. Schematic for a ligand-responsive shRNA-based ON switch. (A) shRNA switches are composed of an RNA aptamer (sensor) coupled to an shRNA (actuator) through a competing strand (transmitter) that translates ligand binding in the aptamer to conformational changes in the shRNA. (B) Switches are designed to sample alternative structural conformations. The most thermodynamically stable conformation changes with the availability of the cognate ligand molecule. An ON switch prefers the shRNA-active conformation in the absence of ligand molecules, leading to shRNA processing by the RNase Dicer and RNAi-mediated knockdown of the target gene (OFF state). In contrast, ligand binding to the sensor component stabilizes the shRNA-inactive conformation, thus abrogating the RNAi pathway and upregulating gene expression (ON state). This figure is adopted from Ref. 55.

In addition to shRNA switches, ligand-responsive miRNA switches have been developed in HEK 293 cells[56] (Figure 1.5). In this system, an RNA aptamer is integrated in the basal segment of a miRNA. Ligand binding to the aptamer imposes a constrained structure in the basal segment, thereby preventing miRNA processing by the RNase Drosha and abrogating gene-silencing activity by the RNAi pathway. Similar to the ribozyme and shRNA switch platforms, miRNA switches are modularly composed and can be systematically modified to respond to various molecular inputs. Furthermore, combinatorial expression strategies can be employed to generate multiple-copy miRNA constructs that mimic natural miRNA clusters and improve regulatory stringency. Importantly, miRNA switches can regulate gene expression both in *cis* and in *trans*. By specifying the miRNA sequence to match the target gene, miRNA switches can direct

gene expression knockdown in *trans* through the RNAi pathway. In addition, the miRNA switch can be inserted in the 3' UTR of a target gene. Processing by the RNase Drosha results in excision of the miRNA from the mRNA, leading to rapid transcript degradation and *cis*-acting gene expression knockdown. Therefore, miRNA devices can be designed to either silence one target gene through two regulatory mechanisms to increase regulatory stringency or simultaneously target two different genes in response to one molecular input.

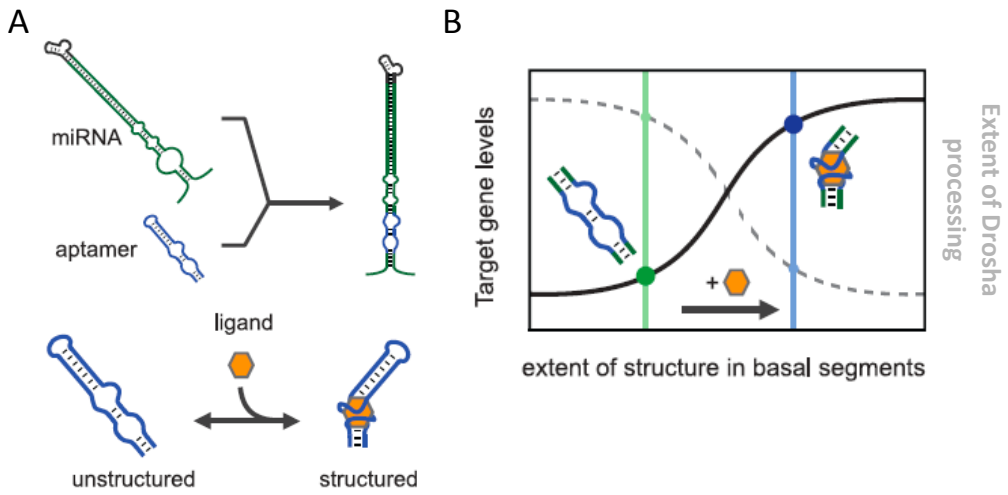

Figure 1.5. Schematic for a ligand-responsive miRNA-based ON switch. (A) miRNA switches are composed of an RNA aptamer (sensor) integrated in the basal segment of a miRNA (actuator). (B) In the absence of ligand, the basal segment has a flexible structure that allows recognition and cleavage by the RNase Drosha, thus enabling proper miRNA processing and RNAi-mediated knockdown of the target gene (OFF state). Increasing ligand concentration increases the likelihood of ligand binding to the sensor component, which results in a constrained structure in the basal segment of the miRNA. This structure inhibits Drosha processing, prevents RNAi-mediated gene silencing, and upregulates gene expression (ON state). The figure is taken from Ref. 56.

The ribozyme, shRNA, and miRNA switches described above represent modular and versatile devices with which integrated regulatory systems may be constructed. Although the three platforms act through different mechanisms, they share the same requirement for ligand-sensing activity. Namely, RNA aptamers specific to the molecular input of interest must be available for the construction of switches responsive to the

desired ligand. Therefore, the ability to generate RNA aptamers to the appropriate molecular inputs is critical to the development of RNA-based control devices for diverse applications.

Aptamers and *In Vitro* Selection Schemes for Novel Ligand-Binding Sequences

Aptamers are nucleic acid species that bind to ligands with high affinity and specificity. While nucleic acid species with ligand-binding activities exist in nature, the expanding repertoire of aptamers is largely a product of *in vitro* selection schemes that have become possible with the development of chemical DNA synthesis, the isolation of reverse transcriptase, and the invention of polymerase chain reaction (PCR). SELEX (Systematic Evolution of Ligands by EXponential enrichment) is the most widely used method for the *in vitro* selection of DNA and RNA aptamers[45, 46]. In this procedure, a pool of 10^{13}–10^{15} unique DNA sequences is amplified by PCR from chemically synthesized DNA templates with a randomized region flanked by fixed primer sequences. For RNA aptamer selection, the DNA library is used as a template for *in vitro* transcription to generate an RNA sequence pool. This RNA library is incubated with the ligand of interest, and the ligand-bound pool is isolated by separation techniques such as column chromatography and membrane filtration[44, 65]. The bound species are collected, reverse transcribed, amplified by PCR, and subjected to iterative rounds of selection following the same protocol. Increased selection pressure may be applied with each cycle to alter the properties of the resultant sequence pool. Such strategies include lowering ligand concentrations or increasing wash volumes to increase binding affinities, lowering Mg^{2+} content in the selection buffer to decrease ion concentration dependence, and

performing appropriate negative selections against related ligand species to tune the specificity of the resultant aptamer pool.

Aptamer sequences to diverse molecular targets have been generated since the advent of SELEX and other *in vitro* selection methods in the early 1990s. However, the aptamers reported thus far have mainly been selected for *in vitro* sensing applications, and many of the existing aptamers are not optimized for activity under physiological conditions. As a result, the great majority of ligand-responsive RNA devices developed to date have relied on the use of a few well-behaved aptamers—particularly those specific to the small molecules theophylline and tetracycline, both of which have considerable cytotoxicity—thus limiting the range of potential applications for these devices. The generation of novel aptamers to clinically suitable molecular targets will enable the construction of RNA-based control devices with diverse applications in health and medicine. In particular, the ability to regulate cellular functions with RNA-based devices can address critical areas for improvement in cell-based immunotherapy.

Synthetic RNA-Based Regulatory Systems for T-Cell Proliferation Control

As discussed above, adoptive T-cell therapy is a promising paradigm for cancer treatment, but its safety and efficacy is dependent on the ability to precisely orchestrate cellular behaviors—particularly proliferation—*in vivo*. The challenge of reprogramming the behaviors of complex biological processes is an area of active research in the field of synthetic biology, and of RNA engineering in particular. The development of RNA-based control devices to date has largely focused on the exploration of individual regulatory mechanisms and the construction of stand-alone devices. This body of knowledge now

enables the development of integrated control systems that can interface with genetic networks and signaling pathways to achieve regulatory functions at a systems level.

With the aim of improving the safety and efficacy of adoptive T-cell immunotherapy, we set out to develop regulatory systems capable of T-cell proliferation control through the use of small molecule–responsive, RNA-based regulatory devices. The paramount criterion of patient safety demands stringent control over the growth of transferred T cells *in vivo*. Conversely, therapeutic efficacy requires robust T-cell proliferation during the treatment period. To achieve both objectives, we focused our efforts on modulating the IL-2 and IL-15 cytokine signaling pathways central to T-cell proliferation, and developed multiple control systems to provide regulatory redundancies that ensure effective control over the fate of transferred T cells *in vivo*. Utilizing both ribozyme- and miRNA-based control devices, we developed synthetic regulatory systems capable of genetic control over both transgenic, growth-promoting cytokines and endogenous cytokine receptor chains. To further expand the applicability of our RNA-based regulatory systems in clinical settings, we also explored the selection of novel RNA aptamers specific to clinically suitable small molecules to serve as the sensor components of ribozyme- and miRNA-based control devices.

Regulatory System Development and Thesis Organization

In this thesis, we present the development of RNA-based regulatory systems capable of ligand-responsive control over T-cell proliferation. In Chapter 2, we discuss the translation of ribozyme switches from yeast to mammalian hosts and examine design parameters that are critical to device portability across organisms. In Chapter 3, we

present a ribozyme-based regulatory system that modulates transgenic expression of the proliferative cytokines IL-2 and IL-15, demonstrating drug-responsive, rapid, and reversible T-cell proliferation control in murine cells and animal models. In Chapter 4, we demonstrate the ability to regulate the growth of primary human central memory T cells with drug-responsive ribozyme switch systems. We further present characterization results on the human natural killer cell line NK-92 as a potential model for device development and optimization in human cells. In Chapter 5, we present the development of drug-responsive miRNA switches that regulate the expression of endogenous IL-2 receptor chains and modulate signaling activities in the IL-2/IL-15 pathways. This *trans*-acting system for endogenous gene expression regulation complements the *cis*-acting ribozyme-based system and expands the repertoire of RNA-based designs for multi-layered gene expression control in mammalian cells. In Chapter 6, we discuss efforts in selecting novel RNA aptamers to clinically suitable small-molecule targets, including phenobarbital, folinic acid, and vitamin B_{12}. Various selection and binding characterization methods were developed and evaluated, and the results serve to inform ongoing efforts in aptamer selection.

Synthetic RNA-based devices have broad applications in areas ranging from energy production to metabolic engineering. The work presented here demonstrates the capabilities and potential applications of RNA-based regulatory systems in improving next-generation treatment options for critical diseases. Although much optimization remains possible, this work illustrates one approach to the engineering of biological systems that may be applied to future endeavors in synthetic biological design.

References

1. Schilsky, R.L. Personalized medicine in oncology: the future is now. *Nat Rev Drug Discov* **9**, 363-366 (2010).
2. Rosenwald, A. et al. The use of molecular profiling to predict survival after chemotherapy for diffuse large-B-cell lymphoma. *N Engl J Med* **346**, 1937-1947 (2002).
3. Potti, A. et al. A genomic strategy to refine prognosis in early-stage non-small-cell lung cancer. *N Engl J Med* **355**, 570-580 (2006).
4. Peppercorn, J., Perou, C.M. & Carey, L.A. Molecular subtypes in breast cancer evaluation and management: divide and conquer. *Cancer Invest* **26**, 1-10 (2008).
5. Blattman, J.N. & Greenberg, P.D. Cancer immunotherapy: a treatment for the masses. *Science* **305**, 200-205 (2004).
6. Finn, O.J. Cancer immunology. *N Engl J Med* **358**, 2704-2715 (2008).
7. Waldmann, T.A. Immunotherapy: past, present and future. *Nat Med* **9**, 269-277 (2003).
8. Weiner, L.M., Surana, R. & Wang, S. Monoclonal antibodies: versatile platforms for cancer immunotherapy. *Nat Rev Immunol* **10**, 317-327 (2010).
9. Brower, V. Approval of Provenge seen as first step for cancer treatment vaccines. *J Natl Cancer Inst* **102**, 1108-1110 (2010).
10. June, C.H. Adoptive T cell therapy for cancer in the clinic. *J Clin Invest* **117**, 1466-1476 (2007).
11. Yee, C. Adoptive T cell therapy: Addressing challenges in cancer immunotherapy. *J Transl Med* **3**, 17 (2005).

12. Rosenberg, S.A., Restifo, N.P., Yang, J.C., Morgan, R.A. & Dudley, M.E. Adoptive cell transfer: a clinical path to effective cancer immunotherapy. *Nat Rev Cancer* **8**, 299-308 (2008).

13. Goldsby, R.A., Kindt, T.J., Osborne, B.A. & Kuby, J. Immunology, Edn. 5. (W. H. Freeman and Company, New York; 2003).

14. Trapani, J.A. & Smyth, M.J. Functional significance of the perforin/granzyme cell death pathway. *Nat Rev Immunol* **2**, 735-747 (2002).

15. Dudley, M.E., Wunderlich, J.R., Shelton, T.E., Even, J. & Rosenberg, S.A. Generation of tumor-infiltrating lymphocyte cultures for use in adoptive transfer therapy for melanoma patients. *J Immunother* **26**, 332-342 (2003).

16. Dudley, M.E. et al. CD8+ enriched "young" tumor infiltrating lymphocytes can mediate regression of metastatic melanoma. *Clin Cancer Res* (2010).

17. Cartellieri, M. et al. Chimeric antigen receptor-engineered T cells for immunotherapy of cancer. *J Biomed Biotechnol* **2010**, 956304 (2010).

18. Kahlon, K.S. et al. Specific recognition and killing of glioblastoma multiforme by interleukin 13-zetakine redirected cytolytic T cells. *Cancer Res* **64**, 9160-9166 (2004).

19. Gonzalez, S. et al. Genetic engineering of cytolytic T lymphocytes for adoptive T-cell therapy of neuroblastoma. *J Gene Med* **6**, 704-711 (2004).

20. Jensen, M.C. et al. Human T lymphocyte genetic modification with naked DNA. *Mol Ther* **1**, 49-55 (2000).

21. Park, J.R. et al. Adoptive transfer of chimeric antigen receptor re-directed cytolytic T lymphocyte clones in patients with neuroblastoma. *Mol Ther* **15**, 825-833 (2007).

22. Morgan, R.A. et al. Cancer regression in patients after transfer of genetically engineered lymphocytes. *Science* **314**, 126-129 (2006).

23. Dudley, M.E. et al. Adoptive transfer of cloned melanoma-reactive T lymphocytes for the treatment of patients with metastatic melanoma. *J Immunother* **24**, 363-373 (2001).

24. Yee, C. et al. Adoptive T cell therapy using antigen-specific CD8+ T cell clones for the treatment of patients with metastatic melanoma: in vivo persistence, migration, and antitumor effect of transferred T cells. *Proc Natl Acad Sci U S A* **99**, 16168-16173 (2002).

25. Mackensen, A. et al. Phase I study of adoptive T-cell therapy using antigen-specific CD8+ T cells for the treatment of patients with metastatic melanoma. *J Clin Oncol* **24**, 5060-5069 (2006).

26. Gattinoni, L., Powell, D.J., Jr., Rosenberg, S.A. & Restifo, N.P. Adoptive immunotherapy for cancer: building on success. *Nat Rev Immunol* **6**, 383-393 (2006).

27. Leen, A.M., Rooney, C.M. & Foster, A.E. Improving T cell therapy for cancer. *Annu Rev Immunol* **25**, 243-265 (2007).

28. Endy, D. Foundations for engineering biology. *Nature* **438**, 449-453 (2005).

29. Elowitz, M.B. & Leibler, S. A synthetic oscillatory network of transcriptional regulators. *Nature* **403**, 335-338 (2000).

30. Tabor, J.J. et al. A synthetic genetic edge detection program. *Cell* **137**, 1272-1281 (2009).

31. Sinha, J., Reyes, S.J. & Gallivan, J.P. Reprogramming bacteria to seek and destroy an herbicide. *Nat Chem Biol* **6**, 464-470 (2010).

32. Anderson, J.C., Voigt, C.A. & Arkin, A.P. Environmental signal integration by a modular AND gate. *Mol Syst Biol* **3**, 133 (2007).

33. Cox, R.S., 3rd, Surette, M.G. & Elowitz, M.B. Programming gene expression with combinatorial promoters. *Mol Syst Biol* **3**, 145 (2007).

34. Weber, W., Kramer, B.P. & Fussenegger, M. A genetic time-delay circuitry in mammalian cells. *Biotechnol Bioeng* **98**, 894-902 (2007).

35. Novina, C.D. & Sharp, P.A. The RNAi revolution. *Nature* **430**, 161-164 (2004).

36. Fedor, M.J. & Williamson, J.R. The catalytic diversity of RNAs. *Nat Rev Mol Cell Biol* **6**, 399-412 (2005).

37. Breaker, R.R. Complex riboswitches. *Science* **319**, 1795-1797 (2008).

38. Mathews, D.H. & Turner, D.H. Prediction of RNA secondary structure by free energy minimization. *Curr Opin Struct Biol* **16**, 270-278 (2006).

39. Isaacs, F.J., Dwyer, D.J. & Collins, J.J. RNA synthetic biology. *Nat Biotechnol* **24**, 545-554 (2006).

40. Wieland, M. & Hartig, J.S. Artificial riboswitches: synthetic mRNA-based regulators of gene expression. *Chembiochem* **9**, 1873-1878 (2008).

41. Win, M.N., Liang, J.C. & Smolke, C.D. Frameworks for programming biological function through RNA parts and devices. *Chem Biol* **16**, 298-310 (2009).

42. Mathews, D.H. et al. Incorporating chemical modification constraints into a dynamic programming algorithm for prediction of RNA secondary structure. *Proc Natl Acad Sci U S A* **101**, 7287-7292 (2004).

43. Zadeh, J.N. et al. NUPACK: Analysis and design of nucleic acid systems. *J Comput Chem* (2010).

44. Wilson, D.S. & Szostak, J.W. In vitro selection of functional nucleic acids. *Annu Rev Biochem* **68**, 611-647 (1999).

45. Ellington, A.D. & Szostak, J.W. In vitro selection of RNA molecules that bind specific ligands. *Nature* **346**, 818-822 (1990).

46. Tuerk, C. & Gold, L. Systematic evolution of ligands by exponential enrichment: RNA ligands to bacteriophage T4 DNA polymerase. *Science* **249**, 505-510 (1990).

47. Mendonsa, S.D. & Bowser, M.T. In vitro selection of aptamers with affinity for neuropeptide Y using capillary electrophoresis. *J Am Chem Soc* **127**, 9382-9383 (2005).

48. Cox, J.C. et al. Automated selection of aptamers against protein targets translated in vitro: from gene to aptamer. *Nucleic Acids Res* **30**, e108 (2002).

49. An, C.I., Trinh, V.B. & Yokobayashi, Y. Artificial control of gene expression in mammalian cells by modulating RNA interference through aptamer-small molecule interaction. *RNA* **12**, 710-716 (2006).

50. Topp, S. & Gallivan, J.P. Random walks to synthetic riboswitches—a high-throughput selection based on cell motility. *Chembiochem* **9**, 210-213 (2008).

51. Win, M.N. & Smolke, C.D. A modular and extensible RNA-based gene-regulatory platform for engineering cellular function. *Proc Natl Acad Sci U S A* **104**, 14283-14288 (2007).

52. Win, M.N. & Smolke, C.D. Higher-order cellular information processing with synthetic RNA devices. *Science* **322**, 456-460 (2008).

53. Salehi-Ashtiani, K. & Szostak, J.W. In vitro evolution suggests multiple origins for the hammerhead ribozyme. *Nature* **414**, 82-84 (2001).

54. Murray, J.B. et al. The structural basis of hammerhead ribozyme self-cleavage. *Cell* **92**, 665-673 (1998).

55. Beisel, C.L., Bayer, T.S., Hoff, K.G. & Smolke, C.D. Model-guided design of ligand-regulated RNAi for programmable control of gene expression. *Mol Syst Biol* **4**, 224 (2008).

56. Beisel, C.L., Chen, Y.Y., Culler, S.J., Hoff, K.G. & Smolke, C.D. Design of small molecule-responsive microRNAs based on structural requirements for Drosha processing. *Nucleic Acids Res* (2010). doi: 10.1093/nar/gkq954.

57. Fire, A. et al. Potent and specific genetic interference by double-stranded RNA in Caenorhabditis elegans. *Nature* **391**, 806-811 (1998).

58. He, L. & Hannon, G.J. MicroRNAs: small RNAs with a big role in gene regulation. *Nat Rev Genet* **5**, 522-531 (2004).

59. Elbashir, S.M. et al. Duplexes of 21-nucleotide RNAs mediate RNA interference in cultured mammalian cells. *Nature* **411**, 494-498 (2001).

60. Dykxhoorn, D.M., Novina, C.D. & Sharp, P.A. Killing the messenger: short RNAs that silence gene expression. *Nat Rev Mol Cell Biol* **4**, 457-467 (2003).

61. Zeng, Y., Wagner, E.J. & Cullen, B.R. Both natural and designed micro RNAs can inhibit the expression of cognate mRNAs when expressed in human cells. *Mol Cell* **9**, 1327-1333 (2002).

62. McManus, M.T., Petersen, C.P., Haines, B.B., Chen, J. & Sharp, P.A. Gene silencing using micro-RNA designed hairpins. *Rna* **8**, 842-850 (2002).

63. Paddison, P.J., Caudy, A.A., Bernstein, E., Hannon, G.J. & Conklin, D.S. Short hairpin RNAs (shRNAs) induce sequence-specific silencing in mammalian cells. *Genes Dev* **16**, 948-958 (2002).

64. Siolas, D. et al. Synthetic shRNAs as potent RNAi triggers. *Nat Biotechnol* **23**, 227-231 (2005).

65. Fitzwater, T. & Polisky, B. A SELEX primer. *Methods Enzymol* **267**, 275-301 (1996).

Chapter 2

Translation of Ribozyme-Based Gene Expression Control Devices from Yeast to Mammalian Cells

Abstract

Engineered biological systems have potential applications in areas ranging from foundational biological studies to biofuel production to cellular therapeutics. Robustly operating systems require effective control mechanisms to achieve fine-tuned performance, and a variety of synthetic, RNA-based control devices capable of gene expression regulation have been demonstrated. The majority of RNA-based control devices reported thus far have been developed in bacteria and yeasts—model organisms with well-characterized tools for genetic manipulation to facilitate the rapid prototyping and optimization of new devices. However, few devices have been shown to function in higher organisms, including human cells. While bacteria and yeasts are important cellular hosts in many research and industrial processes, several important application areas—particularly those in health and medicine—require mammalian systems and compatible control devices. Therefore, the ability to transfer synthetic devices developed in model organisms to mammalian systems is critical to the versatility and practicality of such devices in downstream applications. Here, we systematically examine the translation of ribozyme-based control devices developed in the yeast *Saccharomyces cerevisiae* to gene expression regulation in the model cell line human embryonic kidney (HEK) 293. We demonstrate that the knockdown efficiency of ribozyme-based devices is lower in HEK cells by 2- to 5-fold compared to that observed in yeast, and the switch dynamic range is reduced in HEK cells due to the mammalian hosts' limited capacity to withstand ligand toxicity. We identify several tuning strategies, including thermodynamically based sequence modification and multiple-copy expression, by which regulatory stringency can be improved for applications in mammalian systems, and we demonstrate functional ON,

OFF, and AND-gate switches in HEK 293 cells. We conclude that performance tunability is a device property essential to the transportability of these genetic devices across organisms, and we further identify several system parameters—including actuator efficiency, input signal toxicity, and genomic integration—as critical to the development of ribozyme-based control systems in higher organisms.

Introduction

RNA-based control devices with diverse regulatory mechanisms have been developed in recent years[1], and the great majority of RNA devices described to date have been developed in model organisms such as the bacterium *Escherichia coli* and the yeast *Saccharomyces cerevisiae*. Relatively high growth rates and the ease of genetic manipulation enable faster device prototyping and optimization in these model hosts compared to higher organisms such as mammalian cells. However, not all regulatory mechanisms are transportable across organisms. For example, translation initiation in prokaryotes is mediated by the hybridization of the 16S rRNA to the ribosome binding site (RBS) located 6–7 nucleotides upstream of the start codon. In contrast, translation in eukaryotes is initiated through a 7-methyl guanosine cap that recruits the translation initiation machinery. Therefore, an RNA device designed to regulate translation initiation in bacteria cannot function in eukaryotic hosts and vice versa.

It follows that the versatility of RNA devices depends on the use of components that do not rely on cell-specific machinery in performing regulatory functions. Alternatively, given a defined set of applications, devices can be developed in and tailored for specific host organisms of interest. The latter construction strategy circumvents the need for broad transportability across species, but incurs the potential cost of longer development periods required for designing and optimizing devices in complex organisms. The non-trivial increase in time and resource investments, as well as the technical complexities that accompany development work in higher organisms, has contributed to the relatively small number of functional RNA devices that have been generated in mammalian cells[2-4]. At the same time, many important application areas—

particularly those in health and medicine—require regulatory devices that can function in higher organisms, especially human cells. Therefore, the development of devices that function independently of cell-specific machineries and the demonstration of transportability across different organisms are critical to the versatility of synthetic RNA devices.

Previous work in the Smolke Laboratory presented a framework for assembling ligand-responsive, ribozyme-based devices from modular components in the yeast *S. cerevisiae*[5, 6] (see Chapter 1 for a detailed description). This RNA device assembly platform allows deliberate choice of the input molecule, fine-tuning of basal expression level and dynamic range, and the ability to program higher-order cellular information processing, making it uniquely suited for downstream therapeutic applications. However, the transportability of these ribozyme-based devices to gene expression control in mammalian cells remains to be demonstrated. Since the hammerhead ribozyme's cleavage-based regulatory mechanism is self-catalyzed and independent of cell-specific machinery, we hypothesized that the ribozyme switches should be functional in mammalian hosts, even though the quantitative performance levels of the devices may be affected by differences in the cellular environment. Here, we demonstrate the ability of ribozyme switches to regulate gene expression in human embryonic kidney (HEK) 293 cells. Through the process of transferring ribozyme switches from yeast to human cells, we identify performance tunability as a device property critical to transportability across organisms. Furthermore, we examine several system parameters—including ribozyme-mediated knockdown efficiency, ligand toxicity, and impact of device integration into the

host genome—that are essential to the construction of ribozyme-based gene-regulatory systems in mammalian hosts.

Results

Ribozyme Devices Show Reduced Knockdown Efficiency but Retain Ligand Responsiveness and Performance Tunability in Human Cells. We developed a model system to characterize ribozyme-based devices in mammalian cells, in which EGFP was expressed from a cytomegalovirus (CMV) promoter and ribozyme switches were inserted in the 3' UTR of the EGFP coding region. Transient transfections of the switch constructs were performed in HEK Flp-In 293 cells, and gene expression output was evaluated by EGFP intensity measured with a flow cytometer. Several theophylline- and tetracycline-responsive ON switches with distinct transmitter sequences that program different response properties (i.e., varying basal expression levels and dynamic ranges) were examined in the presence and absence of the appropriate small-molecule input. Ligand molecules were supplied at the maximum concentration that still permitted cell growth. Due to differences in ligand toxicity toward different cell types, the ligand concentration used in HEK transfections was ten-fold lower than that used in yeast characterization studies (Table 2.1)[5, 6].

Results from transient transfection assays indicate that each of the examined devices is capable of gene expression knockdown, with L2bulge8 exhibiting the highest knockdown efficiency and lowest basal expression level. The relative knockdown efficiencies among the devices are consistent with previous characterization results in

yeast, suggesting the tuning capability of the transmitter sequences is retained in the new host organism (Table 2.1, (1x) constructs in Figure 2.1).

Table 2.1. Theophylline-responsive ribozyme switch activities in yeast and HEK cells

Switch Construct	Theophylline Input		Expression Range[a,b]		Switch Activity (Fold)[c]	
	Yeast	HEK	Yeast	HEK	Yeast	HEK
L2bulge1(1x)	10 mM	1 mM	40% - 89%	88% - 89%	2.23	1.01
L2bulge8(1x)			12% - 48%	62% - 73%	4.00	1.18
L2bulge9(1x)			30% - 72%	88% - 104%	2.40	1.18

[a]Data for yeast cells are taken from Ref. 6, Table S1; data for HEK cells are taken from the experiment reported in Figure 2.1.
[b]Expression range indicates fluorescent protein expression levels in the absence (OFF state) and presence (ON state) of theophylline at the concentration indicated for each cell type.
[c]Switch activity is calculated by dividing the ON-state expression level by the OFF-state expression level and reported as a fold-change.

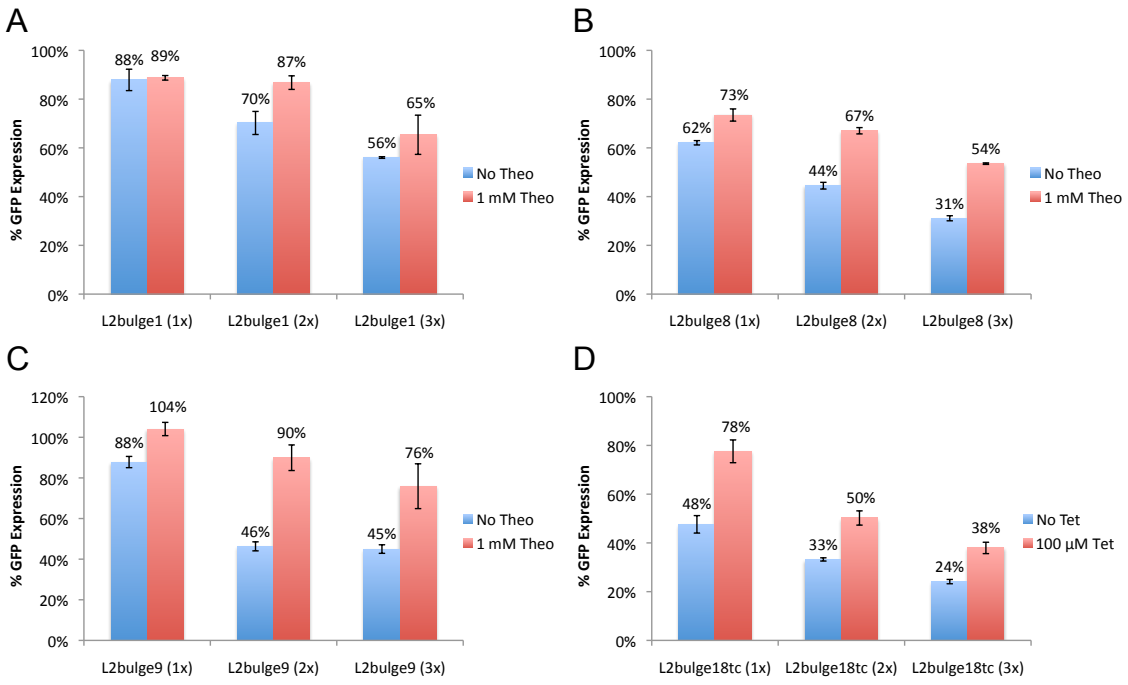

Figure 2.1. Ribozyme switches provide tunable, ligand-responsive gene regulation. GFP expression levels are reported for constructs encoding the theophylline-responsive switches (A) L2bulge1, (B) L2bulge8, and (C) L2bulge9, and the tetracycline-responsive switch (D) L2bulge18tc. Fluorescence values were normalized to those of the inactive ribozyme control cultured at corresponding ligand concentrations. Reported values are mean ± s.d. from triplicates.

Despite their evident knockdown activities, all the devices tested show significantly higher basal expression levels (i.e., gene expression in the absence of ligand input) in HEK cells compared to those observed in yeast, and the switch dynamic ranges are more limited in HEK cells (Table 2.1). The reduced dynamic ranges may have resulted from the lower ligand concentrations used in HEK cultures. However, elevated basal expression levels suggest that cellular mechanisms associated with this gene-regulatory scheme, including ribozyme cleavage activities as well as mRNA and protein synthesis and degradation, likely occur at different rates in the two cell types. The observed reduction in ribozyme-mediated knockdown efficiency in HEK cells is consistent with previously reported data on the transcript levels of reporter genes coupled to the unmodified sTRSV hammerhead ribozyme in yeast (8%)[5] versus HEK cells (20%)[7]. Furthermore, differences in the method of genetic manipulation (i.e., stable transformation in yeast versus transient transfection in HEK cells) may also have contributed to the different activities observed.

Multiple-Copy Expression Fine-Tunes Regulatory Stringency and Improves Switch Dynamic Range. To address the reduction in ribozyme-mediated knockdown efficiency in mammalian cells, we implemented a second tuning strategy based on linking multiple copies of ribozyme switches in the 3' UTR of the transgene. The ribozyme switches are expected to act independently in this design[6], where only one of the switches needs to be in the ribozyme-active state to cleave and inactivate the transcript. Multiple-copy switch devices increase the probability of ribozyme-mediated transcript cleavage, thereby lowering basal expression levels. However, expressing multiple copies of the same or

similar ribozyme switches increases the potential of misfolding of the RNA elements, which would disable the devices. To maintain the structural and functional independence of each switch, we introduced standardized spacer sequences that form stable hairpin structures between each copy of the ribozyme switch (Figure 2.2). We used the RNAstructure software[8] to verify that the most thermodynamically favorable conformation for the entire RNA sequence is one in which each switch is properly folded. Previous studies in yeast have examined the effect of expressing two copies of the ribozyme switches[6]. Given the reduced ribozyme cleavage efficiency observed in HEK cells, we anticipated the need to integrate additional copies of switch devices and devised a sequential cloning strategy to allow for the systematic integration of a theoretically unlimited number of ribozyme switches in the 3' UTR of a given gene (Figure 2.2, see Materials and Methods).

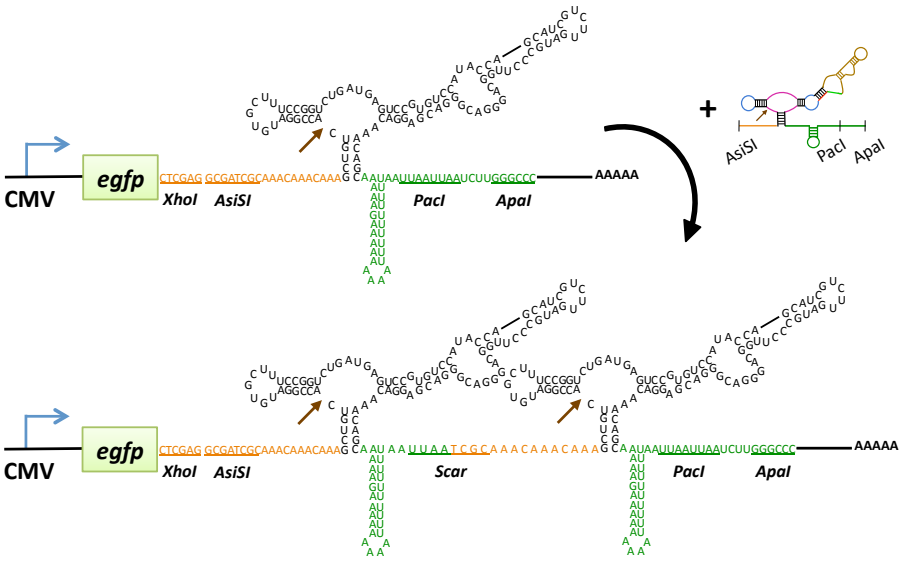

Figure 2.2. Ribozyme switch devices are modularly integrated into mammalian expression vectors. Ligand-responsive ribozyme switch devices (here depicting L2bulge1) are inserted in the 3' UTR of the transgene encoding for EGFP, which serves as a reporter protein for the evaluation of regulatory activities. A modular insertion strategy allows the implementation of multiple copies of ribozyme switches to tune regulatory stringency. The restriction sites AsiSI and PacI, which generate compatible sticky ends, allow reuse of the sites after each switch insertion. Spacer sequences (orange and green) form a stable hairpin structure that provides structural insulation and maintain the functional independence of each switch.

If the cleavage activity of each ribozyme were an independent event, the probability of the transcript remaining intact (i.e., all ribozymes remaining in the inactive state) would be the product of each ribozyme's probability of remaining uncleaved. Therefore, each additional copy of the switch would result in a fixed fold-decrease in basal expression level equivalent to the inverse of the probability of each ribozyme remaining uncleaved. The probability of a ribozyme switch remaining uncleaved can be indirectly measured by the expression levels of single-copy constructs. Therefore, each additional copy of the L2bulge1, L2bulge8, L2bulge9, and L2bulge18tc switches is expected to result in fold-decreases of 1.1-, 2.1-, 1.1-, and 1.6-fold, respectively.

Transient transfection results show that the multiple-copy switch systems lower basal expression levels while maintaining ligand-responsive switch activities (Figure 2.1). With the exception of L2bulge9, each addition copy of a ribozyme switch results in a constant fold-decrease in basal expression levels (1.3-fold for L2bulge1, 1.4-fold for L2bulge8, and 1.4-fold for L2bulge18tc), consistent with independent ribozyme activity. The actual magnitudes of change for L2bulge1 and L2bulge18tc are close to the predicted values, whereas that for L2bulge8 is not. In addition, the L2bulge9 switch exhibits a dramatic decrease in basal expression level with the first additional ribozyme copy but no further improvement with the second additional copy. These behaviors suggest that the assumption of independent cleavage activities may not be valid for all switch designs and additional factors such as cooperativity and kinetic limitations in ribozyme cleavage may be involved. It is also possible that protein expression level is not a perfect surrogate measurement for mRNA cleavage activity, thus introducing discrepancies between theoretical and actual results.

In addition to lowering the basal expression levels, multiple-copy switch systems improve the ligand-responsive dynamic range for the majority of constructs tested (Figure 2.1). Specifically, switches with the highest basal expression levels show the largest improvements in dynamic range measured both in fold change (i.e., ratio of ON-state to OFF-state expression levels) and in absolute values. L2bulge1, which has no switch activity when expressed as a single-copy construct, shows theophylline-responsive gene expression upregulation when implemented in two and three copies. L2bulge8, which has a significantly higher knockdown efficiency than L2bulge1, also exhibits increased switch dynamic range (measured in fold) with each increasing ribozyme copy number. The improvement in switch activity may be attributed to the lowered basal expression level, which effectively broadens the maximum range between the ON and the OFF states. Although the maximum ON state may not be accessible in these model systems due to HEK cells' limited tolerance for the small-molecule ligands used, the ability to increase the potential dynamic range makes multiple-copy expression a valuable tool for fine-tuning the performance of regulatory systems constructed with ribozyme-based devices.

Ribozyme Devices Exhibit Titratable Switch Activity Dependent on Basal Expression Levels. The ability to modulate output signal intensity by adjusting input signal strength is a critical property of genetic control devices. An important characteristic of the ribozyme switch devices is a dose-dependent response to input concentrations. To verify the titratable response of ribozyme switch devices in human cells, we performed transient transfections of constructs harboring ON and OFF switches

responsive to theophylline and tetracycline in HEK cells supplemented with various levels of the appropriate ligands. Results indicate titratable switch activity in the majority of devices tested, with gene expression increasing or decreasing with input concentration as prescribed by the device design (Figure 2.3). Consistent with previous observations, devices with high basal expression levels have relatively poor ligand-responsive ON switch activities (L2bulge1tc, Figure 2.3B). In addition, L2bulgeOFF1tc, a tetracycline-responsive OFF switch, exhibits weak switch activities. Yeast and HEK cells have different sensitivity levels to small-molecule ligands, and toxicity issues limit the maximum tetracycline input in HEK cultures to a concentration substantially lower than that used in yeast cultures (150 μM and 1 mM for HEK and yeast, respectively)[6]. This difference in input signal strength is likely the main cause of the reduced switch dynamic ranges observed in HEK cells.

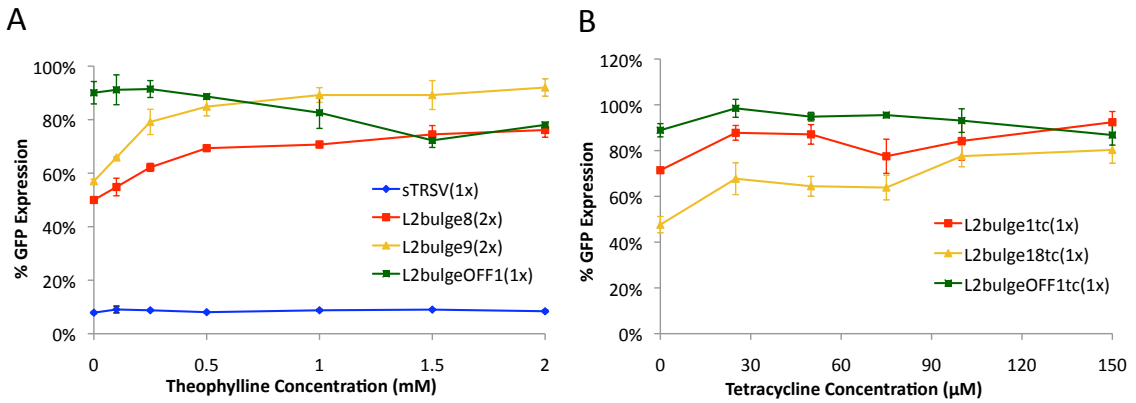

Figure 2.3. Ribozyme switches provide titratable gene regulation. GFP expression levels are reported for constructs encoding (A) theophylline- and (B) tetracycline-responsive switches. (A) L2bulge8(2x) and L2bulge9(2x), ON switches. L2bulgeOFF1(1x), an OFF switch. sTRSV, a non-switch, fully active hammerhead ribozyme control. (B) L2bulge1tc(1x) and L2bulge18tc(1x), ON switches. L2bulgeOFF1tc, an OFF switch. Values are reported as described in Figure 2.1.

Stable Integration of Ribozyme Devices Provides Consistent, Long-Term Regulatory Activity. The performance stability of genetic control devices is a critical system attribute in a wide range of applications, including cellular therapeutics and the industrial production of pharmaceuticals or biofuels using genetically modified cell strains. To evaluate the long-term robustness of ribozyme switch devices in mammalian cells, we performed site-specific integration of the switch devices in HEK Flp-In 293 cells. Site-specific stable integration was chosen for three main reasons. First, long-term characterization cannot be performed on transiently transfected cells, which generally lose transgene expression within one week in the absence of selection pressure due to the loss or dilution of plasmids. Any downstream application that operates for more than a few days will require stably integrated systems. Second, stably integrated cell lines have significantly more consistent gene expression levels compared to transiently transfected cultures. Transient transfections result in heterogeneous populations of cells receiving different numbers of plasmids and thus expressing the encoded transgene at vastly different levels. Stable integration permits the selection of monoclonal cultures with a tight distribution of gene expression levels, enabling more accurate quantification of system performance (Figure 2.4A). Third, site-specific integration with the Flp-In system (Invitrogen) allows direct comparison of various stably integrated cell lines harboring different constructs. Stable integration in mammalian cells can be achieved through several methods, including viral transduction and lipid-based transfection followed by selection. However, such methods generate polyclonal integrants with random insertion sites for the introduced transgene, and more than one copy of the transgene may be integrated into the genome. While it is possible to isolate monoclonal populations for

each cell line by cell sorting or limiting dilution, direct comparisons cannot be made across different cell lines due to differences in integration site and copy number, both of which affect gene expression levels. The Flp-In system generates isogenic cell lines with one copy of the transgene inserted into a specific genomic location, thus allowing accurate comparisons to be made across cell lines harboring different transgenic constructs.

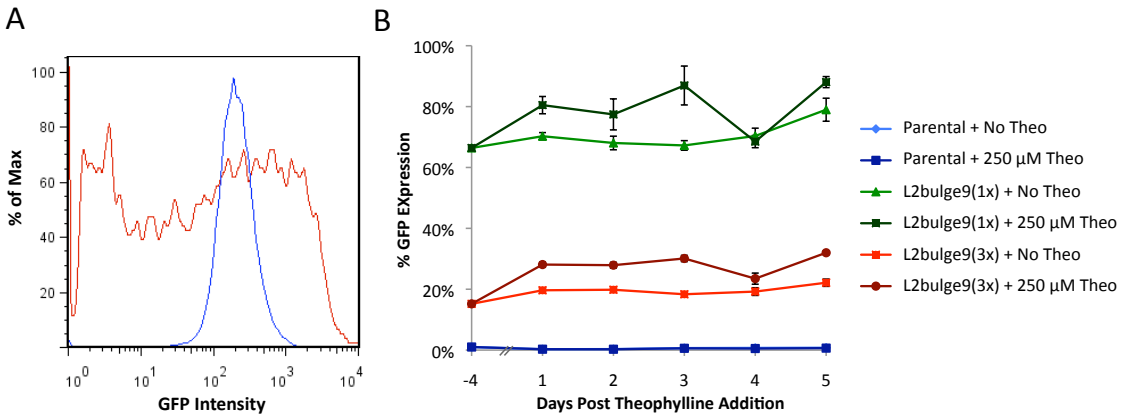

Figure 2.4. Stably integrated cell lines show tight gene expression distributions and demonstrate long-term regulatory activities by ribozyme switches. (A) Stably integrated cell lines show a substantially narrower gene expression distribution compared to transiently transfected cells. Blue, HEK cells stably integrated with a plasmid encoding EGFP coupled to an inactive ribozyme; red, HEK cells transiently transfected with the same plasmid. (B) HEK cell lines stably expressing one or three copies of the theophylline-responsive ribozyme switch L2bulge9 exhibit ligand-responsive ON switch behavior and an increase in knockdown activity with increasing ribozyme copy numbers. Stable cell lines were cultured in the presence or absence of 250 µM theophylline for five days. The parental HEK Flp-In 293 cell line was included as a negative control. Values are reported as described in Figure 2.1.

Stable cell lines expressing one or three copies of the theophylline-responsive ON switch L2bulge9 or an inactive ribozyme (positive control) inserted in the 3' UTR of the *egfp* transgene were generated. The resultant cell lines were characterized for ligand-responsive gene regulatory activities by culturing in the presence or absence of 250 µM theophylline for five days, and the parental HEK Flp-In 293 cell line was included as a negative control. The theophylline concentration used with the stable cell lines was four-

fold lower than that used in transient transfection studies because HEK cells cannot withstand long-term exposure to the higher theophylline concentration. Despite the lowered input concentration, gene expression results indicate theophylline-responsive ON switch activities and an increase in knockdown efficiency with increasing ribozyme copy numbers (Figure 2.4B). Gene expression reached steady-state levels within 24 hours and remained stable through the five-day time-course, supporting a rapid and robust response to the molecular input. Compared to transient transfection results, the stably integrated cell lines show substantially lower basal expression levels and slightly smaller dynamic ranges in response to ligand addition (Table 2.2). The reduced input concentration used in the time-course study is likely a major contributing factor to the decrease in dynamic range. In addition, the substantially different distribution of gene expression levels in transiently transfected samples versus stably integrated cell lines may account for the differences in basal expression levels and dynamic ranges. Specifically, the measured performance of transiently transfected samples reflects the average of heterogeneous cell populations with widely varying expression levels (Figure 2.4A). Measurements made on stably integrated cells, which are isogenic and show a tight distribution of expression levels, are likely to be more accurate reflections of device performance.

Table 2.2. Theophylline-responsive ribozyme switch activities in transiently transfected and stably integrated HEK 293 cells

Switch Construct	Theophylline Input		Expression Range[a,b]		Switch Activity (Fold)[c]	
	Transient	Stable	Transient	Stable	Transient	Stable
L2bulge9(1x)	1 mM	250 μM	88% - 104%	71% - 80%	1.18	1.13
L2bulge9(3x)			45% - 76%	20% - 28%	1.69	1.43

[a]Data for transient transfection are taken from the experiment reported in Figure 2.1C; data for stable integration are taken from the experiment reported in Figure 2.4B, with expression levels reported as the average (arithmetic mean) of data points gathered over the five-day time-course study.
[b]Expression range shows fluorescent protein expression levels in the absence (OFF state) and presence (ON state) of theophylline at the concentration indicated for each experiment type.
[c]Switch activity is calculated by dividing the ON-state expression level by the OFF-state expression level and reported as a fold change.

Translation of Higher-Order Information Processing Devices from Yeast to Mammalian Cells Requires Finely Tuned Designs with Strong Regulatory Performance. Ribozyme-based devices capable of higher-order computation have been demonstrated in yeast cells [6]. To examine the portability of these multi-input devices in mammalian cells, we tested logic-gate devices generated by the combinatorial expression of ON switches responsive to theophylline or tetracycline (Figure 2.5A). Transient transfection results for two AND-gate devices in HEK cells suggest that robust multi-input device activity is dependent on a low basal expression level (Figure 2.5B), consistent with results observed with single-input devices (Figures 2.1, 2.3). Specifically, single-input switches capable of lower basal expression levels and larger dynamic ranges when acting as individual devices (L2bulge8 and L2bulge18tc) can be combined to build AND-gate devices with better performance levels compared to devices composed of single-input switches with higher basal expression levels and narrower dynamic ranges (L2bulge1 and L2bulge1tc). These results suggest that optimized multi-input RNA devices capable of higher-order computation in mammalian cells may be constructed by lowering the basal expression levels of both individual, single-input devices and the

combined ensemble. This could be achieved by reprogramming the transmitter sequence, implementing multiple copies of switch devices, or stably integrating the control devices into the host genome (Figure 2.1, Table 2.2). Furthermore, the use of non-toxic molecular inputs would permit the administration of higher ligand concentrations and enable access to the full switch dynamic range of each control device, which is likely much larger than what is currently achievable in HEK cells based on comparisons against results observed in yeasts.

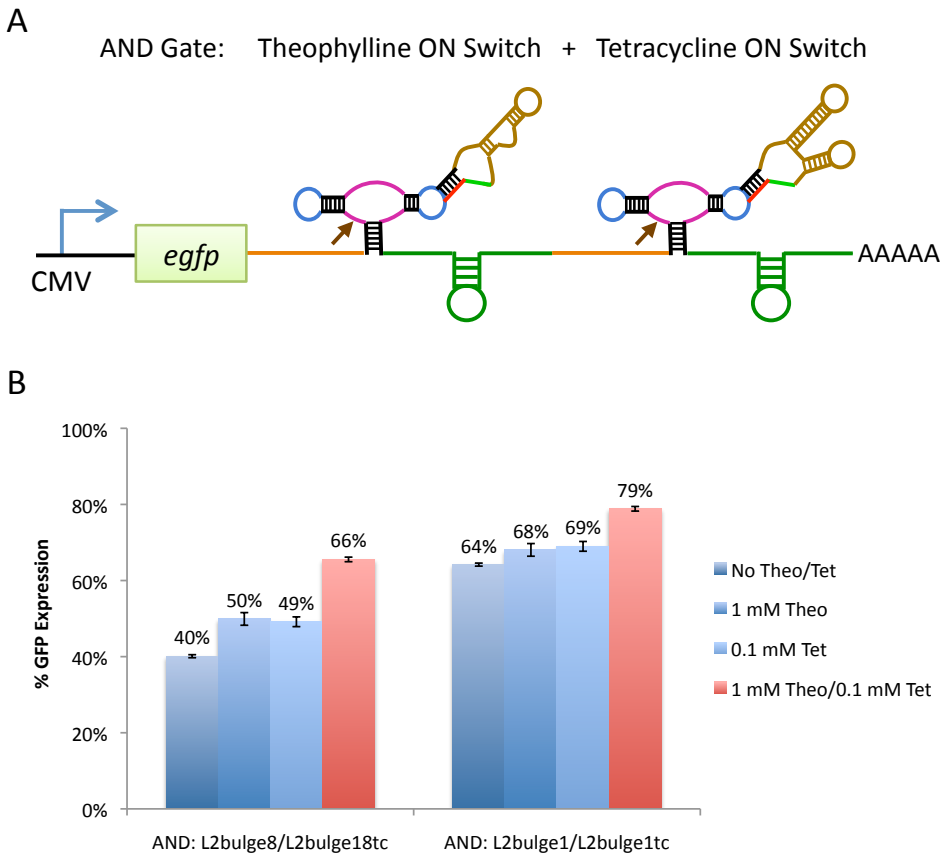

Figure 2.5. Higher-order information-processing devices must be composed of switch components with robust individual performance levels to achieve the prescribed regulatory activity in mammalian cells. (A) AND-gate devices are constructed by the tandem expression of two ON switches responsive to different input molecules. An AND-gate device comprised of theophylline-responsive and tetracycline-responsive ON switches is illustrated. (B) The combination of individual devices with strong regulatory activities enables more effective higher-order information-processing devices. Two devices were examined in HEK Flp-In 293 cells. The first AND gate consists of the L2bulge8 and L2bulge18tc switches inserted in tandem behind the *egfp* gene using the platform described in Figure 2.2. The second AND gate consists of L2bulge1 and L2bulge1tc inserted in tandem. Values are reported as described in Figure 2.1.

Discussion

RNA-based control devices incorporating a variety of regulatory strategies have been developed, mostly in bacteria and yeasts[1, 2, 9]. However, the translation of these devices to higher organisms has been limited due to the incorporation of regulatory mechanisms that require cell-specific machinery. Important application areas such as cell-based therapies and the production of highly glycosylated pharmaceuticals require the use of mammalian systems and compatible control devices. Although a number of RNA-based control devices have been developed directly in mammalian cells[4, 10, 11], important advantages such as high growth rates and the relative ease of genetic manipulations make simpler model organisms, such as *S. cerevisiae,* the preferred hosts for device development. Therefore, the ability to prototype and optimize control devices in simpler organisms and later transport them to more complex cellular systems is highly desirable.

Ausländer et al. recently reported a ribozyme-based OFF switch for gene expression regulation in mammalian cells (Auslander et al.). The theophylline-responsive ribozyme was originally generated through library screening in *E. coli*. Although the switch sequence optimized in bacteria proved functional in mammalian cells, its ligand responsiveness required re-optimization through both rational design and sequence randomization and screening once implemented in the mammalian system. Furthermore, the gene regulatory strategy required fundamental changes when moving from the bacterial system to the mammalian system. Specifically, gene expression regulation in bacteria was achieved by controlling the availability of the Shine-Dalgarno sequence (Wieland and Hartig 2008b), whereas expression control in mammalian cells acted

through mRNA degradation following ribozyme cleavage in the 5' UTR of the target transcript (Auslander et al.). As a result, the device designed as an ON switch in bacteria can only function as an OFF switch in mammalian cells, and the design platform (which is dependent on library screening) does not allow for systematic alterations to reprogram and tune regulatory performance. It is also unclear whether this earlier design can support the construction of multi-input devices capable of higher-order information processing. These results highlight the importance and challenge of designing regulatory devices that are fully translatable across organisms and allow for the implementation of diverse information processing functions.

In the present work, we have demonstrated the translation of ribozyme switch devices previously developed in the yeast *S. cerevisiae* to gene expression regulation in the human cell line HEK 293. We implemented theophylline- and tetracycline-responsive ribozyme switch devices without modification in a mammalian expression system, in which the CMV promoter drives the expression of the reporter gene *egfp* with ribozyme switches inserted in the 3' UTR of the gene. Our characterization results show that the switch devices are capable of gene expression knockdown in HEK cells, exhibiting titratable activities in response to varying ligand input concentrations. However, the knockdown efficiency and switch dynamic range of any given device are generally lower in HEK cells compared to yeast cells. For certain switches, the reduction in knockdown and switch activities is sufficient to render the device largely ineffective. Although the cleavage mechanism that underpins the ribozyme-based regulatory framework is self-catalyzed and independent of cell-specific machinery, the cellular environment in which the ribozyme switches function is expected to influence their activities. Therefore, design

adjustments must be made to realize the full regulatory capabilities of ribozyme-based devices in mammalian cells, and our findings highlight performance tunability as critical to achieving device transportability across organisms.

The ribozyme-based control platform has the unique property of being modularly composed and thus amenable to a variety of performance-tuning strategies, including modifications to the transmitter sequence of individual devices and the expression of multiple ribozyme switches coupled to the same genetic target[5]. Our results show that these strategies are both transportable and essential to achieving effective regulatory activities in mammalian systems. Transmitter sequence modification was employed in the design of the theophylline-responsive ON switches L2bulge8 and L2bulge9 based on L2bulge1. While all three switches are capable of substantial knockdown and ligand-responsive switch activities in yeast, only the modified switches L2bulge8 and L2bulge9 are able to achieve knockdown and switching when expressed as single-copy constructs in mammalian cells. As a second tuning strategy, the implementation of multiple copies of a switch within a single genetic target was shown to lower basal expression levels and increase ligand-responsive dynamic ranges. While reduced ribozyme-mediated knockdown efficiency in mammalian cells can abrogate the switch activity of some devices implemented in single copies (e.g., L2bulge1 (1x), Figure 2.1), multiple-copy switch systems improve knockdown efficiency and restore ligand-responsive activity by increasing the overall probability of transcript cleavage. These results highlight the importance of modularity and tunability in the translation of control devices across organisms, and demonstrate that the ribozyme-switch platform, originally developed in yeast, possesses the required properties for effective function in mammalian hosts.

Although the fine-tuned ribozyme switches are functional in mammalian cells, several system parameters show significant differences between yeast and mammalian cells and should inform future designs of ribozyme-based regulatory systems for mammalian applications. First, our results show that the knockdown efficiency of the sTRSV hammerhead ribozyme is substantially lower in mammalian cells than in yeast. This reduced efficiency leads to a higher basal expression level (or greater "leakiness" in expression) and a smaller dynamic range. Therefore, when prototyping and optimizing devices in yeast cells, it is important to make allowances for this expected decrease in cleavage activity upon transfer to mammalian cells. Furthermore, the previously discussed tuning strategies will likely be necessary in refining the system design upon transferring into mammalian hosts. Finally, these results suggest that highly active ribozymes are necessary for the generation of ribozyme-based control devices that can function effectively in mammalian cells.

Second, different cell types have different sensitivities toward the small-molecule inputs used to regulate the RNA devices. Our results suggest that mammalian cells tend to be more susceptible to ligand toxicity compared to yeast cells. In the ribozyme switch platform, ligand binding dictates the ribozyme cleavage rate by influencing the relative stability of alternative ribozyme conformations. The cleavage rate in turn regulates the target gene expression level and the functional output of the regulatory device. Higher ligand concentrations have greater impacts on the ribozyme switch's conformational change and expand the potential dynamic range of the device. Conversely, toxicity-imposed limitations on input concentrations set constraints on switch activities and the overall performance of the regulatory system. Therefore, even if the model organism used

for device prototyping is able to withstand high input concentrations, the destination organism's tolerance for the ligand molecules must be determined early and applied to the device development process to ensure functionality in the application of interest. Furthermore, these results indicate that sensor components (i.e., aptamers) with high affinity to ligand molecules that exhibit low cellular toxicity are critical to the utility and portability of RNA-based regulatory devices.

Third, the performance of RNA-based devices can vary dramatically depending on whether the devices are transiently or stably expressed in the mammalian host. While characterization studies are more efficiently and thus frequently performed by transient transfection, stable genomic integration is required for applications in which a narrow distribution of expression levels and long-term functionality are important. Our results show that ribozyme switches have greater knockdown efficiencies but slightly smaller dynamic ranges in stably integrated cell lines compared to transiently transfected cultures. The reduced dynamic range is likely due to the limited ligand concentration that can be tolerated for long periods by cell cultures, thus highlighting a system constraint imposed by the aforementioned issue of input toxicity.

To our knowledge, this work presents the first successful translation of an RNA-based control device from the model organism *S. cerevisiae* to gene expression control in mammalian cells. We demonstrated that ribozyme-based devices retain their designed functions when transported from yeast to human cells, and that performance tunability is a critical system attribute that permits portability across diverse organisms. Several system parameters—including actuator efficiency, ligand toxicity, and genetic integration of regulatory devices—must be considered and properly specified to achieve robust and

effective regulatory activity. These findings provide the foundation for the design and construction of ribozyme-based T-cell proliferation control systems presented in the following chapters.

Materials and Methods

Plasmid construction. All plasmids were constructed using standard molecular biology techniques[14]. All oligonucleotides were synthesized by Integrated DNA Technologies and all constructs were sequence verified (Laragen). Cloning enzymes, including restriction enzymes and T4 DNA ligase, were obtained from New England Biolabs, and DNA polymerases were obtained from Stratagene. The coding region of EGFP was inserted into the restriction sites KpnI and XhoI in pcDNA3.1(+) (Invitrogen). A CMV promoter and the coding region of dsRed-Express were also inserted into the plasmid to serve as transfection control. Ribozyme switch sequences were inserted into XhoI/ApaI behind EGFP, and the resulting plasmids were digested with KpnI and ApaI to obtain the EGFP-ribozyme switch sequence insert, which was then cloned into KpnI/ApaI in pcDNA5/FRT (Invitrogen).

A standardized cloning method was developed to allow for the sequential insertion of engineered ribozyme switches and corresponding control constructs in the 3' UTR of the target transgenes (Figure 2.2). The engineered ribozyme switch constructs were generated by PCR amplification using the forward primer Rz XhoI-AsiSI5' (5'AATACTCGAG GCGATCGC*AAACAAACAAA*), where the underlined sequences indicate restriction sites for XhoI and AsiSI, respectively, and the reverse primer Rz ApaI-PacI3' (5'AATA GGGCCCAAGATTAATTAA*AAAAAAAATTTTTATTTTTCTTTT*

*T*GCTGTT), where the underlined sequences indicate restriction sites for ApaI and PacI, respectively. The italicized sequences indicate spacers flanking each ribozyme switch, and the 3' spacer sequence forms a hairpin structure consisting of A-U pairs to provide insulation for each ribozyme switch. The first copy of an engineered ribozyme switch in each plasmid was inserted via the unique restriction sites XbaI and ApaI. All subsequent copies of the engineered ribozyme switches were inserted behind the 3' end of the previous copy of ribozyme switch by digesting the plasmid with PacI and ApaI and the insert with AsiSI and ApaI, where digestions with PacI and AsiSI resulted in identical sticky ends. The resulting ligation product retained unique PacI and ApaI sites while eliminating the AsiSI site, thus allowing the cloning strategy to be repeated for each additional copy of the ribozyme switch inserted into the construct.

Ribozyme switch sequences are listed below. Color schemes: Purple, catalytic core of the ribozyme or actuator component; blue, loop region of the actuator component; brown, aptamer or sensor component; green and red, strands that participate in the competitive hybridization event; italicized, spacer sequences; underlined, restriction sites.

sTRSV hammerhead ribozyme
5'CTCGAG*AAACAAACAAA*GCTGTCACCGGATGTGCTTTCCGGTCTGATGAGTCC
GTGAGGACGAAACAGC*AAAAAGAAAAATAAAAATTTTTTGGAA* TCTAGA

Inactive ribozyme
5'CTCGAGGCGATCGC*AAACAAACAAA*GCTGTCACCGGATGTGCTTTCCGGTAC
GTGAGGTCCGTGAGGACAGAACAGC*AAAAAGAAAAATAAAAATTTTTTTT*TTAAT
TAATCTTGGGCCC

L2bulge1
5'CTCGAGGCGATCGC*AAACAAACAAA*GCTGTCACCGGATGTGCTTTCCGGTCT
GATGAGTCCGTGTCCATACCAGCATCGTCTTGATGCCCTTGGCAGGGACGGG
ACGAGGACGAAACAGC*AAAAAGAAAAATAAAAATTTTTTTT*TTAATTAATCTTGG
GCCC

L2bulge8
5’CTCGAGGCGATCGC*AAACAAACAAA*GCTGTCACCGGATGTGCTTTCCGGTCT
GATGAGTCCGTTGTCCATACCAGCATCGTCTTGATGCCCTTGGCAGGGACGG
GACGGAGGACGAAACAGC*AAAAAGAAAAATAAAAATTTTTTTT*TTAATTAATCTT
GGGCCC

L2bulge9
5’CTCGAGGCGATCGC*AAACAAACAAA*GCTGTCACCGGATGTGCTTTCCGGTCT
GATGAGTCCGTTGTCCAATACCAGCATCGTCTTGATGCCCTTGGCAGTGGATG
GGGACGGAGGACGAAACAGC*AAAAAGAAAAATAAAAATTTTTTTT*TTAATTAATC
TTGGGCCC

L2bulge1tc
5’CTCGAGGCGATCGC*AAACAAACAAA*GCTGTCACCGGATGTGCTTTCCGGTCT
GATGAGTCCGTGTCCAAAACATACCAGATTTCGATCTGGAGAGGTGAAGAAT
TCGACCACCTGGACGGGACGAGGACGAAACAGC*AAAAAGAAAAATAAAAA*TTA
ATTAATCTTGGGCCC

L2bulge18tc
5’CTCGAGGCGATCGC*AAACAAACAAA*GCTGTCACCGGATGTGCTTTCCGGTCT
GATGAGTCCGTTGTCCAAAACATACCAGATTTCGATCTGGAGAGGTGAAGAA
TTCGACCACCTGGACGAGGACGGAGGACGAAACAGC*AAAAAGAAAAATAAAAA*
TTAATTAATCTTGGGCCC

L2bulgeOFF1
5’CTCGAGGCGATCGC*AAACAAACAAA*GCTGTCACCGGATGTGCTTTCCGGTCT
GATGAGTCCGTGTTGCTGATACCAGCATCGTCTTGATGCCCTTGGCAGCAGTG
GACGAGGACGAAACAGC*AAAAAGAAAAATAAAAATTTTTTTT*TTAATTAATCTTG
GGCCC

L2bulgeOFF1tc
55’CTCGAGGCGATCGC*AAACAAACAAA*GCTGTCACCGGATGTGCTTTCCGGTCT
GATGAGTCCGTTGTTGAGGAAAACATACCAGATTTCGATCTGGAGAGGTGAA
GAATTCGACCACCTCCTTATGGGAGGACGAAACAGC*AAAAAGAAAAATAAAAAT*
TTTTTTT TTAATTAA TCTT GGGCCC

AND: L2bulge8/L2bulge18tc
5’CTCGAGGCGATCGC*AAACAAACAAA*GCTGTCACCGGATGTGCTTTCCGGTCT
GATGAGTCCGTTGTCCATACCAGCATCGTCTTGATGCCCTTGGCAGGGACGG
GACGGAGGACGAAACAGC*AAAAAGAAAAATAAAAATTTTTTTT*TTAATCGC*AAAC*
*AAACAAA*GCTGTCACCGGATGTGCTTTCCGGTCTGATGAGTCCGTTGTCCAAA
ACATACCAGATTTCGATCTGGAGAGGTGAAGAATTCGACCACCTGGACGAGG
ACGGAGGACGAAACAGC*AAAAAGAAAAATAAAAA*TTAATTAATCTTGGGCCC

AND: L2bulge1/L2bulge1tc
5’CTCGAGGCGATCGC*AAACAAACAAA*GCTGTCACCGGATGTGCTTTCCGGTCT

GATGAGTCCGTGTCCATACCAGCATCGTCTTGATGCCCTTGGCAGGGACGGG
ACGAGGACGAAACAGC*AAAAAGAAAAATAAAAATTTTTTTT*TTAATCGC*AAACAAA*
*CAAA*GCTGTCACCGGATGTGCTTTCCGGTCTGATGAGTCCGTGTCCAAAACAT
ACCAGATTTCGATCTGGAGAGGTGAAGAATTCGACCACCTGGACGGGACGAG
GACGAAACAGC*AAAAAGAAAAATAAAAA*TTAATTAATCTTGGGCCC

NOR: L2bulgeOFF1/L2bulgeOFF1tc
5'CTCGAGGCGATCGC*AAACAAACAAA*GCTGTCACCGGATGTGCTTTCCGGTCT
GATGAGTCCGTGTTGCTGATACCAGCATCGTCTTGATGCCCTTGGCAGCAGTG
GACGAGGACGAAACAGC*AAAAAGAAAAATAAAAATTTTTTTT*TTAATCGC*AAACA*
*AACAAA*GCTGTCACCGGATGTGCTTTCCGGTCTGATGAGTCCGTTGTTGAGGA
AAACATACCAGATTTCGATCTGGAGAGGTGAAGAATTCGACCACCTCCTTAT
GGGAGGACGAAACAGC*AAAAAGAAAAATAAAAATTTTTTTT*TTAATTAATCTTGG
GCCC

Cell lines and cell culture maintenance. Parental HEK Flp-In 293 cells (Invitrogen) were cultured in D-MEM media (Gibco) supplemented with 10% FBS and 0.1 mg/ml zeocin (Invitrogen). Cells were seeded at 0.05 x 10^6 cells/ml and passaged regularly. HEK cells stably integrated with Flp-In constructs were cultured similarly, except the culture media were supplemented with 0.1 mg/ml hygromycin B (Invitrogen) and no zeocin.

Transient transfection and fluorescence quantification. All transient transfections were performed using FuGENE 6 (Roche) following the manufacturer's protocols. Cells were seeded at 0.05 x 10^6 cells/ml, 500 µl/well, in 24-well plates 24 hours prior to transfection. Each transfection sample received 250 ng of plasmid DNA at a FuGENE:DNA ratio of 4:1. Fluorescence data were obtained 48 hours after transfection using a Quanta Cell Lab Flow Cytometer equipped with a 488-nm laser (Beckman Coulter). Viability was gated by side scatter and electronic volume, and viable cells were further gated for dsRed-Express expression, which served as a transfection control. EGFP

and dsRed-Express were measured through 525/30-nm band-pass and 610-nm long-pass filters, respectively. Flow cytometry data were analyzed using FlowJo (Tree Star). Geometric mean fluorescence values were normalized to those of the inactive ribozyme control cultured at the same input concentration of the appropriate ligand molecule. Mean values from triplicate samples were reported with an error range of ± 1 standard deviation.

Stable HEK Flp-In cell line generation. Six wells in a six-well plate containing 2 ml/well of parental HEK Flp-In 293 cells seeded at 0.05 x 10^6 cells/ml were transfected with FuGENE 6 and cultured in media without antibiotics for 48 hours. Cultures were then passaged into media containing 0.2 mg/ml hygromycin B. Cells were continuously cultured in hygromycin-containing media without passaging for 9 more days. Colonies were pooled together into one well of a six-well plate on day 11 after transfection. Cells were passaged 2 days after pooling and passaged regularly thereafter into media containing 0.1 mg/ml hygromycin B. Construct integration was verified by EGFP detection through fluorescence microscopy and flow cytometry.

Theophylline response assay for stable HEK Flp-In cell lines. Stably integrated HEK cell lines as well as the parental HEK Flp-In 293 cell line were each used to seed 30 wells in 24-well plates with 500 μl of culture per well. Wells were seeded at different densities to allow assaying at different time points through the 5-day time-course study. Twelve wells were seeded at 0.1 x 10^6 cells/ml, another 12 wells were seeded at 0.05 x 10^6 cells/ml, and the remaining 6 wells were seeded at 0.02 x 10^6 cells/ml. At each seeding

density, half of the wells were fed with 250 μM final concentration of theophylline dissolved in water and sterile-filtered with a 0.22 μM syringe filter. Every 24 hours after seeding, 6 wells (3 with and 3 without theophylline) were analyzed by flow cytometery, starting with the wells seeded at the highest cell density. Data analyses were performed as described for transient transfections.

Acknowledgments

We thank S. Culler for generating the HEK Flp-In 293 stable cell lines. This work was supported by the City of Hope's National Cancer Institute–Cancer Center Support Grant, the National Science Foundation (fellowship to Y.Y.C.), the Alfred P. Sloan Foundation (fellowship to C.D.S.), and the National Institutes of Health (grant to C.D.S., RC1GM091298).

References

1. Win, M.N., Liang, J.C. & Smolke, C.D. Frameworks for programming biological function through RNA parts and devices. *Chem Biol* **16**, 298-310 (2009).
2. Isaacs, F.J., Dwyer, D.J. & Collins, J.J. RNA synthetic biology. *Nat Biotechnol* **24**, 545-554 (2006).
3. Yen, L. et al. Exogenous control of mammalian gene expression through modulation of RNA self-cleavage. *Nature* **431**, 471-476 (2004).
4. Yen, L., Magnier, M., Weissleder, R., Stockwell, B.R. & Mulligan, R.C. Identification of inhibitors of ribozyme self-cleavage in mammalian cells via high-throughput screening of chemical libraries. *RNA* **12**, 797-806 (2006).

5. Win, M.N. & Smolke, C.D. A modular and extensible RNA-based gene-regulatory platform for engineering cellular function. *Proc Natl Acad Sci U S A* **104**, 14283-14288 (2007).

6. Win, M.N. & Smolke, C.D. Higher-order cellular information processing with synthetic RNA devices. *Science* **322**, 456-460 (2008).

7. Khvorova, A., Lescoute, A., Westhof, E. & Jayasena, S.D. Sequence elements outside the hammerhead ribozyme catalytic core enable intracellular activity. *Nat Struct Biol* **10**, 708-712 (2003).

8. Mathews, D.H. et al. Incorporating chemical modification constraints into a dynamic programming algorithm for prediction of RNA secondary structure. *Proc Natl Acad Sci U S A* **101**, 7287-7292 (2004).

9. Wieland, M. & Hartig, J.S. Artificial riboswitches: synthetic mRNA-based regulators of gene expression. *Chembiochem* **9**, 1873-1878 (2008).

10. An, C.I., Trinh, V.B. & Yokobayashi, Y. Artificial control of gene expression in mammalian cells by modulating RNA interference through aptamer-small molecule interaction. *RNA* **12**, 710-716 (2006).

11. Beisel, C.L., Bayer, T.S., Hoff, K.G. & Smolke, C.D. Model-guided design of ligand-regulated RNAi for programmable control of gene expression. *Mol Syst Biol* **4**, 224 (2008).

12. Auslander, S., Ketzer, P. & Hartig, J.S. A ligand-dependent hammerhead ribozyme switch for controlling mammalian gene expression. *Mol Biosyst* **6**, 807-814.

13. Wieland, M. & Hartig, J.S. Improved aptazyme design and in vivo screening enable riboswitching in bacteria. *Angew Chem Int Ed Engl* **47**, 2604-2607 (2008).

14. Sambrook, J. & Russell, D.W. Molecular Cloning: A Laboratory Manual, Edn. 3. (Cold Spring Harbor Press, Cold Spring Harbor; 2001).

Chapter 3

T-Cell Proliferation Control with Ribozyme-Based Regulatory Systems

Adapted with permission from Chen, Y.Y., Jensen, M.C., & Smolke, C.D. Genetic control of mammalian T-cell proliferation with synthetic RNA regulatory systems. *Proc Natl Acad Sci USA* **107**, 8531-8536 (2010).

Abstract

RNA molecules perform diverse regulatory functions in natural biological systems, and numerous synthetic RNA-based control devices that integrate sensing and gene-regulatory functions have been demonstrated, predominantly in bacteria and yeast. Despite potential advantages of RNA-based genetic control strategies in clinical applications, there has been limited success in extending engineered RNA devices to mammalian gene expression control and no example of their application to functional response regulation in mammalian systems. Here, we describe a synthetic RNA-based regulatory system and its application in advancing cellular therapies by linking rationally designed, drug-responsive, ribozyme-based regulatory devices to the proliferative cytokines interleukin-2 (IL-2) and interleukin-15 (IL-15) to control mouse T-cell proliferation. We report the development of regulatory devices responsive to the small-molecule drugs theophylline and tetracycline, and demonstrate the ability of the regulatory devices to reversibly modulate target-gene expression levels within 12 hours of drug addition. We further demonstrate the ability of our synthetic controllers to effectively modulate *in vivo* T-cell expansion, achieving a 40% increase in T-cell growth rate in response to theophylline administration. Our RNA-based regulatory system exhibits unique properties critical for translation to therapeutic applications, including adaptability to diverse ligand inputs and regulatory targets, tunable regulatory stringency, and rapid response to input availability. By providing tight gene expression control with customizable ligand inputs, RNA-based regulatory systems can greatly improve cellular therapies and advance broad applications in health and medicine.

Introduction

The ability to control functional responses in mammalian cells with customizable and compact regulatory systems *in vivo* addresses a critical need in diverse clinical applications, particularly in cellular therapies[1, 2]. As an example, adoptive T-cell therapy seeks to harness the precision and efficacy of the immune system against diseases that escape the body's natural surveillance. The adoptive transfer of antigen-specific T cells can reconstitute immunity to viruses and mediate tumor regression[3, 4], and early-stage clinical trials have demonstrated the potential of engineered T cells against cancer[5]. T cells engineered to express tumor-specific T-cell antigen receptors can achieve highly refined target recognition[6, 7], thus minimizing toxic off-target effects associated with conventional chemotherapy. However, considerable research has shown that the persistence of transferred T cells *in vivo* is both central to therapeutic success and elusive to current technology[8, 9]. The efficacy of adoptive immunotherapy in humans is often limited by the failure of transferred T cells to survive in the host[10-12].

Clonal expansion of T cells is a critical component of T-cell activation mediated by cytokines such as interleukin-2 (IL-2) and interleukin-15 (IL-15), which activate JAK-STAT signaling pathways and lead to the expression of genes involved in growth modulation[13]. Sustaining the survival and proliferation of T cells following adoptive transfer is challenging due to the limited availability of homeostatic cytokines (IL-15/IL-7) and stimulatory antigen presenting cells. State-of-the-art strategies for improving the persistence of adoptively transferred lymphocytes require that patients be subjected to myeloablative total body irradiation/chemotherapy and toxic levels of IL-2[14]. Alternative strategies based on the unregulated expression of growth-related genes pose the risk of

uncontrolled lymphoproliferation and leukemic transformation[8]. Thus, the ability to integrate growth stimulatory gene expression with tightly controlled regulatory systems has the potential to greatly improve the safety and efficacy of adoptive T-cell therapy.

As described in Chapter 1, numerous synthetic RNA-based regulatory systems have been developed. However, despite recent advances in the design of RNA devices that process and transmit specified molecular inputs to regulated gene expression events[15, 16], the absence of successful adaptations of these earlier genetic devices to the regulation of functional responses in mammalian cells highlights remaining difficulties in translating designs that regulate reporter gene expression to functional control. Here, we report a synthetic, small-molecule-responsive RNA-based gene regulatory system in mammalian cells and demonstrate its application in advancing cell-based therapies through the control of cell-fate decisions. We develop a genetic strategy for effectively controlling T-cell expansion based on drug-responsive RNA regulators that exert tight control over key upstream signaling molecules in the proliferation pathway. Our work demonstrates an RNA-based regulatory system that exhibits unique properties critical for translation to therapeutic applications, including adaptability to diverse input molecules and genetic targets, tunable regulatory stringency, and rapid input response.

Results

An RNA-Based System Enables Gene Expression and Viability Control in T Cells. We developed an RNA-based regulatory system for mammalian T-cell proliferation based on a platform for assembling RNA devices from modular sensor (aptamer) and gene-regulatory (hammerhead ribozyme) components. The activity of this ribozyme

switch platform had been shown in the microorganism *Saccharomyces cerevisiae*[17, 18], and its ability to regulate gene expression in mammalian cells has been confirmed in human embryonic kidney (HEK) cells (see Chapter 2). However, the ability of ribozyme switch devices to regulate functional outputs in mammalian cells remains to be demonstrated.

Cytokines are potent growth-stimulatory molecules whose effects on cell growth are amplified through the JAK-STAT signaling pathway (Figure 3.1A). The ability to regulate upstream pathway molecules and take advantage of signal amplification through an endogenous pathway toward downstream functional responses is an important design strategy supported by our RNA regulatory system. We developed a cell-intrinsic control system for cytokine production based on ribozyme ON switches, which are RNA devices that convert a small-molecule input to an increased gene expression output (Figure 3.1B). The system design ensures suppression of cell growth as a default state and induction of cell proliferation only in the presence of an administered small-molecule drug input. In this system, the ribozyme-based device is placed in the 3' untranslated region (UTR) of a target transgene encoding a proliferative cytokine, where self-cleavage by the ribozyme results in rapid degradation of the target transcript and decreased cytokine production. The ribozyme device is designed to adopt at least two conformations (input-unbound and input-bound) associated with either a ribozyme-active or -inactive state. The presence of drug input stabilizes the input-bound, ribozyme-inactive conformation, thereby preserving transcript integrity and upregulating cytokine production, resulting in autocrine cell growth. The absence of drug input stabilizes the ribozyme-active

conformation, resulting in transcript degradation, reduced cytokine production, and diminished cell growth.

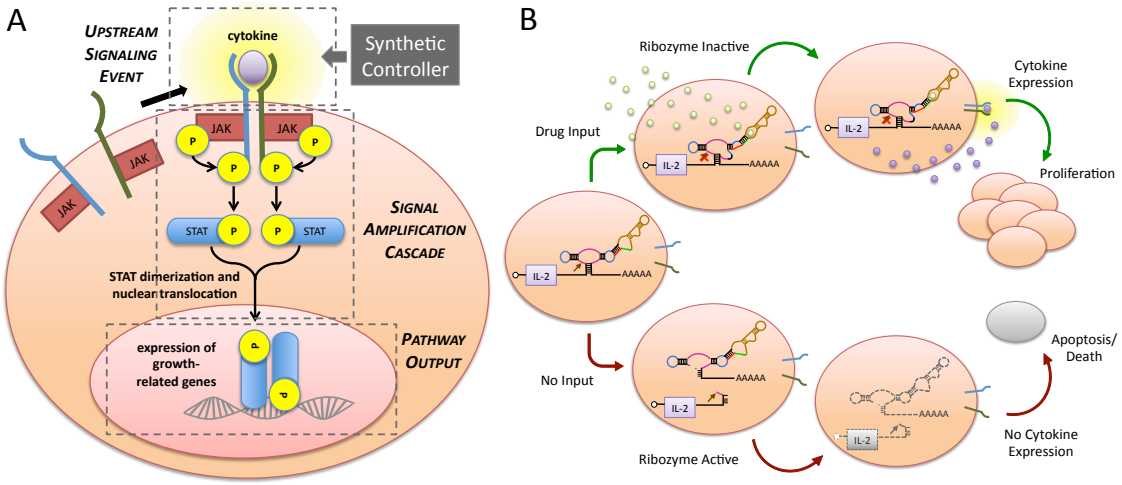

Figure 3.1. An engineered T-cell proliferation regulatory system utilizing a synthetic RNA device to achieve drug-mediated modulation of cell signaling and proliferation. (A) The common γ-chain T-cell proliferation pathway and integration of a synthetic controller targeted to the upstream signaling events. (B) An engineered T-cell proliferation regulatory system based on the programmable drug-mediated regulation of cytokine expression from a synthetic ribozyme switch. Ribozyme color scheme is as described in Ref. 17.

As a model system, a fusion transgene encoding a proliferative cytokine (IL-2) and a quantifiable protein marker (EGFP) served as the regulatory target to permit simultaneous quantification of the regulatory system's performance at the levels of direct gene expression (fluorescence) and downstream pathway output (viability) (Figure 3.2A). The cytokine and reporter proteins were linked through a self-cleaving T2A peptide (see Supplementary Text 3.1 for sequence) to ensure that the ribozyme switch activity was equally effective on the linked target genes but that the proteins folded and functioned as independent molecules. Three theophylline-responsive ribozyme switches (L2bulge1, 8, and 9; see Chapter 2 Materials and Methods for sequences), which had been tuned through sequence modifications to exhibit different regulatory response properties[17], were inserted into the 3' UTR of the *egfp-t2a-il2* fusion gene. Instead of the more commonly

used cytomegalovirus (CMV) immediate early promoter, which has been shown by previous reports[19-21] and our own studies (see Supplementary Text 3.2) to be prone to suppression and silencing upon genomic integration, the elongation factor 1 alpha (EF1α) promoter was used to drive the expression of the target transgene and ribozyme switches. Plasmids incorporating this regulatory system were transiently transfected into the CTLL-2 mouse T-cell line which, like primary human T cells, is dependent on common γ-chain signaling for survival and proliferation[22]. Each of the ribozyme switches resulted in input-responsive regulation over cell viability and fluorescence (Figure 3.2B, Supplementary Figure 3.1A; see Supplementary Text 3.3 for discussion on controls and normalization methods), confirming the prescribed function of these devices in mammalian cells. The ribozyme-based regulatory systems provided titratable response over a range of input concentrations (Figure 3.2C, Supplementary Figure 3.1B), demonstrating the ability to adjust expression levels based on input availability.

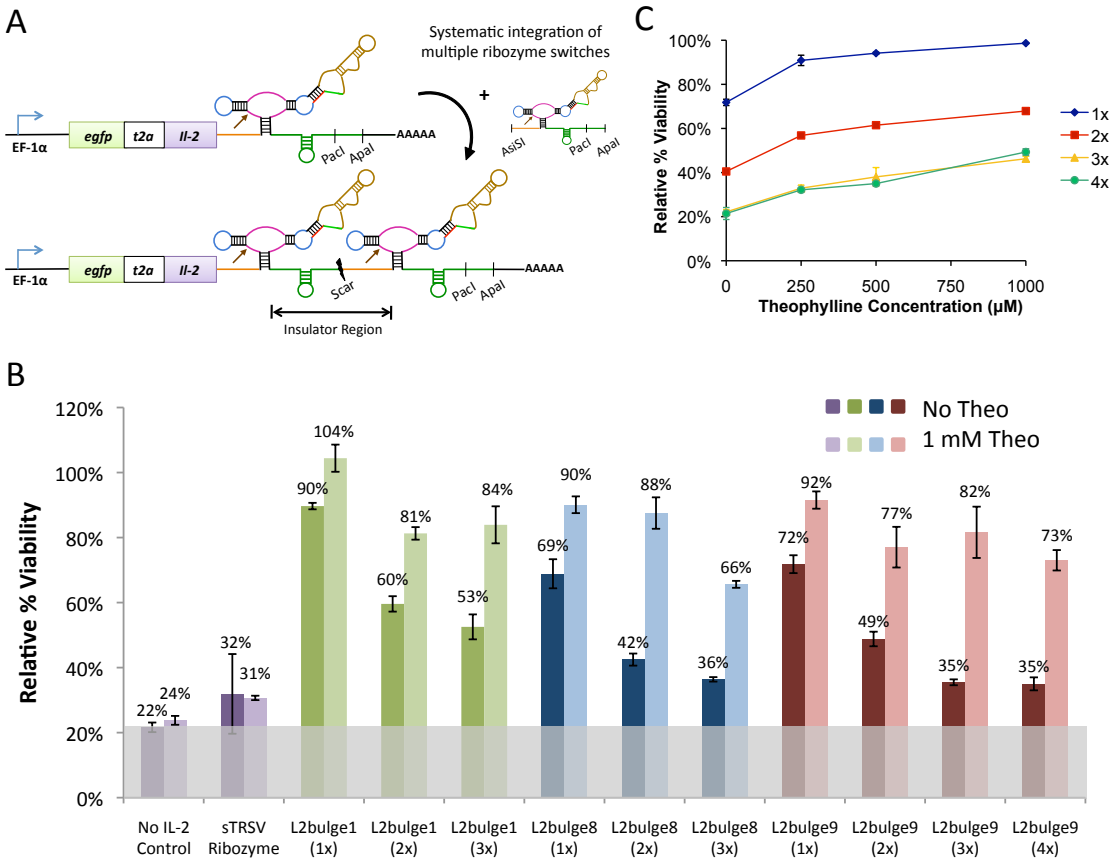

Figure 3.2. Modularly constructed ribozyme switches exhibit tunable, drug-mediated regulation of gene expression and cell growth in mammalian T cells. (A) A modular insertion strategy allows the implementation of multiple copies of ribozyme switches to tune regulatory stringency. Spacer sequences (orange, green) provide structural insulation and maintain the functional independence of each switch. (B) Ribozyme switches provide tunable, small-molecule-mediated regulatory systems. Cell viability levels are reported for constructs encoding theophylline-responsive switches (L2bulge1, 8, 9) in one (1x), two (2x), three (3x), and four (4x) copies through transient transfections in CTLL-2 cells grown in 0 and 1 mM theophylline. No IL-2 Control, construct not encoding a proliferative cytokine; sTRSV Ribozyme, construct encoding a non-switch hammerhead ribozyme. Gray bar indicates background viability level of cells in the absence of cytokine. (C) Ribozyme switches provide titratable regulatory systems. Cell viability levels are reported for the L2bulge9 regulatory systems at various theophylline concentrations. All values were normalized to those of controls expressing the appropriate transgene regulated by an inactive ribozyme and cultured at corresponding theophylline concentrations. Reported values are mean ± s.d. from at least two replicate samples.

A General Strategy for Tuning the Dynamic Range of Ribozyme Switches Allows for Modulation of T-Cell Proliferation Response. The potency of the genetic targets in our T-cell regulatory system requires stringent control over basal cytokine expression levels, such that in the absence of input the engineered T cells exhibit proliferation levels

similar to cells growing in the absence of cytokine. To engineer a more stringent regulatory system, we implemented a second tuning strategy based on linking multiple copies of the ribozyme switches in the 3' UTR of the transgene. As demonstrated by studies performed in HEK 293 cells and described in Chapter 2, multiple-copy expression is expected to lower the basal expression level since only one of the switches needs to be in a ribozyme-active state to cleave and inactivate the transcript. We developed a construction strategy for sequentially inserting ribozyme switches in the 3' UTR of the transgene and insulated the switches through spacer sequences designed to maintain the structural integrity and functional independence of each switch (Figure 3.2A, see Chapter 2 Materials and Methods).

Characterization of the multiple-copy switch systems indicated that this tuning strategy effectively decreased basal expression levels (Figure 3.2B, Supplementary Figure 3.1A) and that the titratable response of the system was maintained (Figure 3.2C, Supplementary Figure 3.1B). Stringent knockdown was achieved with three and four copies of the tightest switch (L2bulge9, Figure 3.2B), which resulted in viability levels comparable to cells transfected with no cytokine or with the fully active, non-switch ribozyme (No IL-2 Control and sTRSV Ribozyme, respectively). Notably, the regulatory performance of the four-copy switch system was similar to that of the three-copy system (Figure 3.2B), indicating that three copies of the tightest switch were sufficient to approach the minimum possible viability levels. The data underscore the non-linear relationship between direct gene expression and functional pathway outputs from the system. Whereas absolute changes in gene expression (fluorescence) in response to drug input remain similar for constructs with varying copies of a ribozyme switch

(Supplementary Figure 3.1A), the absolute changes in pathway output (viability) increased substantially with ribozyme copy number (Figure 3.2B).

Ribozyme Switches Can Be Programmed to Respond to Alternative Drug Molecules. The ON-state expression levels of drug-responsive RNA regulatory systems can be limited by the toxicity and cell permeability of the input molecule[23]. However, an important property of the ribozyme-based regulatory system is that its component functions are modular and thus amenable to changes that support customization for diverse applications, such as reprogramming input responsiveness toward clinically usable pharmaceuticals. To verify this critical property of our prototype T-cell proliferation control system, we replaced the theophylline aptamer[24] with the tetracycline aptamer[25] to construct a tetracycline-responsive switch (L2bulge18tc, Figure 3.3A). *In vitro* assays indicated tetracycline-responsive ON switch activity in CTLL-2 cells (Figure 3.3B). The tetracycline-responsive systems demonstrated lower basal expression levels and increased dynamic ranges in response to lower input concentrations relative to the theophylline-responsive systems. The improved performance can be attributed to several factors, including structural differences between the aptamers resulting in less disruption from the tetracycline aptamer to the ribozyme's activity, higher affinity of the tetracycline aptamer for its ligand[26], and increased membrane permeability of tetracycline relative to theophylline resulting in a higher intracellular concentration of tetracycline under similar extracellular concentrations. Although tetracycline is not a clinically applicable drug input, the tetracycline switch system demonstrates the ability to improve regulatory stringency by incorporating aptamer sequences that cause minimal obstruction

to ribozyme cleavage in the absence of ligand input. Furthermore, the tetracycline switches highlight the ability to significantly increase the switch dynamic range by utilizing aptamers with higher binding affinities and applying input molecules that can be administered to higher intracellular concentrations.

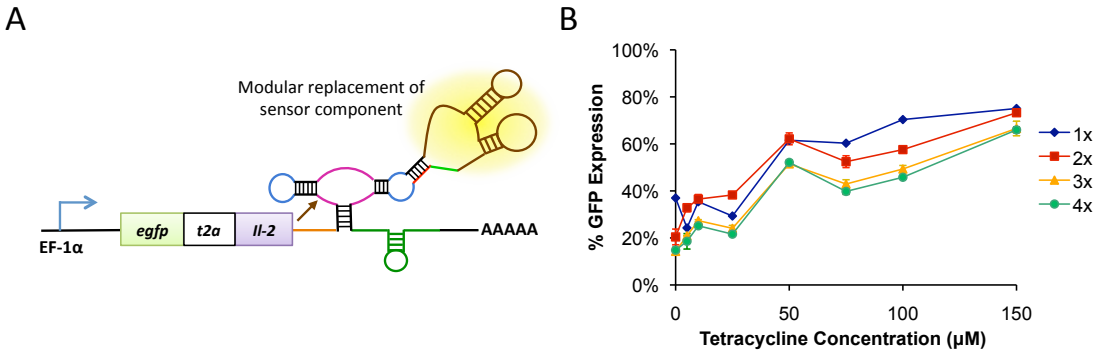

Figure 3.3. Ribozyme switches can be programmed to respond to alternative drug molecules. (A) Direct replacement of the sensor component allows tailoring of the input-responsiveness of the RNA-based regulatory system. (B) Reprogrammed device (L2bulge18tc) demonstrates titratable, tetracycline-responsive gene regulation. Values are reported as described in Figure 3.2, except control samples were cultured at corresponding tetracycline concentrations.

A Clinically Relevant System Controls T-Cell Proliferation Based on Drug-Modulated Regulation of IL-15 Production. Although IL-2 plays a critical role in the stimulation of activated T cells, it is also involved in activation-induced cell death (AICD) and the establishment of peripheral tolerance. Several studies have indicated that an alternative γ-chain cytokine, IL-15, provides potent homeostatic T-cell survival/proliferative signals, inhibits IL-2-mediated AICD, and may be superior to IL-2 in immunotherapy applications[27, 28]. Recently, IL-15 has been shown to function in establishing the long-term persistence of adoptively transferred central memory T (T_{CM}) cells in primates, suggesting significant potential in T-cell therapy for cancer[29]. To develop a more clinically relevant regulatory system, we utilized the modularity of the

ribozyme switch platform and replaced the *egfp-t2a-il2* transgene with a trifunctional fusion transgene (*cd19-tk-t2a-il15*) encoding IL-15, mutant HSV-1 thymidine kinase (ser39TK, a protein marker that can act as a PET reporter and as a suicide protein in the presence of the drug ganciclovir, providing imaging and safety kill-switch functionalities for downstream clinical implementations), and CD19 (a quantifiable protein marker amenable to FACS- and immunomagnetic-based selections). The alternative transgene was placed directly into the theophylline-responsive switch systems based on L2bulge9 (Figure 3.4A). Ribozyme switch systems with the altered target transgene exhibited ON-switch control over cell viability and proliferation in transient transfection experiments (Figure 3.4B), confirming modular coupling between the target transgene and the regulatory device. Samples expressing IL-15 showed higher viability levels compared to those expressing IL-2 with the corresponding switch systems (Figures 3.2C, 3.4B), suggesting IL-15 may be a more potent survival/proliferative cytokine and can better amplify the signal response. Therefore, under a low basal expression level, a small increase in IL-15 expression has the potential to significantly elevate the T-cell proliferation level.

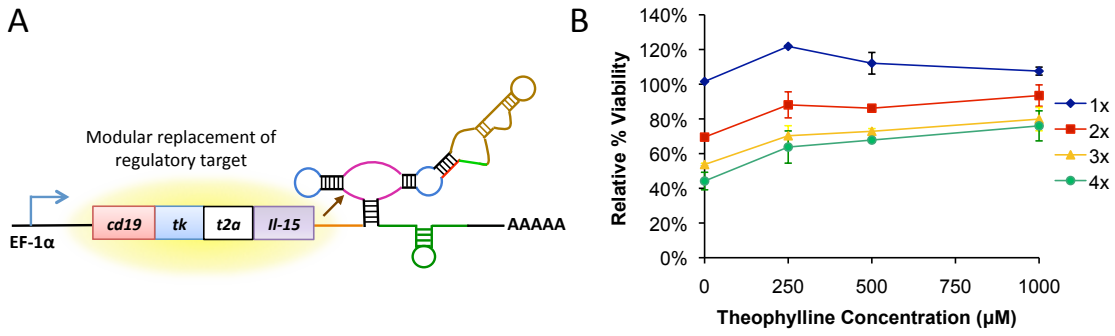

Figure 3.4. Ribozyme switches can be programmed to regulate alternative gene targets. (A) Direct replacement of the target gene allows tailoring of the output of the RNA-based regulatory system. (B) Reprogrammed system with the alternative regulatory target *cd19-tk-t2a-il15* achieves enhanced survival response compared to IL-2-based systems. Values are reported as described in Figure 3.2.

Ribozyme Switches Enable Long-Term, Dynamic Control over Gene Expression. To characterize long-term behavior of the regulatory system, we generated stable T-cell lines expressing the theophylline-responsive ribozyme switch systems. We generated a CTLL-2 cell line (CffLuc) that stably expressed the firefly luciferase (*ffluc*) gene to enable biophotonic imaging of cell populations *in vivo*. We subsequently integrated T-cell proliferation regulatory systems based on one or three copies of L2bulge9 into CffLuc. Stable integrants were initially sorted based on CD19 expression. At the bulk population level, cells stably expressing three copies of the ribozyme switch had a lower basal level and larger switch dynamic range in response to theophylline addition compared to cells stably expressing one copy of the ribozyme switch, consistent with transient transfection results (Supplementary Figure 3.2). We further refined the sorted population by alternating treatment with ganciclovir and IL-2 or with theophylline and no IL-2 (Figure 3.5) to enrich for clones with low basal expression levels and sufficiently high ON-state expression levels to sustain cell survival, respectively. We generated clonal cell lines by a final sorting step for CD19 positive cells in the presence of theophylline.

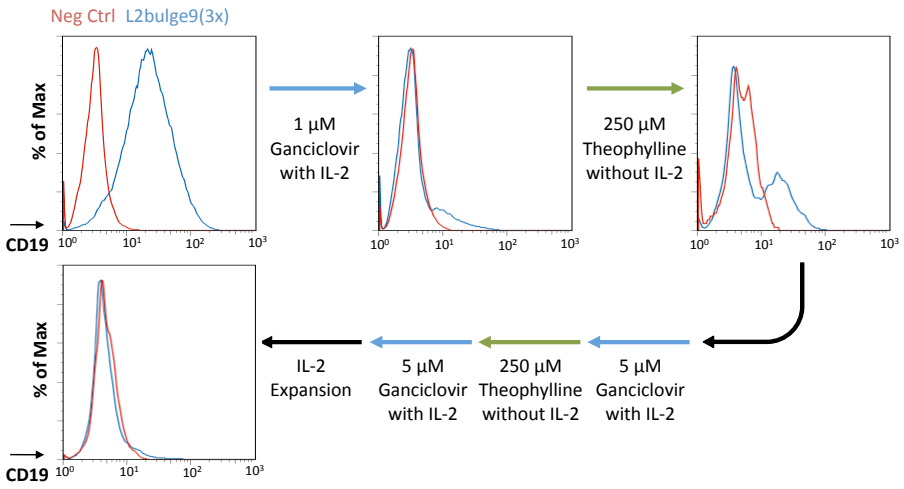

Figure 3.5. The generation of T-cell lines stably expressing ribozyme switch systems through alternate cycles of negative and positive selections. CTLL-2 cells stably expressing a luciferase reporter (CffLuc) were transfected with linearized plasmids encoding ribozyme switch systems based on L2bulge9. Stable integrants were initially sorted for CD19 expression and subsequently subjected to alternate cycles of negative and positive growth selection with ganciclovir and theophylline, respectively. Gene expression levels were monitored by staining with PE-conjugated CD19 antibodies; blue, bulk stable *cd19-tk-t2a-il15*-L2bulge9(3x) cell line; red, CffLuc cell line.

Growth behavior of individual clones was characterized by culturing under various theophylline concentrations. Results indicate that the T-cell proliferation regulatory system retained functionality over long time periods when stably integrated, and that theophylline effectively replaced IL-2 as the trigger for cell proliferation (Figure 3.6A). Fifteen of the sixteen clones examined showed substantial theophylline-responsive increase in cell growth (Supplementary Figure 3.3), supporting that the growth modulation effect is specific to the introduced regulatory system.

Additional assays on a clonal cell line harboring three copies of L2bulge9 (clone 1264-48) were performed to verify the mechanism of growth regulation and examine the dynamic behavior of the regulatory system to variations in theophylline availability. Cell cultures were grown for one week in the presence of 500 µM theophylline and continued for a second week in the absence of theophylline. Theophylline was reintroduced for

another four days at the end of the study. Compared to the identical clone continuously cultured in the absence of theophylline, the cell population exhibited elevated CD19 protein levels within 24 hours of theophylline addition and levels remained elevated throughout the period of theophylline treatment (Figure 3.6B). CD19 expression returned to basal levels within 48 hours of theophylline removal. The theophylline-responsive increase in CD19 expression was repeated upon reintroduction of theophylline to culture media. To determine a more precise time scale at which gene expression elevation occurs, the time course study was repeated with multiple time points taken within 48 hours of theophylline addition. Results indicate that the ribozyme-based system generates a regulatory response at the protein level within 12 hours of drug input addition (Figure 3.6C). IL-15 expression patterns were verified at the transcript level through qRT-PCR (Supplementary Figure 3.4A). Interestingly, the IL-15 protein levels as measured by intracellular antibody staining showed no response to drug input and no difference between cell lines expressing the inactive ribozyme control and the L2bulge9 switch construct despite clear differences in IL-15 mRNA and CD19 protein levels (Supplementary Figure 3.4B). Since CTLL-2 cells continuously export IL-15 in high flux, the signals detected by intracellular staining may indicate the steady-state protein level and thus show no difference among the cell lines and conditions tested. Finally, western blot analysis of phosphorylated STAT5 levels verified activation of the IL-15 receptor-signaling cascade in the presence of theophylline (Supplementary Figure 3.4C). These results highlight the ability of the ribozyme switch system to quickly, effectively, and robustly switch gene expression on and off in response to drug input.

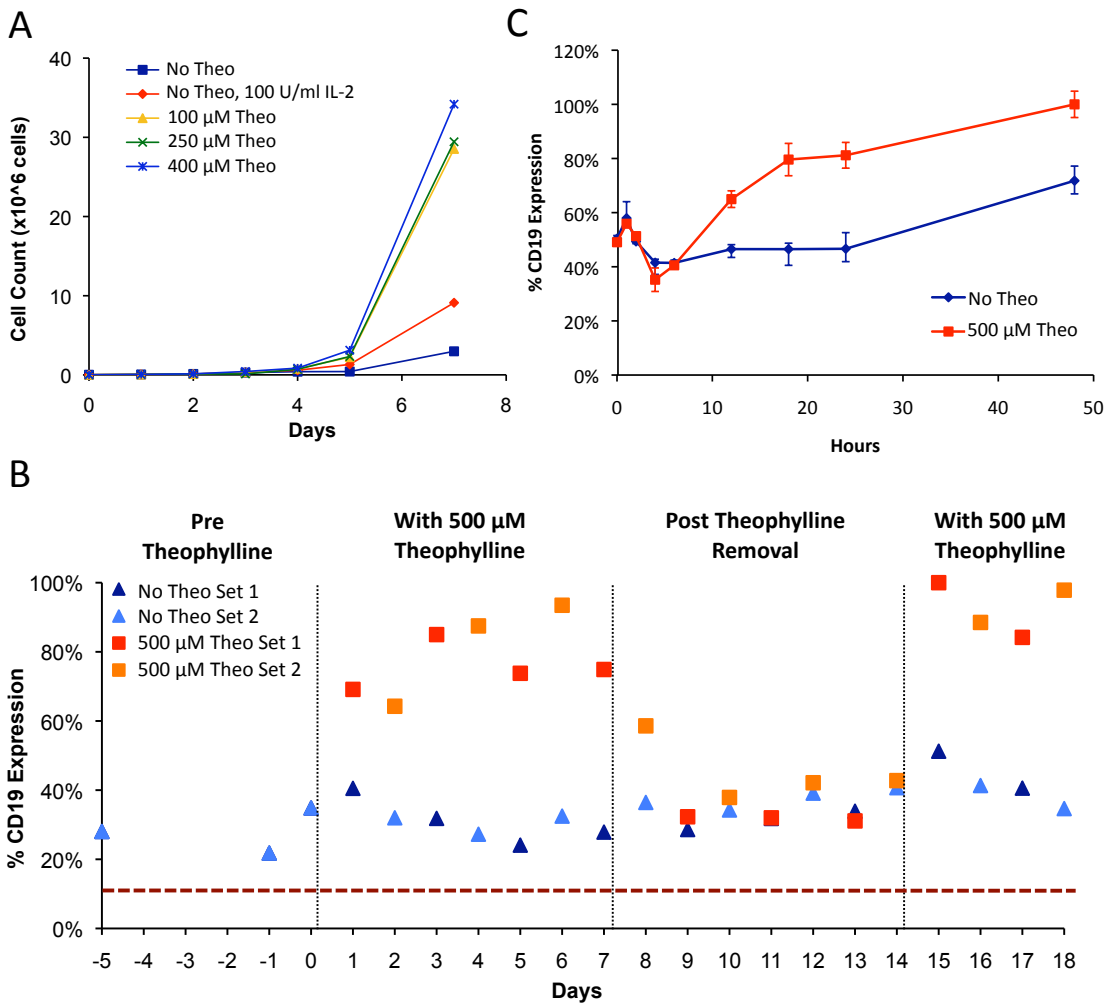

Figure 3.6. T cells stably expressing ribozyme switch systems exhibit drug-mediated regulation of growth over extended time periods *in vitro*. (A) Clonal cell lines stably expressing the ribozyme switch system exhibit drug-mediated growth. Cell growth was monitored by counting viable cells, and data for a representative clone (1264-48, expressing *cd19-tk-t2a-il15*-L2bulge9(3x)) are shown. (B) The ribozyme switch system regulates gene expression in response to changes in input concentrations. Duplicate sets of the clonal cell line 1264-48 were cultured in the presence (red and orange) and absence (light blue and dark blue) of theophylline over 18 days. Expression levels were monitored by staining with PE-conjugated CD19 antibodies, and values were normalized to those from the inactive ribozyme control. The highest expression level was set to 100%. Red dashed line indicates background-staining level of a cell line without a CD19 construct. (C) The ribozyme switch system generates regulatory response within 12 hours of input addition. Duplicate cultures were maintained in the presence (red) and absence (blue) of theophylline for 48 hours. Fluorescence values were obtained and normalized as in (B).

Ribozyme Switches Enable Drug-Modulated Control over T-Cell Proliferation *In Vivo*. To verify *in vivo* functionality of the T-cell proliferation regulatory system, we examined several clonal cell lines for theophylline-dependent growth in mice. Select

clones were encased in a hydrogel matrix that contained either 0 or 500 μM theophylline and injected into the flanks of NOD/SCID-$\gamma_c^{-/-}$ mice. Cell lines lacking the transgene regulatory system or stably expressing the inactive ribozyme construct served as negative and positive controls, respectively. *In vivo* T-cell expansion was not observed from clones lacking cytokine expression (No IL-15 control, Figure 3.7A), demonstrating the need for cytokine expression in sustaining cell growth. Uncontrolled T-cell proliferation was observed in the absence of a functional ribozyme-based regulatory device regardless of theophylline availability (Inactive Rz control, Figure 3.7A). In contrast, the clonal cell line 1264-48, which harbors three copies of L2bulge9, showed a significantly stronger reporter signal at the conclusion of the 14-day study when injected with 500 μM theophylline compared to the same clone injected without theophylline (L2bulge9(3x), Figure 3.7A). Growth rate calculations based on flux measurements over the 14-day period indicated a 32% increase in *in vivo* growth rate in the presence of 500 μM theophylline, leading to a 14-fold increase in luciferase signal (Figure 3.7B, Supplementary Figure 3.5). The *in vivo* study was repeated for clone 1264-48 with replicates, with the inactive ribozyme serving as the positive control. Flux measurements over a 9-day period indicated an average of 40% increase in the growth rate of clone 1264-48 in the presence of 500 μM theophylline (n_1 = 4, n_2 = 6, P = 0.038 by Mann-Whitney U test). In contrast, the positive control did not show statistically significant changes in growth rate (n_1 = 6, n_2 = 6, P = 0.394; Figure 3.7C, Supplementary Figure 3.6), indicating that the input-responsive growth behavior observed in clone 1264-48 was not due to non-specific effects of theophylline.

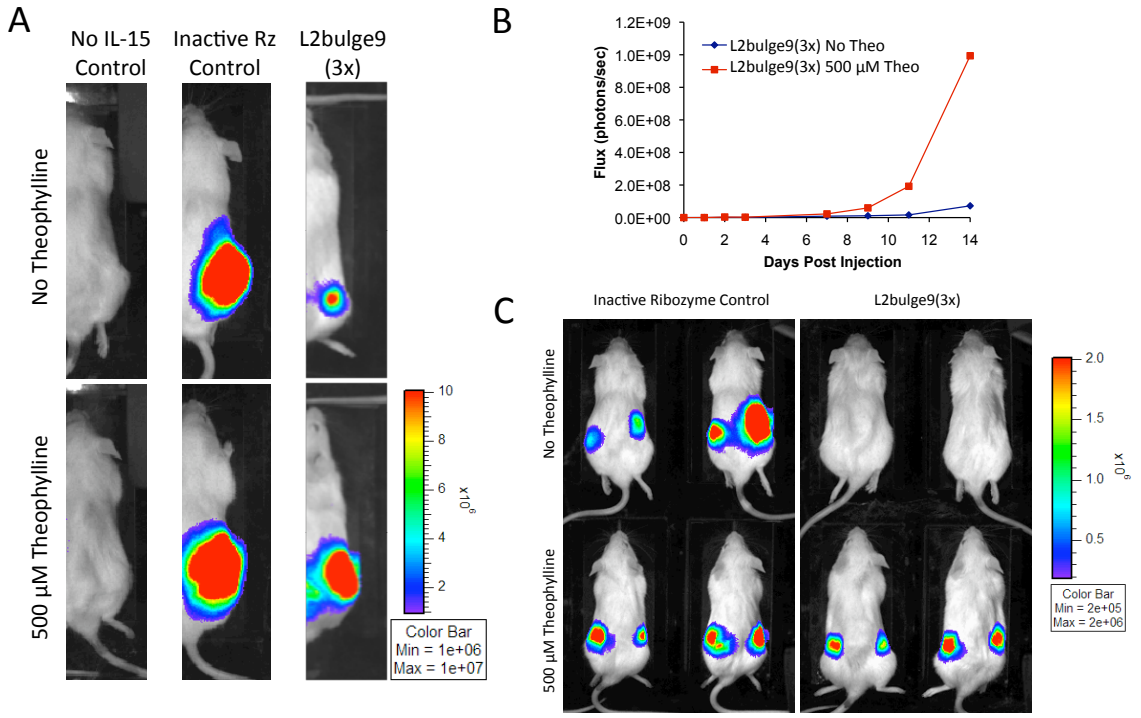

Figure 3.7. T cells stably expressing the ribozyme switch systems exhibit drug-mediated regulation of growth over extended time periods *in vivo*. (A) Both cytokine expression and functional ribozyme switches are required for effective regulation of T-cell proliferation. Images are shown for day 14 after injection of the negative control (No IL-15 Control, CffLuc), positive control (Inactive Rz Control, stable cell line expressing inactive ribozyme), and stable cell line expressing the ribozyme switch system (L2bulge9(3x), clone 1264-48) in the presence and absence of 500 µM theophylline. (B) Total luciferase signal flux over 14 days after injection of T cells is reported from the negative control (CffLuc) and clone 1264-48 (L2bulge9(3x)). (C) The ribozyme switch system demonstrates robust and reproducible small-molecule-mediated control over T-cell proliferation *in vivo*. Images are shown for day 4 after injection of the positive control and clone 1264-48. Identical clones were injected into the two flanks of each mouse in the presence or absence of 500 µM theophylline.

Discussion

Achieving robust, controlled, long-term persistence of transfused T cells *in vivo* is a critical objective in adoptive immunotherapy, where efficacy depends on prolonged T-cell survival and safety demands stringent growth regulation. The T-cell proliferation challenge highlights a broader need for programmable regulatory systems that can modulate functional responses in mammalian cells. While numerous gene-regulatory systems have been developed, successful translation to clinical settings has been limited.

For example, synthetic inducible promoters rely on various transcriptional regulatory proteins, thus requiring multiple vectors and transgene expression systems. However, the stable expression of multiple transgenes in primary cell lines presents a significant challenge. In addition, concerns for potential immunogenicity of heterologous proteins limits the use of inducible promoters in clinical settings. Finally, the input specificity and regulatory dynamic range of such protein-based systems are relatively difficult to reprogram, thus limiting the flexibility and broader application of these system.

An alternative technology that has been pursued in the context of hematopoietic cell growth regulation is based on chemical inducers of dimerization (CIDs), which induce dimerization of pathway components fused to CID-binding domains[30-32]. However, studies conducted with CID-based systems have required lethally irradiated animal subjects to allow the expansion of transfused T cells with the assistance of homeostatic proliferation. In addition, several properties of the CID-based system hinder its broader application. For example, the system is limited to the regulation of homodimerization events, a mechanism that does not apply to many pathways of interest, including the common γ-chain signaling pathway central to T-cell persistence. The CID-based system is also fixed with respect to the input molecule, which is not available as a pharmaceutical drug.

Our synthetic, drug-responsive RNA-based regulatory system features properties that address critical limitations in existing genetic control strategies for clinical applications, including encapsulation within a compact, RNA-only platform (to avoid the use of immunogenic protein-based components) and allowing direct replacement of sensor and target transgene components (to tailor the technology to diverse applications).

This work presents the successful translation of an RNA device to the regulation of a functional response in mammalian cells. The unique capability to program the regulatory device's response properties was key to the effective transition from reporter gene expression regulation to functional control. By developing a rational tuning strategy for the regulatory stringency of our control system and integrating our synthetic controller with upstream signaling components, we were able to substantially enhance control over the functional system response. Furthermore, the observed non-linear relationship between direct gene expression levels and downstream pathway outputs highlights the importance of system design strategies. In particular, the ability to link synthetic controllers with relatively moderate gene regulatory activities to potent upstream pathway components enables dramatic alterations in downstream functional behaviors. The functional and structural independence of the ribozyme switch and its target gene enables the regulation of any transgene of interest and allows a high degree of flexibility in the design of optimal regulatory networks. Therefore, the identification of critical genetic components in a given system is both central to and readily accommodated by ribozyme switch-based regulation.

The unique modularity of our RNA-based device framework supports rapid and effective tailoring of the regulatory system to respond to clinically applicable inputs. Furthermore, the implementation of higher-order information processing devices[18] on platforms that integrate multiple aptamers to both endogenous and exogenous inputs will enable more sophisticated control strategies with applications in autonomous control systems, *in vivo* diagnosis, and precise localization of cellular therapeutics to disease targets. The development of RNA aptamers to pharmaceuticals with minimal off-target

toxicities and high cell permeability and bioavailability will be critical for the translation of these RNA-based regulatory systems to clinical applications. Therefore, the coupling of our modular device framework with advances in aptamer selection processes[33] will more broadly support the tailoring of RNA-based regulatory systems to diverse applications in health and medicine, including diagnostics, cellular therapeutics, gene therapy, and intelligent molecular therapies.

Materials and Methods

Plasmid construction. All plasmids were constructed using standard molecular biology techniques[34]. Plasmid maps are provided in Supplementary Figure 3.7. All oligonucleotides were synthesized by Integrated DNA Technologies and all constructs were sequence verified (Laragen). Cloning enzymes, including restriction enzymes and T4 DNA ligase, were obtained from New England Biolabs and DNA polymerases were obtained from Stratagene.

A fusion of the firefly luciferase (*ffluc*) gene and the *Sh ble* gene encoding zeocin resistance was PCR amplified from pMOD-LucSh (Invivogen) using forward and reverse primers Kozak BamHI5' (5'ATCGGATCCGCCGCCACCATGGAGGATGCCAAGAA TATTAAGAAAGG) and zeocin XbaI3' (5'TATTCTAGATCAGTCCTGCTCCTCTGC CACAAAGTGC), respectively. The plasmid pffLuc:zeo was constructed by inserting the resulting PCR product into pcDNA3.1(+) (Invitrogen) via the unique restriction sites BamHI and XbaI located in the multi-cloning site behind the CMV promoter.

The *cd19* gene was PCR amplified from CD19t-Tk-T2A-IL15op_epHIV7 using forward and reverse primers CD19t BlpI5' (5'ATTGCTGAGCCTAGAGCTGAAG) and

CD19t-mutsr39TK FR (5'CCCGCAGTAGCGTGGGCATTCTTTTCCTCCTCAGGAC CAG), respectively. The thymidine kinase gene *mutsr39tk* was PCR amplified from mutsr39tk_pcDNA3.1(+) using forward and reverse primers CD19t-mutsr39TK FF (5'C TGGTCCTGAGGAGGAAAAGAATGCCCACGCTACTGCGGG) and mutsr39TK-T2A FR (5'CCTCTCCGCCGCCAGATCTGTTAGCCTCCCCCATCTCCC), respectively. The cytokine gene *il-15* was PCR amplified from CD19t-Tk-T2A-IL15op_epHIV7 using forward and reverse primers mutsr39TK FF (5'GGGAGATGGGGGAGGCTAACAGATCTGGCGGCGGAGAGG) and IL15op BsrGI3' (5'TCTCGGTGTACAGGGTGGCG), respectively. PCR products for the three genes were assembled via a fourth PCR reaction using forward and reverse primers CD19t BlpI5' and IL15op BsrGI3', respectively. The plasmid pIL15 was constructed by inserting the assembled PCR product (*cd19-mutsr39tk-t2a-il15*) into CD19t-Tk-T2A-IL15op_epHIV7 via the unique restriction sites BlpI and BsrGI behind the EF1α promoter.

The fluorescence gene *egfp* was PCR amplified from eGFP_pcDNA3.1(+) using forward and reverse primers eGFP KpnI5' (5'CTTGGTACCCGCCACCATGGTGAGC AAG) and T2A-IL2 FR (5'CCACGTCACCGCATGTTAGAAGACTTCCTCTGCCCTC TCCGCTGCCCTTGTACAGCTCGTCCATGCC), respectively. The cytokine gene *il-2* was PCR amplified from IL2_pSK using forward and reverse primers T2A-IL2 FF (5'CT TCTAACATGCGGTGACGTGGAGGAGAATCCCGGCCCTATGTACAGGATGCAA CTCCTGTC) and IL2 XhoI3' (5'AGACTCGAGTCAAGTTAGTGTTGAGATGATGC), respectively. PCR products for the two genes were assembled via a third PCR reaction using forward and reverse primers eGFP KpnI5' and IL2 XhoI3', respectively. The

plasmid eGFP-T2A-IL2_pcDNA3.1(+) was constructed by inserting the assembled PCR product (*egfp-t2a-il2*) into pcDNA3.1(+) via the unique restriction sites KpnI and XhoI behind the CMV promoter. A DNA sequence including the CMV promoter, the *egfp-t2a-il2* fusion gene, and the poly-A sequence was PCR amplified from eGFP-T2A-IL2_pcDNA3.1(+) using forward and reverse primers CMV HpaI5' (5'AATAGTTAACGTTGACATTGATTATTGACTAGTTATTAATAGTAATCAA) and bGHpA SacII3' (5'AATACCGCGGCCATAGAGCCCACCGC), respectively. The PCR product was inserted into dsRed Express_pcDNA3.1(+) via the unique restriction sites HpaI and SacII. The CMV promoter regulating the *egfp-t2a-il2* fusion gene was replaced by the EF1α promoter via the unique restriction sites BglII and KpnI to construct the plasmid pIL2. The EF1α promoter sequence was PCR amplified from pIL15 using forward and reverse primers EF1α BglII5' (5'AATAGATATCTGCTTCGCGA GGATCTGC) and EF1 α KpnI3' (5'AATAGGTACCGGTGGCGGCGCTAG), respectively. Multiple copies of ribozyme switches were inserted into the pIL2 and pIL15 vectors using sequential cloning methods described in Chapter 2.

Mammalian cell culture maintenance. The mouse T-cell line CTLL-2 was obtained from ATCC and maintained in RPMI-1640 media (Lonza) supplemented with 10% heat-inactivated fetal bovine serum (HI-FBS; Hyclone), 2 mM sodium pyruvate (Gibco), and 4.5 g/L D-(-)-glucose (Sigma). Cells were fed 100 U/ml IL-2 every 48 hours and maintained between 0.05 x 10^6 and 0.50 x 10^6 cells/ml. 0.20 mg/ml zeocin (Invivogen) was added to all cell lines stably expressing the ffLuc:zeocin fusion gene.

Transient transfection and fluorescence quantification. All transient transfections into CTLL-2 cells were performed with an Amaxa Nucleofector II and the Mouse T Cell Nucleofector Kit (Amaxa) following the manufacturer's protocols. Electroporations were performed with 2 x 10^6 cells and 3 μg of plasmid DNA. One hour after electroporation, samples were diluted two-fold with supplemented RPMI media and split into 2 wells, one treated with small molecule input and one without input. In experiments testing a range of input concentrations, multiple aliquots of cells were electroporated as described. One hour after electroporation, samples were combined, diluted two-fold, split into the appropriate number of wells, and each treated with the appropriate concentration of small molecule input. Fluorescence and cell viability data were obtained 24 and 48 hours after transfection, respectively, using a Quanta Cell Lab Flow Cytometer (Beckman Coulter) equipped with a 488-nm laser. EGFP, PE, and dsRed-Express were measured through 525/30-nm band-pass, 575/30-nm band-pass, and 610-nm long-pass filters, respectively. Viability was gated based on side scatter and electronic volume, and only viable cells were included in fluorescence measurements. For samples expressing constructs based on pIL2, viable cells were further gated for dsRed-Express expression, which served as a transfection efficiency control, before EGFP intensity values were collected. All fluorescence measurements were reported as the geometric mean intensity observed in the gated population. To control for toxicity and other possible non-specific effects of transfection and input ligand molecules, cells transfected with an inactive (scrambled) hammerhead ribozyme and treated with the corresponding concentration of ligand molecule served as positive controls to which values from cells transfected with active ribozyme switches were normalized. The inactive ribozyme constructs provide controls

for the maximum possible gene expression levels from the ribozyme-based regulatory systems. CD19 antibody staining was performed by washing 1 x 10^6 cells twice with 500 μl HBSS (Gibco), incubating with 10 μl PE-conjugated CD19 antibody (Beckman Coulter) in 50 μl HBSS for 15 min at 4°C in the dark, washing twice with 500 μl HBSS, and analyzing on the flow cytometer. Transient transfection experiments were performed with at least two replicate samples, and reported error bars indicate one standard deviation from the averaged measured value normalized by the inactive ribozyme control.

Stable CTLL-2 cell line generation. To generate a CTLL-2 cell line for *in vivo* imaging, CTLL-2 cells were electroporated with the pffLuc:zeo plasmid, and stable integrants were selected based on resistance to 0.1 mg/ml zeocin. The stable cell line CffLuc was confirmed through a luciferase activity assay, in which 1 x 10^4 cells were resuspended in 100 μl media and aliquoted into 96-well black, clear-bottom plates. Each well was incubated with 20 μl of 1.4 mg/ml D-luciferin diluted in PBS (Xenogen) at 37°C for 10 min, and luciferase signal was detected using a Victor3 1420 Multilabel Counter (Perkin Elmer; Waltham, MA). Signals from six replicates were averaged for each experiment, and CTLL-2 cells not expressing *ffluc* were used as negative controls.

To generate CTLL-2 cells stably expressing constructs encoding the T-cell proliferation regulatory system for *in vivo* imaging, CffLuc cells were electroporated with plasmids derived from the pIL15 plasmid and linearized at the unique NsiI site. Electroporations for stable cell lines were carried out in seven cuvettes each containing 5 x 10^6 cells and 5 μg plasmid DNA. One hour after electroporation, all electroporated samples were combined, diluted to a total volume of 50 ml, and supplemented with IL-2

every 48 hours to a final concentration of 100 U/ml. Cells were stained with PE-conjugated CD19 antibodies 7 days after electroporation and sorted for PE^+ cells by fluorescence-activated cell sorting (FACS) using a BD FACSAria cell sorter (BD Biosciences) equipped with a 488-nm laser. The sorted cells were grown for 13 days and then stained and further sorted via magnetism-automated cell sorting (MACS) using an autoMACS Separator (Miltenyi Biotec) for PE^+ cells. Theophylline was added to cell cultures to a final concentration of 250 μM 2 days prior to each sort.

Following the FACS and MACS sorts a series of selection cycles were performed by alternating between growth in ganciclovir and theophylline. Cells were grown for 2 weeks following AutoMACS sorting in media supplemented with IL-2 every 48 hours to a final concentration of 100 U/ml. The cells were then grown for 7 days in the presence of 1 μM ganciclovir and supplemented with IL-2 every 48 hours to a final concentration of 100 U/ml. The cells were subsequently placed in fresh media supplemented with 250 μM theophylline and allowed to grow for 4 days in the absence of IL-2. Following termination of theophylline treatment, the cells were placed in fresh media supplemented with 100 U/ml IL-2 (added every 48 hours) and 5 μM ganciclovir for 4 days. The theophylline treatment regime then resumed for 8 days, followed by the ganciclovir treatment regime (at 5 μM) for 10 days, and a final theophylline regime for 5 days. Cell density was maintained between 0.05×10^6 cells/ml and 0.5×10^6 cells/ml throughout the cell culture procedure. Following the last theophylline treatment regime, cells were stained with PE-conjugated CD19 antibodies and sorted for single clones into 96-well plates by FACS for low, medium, and high PE levels. The sorted clones (CffLuc-pIL15) were grown in media supplemented with 250 μM theophylline, 50 U/ml

penicillin:streptomycin, and no IL-2. Clones were expanded from the low PE fractions into larger culture volumes and finally maintained in T75 tissue culture flasks (BD Falcon).

***In vitro* growth assay for stable CTLL-2 cell lines.** CffLuc-pIL15 clones were cultured under regular conditions (RPMI 1640 media supplemented with 100 U/ml IL-2 every 48 hours, 0.2 mg/ml zeocin, no theophylline), washed twice with HBSS, and split into five identical aliquots in six-well plates at approximately 0.01 x 10^6 cells/ml (4 ml/well). Each well was supplemented with one of the following: 100 U/ml IL-2, 100 μM theophylline, 250 μM theophylline, 400 μM theophylline, or no IL-2 and no theophylline. Cells were split and passaged as necessary into new six-well plates at approximately 0.03 x 10^6 cells/ml, and IL-2 was added to the appropriate wells to a final concentration of 100 U/ml every 48 hours. Cell count was obtained from 50 μl of each culture daily for 7 days on a Quanta Cell Lab Flow Cytometer by gating for viable cells based on side scatter and electronic volume. Cell density was calculated by dividing the number of detected live cells by the volume analyzed on the flow cytometer.

CTLL-2 time course study. For the 18-day time course, CTLL-2 parental cells, clonal stable cell line 1264-48 (L2bulge9(3x)), and clonal stable cell line 1266-3 (inactive ribozyme) were cultured under regular conditions. On day 0, cells were counted for density and washed twice with HBSS. Each cell line was used to seed two 50-ml cultures at 0.15 x 10^6 cells/ml (Set 1) and two 50-ml cultures at 0.05 x 10^6 cells/ml (Set 2). 500 μM theophylline was added to one flask at each seeding density. 50 U/ml IL-2 was added

to Set 1 flasks and 100 U/ml IL-2 was added to Set 2 flasks to keep IL-2 concentration consistent with seeding cell density and harvesting schedule. On day 1, Set 1 flasks were harvested for CD19 antibody staining (1 x 10^6 cells per sample) and for cell pellet collection for qRT-PCR (12.5 x 10^6 cells per sample, washed once with HBSS, and flash frozen with liquid nitrogen). Each culture was split to 0.05 x 10^6 cells/ml at 50 ml total and supplemented with 100 U/ml IL-2 and the appropriate concentration of theophylline (0 μM or 500 μM). On day 2, the same harvest and subculture procedures were repeated for Set 2 flasks. All cultures were treated in this manner every 48 hours until day 7. On day 7, cell count was obtained for all cultures. After harvesting from Set 1 flasks, all cultures were washed twice with HBSS and resuspended in fresh media without theophylline. Set 1 flasks were seeded at 0.05 x 10^6 cells/ml and supplemented with 100 U/ml IL-2. Set 2 flasks were seeded with all available cells and supplemented with 50 U/ml IL-2. On days 8 and 9, the same harvest and subculture procedures were performed on Set 2 and Set 1 flasks, respectively. All cultures were treated in this manner every 48 hours until day 14. On day 14, cell count was obtained for all cultures. After harvesting from Set 2 flasks, all cultures were washed twice with HBSS and resuspended in fresh media. 500 μM theophylline was added to all cultures that had been treated with theophylline on days 0–7. Set 2 flasks were seeded at 0.05 x 10^6 cells/ml and supplemented with 100 U/ml IL-2. Set 1 flasks were seeded with all available cells and supplemented with 50 U/ml IL-2. On days 15 and 16, samples were harvested for CD19 staining and subcultured as before for Set 2 and Set 1 flasks, respectively. All cultures were treated in this manner every 48 hours until day 18. For the 48-hour time course, CTLL-2 parental cells and the clonal stable cell line 1264-48 (L2bulge9(3x)) were

cultured under regular conditions. On day 0, cells were counted for density and washed twice with HBSS. Each cell line was used to seed four 30-ml cultures at 0.25 x 10^6 cells/ml, each supplemented with 100 U/ml IL-2 and 50 U/ml penicillin streptomycin. 1.5 ml of each culture was sampled for surface staining with PE-CD19 antibody (0 hour time point), and theophylline was then added to two flasks of each cell line to a final concentration of 500 μM. Samples for antibody staining were taken at 1, 2, 4, 6, 12, 18, 24, and 48 hours after theophylline addition. Cultures were not fed with media, cytokine, or theophylline after the initial setup.

Transcript analysis through qRT-PCR. mRNA was purified from frozen cell pellets with the GenElute Direct mRNA MiniPrep Kit (Sigma) following the manufacturer's protocols. mRNA samples were treated with 100 U/ml DNaseI at 37°C for 15 min and purified by phenol-chloroform extraction and ethanol precipitation. Reverse transcription was performed with 300 ng mRNA, 2 pmol of each primer, 10 nmol dNTP, 40 U RNaseOUT, 5 mM DTT, 1x First-Strand Buffer, and 200 U SuperScript III Reverse Transcriptase (Invitrogen) in a 20 μl reaction following the manufacturer's protocols. Gene-specific primers (Hprt1 reverse, 5'TGCTGCCATTGTCGAACA; IL-15 reverse, 5'GGTGTCGTGGATGCTG) were used in the cDNA synthesis reactions. The resulting cDNA samples were subsequently treated with 2.5 U of RNaseH at 37°C for 20 min, followed by heat inactivation at 65°C for 20 min.

qRT-PCR reactions were performed in a 25 μl reaction with 200 nM of each primer, 5 μl cDNA, and 1x SYBR Green SuperMix (Bio-Rad) on an iCycler Real-Time PCR machine (Bio-Rad). Separate reactions were performed for the housekeeping gene

Hprt1 (Hprt1 forward, 5'AGCCAGCGAAGCCAC; Hprt1 reverse) and the target gene *il-15* (IL-15 forward, 5'CAACTGGGTGAACGTGAT; IL-15 reverse). The qRT-PCR protocol included 32 cycles of a 15 sec annealing step at 50°C and a 30 sec extension step at 72°C, followed by a melt curve analysis to verify absence of non-specific products. All reactions were performed in triplicate, and threshold cycle (C_t) values were averaged to obtain the arithmetic mean. Relative IL-15 expression levels were calculated with the following formula [35]:

$$RE = \frac{\varepsilon_{Hprt1}^{(C_{t,Hprt1})}}{\varepsilon_{IL-15}^{(C_{t,IL-15})}}$$

where RE indicates relative IL-15 expression, ε_x indicates primer efficiency for gene x, and $C_{t,x}$ indicates the averaged C_t value for gene x. Standard deviation was calculated with the following formula:

$$STD = \sqrt{\left[RE\ln(\varepsilon_{Hprt1})\right]^2\left(Std_{Hprt1}\right)^2 + \left[RE\ln(\varepsilon_{IL-15})\right]^2\left(Std_{IL-15}\right)^2}$$

where STD indicates standard deviation in relative IL-15 expression and Std_x indicates standard deviation calculated from the triplicate samples for gene x. Reported error bars indicate one standard deviation.

Intracellular IL-15 antibody staining. Approximately 1 x 10^6 cells were harvested and washed once with 1 ml HBSS. The cell pellet was resuspended in 150 μl of BD Cytofix/Cytoperm buffer (BD Biosciences) and incubated on ice in the dark for 20 min. The sample was then washed twice with 1 ml of 1X BD Perm/Wash buffer and resuspended in 95 μl of 1X BD Perm/Wash buffer with 5 μl of anti-human IL-15-fluorescein monoclonal antibody (R&D Systems) and incubated on ice in the dark for 30

min. The sample was then washed twice with 1 ml of 1X BD Perm/Wash buffer, resuspended in 300 μl HBSS, and analyzed using a Quanta Cell Lab Flow Cytometer (Beckman Coulter) with excitation by a 488-nm laser and emission detected through a 525/30 band-pass filter.

Western blot analysis of STAT5 levels. Clonal stable cell lines were cultured under regular conditions (see above), washed twice with HBSS, and split into two identical aliquots. The aliquots were grown in the absence of IL-2 and either in the presence or absence of 500 μM theophylline for 3 days. Approximately 2 x 10^6 cells of each sample were harvested and washed with 1 ml HBSS each day, frozen with liquid nitrogen, and stored at –80°C until lysis. Cell pellets were lysed with 50 μl Triton-X lysis buffer (1% Triton-X, 10 mM Tris-HCl, pH 7.4, 130 mM NaCl, 5 mM EDTA, protease inhibitor, 5% phosphatase inhibitor cocktail II) and incubated on ice for 1 hour. Lysates were centrifuged at 14,000 xg for 20 min at 4°C. The supernatant was collected and immediately frozen at –80°C.

Lysate samples were thawed on ice and a standard Bradford assay using Protein Assay Dye (Bio-Rad) was performed with a BSA standard to determine protein concentrations. Samples were run on NuPAGE 4-12% Bis-Tris Gels (Invitrogen) at 90 V for 2.5 hours, where 50 μg of protein from each sample was loaded. Blotting was performed with Mini Trans-Blot Filter Paper (Bio-Rad) and 0.45 μm Nitrocellulose Membranes (Bio-Rad) wetted with NuPAGE transfer buffer (Invitrogen) and transferred at 40 mA per gel with a Hoefer Semi-Phor Blotter (Hoefer Scientific Instruments). Membranes were blocked with Odyssey Blocking Buffer (Li-Cor) at 4°C for 1 hour and

probed with Rabbit-anti-pSTAT5 antibody (Cell Signaling) or IRDye 800CW-conjugated anti-β-actin antibody (Rockland) at 4°C overnight in the dark. Membranes probed with p-STAT5 antibodies were washed four times with 100 ml TTBS (1x Tris-Buffered Saline (TBS, Bio-RAD), 0.1% Tween 20 (Sigma)) and further stained with IRDye 800CW-conjugated goat-anti-rabbit antibody (Li-Cor) at room temperature for 1 hour. Membranes stained for β-actin and p-STAT5 were washed four times with 100 ml TTBS and once with 100 ml TBS before fluorescent images were acquired and quantified with the Odyssey Infrared Imaging System (Li-Cor). Integrated band intensity was calculated with the Odyssey system using blank gel areas surrounding each band for background subtraction. Relative p-STAT5 expression levels were calculated by normalizing the integrated intensity of the p-STAT5 band by that of the β-actin band from the same protein sample. Data shown are representative of two independent experiments.

In vivo **T-cell proliferation studies in NOD/SCID-IL2(ko) mice.** Various CffLuc-pIL15 cell lines, CffLuc, and a CffLuc-derived cell line stably expressing a cytokine fusion transgene with an inactive ribozyme in the 3' UTR of the transgene were expanded under regular culture conditions. Cells were harvested by centrifugation at 1200 rpm at 4°C for 10 min, washed twice with PBS, resuspended in PBS at a concentration of 2 x 10^6 cells/ml, and split into two 50 μl aliquots. Each aliquot was mixed with 50 μl of either PBS or 2 mM theophylline dissolved in PBS. The 100 μl cell suspension was then mixed with 100 μl of Matrigel (BD Biosciences), for a total of 0.1 x 10^6 cells at a final concentration of 0 μM or 500 μM theophylline. The cell suspensions were injected subcutaneously (s.c.) into the right or left flank of NOD/scid-IL2(ko) mice. All mice were

8 to 10 weeks old and bred in the City of Hope lab animal breeding facility, and experiment protocols were approved by the City of Hope Institute Animal Care and Use Committee. *In vivo* growth of the injected cells was monitored by biophotonic imaging. Clone 1264-48 and the positive control cell line expressing an inactive ribozyme were tested in a second experiment following the procedure described above. Each cell line was injected into both flanks of three mice either with or without 500 μM theophylline, generating six replicates for each experimental condition. One of the mice injected with clone 1264-48 without theophylline exhibited abnormally large engraftments in both flanks. Additional subjects were studied to verify that cell growth in this mouse was aberrant in a statistically significant manner ($P = 0.044$ based on comparison against eight other replicates with the same experimental condition), and data from this mouse were excluded from statistical analyses of the ribozyme switch system.

Biophotonic *in vivo* imaging. Animals received intraperitoneal (i.p.) injections of 4.29 mg per mouse of freshly prepared luciferin substrate (Caliper Life Sciences) suspended in 150 μl of PBS. Mice were then anesthetized with isoflurane (1.5 L oxygen + 4% isoflurane per minute) in an induction chamber. After induction of deep anesthesia, mice were imaged using the IVIS Imaging System 100 Series (Xenogen) consisting of a CCD camera mounted on a light-tight specimen chamber (darkbox), a camera controller, a camera cooling system, and a Windows computer system for data acquisition and analysis. Images were acquired at 10–20 min after luciferin injection with the appropriate exposure time and binning mode to prevent signal saturation. Luciferase activity was

analyzed through Living Image Software 3.1 from Xenogen to quantify tumor region flux (photons per second).

Statistical analysis. Statistical analysis was performed on growth rate data using the Mann-Whitney U test to calculate two-tailed *P* values. The doubling time of injected cells was calculated based on the total luciferase signal flux data collected over the course of each *in vivo* study. Signal flux data were fitted to an exponential curve, and the resulting equation was used to calculate cell-doubling time using the equation:

$$t_D = (t_2 - t_1)\frac{\log(2)}{\log(F_2 - F_1)},$$

where t is time, F is signal flux, and t_D is doubling time.

Acknowledgments

We thank members of the Smolke Lab, Y.A. Chen, and D. Endy for critical reading of the manuscript; M.N. Win for contributing expertise on ribozyme switch design; B. Aguilar, C. Bautista, C. Brown, L. Brown, W. Chang, R. Diamond, A. Hamlett, M. Hunter, D. Perez, G. Raval, J. Wagner, W. Wong, and C. Wright for technical assistance. This work was supported by the City of Hope's National Cancer Institute–Cancer Center Support Grant, the National Science Foundation (fellowship to Y.Y.C.), the Alfred P. Sloan Foundation (fellowship to C.D.S.), and the National Institutes of Health (grant to C.D.S., RC1GM091298).

References

1. Blattman, J.N. & Greenberg, P.D. Cancer immunotherapy: a treatment for the masses. *Science* **305**, 200-205 (2004).
2. June, C.H. Principles of adoptive T cell cancer therapy. *J Clin Invest* **117**, 1204-1212 (2007).
3. Falkenburg, J.H., Smit, W.M. & Willemze, R. Cytotoxic T-lymphocyte (CTL) responses against acute or chronic myeloid leukemia. *Immunol Rev* **157**, 223-230 (1997).
4. Walter, E.A. et al. Reconstitution of cellular immunity against cytomegalovirus in recipients of allogeneic bone marrow by transfer of T-cell clones from the donor. *N Engl J Med* **333**, 1038-1044 (1995).
5. Morgan, R.A. et al. Cancer regression in patients after transfer of genetically engineered lymphocytes. *Science* **314**, 126-129 (2006).
6. Gonzalez, S. et al. Genetic engineering of cytolytic T lymphocytes for adoptive T-cell therapy of neuroblastoma. *J Gene Med* **6**, 704-711 (2004).
7. Kahlon, K.S. et al. Specific recognition and killing of glioblastoma multiforme by interleukin 13-zetakine redirected cytolytic T cells. *Cancer Res* **64**, 9160-9166 (2004).
8. Leen, A.M., Rooney, C.M. & Foster, A.E. Improving T cell therapy for cancer. *Annu Rev Immunol* **25**, 243-265 (2007).
9. Robbins, P.F. et al. Cutting edge: persistence of transferred lymphocyte clonotypes correlates with cancer regression in patients receiving cell transfer therapy. *J Immunol* **173**, 7125-7130 (2004).

10. Dudley, M.E. et al. Adoptive transfer of cloned melanoma-reactive T lymphocytes for the treatment of patients with metastatic melanoma. *J Immunother* **24**, 363-373 (2001).

11. Yee, C. et al. Adoptive T cell therapy using antigen-specific CD8+ T cell clones for the treatment of patients with metastatic melanoma: in vivo persistence, migration, and antitumor effect of transferred T cells. *Proc Natl Acad Sci U S A* **99**, 16168-16173 (2002).

12. Mackensen, A. et al. Phase I study of adoptive T-cell therapy using antigen-specific CD8+ T cells for the treatment of patients with metastatic melanoma. *J Clin Oncol* **24**, 5060-5069 (2006).

13. Johnston, J.A. et al. Tyrosine phosphorylation and activation of STAT5, STAT3, and Janus kinases by interleukins 2 and 15. *Proc Natl Acad Sci U S A* **92**, 8705-8709 (1995).

14. Gattinoni, L., Powell, D.J., Jr., Rosenberg, S.A. & Restifo, N.P. Adoptive immunotherapy for cancer: building on success. *Nat Rev Immunol* **6**, 383-393 (2006).

15. Isaacs, F.J., Dwyer, D.J. & Collins, J.J. RNA synthetic biology. *Nat Biotechnol* **24**, 545-554 (2006).

16. Isaacs, F.J. et al. Engineered riboregulators enable post-transcriptional control of gene expression. *Nat Biotechnol* **22**, 841-847 (2004).

17. Win, M.N. & Smolke, C.D. A modular and extensible RNA-based gene-regulatory platform for engineering cellular function. *Proc Natl Acad Sci U S A* **104**, 14283-14288 (2007).

18. Win, M.N. & Smolke, C.D. Higher-order cellular information processing with synthetic RNA devices. *Science* **322**, 456-460 (2008).

19. Palmer, T.D., Rosman, G.J., Osborne, W.R. & Miller, A.D. Genetically modified skin fibroblasts persist long after transplantation but gradually inactivate introduced genes. *Proc Natl Acad Sci U S A* **88**, 1330-1334 (1991).

20. Choi, K.H., Basma, H., Singh, J. & Cheng, P.W. Activation of CMV promoter-controlled glycosyltransferase and beta-galactosidase glycogenes by butyrate, tricostatin A, and 5-aza-2'-deoxycytidine. *Glycoconj J* **22**, 63-69 (2005).

21. Xia, X., Zhang, Y., Zieth, C.R. & Zhang, S.C. Transgenes delivered by lentiviral vector are suppressed in human embryonic stem cells in a promoter-dependent manner. *Stem Cells Dev* **16**, 167-176 (2007).

22. Gillis, S. & Smith, K.A. Long term culture of tumour-specific cytotoxic T cells. *Nature* **268**, 154-156 (1977).

23. Beisel, C.L. & Smolke, C.D. Design principles for riboswitch function. *PLoS Comput Biol* **5**, e1000363 (2009).

24. Jenison, R.D., Gill, S.C., Pardi, A. & Polisky, B. High-resolution molecular discrimination by RNA. *Science* **263**, 1425-1429 (1994).

25. Berens, C., Thain, A. & Schroeder, R. A tetracycline-binding RNA aptamer. *Bioorg Med Chem* **9**, 2549-2556 (2001).

26. Weigand, J.E. & Suess, B. Tetracycline aptamer-controlled regulation of pre-mRNA splicing in yeast. *Nucleic Acids Res* **35**, 4179-4185 (2007).

27. Hsu, C. et al. Primary human T lymphocytes engineered with a codon-optimized IL-15 gene resist cytokine withdrawal-induced apoptosis and persist long-term in the absence of exogenous cytokine. *J Immunol* **175**, 7226-7234 (2005).

28. Waldmann, T.A., Dubois, S. & Tagaya, Y. Contrasting roles of IL-2 and IL-15 in the life and death of lymphocytes: implications for immunotherapy. *Immunity* **14**, 105-110 (2001).

29. Berger, C. et al. Adoptive transfer of effector CD8+ T cells derived from central memory cells establishes persistent T cell memory in primates. *J Clin Invest* **118**, 294-305 (2008).

30. Blau, C.A., Peterson, K.R., Drachman, J.G. & Spencer, D.M. A proliferation switch for genetically modified cells. *Proc Natl Acad Sci U S A* **94**, 3076-3081 (1997).

31. Neff, T. et al. Pharmacologically regulated in vivo selection in a large animal. *Blood* **100**, 2026-2031 (2002).

32. Zhao, S., Weinreich, M.A., Ihara, K., Richard, R.E. & Blau, C.A. In vivo selection of genetically modified erythroid cells using a jak2-based cell growth switch. *Mol Ther* **10**, 456-468 (2004).

33. Wilson, D.S. & Szostak, J.W. In vitro selection of functional nucleic acids. *Annu Rev Biochem* **68**, 611-647 (1999).

34. Sambrook, J. & Russell, D.W. Molecular Cloning: A Laboratory Manual, Edn. 3. (Cold Spring Harbor Press, Cold Spring Harbor; 2001).

35. Livak, K.J. & Schmittgen, T.D. Analysis of relative gene expression data using real-time quantitative PCR and the 2(-Delta Delta C(T)) Method. *Methods* **25**, 402-408 (2001).

Supplementary Text 3.1

T2A Sequences

T2A DNA sequence
GGCAGCGGAGAGGGCAGAGGAAGTCTTCTAACATGCGGTGACGTGGAGGAG
AATCCCGG

T2A peptide sequence
GSGEGRGSLLTCGDVEENPG

Supplementary Text 3.2

CMV Promoter Silencing in Stably Integrated CTLL-2 Cells. The CMV promoter is a powerful and frequently used driver of transgene expression in mammalian cells. Our initial system for implementing ribozyme-based regulatory devices in mammalian cells used the CMV promoter to express the target transgene coupled to ribozyme switches (Figure 2.3). To study the long-term performance of these regulatory systems in T cells, we stably integrated constructs encoding the *egfp-t2a-il2* transgene linked with one to four copies of the theophylline-responsive L2bulge9 switch into the genome of the CffLuc cell line. The results, discussed in detail below, suggest that the CMV promoter is easily silenced in stably integrated CTLL-2 cells and is unsuited for long-term expression of regulatory systems in this cell line.

In our initial ribozyme-based regulatory system design, one CMV promoter drove the expression of the *egfp-t2a-il2* transgene coupled to ribozyme switches, and a second CMV promoter drove the expression of *dsred-express*, which served as a transfection marker (Supplementary Figure 3.8). CffLuc cells were electroporated with DNA plasmids, selected for plasmid-encoded hygromycin resistance, and subjected to multiple rounds of population refinement by FACS. A cell line expressing *egfp-t2a-il2* coupled to

an inactive ribozyme was included as a positive control. Cultures were first sorted for dsRed$^+$ expression to isolate bulk populations with stable genomic integration on day 19 after electroporation (Supplementary Figure 3.9). Since the plasmid encodes for both EGFP and dsRed-Express, cells were expected to be either EGFP$^-$/dsRed$^-$ (double negative; no genomic integration) or EGFP$^+$/dsRed$^+$ (double positive; with genomic integration). Although varying degrees of EGFP knockdown were anticipated from the L2bulge9 constructs, all five cell lines, including the positive control, showed substantial single-positive populations that were either EGFP$^+$/dsRed$^-$ or EGFP$^-$/dsRed$^+$. These results suggest that a significant portion of the cells either integrated an incomplete fragment of the transfected plasmid, or at least one CMV promoter in the integrated construct had been silenced.

Bulk populations from the first sort were expanded in the presence of hygromycin and then cultured in the presence of 1 mM theophylline for six days prior to a second sort for dsRed$^+$/EGFP$^+$ populations on day 38 after electroporation (Supplementary Figure 3.10). This sorting scheme was designed to isolate bulk populations with high ON-state expression levels. Although the cells had previously been sorted for dsRed$^+$ expression and were cultured in the presence of hygromycin to ensure retention of the integrated transgenes, all four cell lines showed large dsRed$^-$ populations prior to the second sort, indicating that a substantial portion of the bulk population had lost expression from the CMV promoter.

The dsRed$^+$/EGFP$^+$ populations collected from the second sort were expanded in the presence of hygromycin. Cells harboring two and four copies of L2bulge9 were characterized for theophylline-responsive switch activities. Cultures were grown in the

presence of 0 mM, 0.5 mM, or 1 mM theophylline for 12 days, and EGFP expression was monitored by flow cytometry. Results indicate dose-dependent theophylline-responsive ON switch behavior from both the L2bulge9(2x) and the L2bulge9(4x) constructs starting within 24 hours of theophylline addition and continuing through the remainder the time-course experiment (Supplementary Figure 3.11).

To verify the regulation of functional output (i.e., cell proliferation) cells expressing L2bulge9(2x) and L2bulge9(4x) were characterized in mouse models. Cells expressing either no *egfp-t2a-il2* or the transgene coupled to an inactive ribozyme served as negative and positive controls, respectively. One million cells of each cell line were injected subcutaneously into the right flank of each of six mice. Three mice from each group subsequently received two systemic injections of 2.5 mg theophylline on the same day. One day after injections, six of the twelve mice that received theophylline were found dead, suggesting that the theophylline dosage used was too toxic for the animals. The remaining subjects were monitored by biophotonic imaging for ten days, and results indicate that all cell lines expressing *egfp-t2a-il2*, regardless of the ribozyme switch devices coupled to the transgene, were able to engraft *in vivo* (Supplementary Figure 3.12). Engrafted tumors were excised from the mice and analyzed by flow cytometry. Comparison of extracted tumor cells against the original cell lines continuously cultured *ex vivo* indicate that the animal hosts had exerted growth-based selection pressure on the injected cells and yielded a population with greatly elevated gene expression levels (Supplementary Figure 3.13). These results suggest that monoclonal cell populations with consistent and low OFF-state gene expression levels are required for effective growth regulation *in vivo*.

The L2bulge9(4x) bulk cell line was subsequently cultured in the absence of theophylline and sorted on day 109 after electroporation for single clones that were both $dsRed^{+}$ and either $EGFP^{-}$ or $EGFP^{low}$ to ensure low OFF-state expression levels (Supplementary Figure 3.14). The inactive ribozyme bulk cell line was sorted for single clones that were $dsRed^{+}/EGFP^{high}$ to provide a strong positive control. Despite the fact that the cells had been twice sorted for $dsRed^{+}$ expression and were continuously cultured in the presence of hygromycin, the majority of both cell lines fell in the double-negative quadrant during the third sort, indicating that CMV promoter silencing progressed as the cells remained in continuous culture.

Five clonal cell lines expressing L2bulge9(4x) were tested in mouse models with a clonal cell line expressing the inactive ribozyme serving as the positive control. CffLuc cells were also included as a negative control in the study. 0.1×10^{6} cells of each cell line was injected subcutaneously into the right flank of a mouse, and cell proliferation was monitored by biophotonic imaging for 19 days. Results show that the positive control achieved robust engraftment while none of the L2bulge9(4x) cell lines expanded beyond background levels, indicating that the OFF-state expression levels were sufficiently low to avoid cell proliferation in the absence of theophylline (Supplementary Figure 3.15).

To test for theophylline-responsive switch behavior without using lethal doses of theophylline, 0.1×10^{6} cells of each of five clonal L2bulge9(4x) cell lines were encased in a hydrogel matrix containing 200 μM theophylline and injected subcutaneously into the flanks of mice. The animals were monitored by biophotonic imaging for 15 days. By day 4 after injection, none of the L2bulge9(4x) cell lines showed engraftment (Supplementary Figure 3.16). Several of the animal subjects died prior to the end of the

experiment, but the cause of death is believed to be the general vulnerability of irradiated, immunosuppressant mice rather than the specific experimental conditions used. Based on the available data, none of the L2bulge9(4x) cell lines showed engraftment by day 8 after injection, suggesting that the cell lines either had lost the *egfp-t2a-il2* transgene or was unable to express the transgene at sufficiently high levels in the presence of 200 μM theophylline to sustain T-cell proliferation *in vivo*.

To verify that the *egfp-t2a-il2* transgene was still present in the genome, genomic DNA was extracted from each of the five L2bulge9(4x) clonal cell lines. The CffLuc cell line served as a negative control. Two positive controls were included: 1) a clonal cell line expressing *egfp-t2a-il2* coupled to the inactive ribozyme control and 2) a cell line expressing *egfp-t2a-il2* without any ribozyme device attached. PCR using a forward primer annealing to *egfp* and a reverse primer annealing to *il-2* was performed, and all cell lines other than the negative control showed the expected PCR product band, indicating that the *egfp-t2a-il2* transgene was stably integrated (Supplementary Figure 3.17A). Total RNA was extracted from each of the cell lines and qRT-PCR was performed using the forward and reverse primers mentioned above. L2bulge9(4x) Clone #4 showed no detectable signal while the other four L2bulge9(4x) clones showed less than 4% EGFP-T2A-IL2 expression relative to the inactive ribozyme, suggesting that the expression levels was likely too low to support T-cell proliferation *in vivo* (Supplementary Figure 3.17B).

In light of the extensive CMV promoter silencing observed in the process of stable cell line generation, we modified our regulatory systems and used the EF1α promoter to drive the expression of the target transgene and ribozyme switch devices

(Figure 3.2A). The EF1α promoter is weaker than the CMV promoter, but it has also been reported to have more stable long-term expression capabilities[21]. As presented in this chapter, the modified system is sufficiently robust to generate effective T-cell proliferation control systems in CTLL-2 cells.

Supplementary Text 3.3

Controlling for Toxicity and Non-specific Effects of Nucleofection and Small-Molecule Ligand Inputs on Growth and Gene Expression. Gene expression can be sensitive to a myriad of external factors, and accurate characterization of phenotypic responses, such as cell growth and viability, requires appropriate controls to account for potential non-specific effects of experimental procedures applied to the cells. In particular, the toxicity and other non-specific effects of transfection and small-molecule ligand addition were of concern in the characterization of the ligand-responsive, ribozyme-based regulatory systems described here. Careful controls were included in the experiments reported in this study to ensure accurate accounting of any potential non-specific effects.

Like most T cell lines, CTLL-2 cells cannot be effectively transfected by lipid-based transfection reagents. Therefore, electroporation with Amaxa Nucleofector technology is the method of choice for transfecting CTLL-2 cells. The trauma of nucleofection results in high cell mortality and affects the health of surviving cells. To account for the toxicity of nucleofection, all experiments conducted in this study included as a positive control cells nucleofected with a similar DNA construct harboring an inactive, scrambled ribozyme that lacks an attached aptamer. This control construct has

no ribozyme-based knockdown activity and no ligand-responsive cleavage activity, and it represents the maximum possible expression level from the regulatory system. Viability and fluorescence data from all other samples were reported relative to those of the positive control treated with the same concentration of small-molecule ligand. It has been verified by multiple nucleofection experiments that nucleofection toxicities from similar DNA constructs purified in the identical manner are similar.

The reproducible agreement between two characterization methods—viability (a phenotypic response) and fluorescence (a measure of reporter gene expression)—provided further confirmation of ligand-responsive gene-regulatory activity (Figure 3.2, Supplementary Figure 3.1). To verify that growth cytokine withdrawal (and not nucleofection toxicity) is responsible for the decrease in viability levels observed for cells transfected with active ribozyme switch constructs, transfected samples were split into two identical aliquots, one of which was fed with 100 U/ml of exogenous IL-2, a concentration that is sufficient to sustain healthy expansion of CTLL-2 cells during routine culture maintenance. The IL-2-treated samples had significantly higher viability levels compared to identical samples not treated with exogenous IL-2 (Supplementary Figure 3.18A). Furthermore, the inverse correlation between viability and ribozyme switch copy number disappears in the presence of exogenous IL-2, suggesting that the reduced viability at high switch copy numbers is specifically caused by more efficient gene expression knockdown and the resultant cytokine withdrawal in the absence of exogenous IL-2. In contrast, the addition of exogenous IL-2 does not affect fluorescence levels (Supplementary Figure 3.18B). Taken together, these results indicate that the observed variations in viability levels are specific to the regulatory systems.

The toxicity and potential pleiotropic effects of the small-molecule ligands theophylline and tetracycline were also considered (see Appendix 1 for toxicity curves of various small-molecule ligands in CTLL-2 cells). In transient transfection experiments the fluorescence and viability values of all samples were normalized to that of the inactive ribozyme control treated with the same concentration of the small molecule ligand (as described above) to account for non-aptamer-mediated effects of the ligand, as it is assumed that the non-specific effects of the ligand will be similar for the sample and the control. Negative controls, such as cells transfected with vectors that encode either no growth cytokine or a growth cytokine gene coupled to a fully active, non-switch hammerhead ribozyme control (sTRSV), were included in all transient transfection experiments. The relative viability and fluorescence levels from the negative control samples exhibited no response to ligand addition, indicating that the normalization method adequately accounts for the toxicity and pleiotropic effects of the small-molecule ligands (Figure 3.2B, Supplementary Figure 3.1A).

By using the inactive ribozyme as the normalizing control for all switch constructs in all transient transfection studies, we report the regulatory output of the switches relative to the maximum possible expression range. Compared to the more commonly used method of internal normalization, where each switch construct is normalized to its own internal high value, our method has the effect of reducing the apparent dynamic range of each switch. However, the reporting of switch output to a consistent standard control allows for direct and accurate comparison of the various switches, which is important for system development and characterization. The internal normalization method is employed for *in vitro* gene expression assays on stably

integrated cell lines (Figure 3.6B, C, Supplementary Figure 3.4A), because the maximum expression level of each clone is dependent on the integration site, which varies from clone to clone.

In the characterization of cell lines stably expressing the ribozyme switch constructs, a clonal cell line expressing the positive control construct (inactive ribozyme) was included to identify any non-specific effects of theophylline. As an example, an *in vitro* growth assay was performed on clonal cell lines in the presence or absence of 500 μM theophylline. The cell line expressing the inactive ribozyme exhibited a decreased growth rate in the presence of theophylline (Supplementary Figure 3.18C), indicating theophylline toxicity and verifying that the theophylline-induced increase in absolute growth rate observed from clones expressing the active ribozyme switches were not due to any non-specific growth-stimulatory effects of theophylline (Figure 3.6A, Supplementary Figure 3.3). As another example, positive and negative control cell lines were included in the animal studies and no significant theophylline-dependent differences were observed in the *in vivo* growth pattern of cells that either do not express growth cytokines or express the inactive ribozyme control (Figures 3.7A, 3.7C). In contrast, the *in vitro* and *in vivo* growth rates of clonal cell lines expressing functional ribozyme switch systems show increases in absolute growth rate (not normalized to the inactive ribozyme control) in response to theophylline addition (Figures 3.6A, 3.7B, Supplementary Figures 3.3, 3.6). Taken together, these results indicate that the observed T-cell growth behaviors were specific to the ligand-responsive regulatory system.

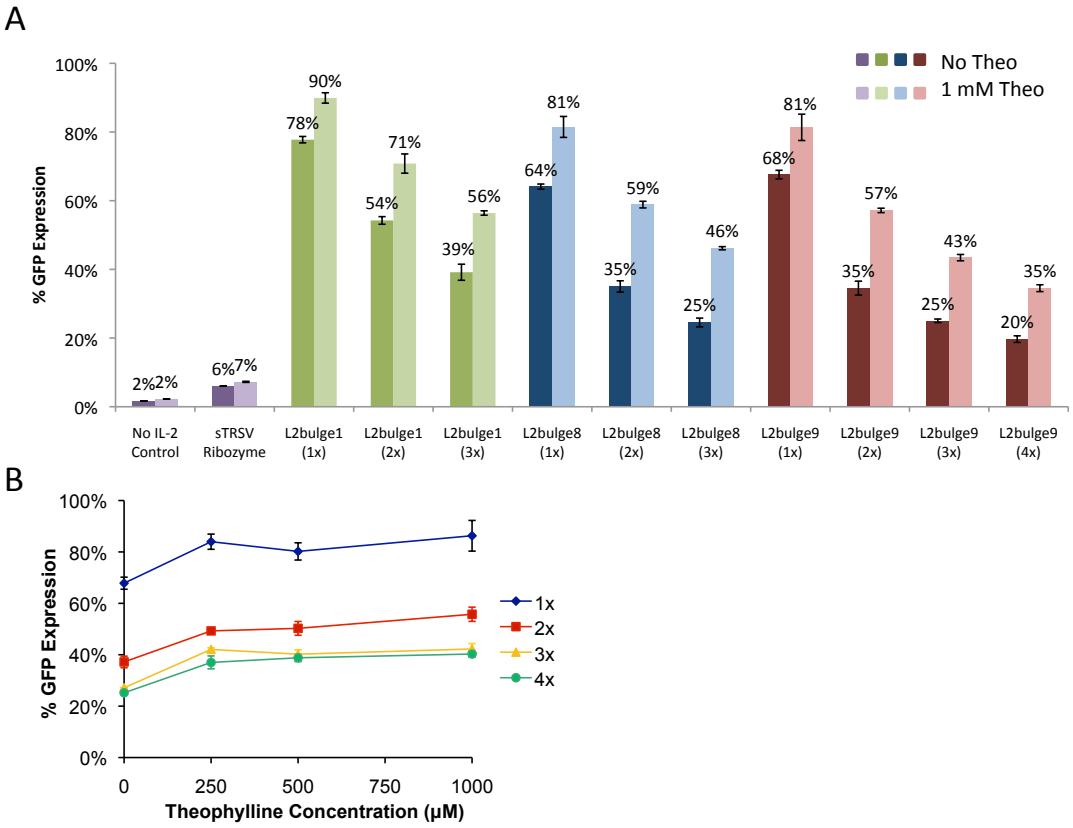

Supplementary Figure 3.1. Tunable, small molecule–mediated regulation of gene expression in mammalian cells by ribozyme switches. (A) GFP expression levels are reported for constructs encoding theophylline-responsive switches (L2bulge1, 8, 9) in one (1x), two (2x), three (3x), and four (4x) copies through transient transfections in CTLL-2 cells grown in 0 and 1 mM theophylline. No IL-2 Control, construct not encoding a proliferative cytokine; sTRSV Ribozyme, construct encoding a non-switch hammerhead ribozyme. (B) GFP expression levels are reported for multiple-copy L2bulge9 regulatory systems at various theophylline concentrations. Fluorescence values were normalized as described in Figure 3.2. Values are mean ± s.d. from at least two replicate samples. Fluorescence and viability measurements yielded consistent results, thus validating the use of a fusion transgene as the regulatory target.

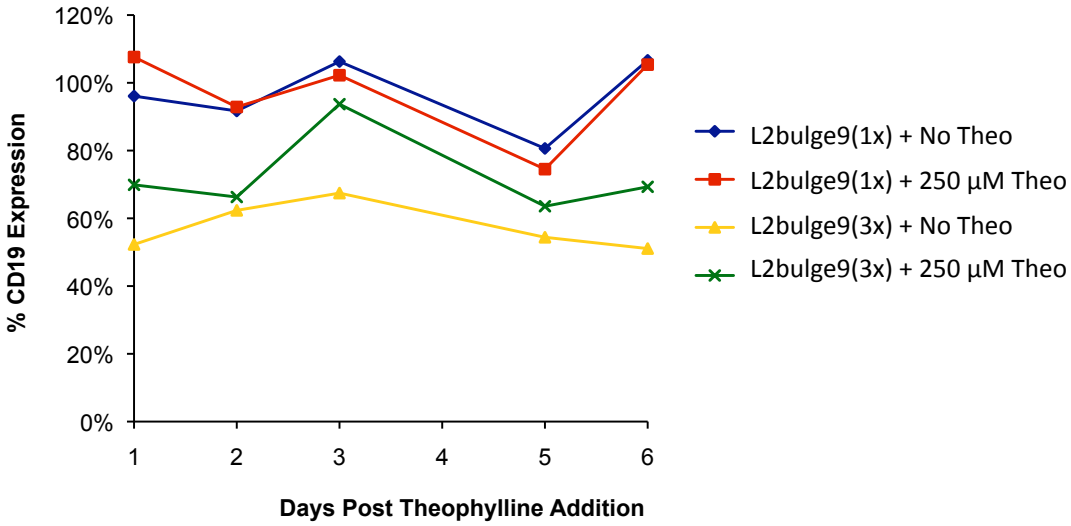

Supplementary Figure 3.2. Stable cell lines expressing multiple ribozyme switches exhibit lowered basal level and increased switch dynamic range. Stable integrants were selected by fluorescence-based cell sorting for $CD19^{+}$ populations. Bulk-sorted cells were cultured either with or without 250 µM theophylline for six days and CD19 expression levels were monitored by staining with PE-conjugated CD19 antibodies. Although bulk cell lines stably expressing the single-copy ribozyme switch system did not exhibit significant increases in gene expression in response to 250 µM theophylline, individual clones that exhibited low basal expression levels and significant theophylline-responsive increases in expression were successfully isolated from this bulk population (see Supplementary Figure 3.3).

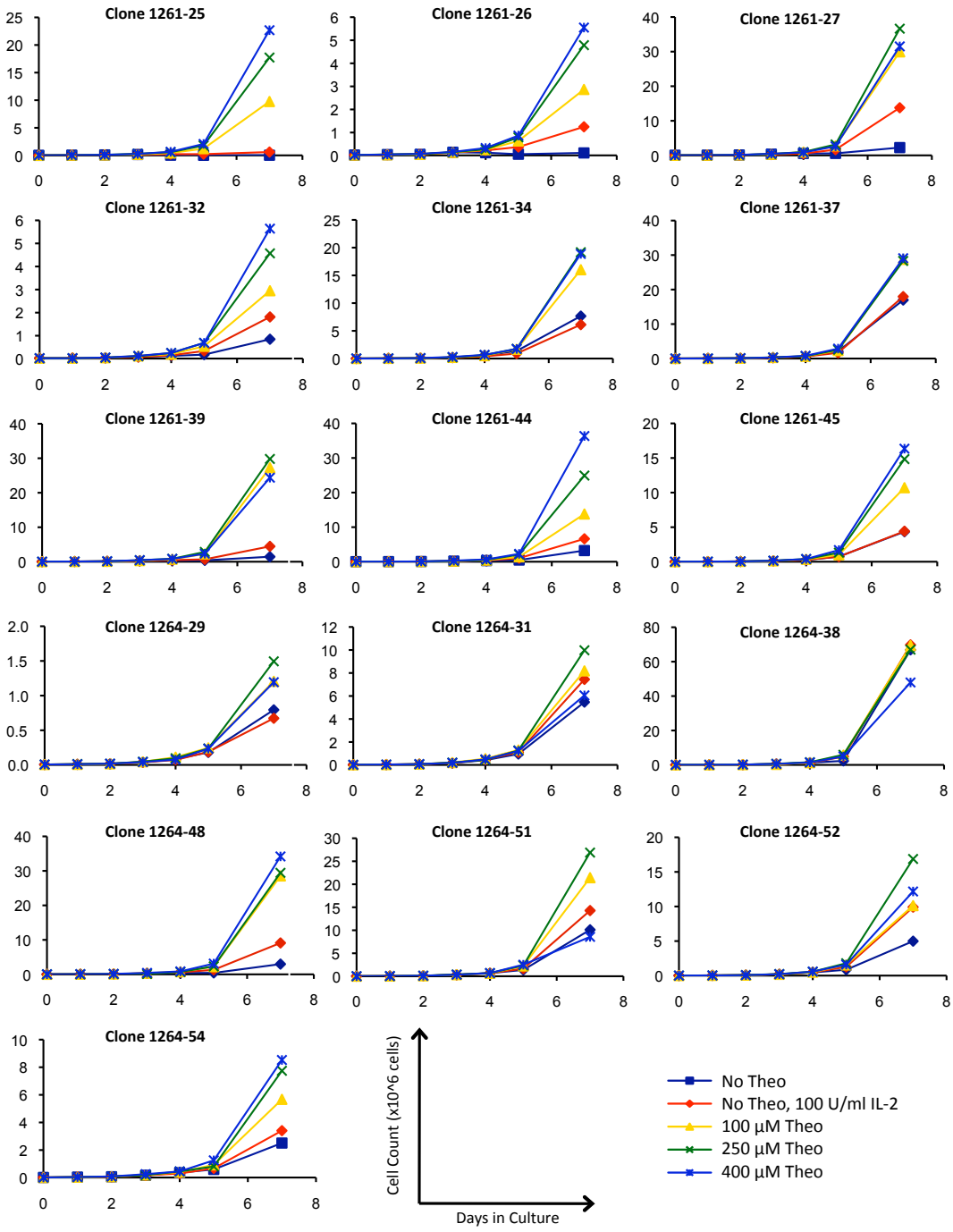

Supplementary Figure 3.3. Clonal CTLL-2 cell lines stably expressing engineered ribozyme switch systems exhibit effective theophylline-responsive growth regulation. The cell lines were cultured at various theophylline concentrations, and cell growth was monitored by counting viable cells. Clones indicated as 1261-xx stably express *cd19-tk-il15*-L2bulge9(1x). Clone 1264-xx stably expresses *cd19-tk-il15*-L2bulge9(3x). Growth behaviors differ from clone to clone, as would be expected from non-site-specific integration of the transgene into the host chromosomes. Theophylline-responsive increase in cell growth is evident in 15 of the 16 tested clones, and the growth enhancement is statistically significant for the sample set (P = 0.0150, 0.0011, 0.0013 for 100 µM, 250 µM, and 400 µM, respectively, by Whitney-Mann U test).

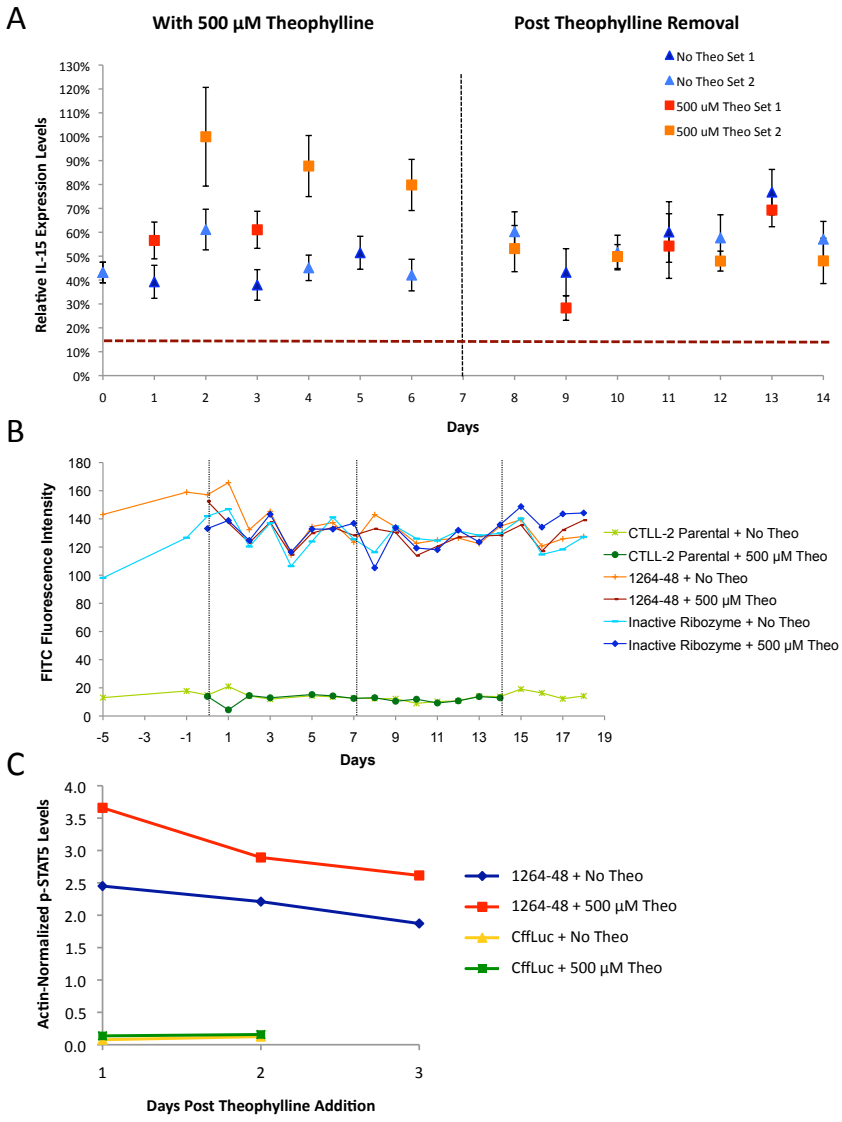

Supplementary Figure 3.4. Cells stably expressing the T-cell proliferation regulatory system exhibit theophylline-responsive increases in IL-15 transcription and signal transduction through the JAK-STAT pathway. (A) Relative IL-15 mRNA levels are elevated in the presence of theophylline and return to basal levels upon theophylline removal. qRT-PCR was performed on mRNA extracted from a CTLL-2 cell line stably expressing *cd19-tk-il15*-L2bulge9(3x) (clone 1264-48). IL-15 expression levels were normalized to expression levels of the housekeeping gene *hprt1*, and relative IL-15 expression levels were obtained by normalizing to the inactive ribozyme control. The highest expression level was set to 100%. Reported values are mean ± s.d. from three replicate samples. Samples shown in this figure were collected from the same cultures as described in Figure 3.6B. Red dashed line indicates background signal from a cell line without a CD19 expression construct. (B) Staining with FITC-conjugated IL-15 antibodies shows no ribozyme-mediated knockdown of intracellular IL-15 protein levels. (C) Western blot analysis was performed on protein extracts from CTLL-2 cell lines for p-STAT5. p-STAT5 levels were normalized to that of β-actin. The 1264-48 cell line, which stably expresses *cd19-tk-il15*-L2bulge9(3x), shows increased p-STAT levels in response to theophylline, indicating an increase in IL-15 signaling. The CffLuc cell line, which lacks the ribozyme switch system, serves as a negative control and verifies that theophylline does not nonspecifically activate the JAK-STAT pathway. The CffLuc cell line cannot survive beyond two days without exogenous IL-2, further demonstrating that autocrine growth cytokine production is necessary for sustaining CTLL-2 survival and proliferation in the absence of exogenous cytokine supplies.

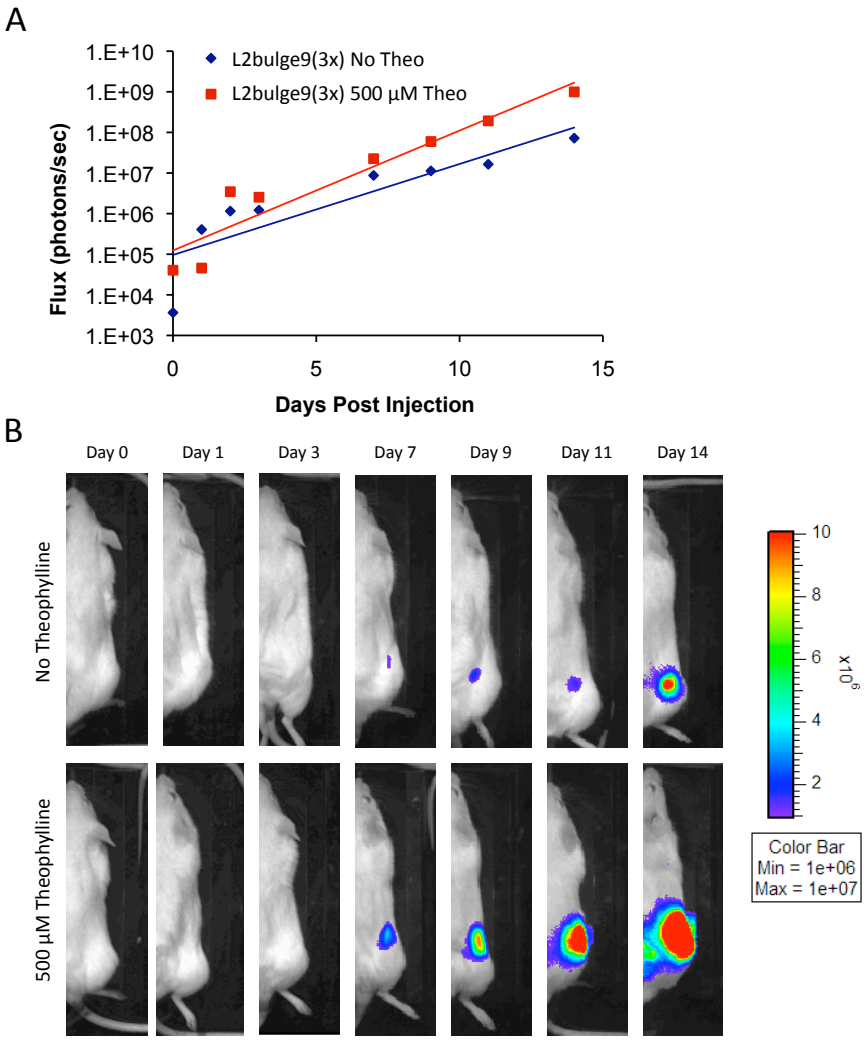

Supplementary Figure 3.5. The clonal cell line 1264-48 exhibits accelerated T-cell proliferation in response to small-molecule input. (A) Total luciferase signal flux measurements collected over a 14-day period were fitted to exponential curves and used to calculate the *in vivo* growth rates of injected cells. (B) Images of clone 1264-48 over time. The day of imaging after injection of the stable cell line is indicated.

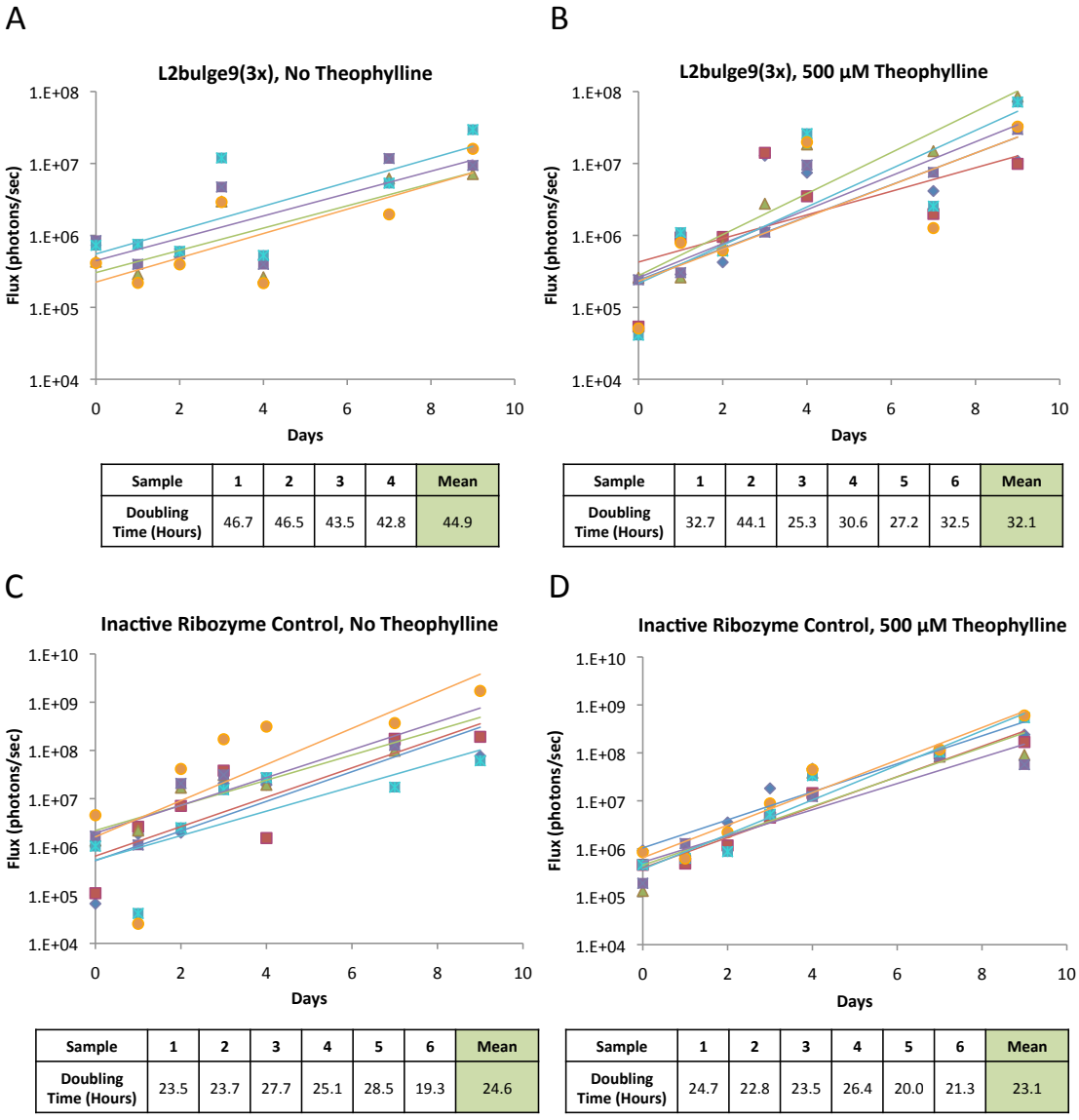

Sample	1	2	3	4	Mean
Doubling Time (Hours)	46.7	46.5	43.5	42.8	44.9

Sample	1	2	3	4	5	6	Mean
Doubling Time (Hours)	32.7	44.1	25.3	30.6	27.2	32.5	32.1

Sample	1	2	3	4	5	6	Mean
Doubling Time (Hours)	23.5	23.7	27.7	25.1	28.5	19.3	24.6

Sample	1	2	3	4	5	6	Mean
Doubling Time (Hours)	24.7	22.8	23.5	26.4	20.0	21.3	23.1

Supplementary Figure 3.6. A clonal cell line stably expressing a functional ribozyme-based regulatory system exhibits theophylline-responsive increases in *in vivo* growth rate. Total luciferase signal flux measurements collected over a 9-day period from replicate mice were fitted to exponential curves and used to calculate the *in vivo* growth rate of the injected cells. (A, B) Clone 1264-48 injected in the absence (A) or presence (B) of 500 µM theophylline. (C, D) Inactive ribozyme control cells injected in the absence (C) or presence (D) of 500 µM theophylline. Results indicate a 40% increase in the growth rate of clone 1264-48 in response to 500 µM theophylline and no statistically significant difference in the growth rate of the inactive ribozyme control in the presence and absence of theophylline.

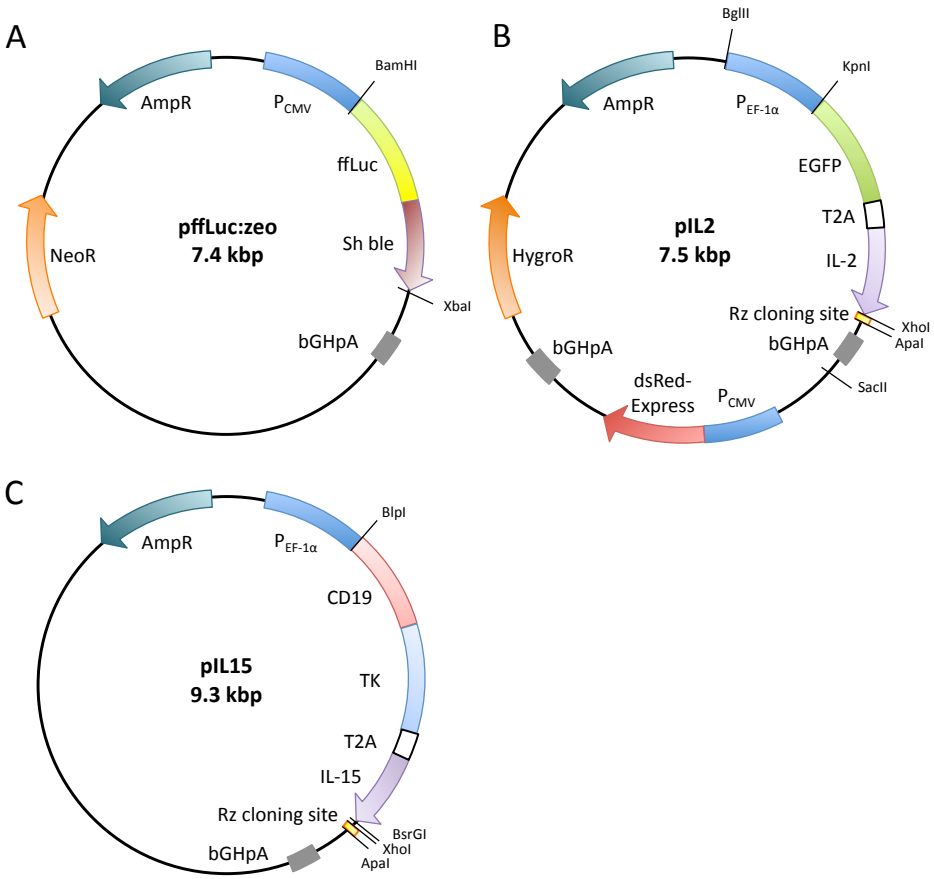

Supplementary Figure 3.7. Plasmid maps of T-cell proliferation constructs. (A) pffLuc:zeo was used in generating T cell lines stably expressing firefly luciferase for *in vivo* imaging; (B, C) pIL2 and pIL15 are the base T-cell proliferation expression constructs into which the ribozyme-based regulatory devices are inserted.

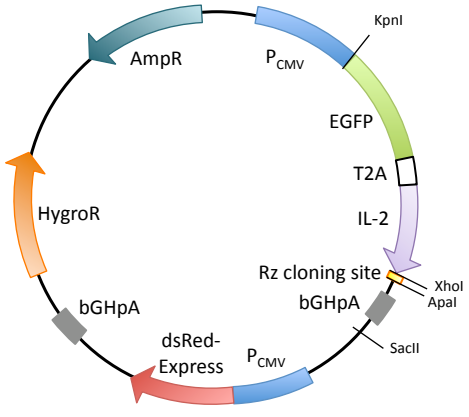

Supplementary Figure 3.8. Plasmid map of T-cell proliferation constructs expressed from a CMV promoter. One CMV promoter drives the expression of the regulatory target transgene, *egfp-t2a-il2*, with ribozyme switch devices inserted in the transgene's 3' UTR. A second CMV promoter drives the expression of *dsred-express*, which serves as a transfection marker. The plasmid also encodes for hygromycin resistance, which allows for antibiotic-based selection of stable integrants.

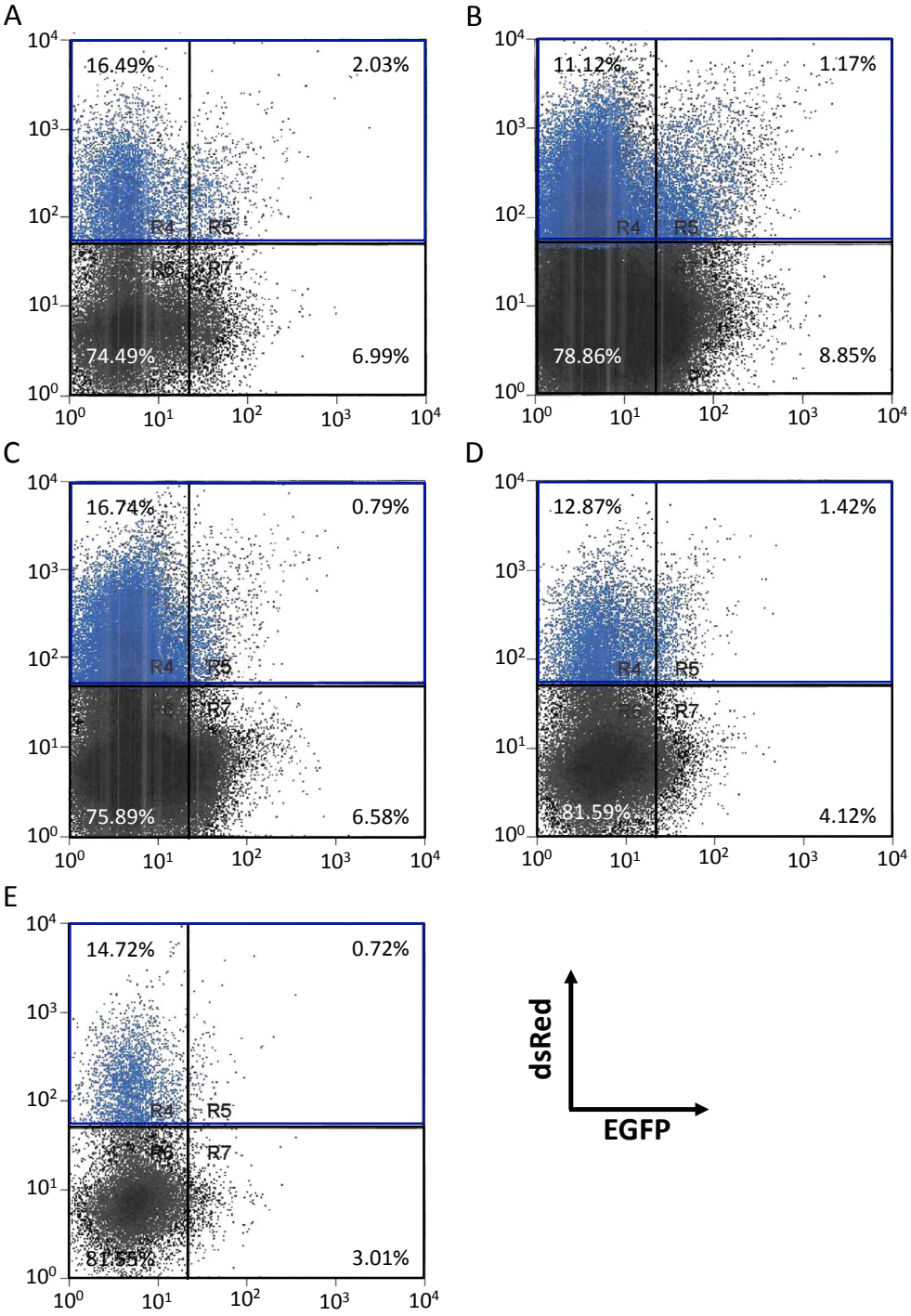

Supplementary Figure 3.9. Stable integrants show partial integration and/or CMV promoter silencing. Cells transfected with constructs based on the plasmid shown in Supplementary Figure 3.8 were analyzed and sorted by FACS 19 days after electroporation. All five cell lines showed significant single-positive populations prior to the sort, indicating that one of the two CMV promoters in the construct was either not integrated into the genome or silenced after integration. FACS data are shown for (A) inactive ribozyme control, (B) L2bulge9(1x), (C) L2bulge9(2x), (D) L2bulge9(3x), and (E) L2bulge9(4x). Percentages shown indicate population distribution in the four quadrants delineated by black lines. The blue gate marks the collection window; blue data points indicate collected dsRed^{+} cells.

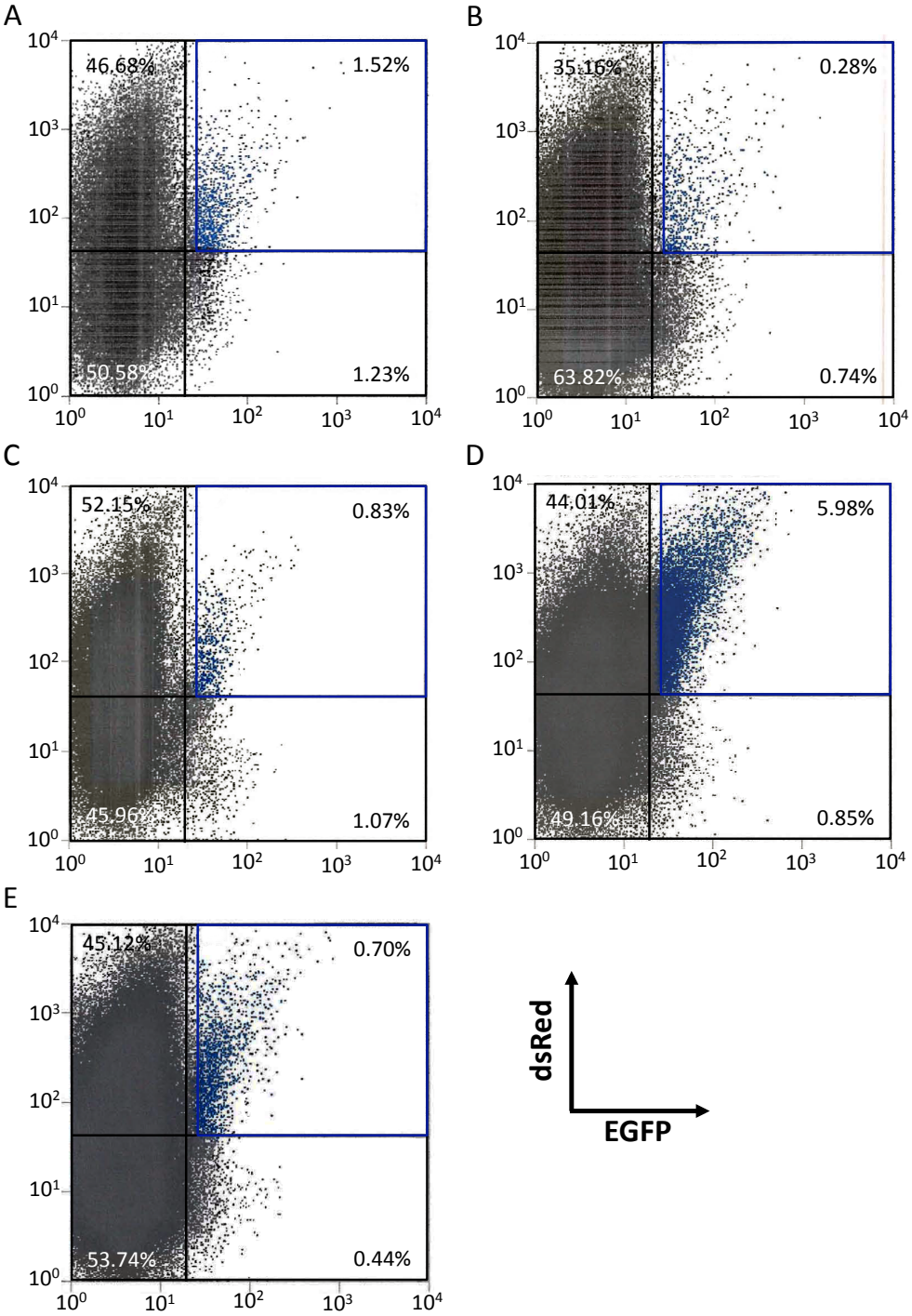

Supplementary Figure 3.10. Sorted stable integrants show CMV promoter silencing. Cells previously sorted for dsRed^{+} expression were analyzed and sorted again by FACS 38 days after electroporation. All five cell lines showed significant dsRed^{-} populations, indicating extensive CMV promoter silencing since the first sort. FACS data are shown for (A) inactive ribozyme control, (B) L2bulge9(1x), (C) L2bulge9(2x), (D) L2bulge9(3x), and (E) L2bulge9(4x). Percentages shown indicate population distribution in the four quadrants delineated by black lines. The blue gate marks the collection window; blue data points indicate collected dsRed^{+}/EGFP^{+} cells.

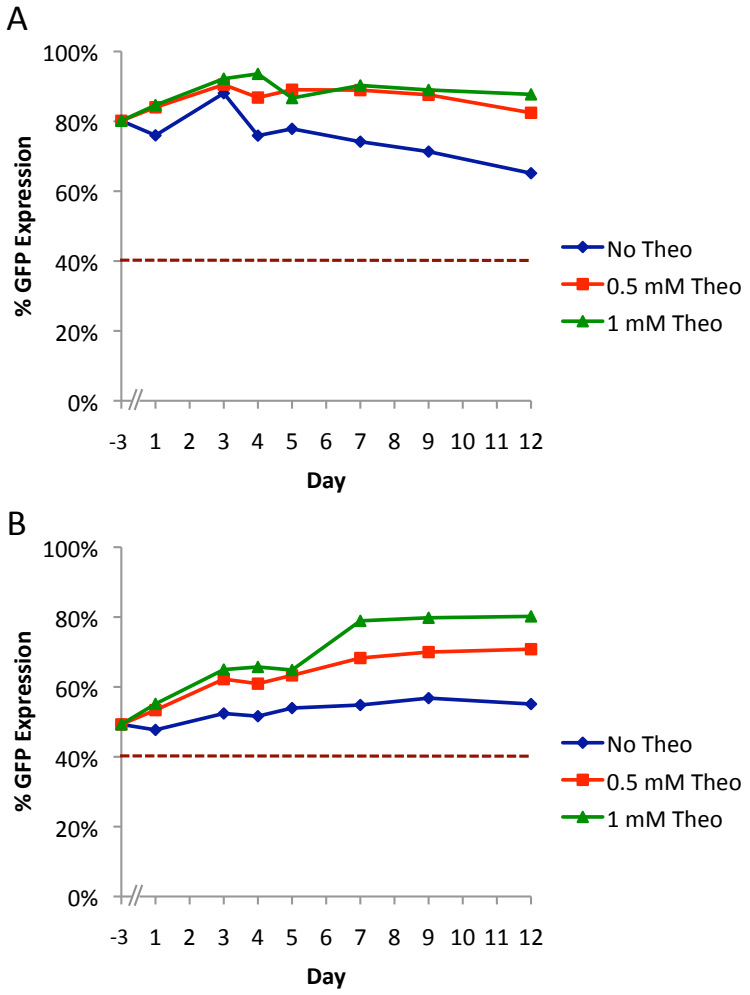

Supplementary Figure 3.11. Bulk cell lines stably expressing ribozyme switch systems exhibit gene expression regulation in response to small-molecule input. CTLL-2 cells stably expressing (A) two copies or (B) four copies of the theophylline-responsive L2bulge9 switch demonstrate rapid, dose-dependent upregulation of gene expression in response to theophylline addition. Red dashed line indicates background autofluorescence level of a cell line that does not express GFP (CffLuc).

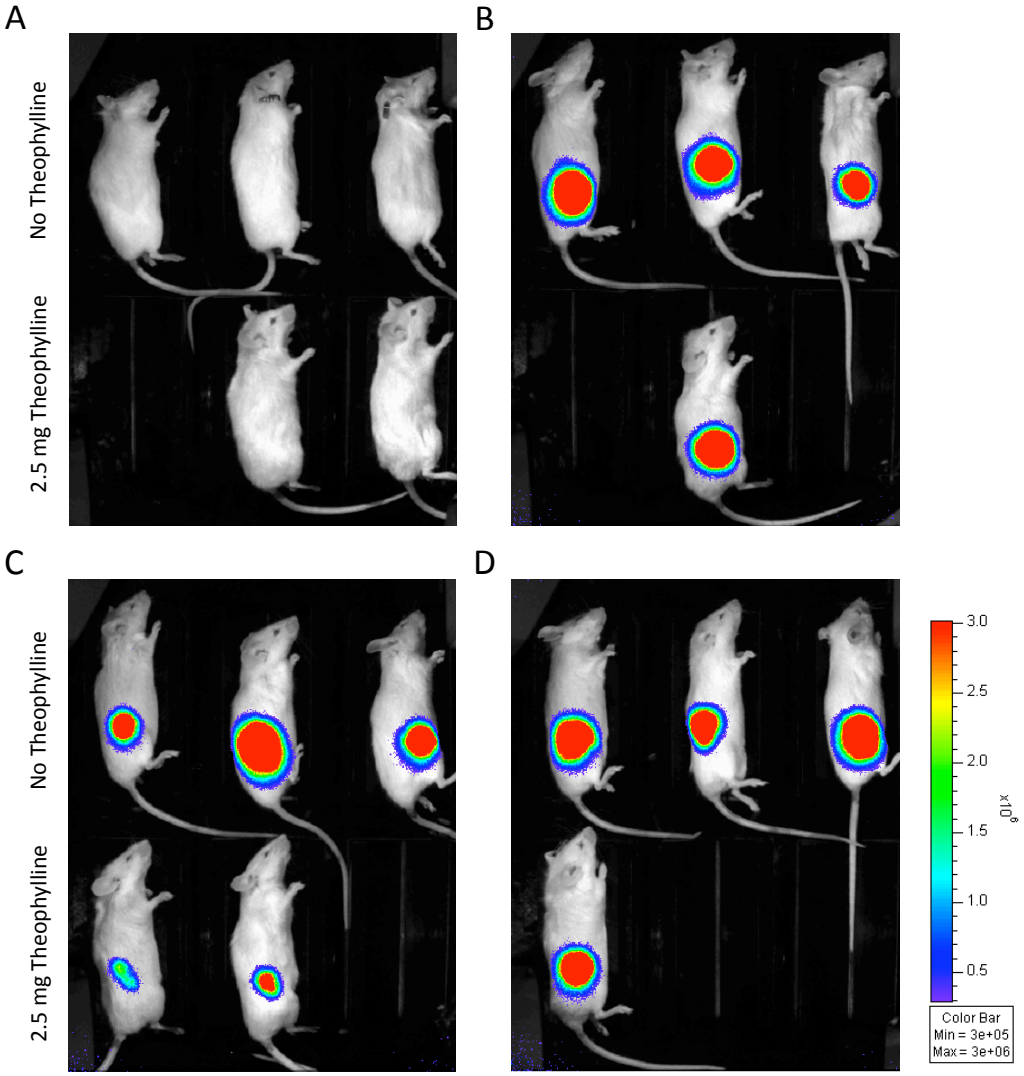

Supplementary Figure 3.12. Bulk cell lines stably expressing ribozyme switch systems show excessively high basal growth levels *in vivo*. Clonal cell lines were injected into the right flanks of mice and monitored by biophotonic imaging of luciferase signals. Two systemic injections of 2.5 mg theophylline were given to half of the animal subjects on the day of cell injections. Three animals were included for each experimental condition; missing subjects died on the first day, possibly due to theophylline toxicity. Images are shown for day 10 after injection. All cell lines except the negative control showed engraftment *in vivo* regardless of theophylline availability, indicating the OFF-state expression level was too high to prevent T-cell proliferation. Images are shown for the following injected cell lines: (A) CffLuc (no IL-2 negative control), (B) Inactive ribozyme (positive control), (C) L2bulge9(2x), and (D) L2bulge9(4x).

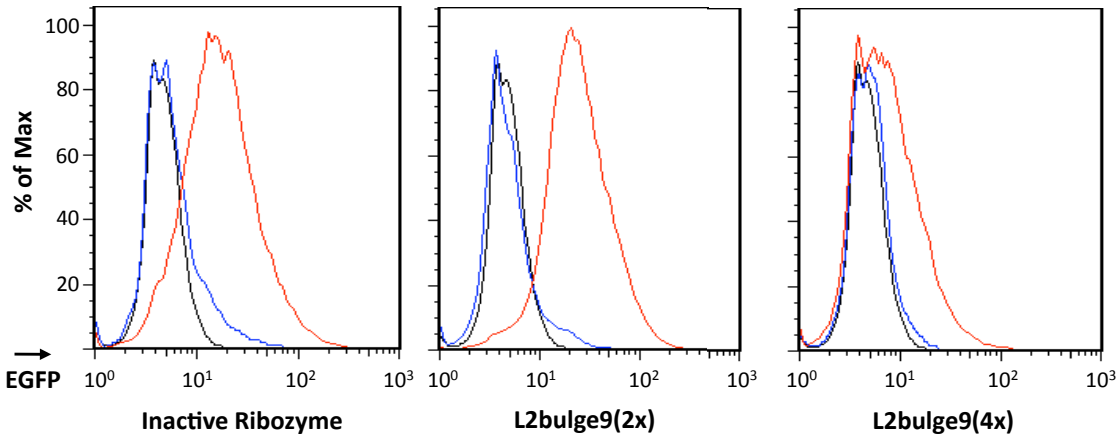

Supplementary Figure 3.13. Bulk cell lines stably expressing ribozyme switch systems are selected for high expression levels *in vivo*. Engrafted tumors were excised from the animal subjects shown in Supplementary Figure 3.12. Extracted tumor cells were analyzed for EGFP expression by flow cytometry and showed elevated expression levels compared to corresponding cell lines that had been continuously cultured *ex vivo*. Black, CffLuc (negative control); blue, *ex vivo* cultured cells; red, extracted tumor cells.

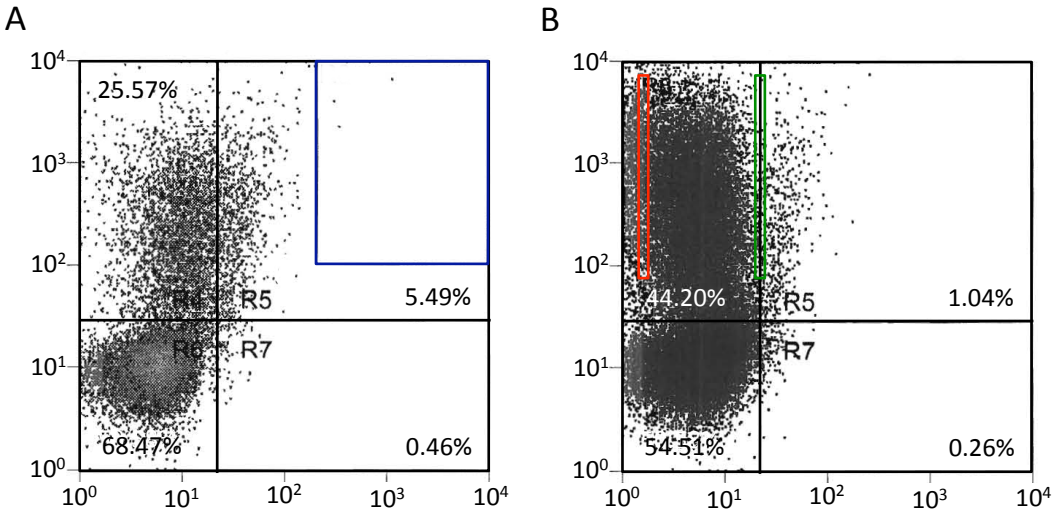

Supplementary Figure 3.14. Sorted stable integrants show continuous CMV promoter silencing. Cells previously sorted for dsRed^{+}/EGFP^{+} expression were analyzed and sorted again by FACS 109 days after electroporation. Cell lines expressing (A) the inactive ribozyme and (B) L2bulge9(4x) both show over 50% dsRed^{-}/EGFP^{-} populations, indicating extensive CMV promoter silencing since the previous sort. Percentages shown indicate population distribution in the four quadrants delineated by black lines. The blue gate marks the dsRed^{+}/EGFP^{high} collection window for the inactive ribozyme cell line. Red and green gates mark the dsRed^{+}/EGFP^{-} and dsRed^{+}/EGFP^{low} collection windows, respectively, for the L2bulge9(4x) cell line.

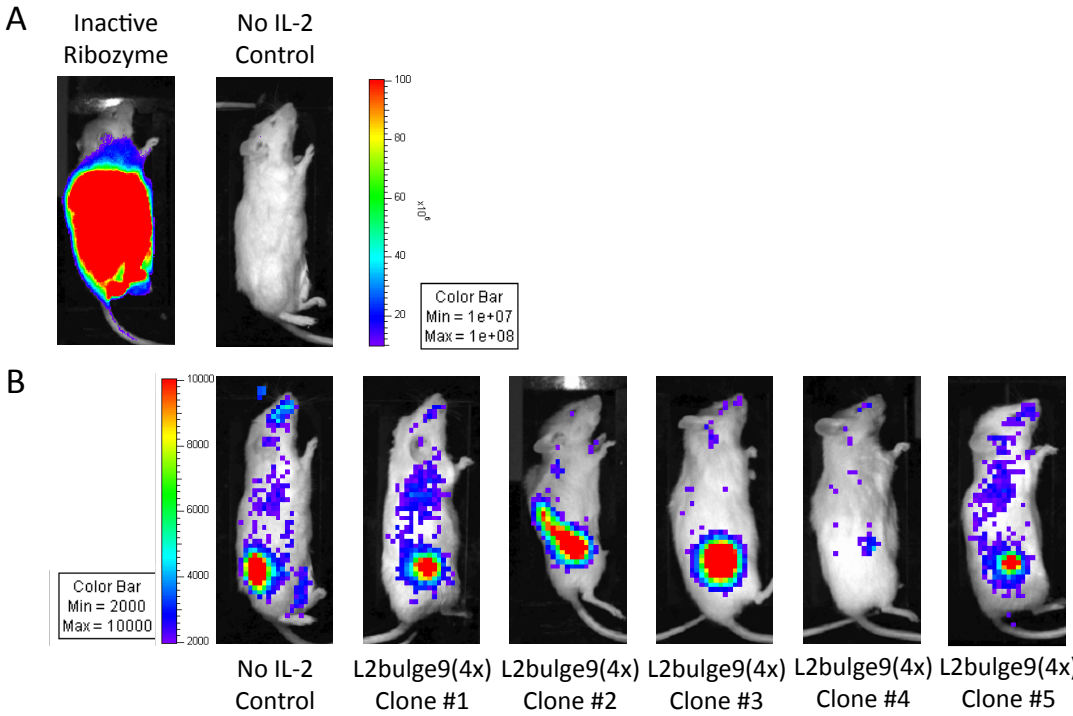

Supplementary Figure 3.15. Clonal cell lines stably expressing ribozyme switch systems show stringent OFF-state expression control *in vivo*. Five clonal cell lines expressing L2bulge9(4x) were injected into the right flanks of mice in the absence of theophylline. A clonal cell line expressing an inactive ribozyme and the CffLuc cell line served as the positive and negative (no IL-2) controls, respectively. Images are shown for day 19 after injection. Due to significantly different engraftment and luciferase signal levels between the positive control and the remaining samples, two image settings were used. Signal intensity for each image setting is indicated by the color bars to the side of each panel. (A) Small-binning image for high-intensity samples. (B) Large-binning image for low-intensity samples. The negative control was included in both image settings to allow comparison between groups. None of the L2bulge9(4x) cell lines showed cell expansion beyond background levels, indicating tight expression control in the OFF state .

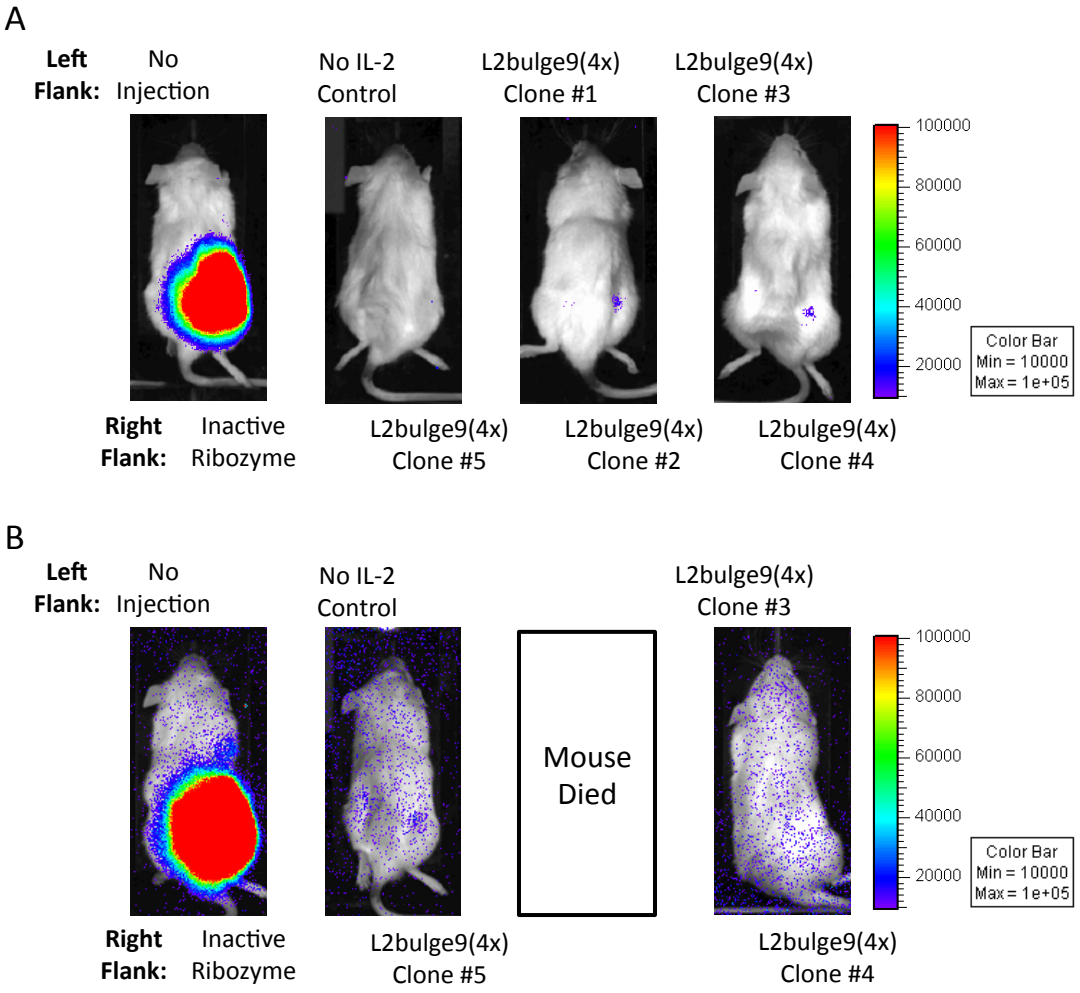

Supplementary Figure 3.16. Clonal cell lines stably expressing ribozyme switch systems lack sufficiently high ON-state expression levels to sustain proliferation *in vivo*. Five clonal cell lines expressing L2bulge9(4x) were injected into the flanks of mice in the presence of 200 μM theophylline. A clonal cell line expressing an inactive ribozyme and the CffLuc cell line served as the positive and negative (no IL-2) controls, respectively. Images are shown for (A) day 4 and (B) day 8 after injection. Mice in the same figure panel were imaged simultaneously. Noise seen in panel B is the effect of signal saturation from the inactive ribozyme control sample.

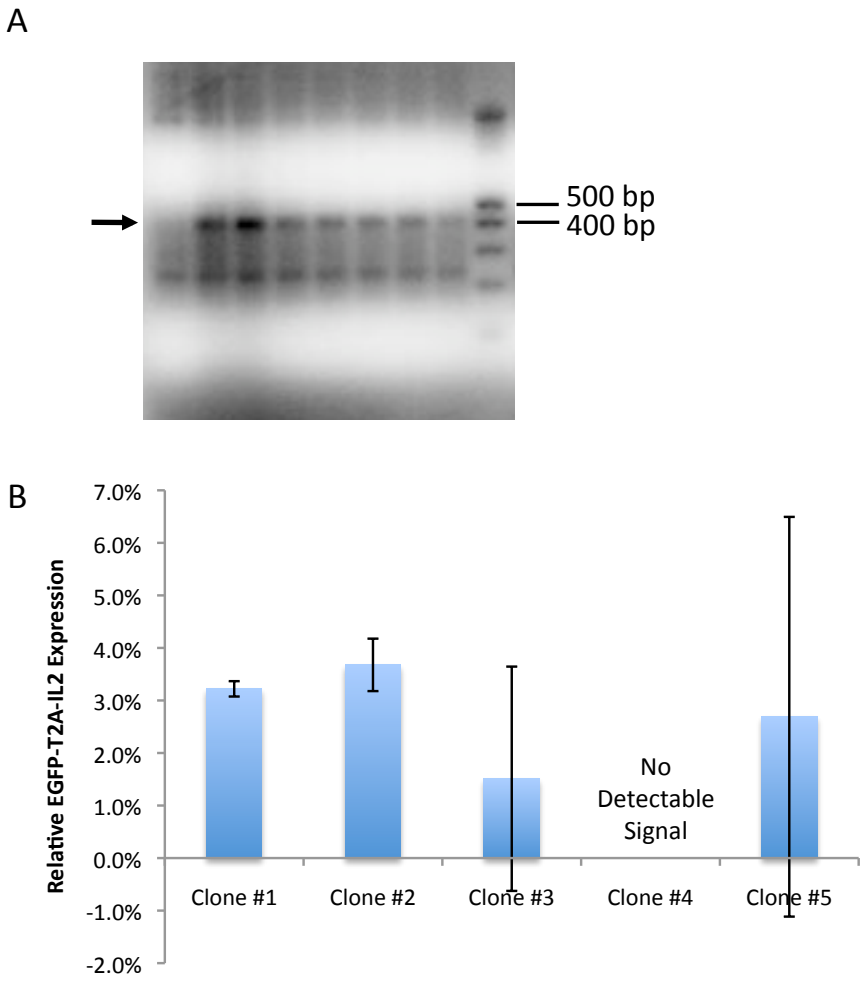

Supplementary Figure 3.17. The *egfp-t2a-il2* transgene is stably integrated but expressed at low levels in clonal cell lines. (A) Genomic PCR confirms stable integration of the *egfp-t2a-il2* transgene in all the clonal cell lines tested in the animal study shown in Supplementary Figure 3.16. Genomic DNA was extracted from clonal cell lines, and PCR reactions using forward and reverse primers that anneal to *egfp* and *il2*, respectively, yielded the expected product band (404 bp; marked by arrow). Lane 1, CffLuc (negative control); lane 2, CTLL-2 cell line stably expressing *egfp-t2a-il2* with no ribozyme device attached; lane 3, inactive ribozyme control; lanes 4–8, L2bulge9(4x) Clone #1-#5; lane 9, 100 bp DNA ladder. (B) Clonal cell lines stably integrated with ribozyme switch systems show low EGFP-T2A-IL2 mRNA levels. qRT-PCR was performed on total RNA extracted from clonal cell lines. EGFP-T2A-IL2 expression levels were normalized to expression levels of the housekeeping gene *gapdh*, and relative EGFP-T2A-IL2 expression levels were obtained by normalizing to the inactive ribozyme control. Reported values are mean ± s.d. from duplicate samples.

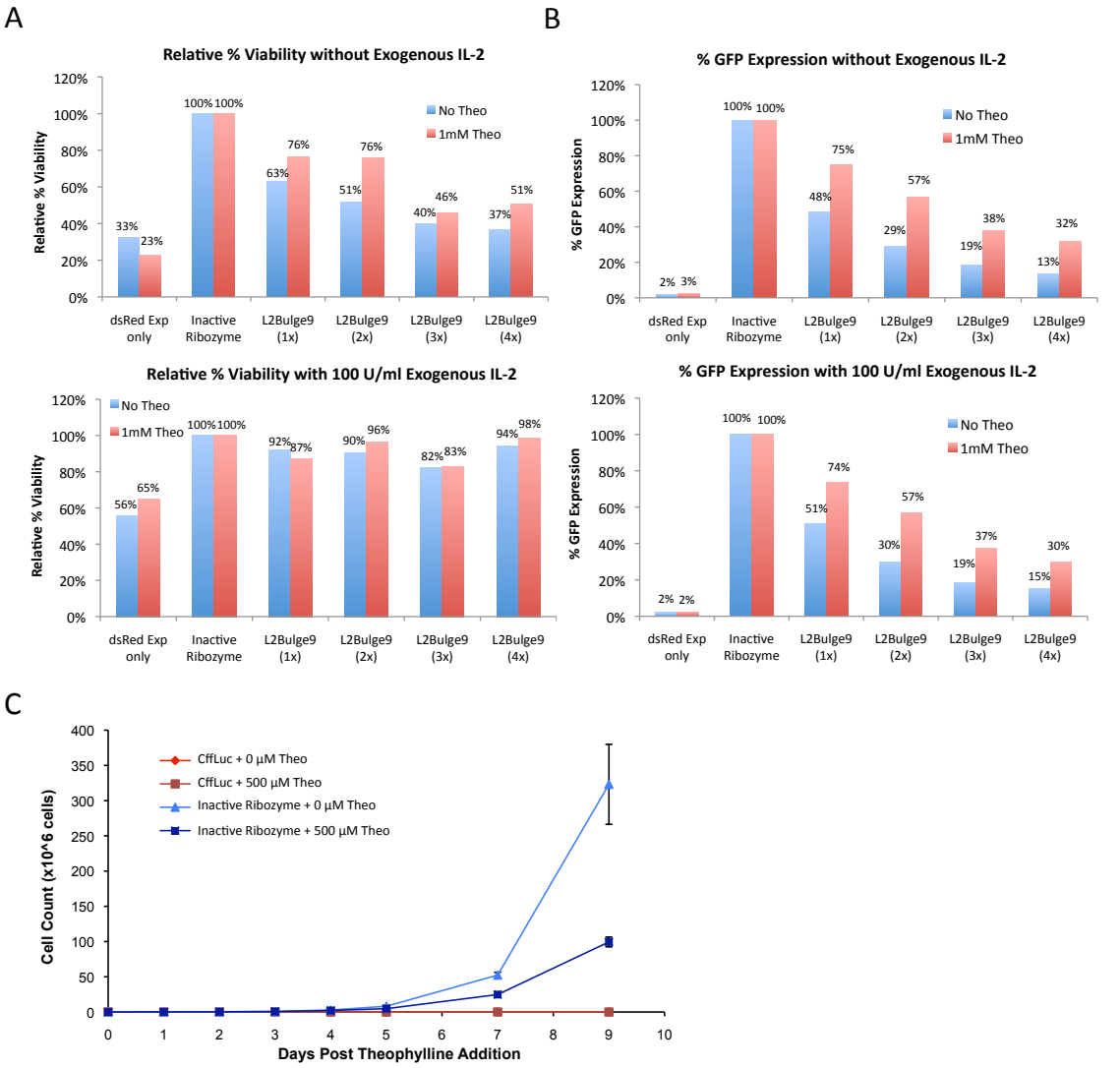

Supplementary Figure 3.18. Appropriate controls confirm that observed ligand-responsive switch activities are due to specific effects of cytokine withdrawal. (A) Relative viability of CTLL-2 cells transiently transfected with ribozyme-based regulatory systems as measured by flow cytometry. The presence of exogenous IL-2 elevates viability in all samples and abolishes the inverse correlation between viability and ribozyme switch copy number observed in the absence of exogenous IL-2. These results suggests that the reduced viability at high switch copy numbers observed in the absence of exogenous IL-2 is specifically caused by more efficient knockdown of the cytokine transgene encoded by the regulatory system and the resultant cytokine withdrawal. (B) GFP expression in CTLL-2 cells transiently transfected with ribozyme-based regulatory systems. Fluorescence values were normalized as described in Figure 3.2. The samples shown here correspond to those shown in (A). In contrast to viability behaviors shown in (A), switch activity as measured by fluorescence is unaffected by the presence of exogenous IL-2, indicating that the gene expression modulation is specific to the regulatory system. (C) Theophylline inhibits growth in CTLL-2 cells. CffLuc cells and a clonal cell line stably expressing the inactive ribozyme were cultured in the presence or absence of 500 µM theophylline without exogenous IL-2. Cell count was monitored for nine days by flow cytometry. CffLuc cells failed to expand due to lack of growth cytokines. The inactive ribozyme control, which expresses high levels of cytokine independent of theophylline, showed reduced growth in the presence of theophylline, indicating theophylline toxicity.

Chapter 4

Proliferation Control of Human Lymphocytes with Ribozyme-Based Regulatory Systems

Partially adapted, with permission, from Chen, Y.Y., Jensen, M.C., & Smolke, C.D. Genetic control of mammalian T-cell proliferation with synthetic RNA regulatory systems. *Proc Natl Acad Sci USA* **107**, 8531–8536 (2010).

Abstract

Cellular immunotherapy utilizing the adoptive transfer of antigen-specific lymphocytes has achieved clinical success in the treatment of some virus-associated malignancies and cancers, particularly metastatic melanoma. However, objective clinical response from adoptive cell therapy is strongly correlated with the persistence of transferred cells in the patient, and the ability to regulate the proliferative response of human lymphocytes is critical to the safety and efficacy of adoptive immunotherapy. We have demonstrated that ribozyme-based regulatory systems are capable of drug-responsive control over T-cell proliferation in mouse models. Here, we demonstrate the application of ribozyme-based regulatory systems to proliferation control in human lymphocytes.

Given the central importance of human cells in immunotherapy and other applications in health and medicine, the ability to characterize and optimize new RNA-based control devices directly in human cells can greatly facilitate the development of gene-regulatory systems for clinical use. The human natural killer (NK) cell line NK-92, a candidate for adoptive cell therapy, is evaluated here as a model cell line for RNA-based device development. We verify the ability to reduce gene expression by 25%—and recover 18% of the expression in response to ligand addition—with only one copy of a theophylline-responsive ribozyme ON switch in NK-92 cells. However, we also demonstrate the unsuitability of NK-92 cells as a human cellular host for the characterization and optimization of novel RNA-based regulatory systems due to the inability to execute rapid and efficient genetic manipulation in this cell line.

Primary human central memory T (T_{CM}) cells represent another class of human lymphocytes currently under intensive investigation for clinical use. Here, we describe the generation of primary human T_{CM} cells stably expressing ribozyme switch systems using protocols readily adaptable to clinical-grade manufacturing standards. Engineered T_{CM} cells are shown to express the proper surface receptors for therapeutic applications, and the cell population can be effectively controlled with the use of the thymidine kinase suicide gene. A ribozyme-based regulatory system capable of modulating the production of the proliferative cytokine interleukin-15 (IL-15) is shown to function robustly in primary human T_{CM} cells, leading to a 24% increase in cell survival and a 54% reduction in apoptosis in response to theophylline treatment in a bulk, unsorted, lentivirally transduced T_{CM} population. These results highlight the portability of ribozyme-based control devices across organisms and demonstrate the applicability of ribozyme switch systems to the regulation of functional outputs in human cells suitable for clinical applications.

Introduction

Adoptive immunotherapy is a promising method for targeted treatment of virus-associated malignancies[1-4] and various cancers[5-8]. Unlike conventional cancer treatment strategies such as chemotherapy and radiation therapy, which are characterized by substantial off-target toxicities, the adoptive transfer of antigen-specific lymphocytes can precisely deliver therapeutic payloads to targeted tumors[9, 10]. A critical task in the development of adoptive immunotherapy is the identification of suitable lymphocyte lineages and manipulation methods to generate safe and potent candidates for clinical applications. Numerous types of lymphocytes have been evaluated as therapeutic candidates with varying degrees of success[11-17]. Among these, antigen-specific $CD8^+$ T cell clones derived from T_{CM} cells[18, 19] and the established cell line NK-92[20] have shown exciting potential for clinical applications.

$CD8^+$ T cells can be derived from either naïve T cells or antigen-experienced memory T cells, the latter being divided into central memory (T_{CM}) and effector memory (T_{EM}) subsets. T_{CM} cells constitutively express CD62L and CCR7, which facilitate cellular extravasation and migration to lymph nodes. In contrast, the $CD62L^{low}/CCR7^-$ T_{EM} cells are found in both lymphoid and peripheral tissues[21]. While T_{EM} cells have been the dominant choice in early clinical studies due to their strong lytic capacity and high IFN-γ production levels, several recent studies have reported that T_{CM} cells may be superior to T_{EM} cells in both long-term persistence and anti-tumor effects[18, 22]. For instance, Riddell and colleagues showed that antigen-specific $CD8^+$ T cell clones derived from T_{CM} cells, but not from T_{EM} cells, could achieve long-term persistence and occupy

memory T cell niches in primates, suggesting T_{CM} cells as a promising candidate for adoptive T-cell therapy[19].

The transplantation of NK cells represents an alternative paradigm in cellular immunotherapy[23]. NK cells are large, granular lymphocytes whose cytotoxic activities are regulated by the balance of various activating and inhibitory signals. Recognition of non-self major histocompatibility complex (MHC) and binding to certain ligands on tumor cells can trigger the release of granzyme and perforin from NK cells[24]. Conversely, recognition of self MHC results in the inactivation of NK cells mediated by killer immunoglobulin-like receptors (KIRs)[25]. Researchers have navigated this intricate signal balance and reported graft-versus-leukemia effects with the transplantation of allogeneic NK cells into human leukocyte antigen (HLA)-mismatched hosts[26, 27]. NK-92 is an NK tumor cell line with cytotoxic activity against a wide range of cancer cells and has demonstrated efficacy against both xenografted human leukemia and malignant melanoma in SCID mouse models[20, 28, 29]. Significantly, NK-92 cells express very low levels of KIRs but retain perforin and granzyme B–mediated cytolytic activities toward cancer cells[30]. In addition, they display no cytotoxicity toward non-malignant allogeneic cells[29], making them uniquely suited for adoptive immunotherapy.

Despite the diversity of potential candidates, cellular immunotherapy is constrained by the fact that the long-term survival and cytotoxicity of lymphocytes are dependent on cytokines such as interleukin 2 (IL-2) and interleukin 15 (IL-15). For instance, primary T_{CM} cells require IL-15 to establish persistent T-cell memory *in vivo*[19, 31], and the cytotoxicity of NK-92 cells declines to approximately 10% three days after IL-2 removal[32]. As discussed in Chapters 1 and 3, the ability to integrate growth stimulatory

gene expression with tightly controlled genetic regulatory systems has the potential to greatly improve the safety and efficacy of cellular immunotherapy.

We have demonstrated T-cell proliferation control in mouse models using RNA-based regulatory systems (Chapter 3), yet the ability to generate engineered human lymphocytes with the stringent quality standards and rapid time scale required for clinical applications remains to be shown. Furthermore, although we have demonstrated that RNA-based control devices developed in yeasts can be effectively transported into mammalian cells, the ability to prototype and optimize new devices directly in human cells would allow more efficient construction of RNA-based regulatory systems suitable for applications in health and medicine. To establish a protocol for developing regulatory systems that can readily interface with clinical applications, we investigated the NK-92 cell line's suitability as a model host for the characterization and optimization of ribozyme-based switch devices. As an established cell line, NK-92 cells have the advantage of being more readily available and easily cultured compared to primary human cells. These properties, coupled with the cell line's promise as a therapeutic agent, make NK-92 cells a potentially powerful host for the development of synthetic control systems. However, our studies show that NK-92 cells are not amenable to transient transfections and that detailed characterization of device performance in this cell line requires stable integration by lentiviral transduction, which significantly increases the time and resource consumption required for device optimization and renders NK-92 cells unsuited for high-throughput developmental work. Nevertheless, we demonstrate that ribozyme switch devices are capable of gene expression knockdown in NK-92 cells,

indicating that ribozyme-based regulatory systems may be useful in the functional control of NK-92 cells as a candidate for cellular immunotherapy.

Furthermore, we examine the performance of ribozyme-based regulatory systems in primary human T_{CM} cells, which have shown promise in adoptive T-cell therapy. Here, we report drug-responsive regulation of both gene expression and cell fate in T_{CM} cells using ribozyme switch devices. We describe the generation of engineered T_{CM} cells using protocols readily adaptable to clinical-grade manufacturing practices and demonstrate the effective regulation of functional output. Although we have been unable to identify a human lymphocyte cell line suitable for rapid characterization and optimization of ribozyme-based regulatory systems, our results show that ribozyme switch devices prototyped in yeast and optimized in a mouse T-cell line are functional in both established and primary human lymphocytes. This model of developing regulatory systems in progressively more complex cellular organisms for eventual applications in human cells may inform future work on the development of synthetic RNA-based regulatory systems.

Results

Transfection Optimization in NK-92 Cell Line. Both primary lymphocytes and established cell lines have been examined as candidates for adoptive immunotherapy. While each cell type has advantages over the other, established cell lines are more readily available and easily cultured. Furthermore, established cell lines generally have higher growth rates and more stable phenotypes compared to primary cells, whose phenotypic outcome can be highly sensitive to procedural details in the isolation and *in vitro* expansion protocols[33]. For these reasons, established cell lines such as NK-92 are potentially well suited for the rapid characterization and optimization of control devices in the development of synthetic gene regulatory systems.

NK-92 cells are IL-2-dependent and are therefore not fully transformed. This cytokine dependence has limited the therapeutic efficacy of NK-92 cells, but it also presents an opportunity for engineered proliferation control using RNA-based regulatory systems. Specifically, viability as a functional output can serve as a useful tool for the evaluation of control devices. We examined the sensitivity of NK-92 cells to various small-molecule ligands and verified that this cell line is equally or more robust than CTLL-2 cells in response to almost all of the ligands tested (Appendix 2), supporting NK-92 as a potentially useful host for the development of ligand-responsive regulatory systems. To examine the portability of ribozyme-based regulatory systems to NK-92 cells, we attempted to characterize previously described constructs (pIL2-based plasmids, Chapter 3) by transient transfection. However, NK cells are known to be highly resistant to transfection[34], and the NK-92 cell line also proved intransigent to commercially available electroporation protocols purportedly optimized for NK-92 transfection.

Electroporation of GFP-encoding plasmids into NK-92 cells was performed using the Amaxa Nucleofector Kit R following manufacturer's protocols, and results show essentially zero transfection efficiency (as defined by the percent of all viable cells that are fluorescent above background levels) for all plasmids tested except for the pmaxGFP control plasmid supplied by the electroporation kit manufacturer Amaxa (Figure 4.1).

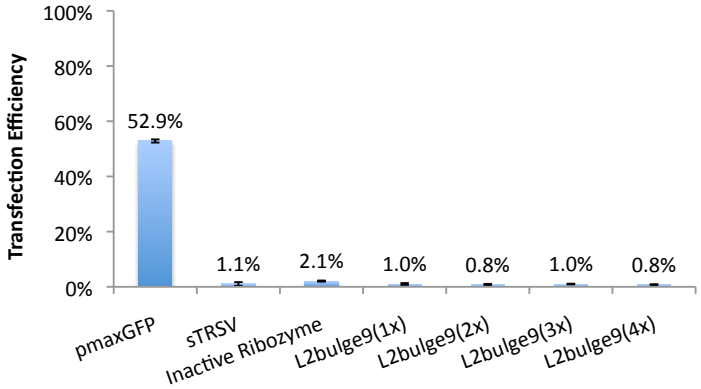

Figure 4.1. NK-92 cells cannot be effectively transfected by electroporation with DNA plasmids based on the pIL2 expression vector. NK-92 cells were transfected using an Amaxa Nucleofector II and the reagent kit and electroporation protocol optimized for NK-92 cells. The control plasmid, pmaxGFP, supplied by Amaxa was included as a positive control. pIL2-based plasmids expressing ribozyme constructs in the 3' UTR of the *egfp-t2a-il2* fusion gene from an EF1α promoter failed to transfect NK-92 cells. All plasmids other than pmaxGFP were prepared from DH10B cells using the Promega Wizard Plus SV Miniprep kit. Transfection efficiency was measured by the percent of total viable cells that are fluorescent. Reported values are the mean of duplicate samples ± s.d.

Several factors may have contributed to the observed difference in transfection efficiencies. First, expression of the reporter construct in pmaxGFP is driven by the cytomegalovirus (CMV) promoter while expression from the pIL2-based plasmids is driven by the elongation factor one alpha (EF1α) promoter. The two promoters exhibit different strengths in different cell types[35, 36] and may have caused the disparate transfection efficiencies observed in NK-92 cells. Second, the pmaxGFP plasmid was supplied by Amaxa and was therefore prepared separately from the other plasmids tested. Differences in plasmid purification methods may have affected transfection efficiencies. Third, the fluorescent protein encoded by pmaxGFP is derived from the copepod

Pontellina plumata and has significantly higher fluorescence intensity compared to the EGFP-T2A-IL2 fusion protein encoded by the other plasmids presented in Figures 4.1 (see Supplementary Text 3.1 and Supplementary Figure 4.1 for fluorophore comparisons). The relatively weak intensity of the fusion protein may have contributed to the low transfection efficiencies observed from plasmids encoding this fluorescent reporter. Finally, the pmaxGFP vector may possess yet-unidentified properties that enhance the expression of its encoded transgene. We performed additional electroporation studies to examine each of these factors.

To evaluate the effect of promoter strength, we inserted the *egfp-t2a-il2* fusion transgene into pcDNA3.1(+) and pcDNA5/FRT—two of the most commonly used mammalian expression vectors with the same CMV promoter as the pmaxGFP plasmid—and compared them against pmaxGFP. Results indicate that while pmaxGFP consistently achieves high transfection efficiency, the pcDNA3.1(+)- and pcDNA5/FRT-based plasmids are ineffective in transfecting NK-92 cells, suggesting that promoter strength is not the sole contributor to transfection efficiency in this cell line (Figure 4.2).

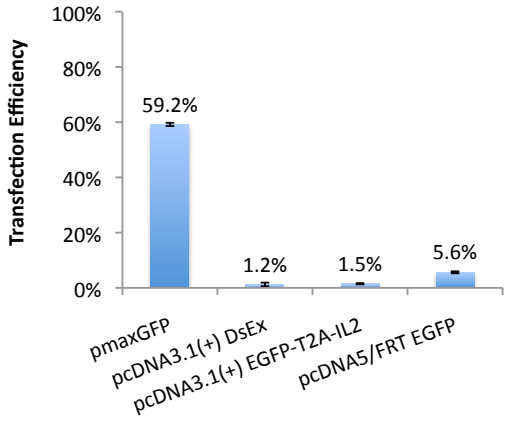

Figure 4.2. NK-92 cells cannot be effectively transfected by electroporation with DNA plasmids based on the pcDNA3.1(+) and pcDNA5/FRT expression vectors. NK-92 cells were transfected as described in Figure 4.1. pcDNA3.1(+)- and pcDNA5/FRT-based plasmids expressing dsRed-Express (DsEx), EGFP-T2A-IL2, or EGFP alone from a CMV promoter were ineffective at transfecting NK-92 cells. All plasmids other than pmaxGFP were prepared from DH10B cells using the Promega Wizard Plus SV Miniprep kit. Data are reported as described in Figure 4.1.

We next investigated whether plasmid preparation methods affect transfection efficiency. The pmaxGFP plasmid was transformed into two electrocompetent *Escherichia coli* strains, DH10B and DH5α, and plasmids were prepared from overnight liquid cultures using three different commercially available plasmid purification kits (Promega Wizard Plus SV Miniprep, Promega Pure Yield Miniprep, and Qiagen EndoFree Maxiprep). Results show that transfection efficiency is dependent on both the bacterial cell strain and the plasmid preparation method used, with DH10B and the Qiagen EndoFree Maxiprep kit being the optimum combination among those tested (Figure 4.3A). However, a pcDNA3.1(+)-based plasmid expressing the EGFP-T2A-IL2 fusion protein prepared from DH10B cells using the Qiagen kit still failed to transfect NK-92 cells (Figure 4.3B), indicating that additional requirements must be met to achieve efficient transfection.

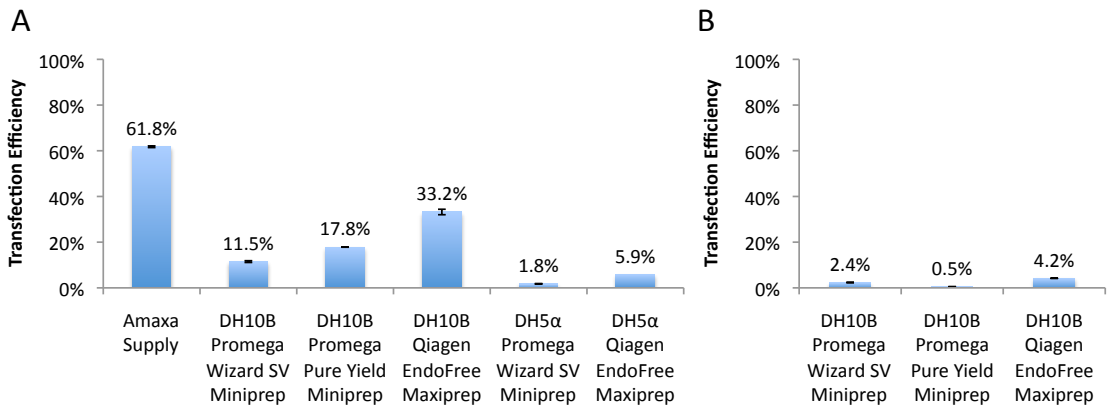

Figure 4.3. Appropriate bacterial strain and purification method used to prepare DNA plasmids are necessary but not sufficient for achieving high transfection efficiency in NK-92 cells. (A) The pmaxGFP plasmid was transformed into both DH10B and DH5α strains of *E. coli* and plasmids were purified from overnight liquid cultures using the Promega Wizard Plus SV Miniprep kit, the Promega Pure Yield Miniprep kit, or the Qiagen EndoFree Maxiprep kit. Plasmids purified from DH10B cells using the Qiagen kit showed the highest transfection efficiency among test samples but were still less efficient than control plasmids supplied directly by Amaxa. (B) A pcDNA3.1(+)-based plasmid expressing *egfp-t2a-il2* from a CMV promoter was unable to achieve high transfection efficiency regardless of the plasmid purification methods used. Transfection efficiency values are reported as in Figure 4.1.

We next investigated whether a stronger fluorophore expressed from the pcDNA3.1(+) vector could achieve higher efficiencies. As shown in Figure 4.2, electroporation with a pcDNA3.1(+)-based plasmid encoding the weak reporter EGFP-T2A-IL2 failed to generate any appreciable fluorescent population. In contrast, cells electroporated with a pcDNA3.1(+)-based plasmid encoding a stronger reporter, EGFP alone, showed a 19% $EGFP^+$ population (Figure 4.4A), suggesting the low percent $EGFP^+$ seen with previously tested plasmids could be artificially low due to weak fluorescence intensity rather than low transfection efficiencies. These results also indicate that NK-92 cells may exhibit lower expression levels overall compared to cell lines such as CTLL-2 and HEK, thus requiring stronger fluorophores for effective signal detection by flow cytometry.

In contrast to the pcDNA3.1(+)-based plasmid, the pcDNA5/FRT-based plasmid expressing EGFP showed significantly lower transfection efficiency (7%) and fluorescence intensity (Figure 4.4A, B), indicating that a strong fluorophore alone is insufficient to achieve high transgene expression in NK-92 cells. We hypothesized that the pmaxGFP plasmid backbone has unique properties that enhance the expression of transgenes encoded by this plasmid. To verify, we replaced the maxGFP reporter in pmaxGFP with the weaker EGFP-T2A-IL2 fusion protein to create the "pmaxGFP EGFP-T2A-IL2" construct and measured both transfection efficiency and fluorescence intensity from transiently transfected samples. Results show that while EGFP-T2A-IL2 has a lower fluorescence intensity compared to both maxGFP and EGFP as expected (Figure 4.4B), pmaxGFP EGFP-T2A-IL2 achieved higher transfection efficiency (33.2%, Figure 4.4A) compared to pcDNA3.1(+)-based plasmids expressing either EGFP-T2A-

IL2 (1.5%, Figure 4.2) or EGFP (18.6%, Figure 4.4A). These results suggest that the vector backbone has a stronger influence over transfection efficiency than the specific protein being expressed. It should be noted that the EGFP-T2A-IL2 fusion protein yielded the lowest intensity among all the samples shown in Figure 4.4 despite having the second largest GFP^+ population, indicating that the transfection efficiency measured is not completely dependent on fluorophore strength. However, fluorescence intensity is affected by transfection efficiency, as indicated by the fact that the pcDNA5/FRT EGFP construct showed markedly lower intensity compared to the pcDNA3.1(+) EGFP construct despite having the same fluorophore as a reporter protein (Figure 4.4B).

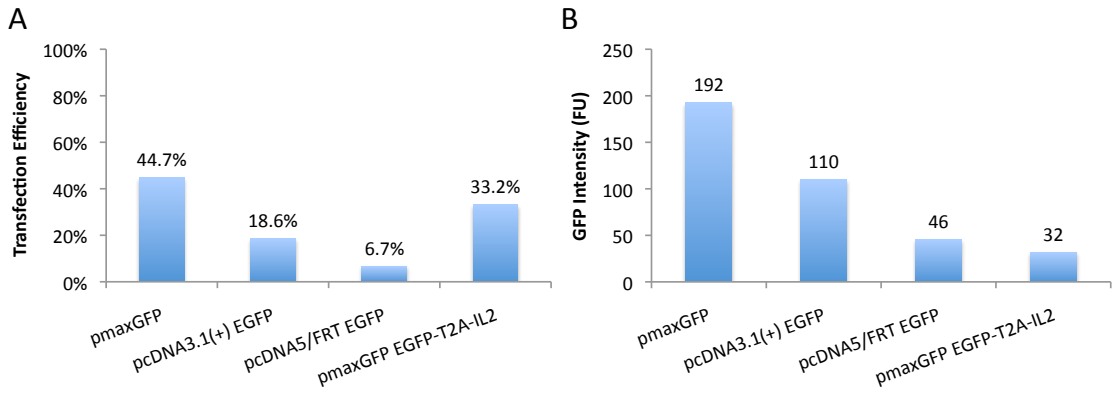

Figure 4.4. Vector backbone has greater influence on transfection efficiency in NK-92 cells than the specific fluorophore encoded by the vector. (A) Plasmids encoding variants of GFP in different vector backbones show varying degrees of transfection efficiency, with the pmaxGFP vector achieving the highest transfection efficiency regardless of the relative strengths of the fluorophores being expressed. (B) The fluorescence intensity expressed by transiently transfected NK-92 cells is dependent on both transfection efficiency and the strength of the particular fluorophore used. Transfection efficiency was measured by the percent of total viable cells that are fluorescent. Reported GFP intensity is the geometric mean fluorescence of the viable, GFP^+ gated population.

Taken together, the results suggest the optimized system for electroporating NK-92 cells requires pmaxGFP-based vectors prepared from DH10B cells using the Qiagen EndoFree Maxiprep kit. Furthermore, a strong fluorophore serving as reporter protein would facilitate flow cytometry analysis and achieve higher measurable levels of transfection efficiency. Since viability cannot be evaluated after gating for transfected

populations (because transfected populations are defined as viable, fluorescent cells), viability measurements must be based on the entire culture sample. As a result, the accuracy of viability measurements is strongly dependent on having high transfection efficiencies in all samples. Our transient transfection results indicate that transfection efficiency is limited to approximately 35% using the EGFP-T2A-IL2 fusion protein as the reporter, and such low transfection levels prevent accurate quantification of viability knockdown. As such, NK-92 cells cannot serve as a robust human cell model for the characterization and optimization of T-cell proliferation control systems. However, as a potential candidate for immunotherapy, NK-92 cells may still benefit from the regulatory functions of ribozyme-based control systems. Therefore, we reconfigured the characterization system and inserted ribozyme switch devices behind the *maxgfp* gene in pmaxGFP, thus permitting the quantification of gene expression regulation by fluorescence measurements.

Ribozyme Switches Achieve Gene Expression Knockdown in NK-92 Cells. To evaluate the performance of ribozyme-based regulatory systems in NK-92 cells, we performed transient transfections of a construct encoding one copy of the theophylline-responsive ON switch L2bulge9 in the 3' UTR of the *maxgfp* gene. Constructs encoding an inactive ribozyme and the non-switch, fully active satellite RNA of tobacco ringspot virus (sTRSV) hammerhead ribozyme were included as positive (maximum expression) and negative (minimum expression) controls, respectively. The unmodified pmaxGFP plasmid was also included for comparison. Percent GFP expression was calculated by normalizing to the inactive ribozyme control, and results indicate both gene expression

knockdown and theophylline-responsive ON switch activity by the L2bulge9 switch (Figure 4.5A). However, unlike the device performance observed in CTLL-2 cells (Figure 3.2), the sTRSV ribozyme also appears to respond to theophylline as an ON switch in NK-92 cells (Figure 4.5A).

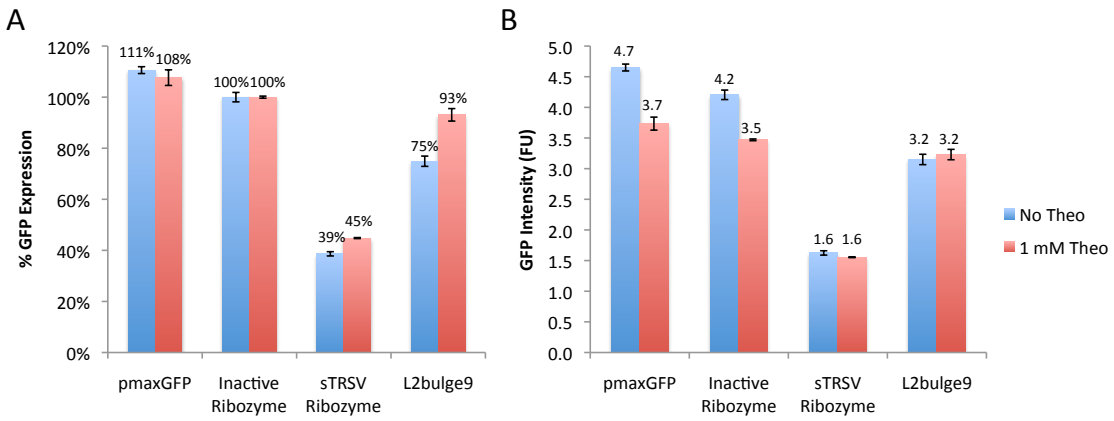

Figure 4.5. A ribozyme switch device is capable of gene expression knockdown in NK-92 cells. NK-92 cells were transfected as described in Figure 4.1 with plasmids constructed by inserting various ribozymes in the 3' UTR of the *maxgfp* gene in pmaxGFP and cultured in the absence or presence of 1 mM theophylline. (A) GFP expression levels normalized to the inactive ribozyme control show theophylline-responsive ON switch behavior by the sTRSV ribozyme and the L2bulge9 ribozyme switch. (B) Theophylline addition has no impact on the absolute fluorescence intensity of sTRSV ribozyme and L2bulge9 samples but results in decreased fluorescence in the pmaxGFP (no ribozyme control) and inactive ribozyme control samples.

Closer inspection of transfection results reveals that the absolute fluorescence levels of the sTRSV ribozyme and L2bulge9 samples remained constant while those of the inactive ribozyme control and pmaxGFP samples decreased in response to theophylline addition (Figure 4.5B). Although non-specific effects of theophylline on gene expression and fluorescence intensity have been observed in previous studies in CTLL-2 and HEK cells, these effects were proportional across different devices and were corrected by normalizing to the inactive ribozyme control. The behavior observed in NK-92 cells appears to be unique and not fully accounted for by the normalization scheme employed. Therefore, we conclude that the ribozyme device is capable of gene expression

knockdown in NK-92 cells, but ligand-responsiveness cannot be confirmed in this cell line.

Stable Integration of Ribozyme-Based Regulatory Systems in Primary Human T_{CM} Cells. The use of primary human T cells in adoptive immunotherapy is well established[37], and primary human T_{CM} cells show great promise as an immunotherapeutic agent given their ability to achieve long-term persistence in primates in the presence of IL-15[19]. To demonstrate the ribozyme-based regulatory system's portability to human T lymphocytes and translatability to clinical applications, we stably integrated ribozyme-based regulatory systems into primary human T_{CM} cells by lentiviral transduction. T_{CM} cells were isolated from peripheral blood mononuclear cells (PBMCs) by magnetic sorting using the autoMACS system (Miltenyi), a method chosen for its ready adaptation to clinical-grade manufacturing processes using the CliniMACS system (Miltenyi). PBMCs were depleted of $CD4^+$, $CD14^+$, and $CD45RA^+$ populations and subsequently enriched for $CD62L^+$ cells. The isolated T_{CM} cells were then transduced with lentiviral vectors encoding the *cd19-tk-t2a-il15* transgene coupled to three copies of the L2bulge9 switch or to an inactive ribozyme.

To verify stable integration of the regulatory system, T_{CM} cells transduced with ribozyme switch systems were tested for sensitivity to ganciclovir conferred by the mutant HSV-1 thymidine kinase (*tk*) gene. Transduced cells cultured in the presence of 5 μM ganciclovir showed decreased viability and growth while parental T_{CM} cells showed no sensitivity to the drug, confirming stable construct integration and demonstrating that the suicide switch programmed into the regulatory system as a safety mechanism is fully

functional (Figure 4.6). To verify that the transduced T_{CM} cells retained phenotypes critical for therapeutic functions, we performed surface antibody staining for the T-cell receptor (TCR), CD4, and CD8. As anticipated, transduced T_{CM} cells retained TCR and CD8 expression and remained $CD4^-$ (Figure 4.7). These results indicate that engineered T_{CM} cells stably expressing the ribozyme-based regulatory system can be efficiently generated without altering critical cell phenotypes.

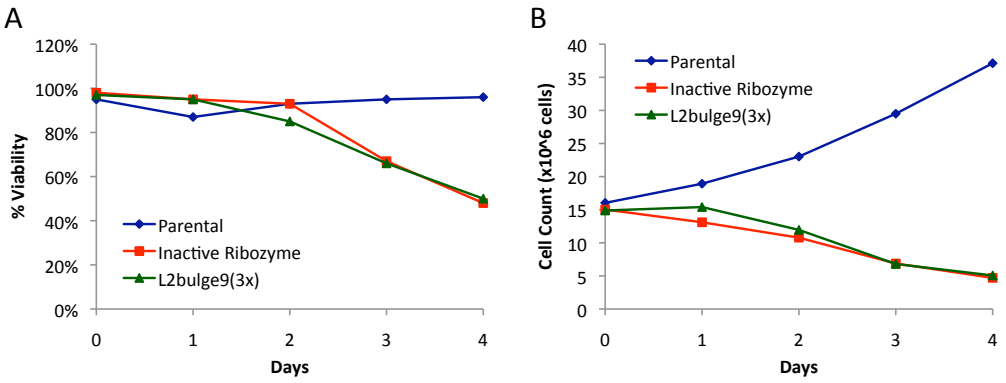

Figure 4.6. The suicide-gene safety switch programmed in ribozyme-based proliferation control systems is functional in primary human T_{CM} cells. T_{CM} cells lentivirally transduced with constructs encoding the *cd19-tk-t2a-il15* gene and ribozyme switches were cultured in the presence of 5 μM ganciclovir for four days. Compared to parental T_{CM} cells that do not express thymidine kinase (tk), the transduced cells show reduced (A) % viability and (B) total viable cell count in response to ganciclovir treatment.

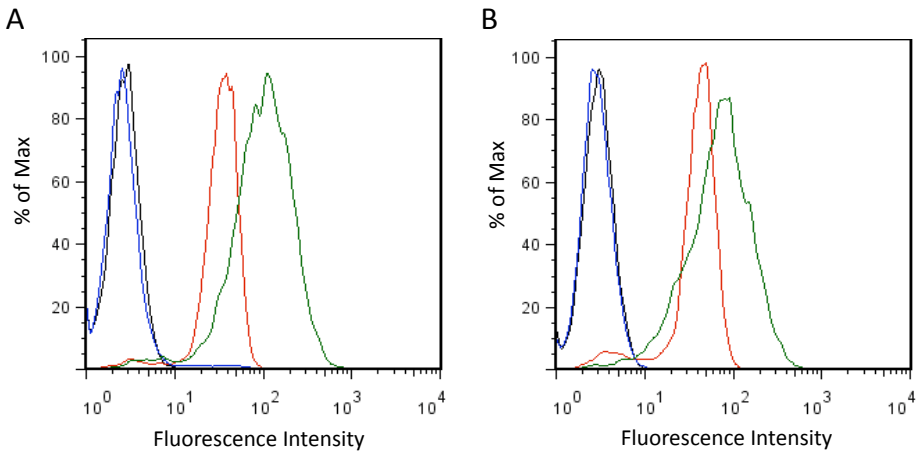

Figure 4.7. T_{CM} cells stably expressing ribozyme switch systems exhibit the proper phenotype for therapeutic applications. T_{CM} cells lentivirally transduced with constructs encoding the *cd19-tk-t2a-il15* gene and (A) the inactive ribozyme control or (B) the theophylline-responsive L2bulge9(3x) ribozyme switch are shown to be $TCR^+/CD4^-/CD8^+$ by surface antibody staining. Black, isotype control; red, TCR; blue, CD4; green, CD8.

Ribozyme Switches Enable Proliferation Control in Engineered T_{CM} Cells. Since short production timelines and streamlined processing are critical in clinical applications, we conducted regulatory performance evaluations on bulk transduced, unsorted T_{CM} populations to examine the robustness of the regulatory system under no population refinement. Transduced cells were cultured in the presence and absence of 500 μM theophylline for five days, with daily monitoring of CD19 levels and cell viability. Cells expressing L2bulge9 show up to 15% increase in CD19 expression levels (Figure 4.8A), 24% increase in the live cell population (Figure 4.8B), and 54% reduction in the apoptotic cell population (Figure 4.8C) in the presence of theophylline compared to the inactive ribozyme control, indicating drug-responsive ON switch behavior in gene expression and cell growth. The measured change in CD19 expression is comparable to that observed in bulk CTLL-2 stable cell lines (Supplementary Figure 3.2), and the shift in population distribution between live and apoptotic cells supports that the regulatory system is effective in controlling the fate of primary human T_{CM} cells.

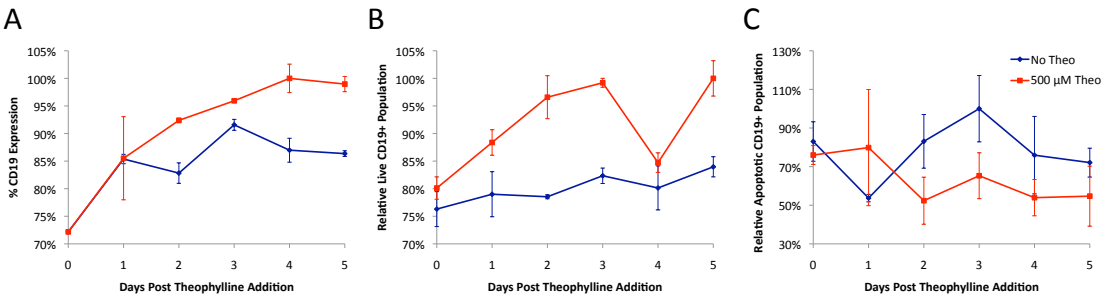

Figure 4.8. The ribozyme switch system effectively regulates gene expression and cell fate in primary human T_{CM} cells. (A) CD19 expression levels are elevated in the presence of theophylline. The populations of cells that are (B) live and $CD19^+$ or (C) apoptotic and $CD19^+$ indicate an increase in live cells and decrease in apoptotic cells in response to theophylline. Values for the L2bulge9(3x) sample are normalized to those of the inactive ribozyme control cultured at the same theophylline concentration. Reported values are mean ± s.d. from triplicate samples. The highest level is set to 100%.

Discussion

The ability to regulate gene expression and cell fate in primary human T cells using compact, programmable control systems is a significant step toward more effective adoptive immunotherapy. Multiple clinical trials have shown that the long-term persistence of adoptively transferred tumor-targeting cells is tightly correlated with the objective response rate[38]. However, maintaining and controlling the survival and expansion of transferred cells *in vivo* remain challenging. As discussed in Chapter 3, we have demonstrated that ribozyme-based regulatory systems can effectively control the proliferation of engineered T cells in mouse models by modulating the expression of growth-related cytokines in a ligand-responsive manner. In this work, we expand the functional range of the ribozyme-based regulatory systems into human cells. We seek to both identify a suitable human lymphocyte for the rapid characterization and optimization of RNA-based control devices and demonstrate the ligand-responsive gene-regulatory capabilities of ribozyme-based systems in established and primary human cells.

Similar to engineered mechanical systems, gene-regulatory systems consisting of biologically engineered control devices are products of a development process that encompasses initial design, prototyping, characterization, optimization, and final implementation. As discussed in Chapter 2, most of the RNA-based control devices published to date have been developed in model organisms such as yeasts and bacteria, primarily due to the high growth rate, ease of culture maintenance, and wide range of genetic manipulation tools available to these organisms. These characteristics enable rapid prototyping, characterization, and optimization of new devices. However, additional modifications are likely necessary during the implementation stage if the

desired application required different cellular hosts than the model organisms used for initial device development. An alternative strategy is to perform the development process in either the application's required cell type or a closely related organism. In the context of cellular immunotherapy, the goal is to implement regulatory systems capable of proliferation control in human lymphocytes. To identify a cellular host suitable for the development of such RNA-based control devices, we sought human lymphocytes that fulfill the following criteria: ready availability, ease of culture, cytokine dependence for growth (to allow for proliferation control via modulation of cytokine production), and amenability to rapid and effective genetic manipulation.

NK-92 was the first established NK cell line to be tested in clinical trials and continues to be a promising candidate for therapeutic applications. Importantly, it satisfies the first three criteria listed above for an ideal host for the development of RNA-based control devices. As an established cell line, NK-92 is readily available from cell banks such as the American Type Culture Collection (ATCC) and can be cultured in commercially available media without the need for antigen stimulation. NK-92 cells are dependent on cytokines (IL-2 or IL-15) for growth, making it a suitable candidate for proliferation control by RNA-based modulation of cytokine expression. However, the genetic manipulation of NK-92 cells has been hampered by difficulties in achieving efficient transfection by both lipid-based and electroporation methods. Lentiviral transduction has shown greater success in achieving transient expression in NK-92 cells, but the stable expression of transgenes remains challenging in this cell line. Furthermore, viral transduction requires greater infrastructural investments and is significantly more time consuming than lipid-based or electroporation methods for transient studies. Here,

we examined various parameters in the electroporation of NK-92 cells and identified a specific expression vector (pmaxGFP) and plasmid purification method (from DH10B cells using Qiagen EndoFree Maxiprep kit) that are critical to efficient transfections. By constructing ribozyme-based regulatory systems using the identified expression vector, we confirmed the gene expression knockdown activity of a ribozyme switch in NK-92 cells. However, our studies also show that the efficiency of transient transfections in NK-92 cells is too low for accurate quantification of the regulatory systems' impacts on cell viability. The alternative strategy of stable integration by lentiviral transduction significantly increases the time and resources required to evaluate each control device, thus precluding NK-92 as a suitable host for the characterization and optimization of new devices.

In contrast to established cell lines such as NK-92, primary human T cells must be obtained from fresh donor blood supplies, require regular antigen stimulation for *in vitro* expansion, and have a limited lifetime. Furthermore, primary T cells are generally resistant to rapid genetic manipulation strategies such as lipid-based transfection and electroporation, making them unsuited for hosting development work on RNA-based regulatory systems. Nevertheless, primary human T cells represent the most common cell type for adoptive cell therapy, and primary human T_{CM} cells in particular have shown promise as therapeutic agents. Therefore, the ability to maintain and control the proliferation of primary human T_{CM} cells can greatly contribute to the improvement of cellular immunotherapy. Our work presents the successful generation of primary human T_{CM} cells that stably express ribozyme-based regulatory systems capable of drug-responsive modulation of functional outputs. The T_{CM} cells were prepared using

protocols that are readily adaptable to clinical-grade manufacturing standards, and the resulting engineered population exhibits proper phenotypes for therapeutic applications. Significantly, T_{CM} cells transduced with the ribozyme switch system show drug-responsive regulation of both gene expression and cell-fate decisions without population refinement, confirming the robustness of the regulatory system and suggesting the potential for further performance improvement via isolation of clonal populations with the optimal behavioral outputs.

The examination of NK-92 and T_{CM} cells presented in this work confirms that the ribozyme-based regulatory system can be applied across multiple cell types through diverse genetic manipulation methods, including lipid-based transfection (in HEK cells, Chapter 2), electroporation (in CTLL-2 cells, Chapter 3), and lentiviral transduction (in T_{CM} cells). This flexibility in integration method and versatility across established cell lines as well as primary human cells will likely be critical to the implementation of ribozyme-based regulatory systems in diverse applications. In this study we also demonstrate that neither NK-92 cells nor primary human T cells are ideal hosts for the rapid characterization and optimization of RNA-based control devices due to limitations in cell availability and culture maintenance requirements (for primary T cells) as well as difficulties in achieving rapid genetic manipulations (for both NK-92 and primary T cells). Although characterization results of ribozyme-based regulatory systems in NK-92 and T_{CM} cells demonstrate that control devices prototyped and optimized in model organisms (yeast in this case) can be efficiently implemented in higher organisms useful for end applications such as adoptive immunotherapy, continued effort on identifying a human cell type suitable for the development of RNA-based control devices will further

improve the development process of engineered gene regulatory systems. The need for ready availability and ease of culture suggests that established cell lines are more promising candidates than primary cells. For systems that do not require cytokine-dependent growth as a functional criterion, numerous human lymphocyte lines, such as the well-characterized Jurkat cells, could be evaluated for suitability in hosting the characterization and optimization of RNA-based control devices. Future work in this area will facilitate the development of new RNA-based regulatory systems that can readily interface with clinical and other downstream applications requiring the use of human cells.

Materials and Methods

Plasmid construction. All plasmids were constructed using standard molecular biology techniques[39]. All oligonucleotides were synthesized by Integrated DNA Technologies or the Stanford Protein and Nucleic Acid Facility. All constructs were sequence verified (Elim Biopharmaceuticals). Cloning enzymes, including restriction enzymes and T4 DNA ligase, were obtained from New England Biolabs, and DNA polymerases were obtained from Stratagene. Construction of pcDNA5/FRT- and pcDNA3.1(+)-based plasmids was described in Chapters 2 and 3, respectively. The ribozyme sTRSV was cloned into the vector pmaxGFP (Amaxa) by annealing 5'-phosphorylated oligos for the sTRSV ribozyme (sTRSV BglII-P Fwd, 5'PGATCTTCGAGGCGATCGCAAACAAAC AAAGCTGTCACCGGATGTGCTTTCCGGTCTGATGAGTCCGTGAGGACGAAAC AGCAAAAAGAAAAATAAAAATTTTTTTTTAATTAATCTTGGGCCGAGCT; sTRSV SacI-P Rev, 5'PCGGCCCAAGATTAATTAAAAAAAAATTTTTATTTTT

CTTTTTGCTGTTTCGTCCTCACGGACTCATCAGACCGGAAAGCACATCCGGTG ACAGCTTTGTTTGTTTGCGATCGCCTCGAA) and inserting into the restriction sites BglII and SacI in the vector. The inactive ribozyme sTRSV Ctrl was similarly constructed using forward primer sTRSV Ctrl BglII-P Fwd (5'PGATCTTCGAGGCGATCGCAAACAAACAAAGCTGTCACCGGATGTGCTTTC CGGTACGTGAGGTCCGTGAGGACAGAACAGCAAAAAGAAAAATAAAAATTT TTTTTTTAATTAATCTTGGGCCGAGCT) and reverse primer sTRSV Ctrl SacI-P Rev (5'PCGGCCCAAGATTAATTAAAAAAAAAATTTTTATTTTTCTTTTTGCTGTTCT GTCCTCACGGACCTCACGTACCGGAAAGCACATCCGGTGACAGCTTTGTTTGT TTGCGATCGCCTCGAA). The L2bulge9 ribozyme switch sequence was PCR amplified from previously constructed plasmids using forward primer BglII Pre-Rz Fwd (5'AATAAGATCTTCGAGGCGATCGC AA) and reverse primer SacI Post-Rz Rev (5'AATAGAGCTCGGCCCAAGATTAATTAA AA) and inserted into BglII and SacI in pmaxGFP. The *egfp-t2a-il2* fusion gene was cloned into pmaxGFP via the KpnI and XhoI sites, thereby replacing the original gene encoding maxGFP.

Derivation of T_{CM} cells from human PBMCs. 5 x 10^8 PBMCs were isolated from donor apheresis products, washed twice with 35 ml MACS buffer (2 mM EDTA and 0.5% BSA in PBS), resuspended in 1.5 ml MACS buffer. Washed cells were stained with 0.75 ml each of CD4, CD14, and CD45RA microbeads (Miltenyi Biotec), and depleted for CD4, CD14, and CD45RA using an autoMACS Separator (Miltenyi). Depleted cells were washed once with 35 ml MACS buffer, resuspended in 3.5 ml MACS buffer with 10.5 μl anti-CD62L DREG56-biotin antibody (City of Hope Center for Biomedicine and

Genetics), and incubated for 20 min in the dark at 4°C. Cells were washed twice with 35 ml MACS buffer and resuspended in 1.2 ml MACS buffer with 300 μl anti-biotin microbeads (Miltenyi). Cells were enriched for CD62L using an autoMACS Separator, placed in fresh RPMI 1640 media supplemented with 10% FBS and stored in a 37°C incubator.

Mammalian cell culture maintenance. Primary human T_{CM} cells were maintained in RPMI-1640 media (Lonza) supplemented with 10% heat-inactivated FBS (Hyclone). Cells were fed 50 U/ml IL-2 and 0.5 ng/ml IL-15 every 48 hr and maintained between 0.2 x 10^6 and 1.0 x 10^6 cells/ml. NK-92 cells were maintained in X-VIVO 20 media (Lonza) and fed 500 U/ml IL-2 every 48 hours. Cultures were maintained between 0.08 x 10^6 cells/ml and 0.4 x 10^6 cells/ml. T_{CM} cell count and viability measurements were performed using the Guava Personal Cell Analysis System following manufacturer's protocols.

DNA plasmid preparation. Plasmids were prepared from 5 ml overnight liquid cultures supplemented with the appropriate antibiotics and inoculated directly from frozen *E. coli* stocks. Promega Wizard Plus SV Miniprep, Promega Pure Yield Miniprep, and Qiagen EndoFree Maxiprep kits were used for DNA purification following manufacturers' protocols.

Transient transfection and fluorescence quantification. Transfection of NK-92 cells was performed with an Amaxa Nucleofector II and Nucleofector Kit R (Amaxa)

following manufacturer's protocols. Each electroporation sample contained 2 x 10^6 cells transfected with 3 μg of plasmid DNA. Fluorescence data were obtained 48 hours after transfection using a Quanta Cell Lab Flow Cytometer equipped with a 488-nm laser (Beckman Coulter). GFP and dsRed-Express were measured through 525/30-nm band-pass and 610-nm long-pass filters, respectively. Viability was gated based on side scatter and electronic volume, and only viable cells were included in fluorescence measurements. All fluorescence measurements were reported as the geometric mean intensity observed in the gated population. Transfection efficiency was measured by the percent of total population that is GFP^+ or dsRed-$Express^+$, depending on the plasmids used. To control for toxicity and other possible non-specific effects of transfection and input ligand molecules, cells transfected with an inactive (scrambled) hammerhead ribozyme and treated with the corresponding concentration of ligand molecule served as positive controls to which values from cells transfected with active ribozyme switches were normalized. The inactive ribozyme constructs provide controls for the maximum possible gene expression levels from the ribozyme-based regulatory systems. Ribozyme sequences are as reported in Chapter 3. Reported error bars indicate one standard deviation.

Lentivirus production. 5.0 x 10^6 293T cells were seeded in a final volume of 9 ml per 10-cm tissue culture plate and transfected with 1 ml solution containing vector DNA, 62 mM $CaCl_2$, and 1X HEPES buffered saline. Cells were washed twice with 5 ml 1X PBS without magnesium and calcium the following morning and fed 10 ml of complete DMEM with 60 mM sodium butyrate. At 24-, 48-, and 72-hr post transfection, viral

supernatants were harvested by centrifugation at 2,000 rpm for 10 min at 4°C and filtered through 0.45 μM vacuum filtration unit. Viral supernatants from all time points were pooled and mixed with ¼ volume of 40% PEG. After rotating overnight at 4°C, samples were centrifuged at 3,000 rpm for 20 min at 4°C and the supernatants discarded. Pellets were resuspended in 35 ml serum-free DMEM and ultracentrifuged at 24,500 rpm for 1.5 hr at 4°C. Resulting pellets were resuspended in 50 μl serum-free FBS and vortexed at 4°C for 2 hr. 10% FBS was added and the samples stored at –80°C until titering and use.

Lentiviral transduction of T_{CM} cells. 0.5 x 10^6 T_{CM} cells were seeded in a total volume of 500 μl per well in 48-well plate. 1.5 x 10^6 anti-CD3/anti-CD28 Dynabeads (Invitrogen) were washed with 1% heat-inactivated human serum in PBS (pH 7.4), resuspended in 500 μl T-cell media (RPMI 1640 supplemented with 10% heat-inactivated fetal bovine serum) containing 0.5 x 10^6 T_{CM} cells, and added to each of 2 wells in a 48-well plate. Each well was fed with 50 U/ml IL-2 and 0.5 ng/ml IL-15, infected with viruses at a multiplicity of infection (MOI) of 5, and treated with protamine sulfate at a final concentration of 5 μg/ml. The plate was centrifuged at 2100 rpm for 30 min at 32°C and incubated at 37°C for 4 hr. 500 μl of warm T-cell media was added to each well and the plate was incubated at 37°C. Cells were assayed by flow cytometry on day 8 post transduction and Dynabeads were removed on day 14 post transduction.

Surface antibody staining. Surface staining of T_{CM} and NK-92 cells was performed by washing 1 x 10^6 cells twice with 500 μl HBSS (Gibco), incubating with FITC- or PE-conjugated antibodies at the appropriate dilution in 50 μl HBSS for 15 min at 4°C in the

dark, washing twice with 500 μl HBSS, and analyzing on the flow cytometer. FITC and PE signals were excited by a 488-nm laser and detected through 525/30-nm and 575/30-nm band-pass filters, respectively, using a Quanta Cell Lab Flow Cytometer.

T_{CM} cell time-course study. T_{CM} cells transduced with the *cd19-t2a-il15*-L2bulge9(3x) or *cd19-t2a-il15*-inactive ribozyme constructs were stimulated with 100 x 10^6 PBMCs, 10 x 10^6 TM-LCLs, and 30 ng/ml OKT2 for each T75 flask and cultured under regular conditions for 12 days. On day 12 after stimulation, each cell line was washed twice with HBSS and used to seed 25-ml cultures at 0.45 x 10^6 cells/ml. Cell media were supplemented with either no theophylline or 500 μM theophylline, and no IL-2 or IL-15 was added. The CD19 expression level study was performed with duplicate cultures and the apoptosis staining study was performed with triplicate cultures. 500 μl of each culture was sampled every 24 hr for surface staining with PE-conjugated CD19 antibody (Beckman Coulter). For the apoptosis study, CD19-stained samples where subsequently stained with Pacific Blue-conjugated annexin V and SYTOX AAD dead cell stain (Invitrogen) following manufacturer's protocols. Fluorescence data were obtained using a Quanta Cell Lab Flow Cytometer with both a 488-nm laser and a UV arc lamp. Pacific Blue, PE, and SYTOX AAD were detected through 465/30-nm band pass, 575/30-nm band pass, and 610-nm long-pass filters, respectively. Percent CD19 expression was calculated by measuring the PE expression level of PE^+ gated cells and normalizing results of the L2bulge9(3x) sample by those of the inactive ribozyme sample cultured at the same theophylline concentration. Only SYTOX AAD^- cells were included in data analyses for the apoptosis study. The population of live $CD19^+$ cells was determined by

gating for annexin V^-/PE^+ cells and the population of apoptotic $CD19^+$ cells was determined by gating for annexin V^+/PE^+ cells. Relative population distribution was calculated by normalizing results of the L2bulge9(3x) sample to those of the inactive ribozyme sample cultured at the same theophylline concentration.

Acknowledgments

We thank C. Bautista and E. Ferkassian for technical assistance. This work was supported by the City of Hope's National Cancer Institute–Cancer Center Support Grant, the Alfred P. Sloan Foundation (fellowship to C.D.S.), and the National Institutes of Health (grant to C.D.S., RC1GM091298).

References

1. Riddell, S.R. et al. Restoration of viral immunity in immunodeficient humans by the adoptive transfer of T cell clones. *Science* **257**, 238-241 (1992).
2. Walter, E.A. et al. Reconstitution of cellular immunity against cytomegalovirus in recipients of allogeneic bone marrow by transfer of T-cell clones from the donor. *N Engl J Med* **333**, 1038-1044 (1995).
3. Rooney, C.M. et al. Infusion of cytotoxic T cells for the prevention and treatment of Epstein-Barr virus-induced lymphoma in allogeneic transplant recipients. *Blood* **92**, 1549-1555 (1998).
4. Bollard, C.M. et al. Cytotoxic T lymphocyte therapy for Epstein-Barr virus+ Hodgkin's disease. *J Exp Med* **200**, 1623-1633 (2004).

5. Brentjens, R.J. et al. Eradication of systemic B-cell tumors by genetically targeted human T lymphocytes co-stimulated by CD80 and interleukin-15. *Nat Med* **9**, 279-286 (2003).

6. Dudley, M.E. et al. Adoptive cell transfer therapy following non-myeloablative but lymphodepleting chemotherapy for the treatment of patients with refractory metastatic melanoma. *J Clin Oncol* **23**, 2346-2357 (2005).

7. Morgan, R.A. et al. Cancer regression in patients after transfer of genetically engineered lymphocytes. *Science* **314**, 126-129 (2006).

8. Park, J.H. & Brentjens, R.J. Adoptive immunotherapy for B-cell malignancies with autologous chimeric antigen receptor modified tumor targeted T cells. *Discov Med* **9**, 277-288.

9. Blattman, J.N. & Greenberg, P.D. Cancer immunotherapy: a treatment for the masses. *Science* **305**, 200-205 (2004).

10. June, C.H. Adoptive T cell therapy for cancer in the clinic. *J Clin Invest* **117**, 1466-1476 (2007).

11. Antony, P.A. et al. CD8+ T cell immunity against a tumor/self-antigen is augmented by CD4+ T helper cells and hindered by naturally occurring T regulatory cells. *J Immunol* **174**, 2591-2601 (2005).

12. Powell, D.J., Jr., Dudley, M.E., Robbins, P.F. & Rosenberg, S.A. Transition of late-stage effector T cells to CD27+ CD28+ tumor-reactive effector memory T cells in humans after adoptive cell transfer therapy. *Blood* **105**, 241-250 (2005).

13. Ahmed, N. et al. HER2-specific T cells target primary glioblastoma stem cells and induce regression of autologous experimental tumors. *Clin Cancer Res* **16**, 474-485 (2010).

14. Kobayashi, H., Tanaka, Y., Shimmura, H., Minato, N. & Tanabe, K. Complete remission of lung metastasis following adoptive immunotherapy using activated autologous gammadelta T-cells in a patient with renal cell carcinoma. *Anticancer Res* **30**, 575-579 (2010).

15. Kuci, S. et al. Efficient lysis of rhabdomyosarcoma cells by cytokine-induced killer cells: implications for adoptive immunotherapy after allogeneic stem cell transplantation. *Haematologica* (2010).

16. Merlo, A. et al. Virus-Specific Cytotoxic CD4+ T Cells for the Treatment of EBV-Related Tumors. *J Immunol* (2010).

17. Wang, L.X. & Plautz, G.E. Tumor-Primed, In Vitro-Activated CD4+ Effector T Cells Establish Long-Term Memory without Exogenous Cytokine Support or Ongoing Antigen Exposure. *J Immunol* (2010).

18. Klebanoff, C.A. et al. Central memory self/tumor-reactive CD8+ T cells confer superior antitumor immunity compared with effector memory T cells. *Proc Natl Acad Sci U S A* **102**, 9571-9576 (2005).

19. Berger, C. et al. Adoptive transfer of effector CD8+ T cells derived from central memory cells establishes persistent T cell memory in primates. *J Clin Invest* **118**, 294-305 (2008).

20. Klingemann, H.G., Wong, E. & Maki, G. A cytotoxic NK-cell line (NK-92) for ex vivo purging of leukemia from blood. *Biol Blood Marrow Transplant* **2**, 68-75 (1996).

21. Roberts, A.D. & Woodland, D.L. Cutting edge: effector memory CD8+ T cells play a prominent role in recall responses to secondary viral infection in the lung. *J Immunol* **172**, 6533-6537 (2004).

22. Wherry, E.J. et al. Lineage relationship and protective immunity of memory CD8 T cell subsets. *Nat Immunol* **4**, 225-234 (2003).

23. Klingemann, H.G. Natural killer cell-based immunotherapeutic strategies. *Cytotherapy* **7**, 16-22 (2005).

24. Cantoni, C. et al. NKp44, a triggering receptor involved in tumor cell lysis by activated human natural killer cells, is a novel member of the immunoglobulin superfamily. *J Exp Med* **189**, 787-796 (1999).

25. Long, E.O. et al. Killer cell inhibitory receptors: diversity, specificity, and function. *Immunol Rev* **155**, 135-144 (1997).

26. Ruggeri, L. et al. Effectiveness of donor natural killer cell alloreactivity in mismatched hematopoietic transplants. *Science* **295**, 2097-2100 (2002).

27. Ruggeri, L. et al. Role of natural killer cell alloreactivity in HLA-mismatched hematopoietic stem cell transplantation. *Blood* **94**, 333-339 (1999).

28. Tam, Y.K., Miyagawa, B., Ho, V.C. & Klingemann, H.G. Immunotherapy of malignant melanoma in a SCID mouse model using the highly cytotoxic natural killer cell line NK-92. *J Hematother* **8**, 281-290 (1999).

29. Yan, Y. et al. Antileukemia activity of a natural killer cell line against human leukemias. *Clin Cancer Res* **4**, 2859-2868 (1998).

30. Tonn, T., Becker, S., Esser, R., Schwabe, D. & Seifried, E. Cellular immunotherapy of malignancies using the clonal natural killer cell line NK-92. *J Hematother Stem Cell Res* **10**, 535-544 (2001).

31. Berger, C. et al. Safety and immunological effects of IL-15 administration in nonhuman primates. *Blood* (2009).

32. Gong, J.H., Maki, G. & Klingemann, H.G. Characterization of a human cell line (NK-92) with phenotypical and functional characteristics of activated natural killer cells. *Leukemia* **8**, 652-658 (1994).

33. Sauce, D. et al. Influence of ex vivo expansion and retrovirus-mediated gene transfer on primary T lymphocyte phenotype and functions. *J Hematother Stem Cell Res* **11**, 929-940 (2002).

34. Grund, E.M. & Muise-Helmericks, R.C. Cost efficient and effective gene transfer into the human natural killer cell line, NK92. *J Immunol Methods* **296**, 31-36 (2005).

35. Hong, S. et al. Functional analysis of various promoters in lentiviral vectors at different stages of in vitro differentiation of mouse embryonic stem cells. *Mol Ther* **15**, 1630-1639 (2007).

36. Qin, J.Y. et al. Systematic comparison of constitutive promoters and the doxycycline-inducible promoter. *PLoS One* **5**, e10611 (2010).

37. Rosenberg, S.A., Restifo, N.P., Yang, J.C., Morgan, R.A. & Dudley, M.E. Adoptive cell transfer: a clinical path to effective cancer immunotherapy. *Nat Rev Cancer* **8**, 299-308 (2008).

38. Robbins, P.F. et al. Cutting edge: persistence of transferred lymphocyte clonotypes correlates with cancer regression in patients receiving cell transfer therapy. *J Immunol* **173**, 7125-7130 (2004).

39. Sambrook, J. & Russell, D.W. Molecular Cloning: A Laboratory Manual, Edn. 3. (Cold Spring Harbor Press, Cold Spring Harbor; 2001).

Supplementary Text 4.1

To decouple the relationship between transfection efficiency and the natural intensity of various fluorophores used in this study, transient transfections were performed in CTLL-2 cells—a cell line capable of relatively high transfection efficiencies by electroporation and is relatively insensitive to the specific expression vectors used compared to NK-92 cells—to compare the intensities of different GFP variants. Each fluorophore tested was expressed from a CMV promoter, and the following constructs were tested in parallel: a pcDNA3.1(+)-based plasmid encoding EGFP-T2A-IL2, a pcDNA3.1(+)-based plasmid encoding EGFP, and pmaxGFP encoding maxGFP. Transfection and flow cytometry analyses were performed as described in Chapter 3. Transfection results, in order of increasing fluorescence intensity, are as follows: EGFP-T2A-IL2, EGFP, and maxGFP (Supplementary Figure 4.1).

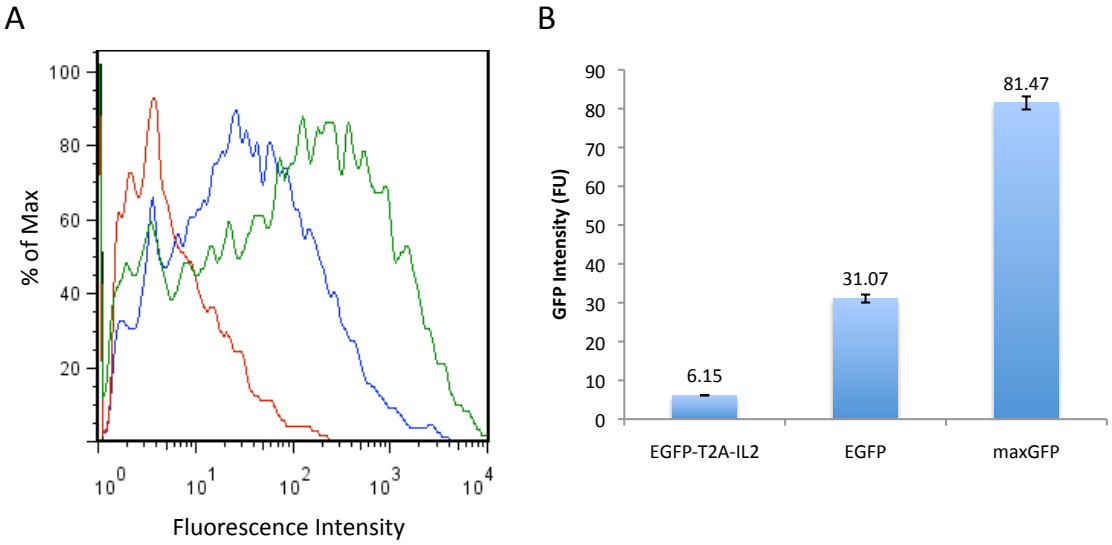

Supplementary Figure 4.1. Different GFP variants show different fluorescence intensities in transiently transfected CTLL-2 cells. (A) Fluorescence histogram of samples transiently transfected with various GFP reporters. Black, negative control (untransfected CTLL-2 cells); red, EGFP-T2A-IL2; blue, EGFP; green, maxGFP. (B) Geometric mean GFP intensity of viable, GFP^+ cells. Reported values are the mean of duplicate samples ± s.d.

Chapter 5

T-Cell Proliferation Control with RNAi-Based Regulatory Systems

Abstract

The safety and efficacy of adoptive T-cell transfer therapy depend not only on a robust *in vivo* proliferative response of transferred T cells, but also on the effective curtailing or elimination of the T-cell population at the conclusion of the treatment period. Natural T-cell proliferation is closely monitored and regulated by coordinated control networks, with the interleukin-2 (IL-2) and interleukin-15 (IL-15) signaling pathways playing key roles in its initiation and long-term maintenance. Previous work has demonstrated a synthetic T-cell proliferation control system based on the modulation of IL-2 and IL-15 production levels with drug-responsive, ribozyme-based regulatory devices. To advance the design of integrated genetic control systems for immunotherapy applications, we have developed a novel regulatory system for the modulation of endogenous cytokine receptor chains essential to the IL-2 and IL-15 signaling pathways. Here, we describe the development of microRNA (miRNA) switches capable of *trans*-acting, ligand-responsive control over endogenous IL-2 receptor β (IL-2Rβ) and common γ (γ_c) chain levels in CTLL-2 mouse T cells. We systematically examine the sequence and structural requirements for the construction of miRNA switches with high knockdown efficiency and ligand responsiveness, and we demonstrate strategies for achieving stringent receptor chain knockdown based on the combinatorial expression of miRNA sequences. We report the construction of theophylline-responsive miRNA switch clusters capable of up to 80% knockdown in cytokine receptor chain expression levels, with switch dynamic ranges of up to 20% and 46% for the IL-2Rβ and γ_c chains, respectively. Finally, we present a framework for building multi-layered regulatory systems capable of simultaneous control over diverse targets based on the

implementation of multiple RNA regulatory devices, thus enabling stringent and robust control over T-cell proliferation.

Introduction

Cytokine signaling plays a central role in T-cell activation and proliferation. In particular, the interleukin-2 (IL-2) and interleukin-15 (IL-15) signaling pathways are critical to both clonal T-cell expansion and the establishment of memory T cells[1]. While each component in these signaling pathways represents a potential regulatory checkpoint in synthetic control systems, studies have shown that components associated with upstream signaling events are particularly effective control points for T-cell proliferation, as regulation exerted at this level takes advantage of signal amplification through the downstream phosphorylation cascade (Figure 3.1). For example, RNA-based regulatory devices have been used to modulate the production of cytokines[2], which initiate the signaling cascade upon binding to their cognate receptor chains. To develop an integrated control system for T-cell proliferation with more robust regulatory properties, we examined the extension of the control system to target other upstream components required for cytokine signaling.

IL-2 and IL-15 share the IL-2 receptor β chain (IL-2Rβ) and the common γ chain (γ_c) that, in the form of a heterodimer, are both necessary and sufficient for IL-2 and IL-15 signaling[3]. In addition, each cytokine has a unique receptor α chain that serves to modulate both cytokine presentation and receptor binding kinetics[4-6]. The IL-2/IL-2R complex exists in three forms. IL-2 can bind to IL-2Rα alone with low affinity ($K_D \approx 10^{-8}$ M), or it can bind to the IL-2Rβ/γ_c heterodimer with intermediate affinity ($K_D \approx 10^{-9}$ M). In addition, IL-2 binding to IL-2Rα promotes association with IL-2Rβ and γ_c, and the stable quaternary structure constitutes the high-affinity IL-2 receptor complex ($K_D \approx 10^{-11}$ M)[7]. Crystal structures of the quaternary IL-2/IL-2R complex show that IL-2Rα forms the

most extensive interface with IL-2 among the three receptor chains, consistent with its ability to bind to IL-2 independently of the other two chains[8]. In contrast, γ_c forms degenerate contacts with IL-2, consistent with its role as a promiscuous receptor shared by IL-2, IL-4, IL-7, IL-9, IL-15, and IL-21[9]. Similar to IL-2, IL-15 can signal through the IL-2Rβ/γ_c heterodimer by triggering the phosphorylation of JAK1, JAK3, STAT3, and STAT5[3]. However, unlike IL-2Rα, IL-15Rα binds to IL-15 with high affinity ($K_D \approx 10^{-11}$ M) and presents IL-15 in *trans* to neighboring cells that express IL-2Rβ/γ_c[4, 10].

The central role of IL-2Rβ and γ_c in IL-2 and IL-15 signaling indicates that they may be effective targets for RNA-based T-cell proliferation control systems. However, the targeting of endogenous cytokine receptor chains demands *trans*-acting control devices with regulatory mechanisms that do not require the device to be physically coupled to the genetic target at the transcript level. As an alternative to *cis*-acting, ribozyme-based control devices previously employed for cytokine regulation, microRNA (miRNA)-based devices can be utilized for the modulation of receptor chain expression.

miRNAs are a class of RNA interference (RNAi) substrates that direct sequence-specific silencing of targeted genes[11]. Long primary miRNA transcripts are processed to 60-70-nt stem-loop intermediates known as precursor miRNAs (pre-miRNAs) in the nucleus by the endogenous RNase Drosha. The pre-miRNAs are exported to the cytoplasm and subsequently processed by the RNase Dicer into 21-23-nt double-stranded mature miRNAs. Following Dicer cleavage, one of the two strands is selectively incorporated into the RNA-induced silencing complex (RISC), and the complementary strand is rapidly degraded. The activated RISC recognizes its regulatory target by

sequence complementation to the loaded miRNA guide strand, and it silences target gene expression by either direct cleavage or translational inhibition of the target transcript[11].

The ability of RNAi substrates to act in *trans* allows for silencing of both transgenic and endogenous genetic targets, thus presenting a potentially versatile regulatory mechanism for a new class of RNA devices[12]. Recently, we developed a modular and tunable platform for the construction of small-molecule-responsive miRNA switches[13]. This class of genetic devices is generated by integrating an RNA aptamer into the basal segment of the miRNA stem-loop structure, where ligand binding stabilizes a constrained or "structured" conformation that inhibits Drosha processing. As a result, the presence of ligand molecules leads to a reduction in RNAi-mediated gene silencing and an increase in target gene expression[13] (Figure 1.5). In the described platform, the aptamer and the miRNA stem sequence independently specify the ligand input and the regulatory target, respectively. Therefore, miRNA switches responsive to diverse ligand molecules and specific for theoretically any target of interest can be constructed through direct replacement of these sequences in the RNA device. Previous work has shown that miRNA switches can function in human cells to regulate both transgenic and endogenous targets in response to diverse small molecule inputs[13].

Here, we present the development of theophylline-responsive miRNA switches for the regulation of endogenous IL-2Rβ and γ_c expression levels. We show that ligand-responsive miRNA switches have greater silencing efficiency and comparable switch dynamic range relative to non-switch miRNAs expressed from an inducible promoter system. Furthermore, we demonstrate that the structure and sequence specificity of both the upper portion and the basal segment of the miRNA stem-loop have significant impact

on the silencing efficiency and switch dynamic range of the miRNA switches. Finally, we describe a framework for combining ribozyme- and RNAi-based regulatory devices in the construction of integrated T-cell proliferation control systems with stringent regulation over signaling pathways and their functional outputs.

Results

Ligand-Responsive miRNA Switch System Exhibits Comparable Gene Regulatory Activities as the Tet-Inducible Promoter System. Ligand-responsive miRNA switches enable gene expression regulation in response to researcher-specified small molecules. In order to examine the utility of this RNA-based platform relative to standard ligand-responsive gene-regulatory systems, we compared the performance of the miRNA switch system to a commonly used inducible promoter system. Specifically, we compared a theophylline-responsive, EGFP-targeting miRNA ON switch (th1)[13] with a comparable transcription-based, tet-inducible control system. The EGFP-targeting miRNA switch was expressed in the 3' UTR of a dsRed-Express gene from a CMV promoter. A non-switch, EGFP-targeting miRNA (wt)[13] was expressed from a similar construct except that the CMV promoter was replaced by a tetO-CMV promoter. Expression from the tetO-CMV promoter is induced by the tet transcriptional activator (tTA) and inhibited by the presence of doxycycline, which binds to tTA and prevents promoter activation (Tet-OFF system). Therefore, the presence of doxycycline will reduce miRNA expression and de-repress EGFP, resulting in an ON-switch behavior in response to ligand addition (similar to the miRNA switch profile).

We optimized several experimental parameters for the Tet-OFF system, including the promoter-to-tTA ratio and the inducer molecule concentration, prior to comparison with the miRNA switch system (Supplementary Text 5.1). The optimized Tet-OFF system was tested for gene silencing and switch activities by transient transfection in human embryonic kidney (HEK) 293 cells stably expressing EGFP. The Tet-OFF promoter system shows minimal leakiness, ensuring low miRNA production and 100% EGFP expression (relative to the level of control samples that do not express any miRNA) at high doxycycline concentrations (Figure 5.1A). However, the maximum knockdown efficiency is substantially lower with the inducible promoter system compared to the miRNA switch system, indicating that miRNA expression from the tetO-CMV promoter system is considerably weaker than that from a constitutive CMV promoter system (Figure 5.1A, B). The resulting increase in basal EGFP expression level limits the dynamic range of the inducible promoter system, leading to a smaller maximum fold-change in response to inducer molecules compared to the theophylline-responsive miRNA switch system (Figure 5.1A, B).

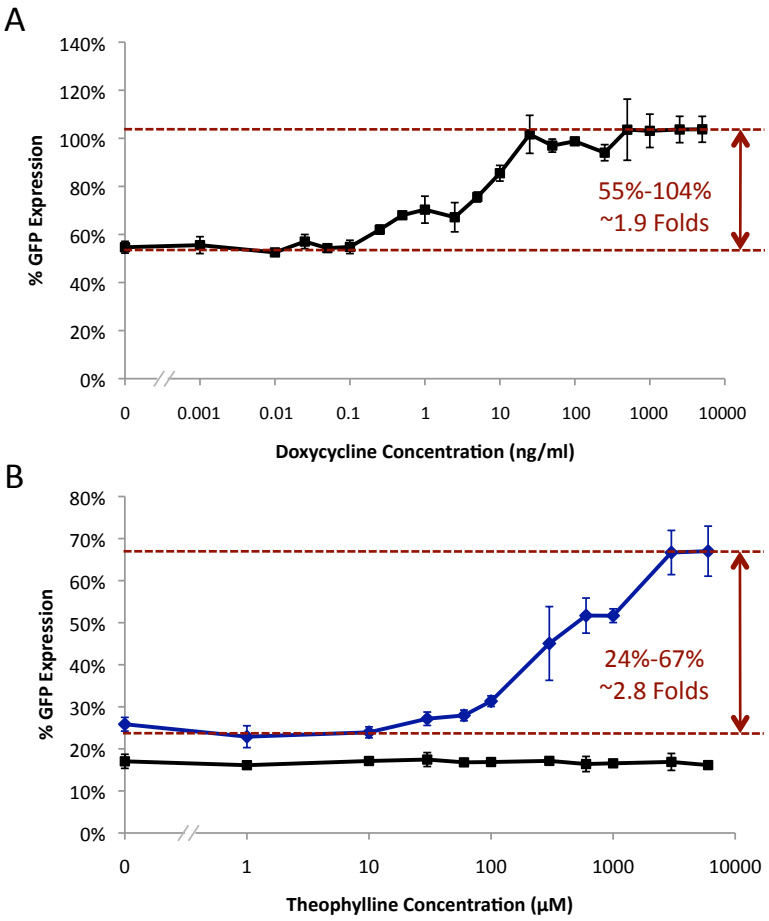

Figure 5.1. A single-copy miRNA regulated by the Tet-OFF inducible promoter system has lower knockdown efficiency and smaller switch dynamic range compared to a single-copy ligand-responsive miRNA switch construct. (A) The non-switch, EGFP-targeting wt miRNA expressed in single copy from a tetO-CMV promoter exhibits high basal expression levels and a modest fold change in response to doxycycline administration. (B) The theophylline-responsive, EGFP-targeting th1 miRNA switch (blue) expressed in single copy from a constitutive CMV promoter shows greater knockdown activity and a larger fold-change compared to the wt miRNA expressed from the Tet-OFF promoter system. The wt miRNA (black) expressed from a constitutive promoter shows significantly greater knockdown activity compared to the construct shown in (A), indicating weaker transgene and miRNA expression from the tetO-CMV promoter system. All constructs were evaluated by transient transfection in HEK 293 cells stably expressing EGFP. EGFP expression levels were normalized to those of control samples transfected with a construct lacking any miRNA sequence and treated at the same doxycycline or theophylline concentration. Reported values in (A) are mean ± s.d. from three independent samples. Data for (B) are taken from Ref. 13.

Multiple-copy miRNA expression increases silencing efficiency and reduces basal expression levels in both the inducible promoter and the ligand-responsive miRNA switch systems (Figure 5.2). Importantly, tight suppression of the tetO-CMV promoter in

the presence of doxycycline enables full EGFP expression in the ON state even with four copies of the miRNA (Figure 5.2A). This consistently high ON-state expression level, combined with lowered basal expression levels with additional miRNA copies, leads to an expanded switch dynamic range with multiple-copy expression and illustrates an important advantage of the inducible promoter system. However, at any given miRNA copy number the basal expression level remains considerably lower with the ligand-responsive miRNA switch system compared to the inducible promoter system (Figure 5.2B). The ability to effectively silence gene expression is critical in some applications, including stringent control over IL-2 receptor chain expression and T-cell proliferation. These results suggest that the miRNA switch system is capable of robust regulatory activity compared to one of the most commonly used inducible promoter systems. Since tetracycline and doxycycline are both highly toxic to T cells (Appendix Figures 1.2, 1.3), the miRNA switch system presents a critical advantage by allowing the use of better-tolerated molecules as regulatory inputs in a synthetic T-cell proliferation control system.

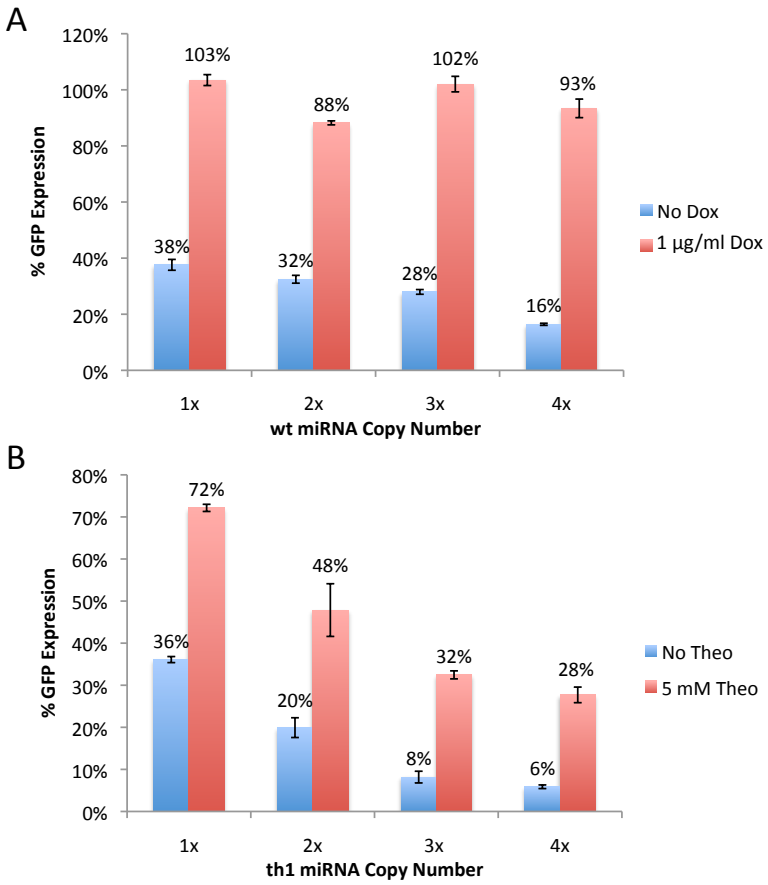

Figure 5.2. Multiple-copy expression of miRNAs improves the knockdown efficiency and the fold-change in gene expression in response to ligand induction. (A) The Tet-OFF promoter system shows consistently high ON-state expression but relatively weak knockdown efficiency. The wt miRNA was expressed in one to four copies from a tetO-CMV promoter and evaluated as described in Figure 5.1. (B) The ligand-responsive miRNA switch system shows efficient gene expression knockdown but also reduced ON-state expression levels with increasing miRNA copy numbers. The th1 miRNA switch was expressed in one to four copies from a constitutive CMV promoter. Reported values in (A) are mean ± s.d. from three independent samples. Data for (B) are taken from Ref. 13

Synthetic miRNAs Effectively Knockdown IL-2Rβ and γ_c Expression in Mouse T Cells. RNAi substrates identify genetic targets in a sequence-specific manner, such that each new target requires unique RNAi substrate sequences to be identified through screening strategies. The silencing efficiency of RNAi substrates is dependent on several factors—including sequence complementarity[14], length[12, 15], secondary structure[16-18] (Supplementary Text 5.2), and the relative thermodynamic stability at different

nucleotide positions[14, 19, 20]—that influence Drosha and Dicer processing efficiencies and biases in the loading of guide strands into RISCs. Although the precise mechanism by which RNAi substrates are processed has not been fully elucidated, current understanding has enabled the development of algorithms that support the design of short interfering RNAs (siRNAs), short hairpin RNAs (shRNAs), and miRNAs to researcher-specified genetic targets[20, 21].

We utilized the web-based Invitrogen BLOCK-iT^{TM} RNAi Designer tool to identify candidate miRNA sequences specific for mouse IL-2Rβ and γ_c (see Supplementary Text 5.3 for sequences). miRNA sequences were inserted into the 3' UTR of a transgene encoding for chloramphenicol acetyl transferase (CAT) expressed from a CMV promoter and evaluated by transient transfections in CTLL-2 mouse T cells. The surface expression levels of IL-2Rβ and γ_c were measured by antibody staining and flow cytometry. We selected sequences with the highest knockdown efficiencies for further characterization (Bm5 for IL2-Rβ; Gm1 and Gm8 for γ_c; Supplementary Figure 5.1). The miRNA sequences were expressed in multiple copies, and results demonstrate increasing knockdown efficiency with increasing copy numbers, confirming multiple-copy expression as an effective strategy for tuning regulatory stringency (Figure 5.3). Constructs expressing three copies of the IL-2Rβ- and γ_c-targeting miRNAs are capable of >80% knockdown of the respective receptor chains, indicating efficient silencing of the target genes.

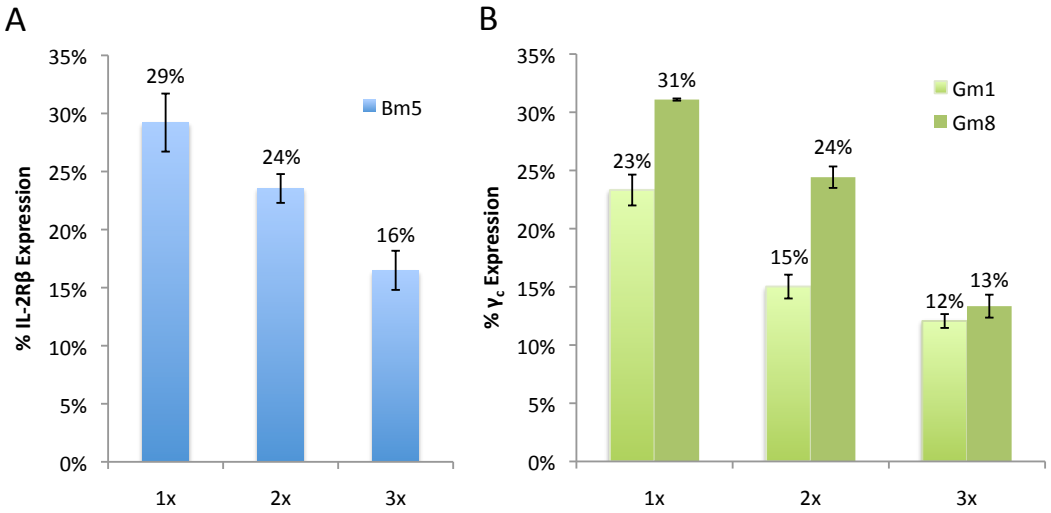

Figure 5.3. Multiple-copy expression of IL-2Rβ- and γ_c-targeting miRNAs improves knockdown efficiency. (A) The IL-2Rβ-targeting miRNA Bm5 and (B) γ_c-targeting miRNAs Gm1 and Gm8 were inserted in one to three copies in the 3' UTR of the CAT gene expressed from a CMV promoter. Constructs were tested by transient transfection in CTLL-2 cells, and surface antibody staining was performed to evaluate the expression level of the relevant receptor chain. Expression levels were normalized to those of control samples transfected with a construct lacking any miRNA sequence. Background expression levels were determined by isotype staining and set to 0% on the normalized scale (see Materials and Methods for details). Reported values are mean ± s.d. from two samples.

Combinatorial Expression of miRNAs Improves Regulatory Stringency. Although both IL-2Rβ and γ_c are necessary for IL-2 and IL-15 signaling, previous studies suggest that CTLL-2 cell proliferation is significantly reduced only when both receptor chains are inhibited[22]. Therefore, we examined the ability to knockdown IL-2Rβ and γ_c concurrently through combinatorial expression of miRNA sequences targeting each receptor chain. This implementation strategy mimics natural miRNA clusters capable of coordinated regulation over endogenous gene expressions[23]. Results show that each miRNA specifically reduces the expression of its intended target and has minimal off-target effects (Figure 5.4). Co-expression of IL-2Rβ- and γ_c-targeting miRNAs results in efficient knockdown of both receptor chains, indicating that simultaneous regulation of

multiple targets can be achieved through the combinatorial expression of miRNA sequences.

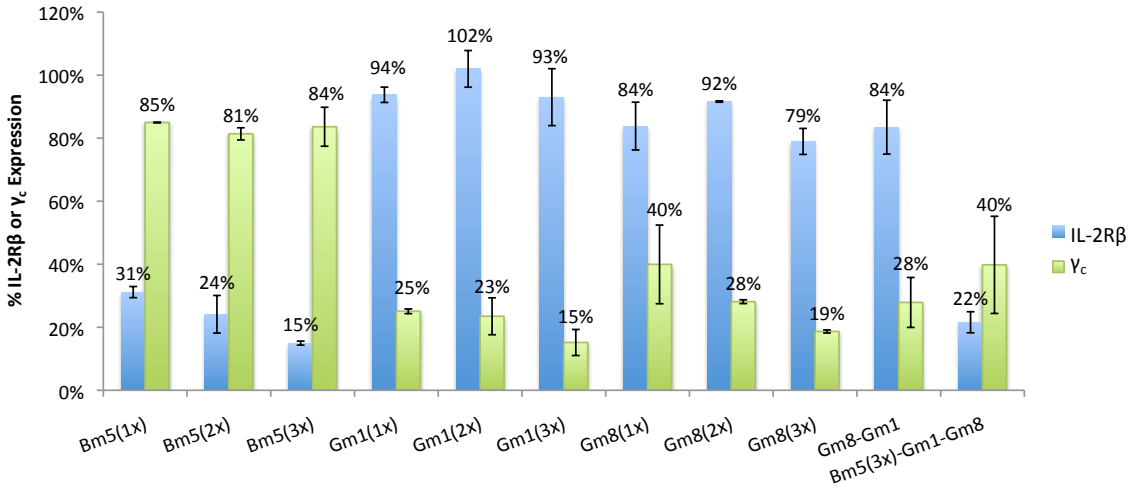

Figure 5.4. Combinatorial expression of IL-2Rβ- and γ_c-targeting miRNAs achieves effective receptor chain knockdown with high target specificity. IL-2Rβ- and γ_c-targeting miRNAs were expressed either in multiple copies or in combination with each other. Transiently transfected CTLL-2 cells were analyzed by surface antibody staining for both IL-2Rβ and γ_c. Normalization and background subtraction were performed as described in Figure 5.3. Reported values are mean ± s.d. from two samples.

Although multiple copy expression can improve overall knockdown activity, data on combinatorial constructs show evidence for reduced gene silencing by individual miRNAs in multiple-miRNA constructs. For example, the Bm5(3x) and Gm8-Gm1 constructs show stronger IL-2Rβ and γ_c knockdown activities, respectively, compared to the Bm5(3x)-Gm1-Gm8 construct, which encodes for all five miRNAs (Figure 5.4). Similar behavior has been observed with other multiple-copy constructs (Supplementary Figure 5.2A), suggesting the existence of an optimal miRNA copy number beyond which additional miRNAs would result in diminishing returns in knockdown efficiency. However, the results also indicate that, at the copy numbers tested, the decrease in individual miRNA processing efficiency is generally more than compensated by the

increase in overall knockdown efficiency when multiple miRNAs with the same target are co-expressed (Figures 5.3 and 5.4; Supplementary Figure 5.2B).

Secondary Structure Affects the Knockdown Efficiency and Switch Dynamic Range of Ligand-Responsive miRNA Switches. Previous work has demonstrated that ligand-responsive miRNA switches can be generated by incorporating an RNA aptamer into the basal segment of the miRNA stem-loop structure[13]. However, the relationship between the structure of the upper portion of the miRNA and the knockdown efficiency and dynamic range of the miRNA switch has not been fully examined. To evaluate the structural significance of the upper portion of the miRNA, we designed various switches based on structures from both the BLOCK-iT™ RNAi Designer tool (Supplementary Figure 5.3A, hereafter termed structure A) and the natural miRNA-30a (Supplementary Figure 5.3B, hereafter termed structure B), the latter being the template for the original ligand-responsive miRNA switch designs[13].

We first constructed ligand-responsive miRNAs to IL-2Rβ based on the IL-2Rβ-targeting miRNA sequence found to have the greatest silencing activity (Bm5, Supplementary Figure 5.1). We converted structure A into switches by replacing either the bottom or the top bulge in the basal segment of the miRNA with a theophylline aptamer (Figure 5.5A, B). Two additional switches were constructed by inserting the same IL-2Rβ-targeting sequence in either the 3' or the 5' side of a structure B-based miRNA stem, following the template of previously developed switch structures[13] (Figure 5.5C, D).

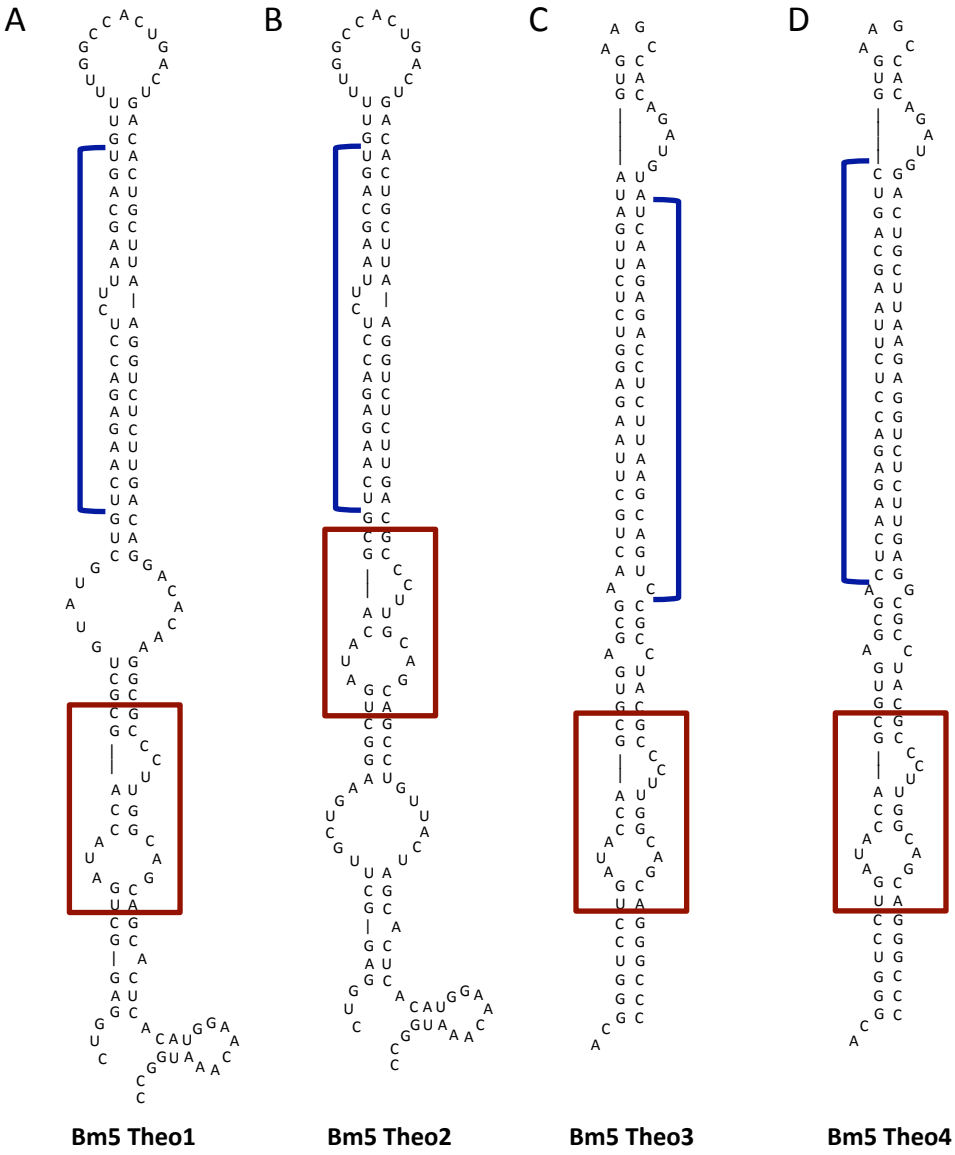

Figure 5.5. Secondary structures of miRNA switches. (A) Bm5 Theo1 and (B) Bm5 Theo2 were constructed by replacing the bottom or top bulge, respectively, in the basal segment of the IL-2Rβ-targeting miRNA Bm5 with the theophylline aptamer. (C) Bm5 Theo3 and (D) Bm5 Theo4 were constructed by inserting the same targeting sequence into either the 3' or the 5' side, respectively, of the mature miRNA stem in a switch structure based on miRNA-30a. Blue brackets indicate the miRNA targeting sequence that is complementary to the regulatory target. Red boxes delineate the theophylline aptamer.

Transient transfection results indicate that placing the theophylline aptamer immediately below the miRNA stem abolishes silencing activity (Bm5 Theo2, Figure 5.6), whereas integrating the theophylline aptamer lower in the miRNA stem preserves knockdown efficiency but fails to confer ligand-responsiveness in structure A–based

constructs (Bm5 Theo1, Figure 5.6). In contrast, a structure B–based design is capable of ligand-responsive ON switch behavior, but its knockdown efficiency is greatly compromised compared to the original miRNA sequence (Bm5 Theo4, Figure 5.6).

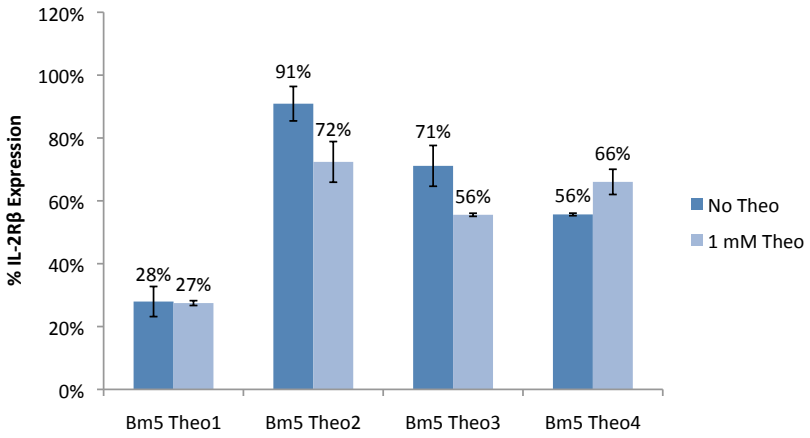

Figure 5.6. Secondary structure has substantial impact on miRNA switch dynamic range and knockdown efficiency. miRNA switches depicted in Figure 5.5 were tested by transient transfection in CTLL-2 cells and assayed by surface antibody staining for IL-2Rβ. Bm5 Theo1 shows the strongest knockdown activity, whereas Bm5 Theo4 is the only device that exhibits ON switch behavior in response to theophylline. Normalization and background subtraction were performed as described in Figure 5.3. Reported values are mean ± s.d. from two samples.

We designed a second panel of switches by combining features from structures A and B to merge the strengths of the two structures. Specifically, to improve the ligand responsiveness of structure A-based designs, we either shortened (Figure 5.7A) or modified the basal segment of Bm5 Theo1 to more closely resemble structure B-based constructs, such that the distances between the mature miRNA and the theophylline aptamer are 11- and 9-nt on the 5' and 3' sides, respectively (Figure 5.7B-D). These length specifications were guided by previous reports on the structural requirements for Drosha processing[16]. In addition, to improve the knockdown efficiency of structure B-based designs, Bm5 Theo4 was modified to incorporate the terminal loop and/or internal bulge present in the miRNA stem of structure A (Figure 5.8A-C).

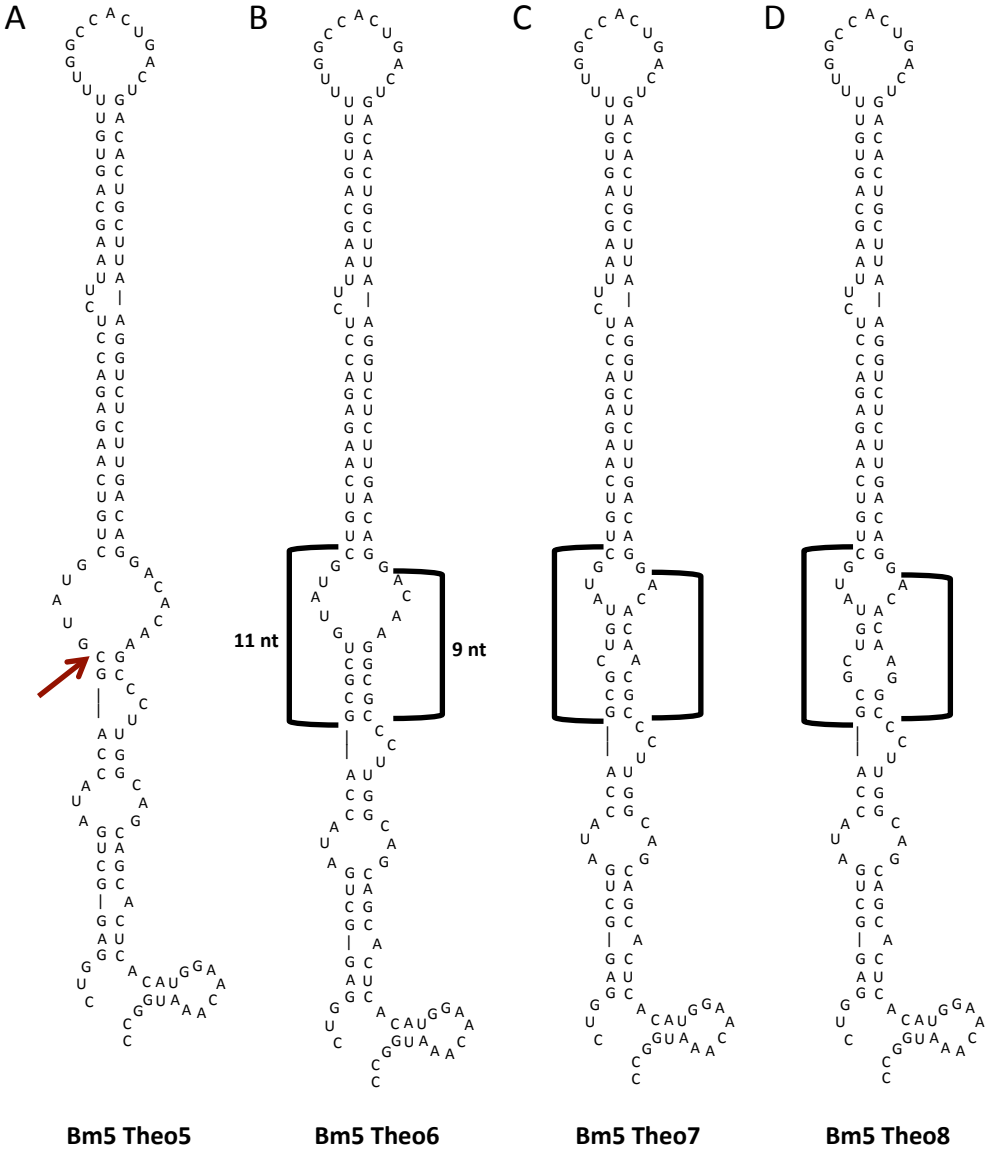

Figure 5.7. Secondary structures of modified miRNA switches based on Bm5 Theo1. (A) Three base pairs between the theophylline aptamer and the top bulge in the basal segment of Bm5 Theo1 (position noted by red arrow) were removed to construct Bm5 Theo4. (B-C) Two nucleotides on the 3' side of the basal segment of Bm5 Theo1 were removed to construct Bm5 Theo5-8. Black brackets indicate the 11-nt and 9-nt distances between the end of the mature miRNA stem-loop and the top bulge of the theophylline aptamer.

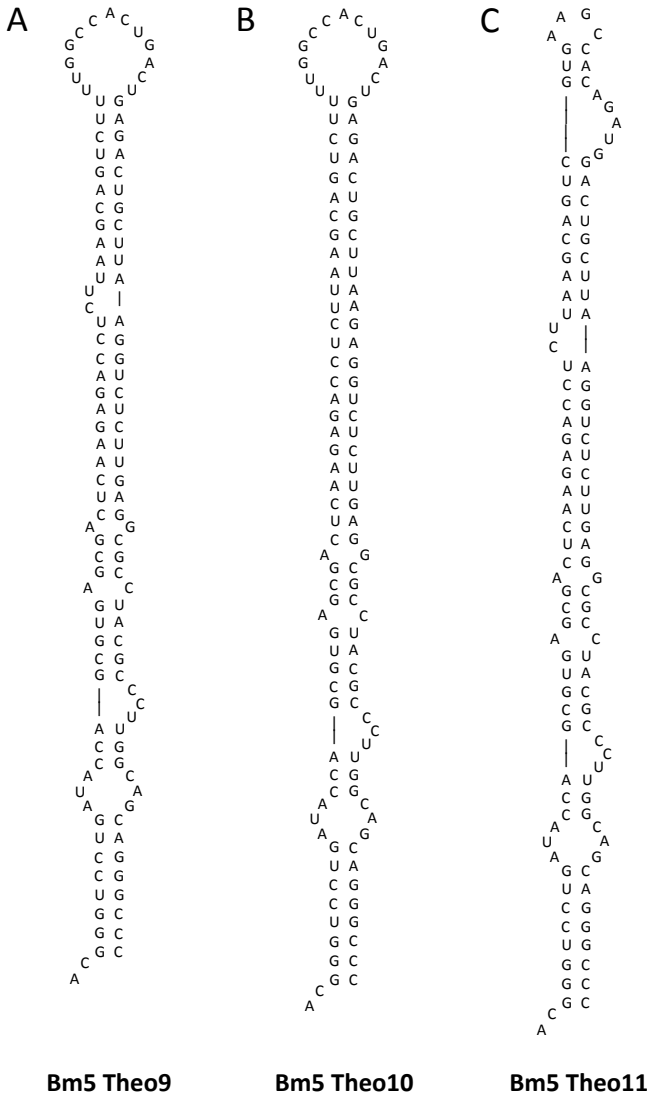

Figure 5.8. Secondary structures of modified miRNA switches based on Bm5 Theo4. (A) The terminal loop and internal bulge in the mature miRNA stem of Bm5 Theo1 were inserted into Bm5 Theo4 to construct Bm5 Theo9. Only (B) the terminal loop or (C) the internal bulge was inserted to construct Bm5 Theo10 and Bm5 Theo11, respectively.

Transient transfection results indicate that knockdown efficiency is highly sensitive to the distance between the miRNA stem and the aptamer, such that the elimination of three base pairs reduces knockdown efficiency by more than four-fold (Bm5 Theo1 vs. Bm5 Theo5, Figure 5.9). Furthermore, minor sequence changes in the basal segment have substantial impacts on knockdown activity. Specifically, two devices

with a single-nucleotide difference exhibit a 19% difference in knockdown efficiency (Bm5 Theo7 vs. Bm5 Theo8, Figure 5.9), highlighting the importance of small sequence discrepancies in the basal segment and their resulting structural changes. Our optimization strategies did achieve a ligand-responsive switch capable of significant knockdown activity—Bm5 Theo9. The optimized IL-2Rβ-targeting miRNA switch integrated the terminal loop and internal bulge from structure A and the basal segment from structure B (Figure 5.8A). This structure was adopted for all subsequent switch designs.

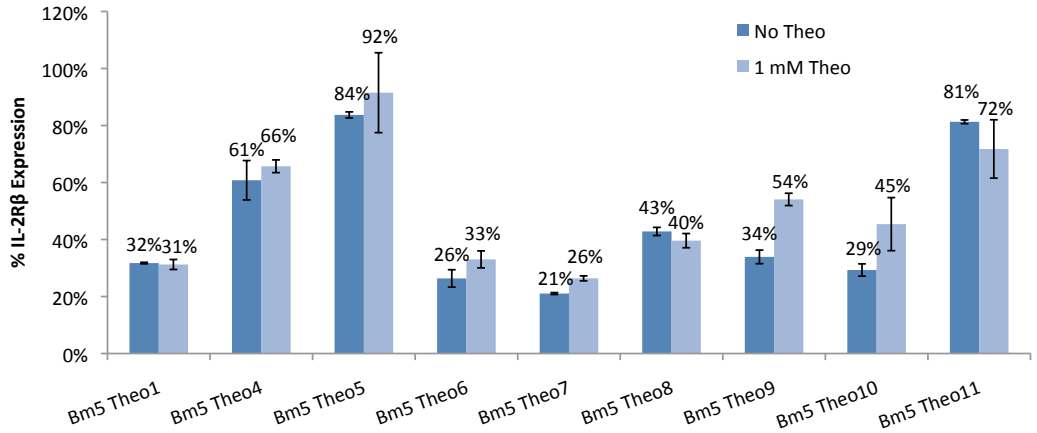

Figure 5.9. Combining features from different miRNA secondary structures exhibiting either strong knockdown efficiency or ligand responsiveness results in improved switch designs. miRNA switches depicted in Figures 5.7 and 5.8 were evaluated for knockdown efficiency and theophylline responsiveness by transient transfection in CTLL-2 cells and surface antibody staining for IL-2Rβ. Bm5 Theo9 shows the best combination of knockdown efficiency and switch dynamic range among the constructs tested. Normalization and background subtraction were performed as described in Figure 5.3. Reported values are mean ± s.d. from two samples.

miRNA Switches Demonstrate Tunable, Theophylline-Responsive Knockdown of IL-2Rβ Surface Expression Levels. The Bm5 Theo9 switch was cloned in multiple copies and evaluated by transient transfection. Results show increasing knockdown activity with increasing copy numbers (up to three copies) while maintaining the fold-increase in IL-2Rβ expression in response to theophylline, thus demonstrating tunable,

ligand-dependent regulatory function (Figure 5.10). However, the inclusion of a fourth miRNA copy shows no increase in knockdown efficiency and results in a reduced switch dynamic range, indicating a point of negative return in the relationship between miRNA copy number and switch activity. Since the switch construct has a lower knockdown efficiency than the non-switch miRNA (Bm5(1x) vs. Bm5T9(1x) in Figure 5.10), the Bm5T9(3x) design likely represents the optimal combination of IL-2Rβ knockdown and theophylline-responsive switch activity achievable with this particular switch sequence, even though its basal level is still higher than that achieved by the non-switch version of the miRNA (Bm5(3x), Figure 5.4). Further improvements will likely require the identification of more efficient miRNA target sequences or the simultaneous expression of multiple-copy miRNA constructs cloned in the 3' UTR of different genes (i.e., not all in tandem behind one gene).

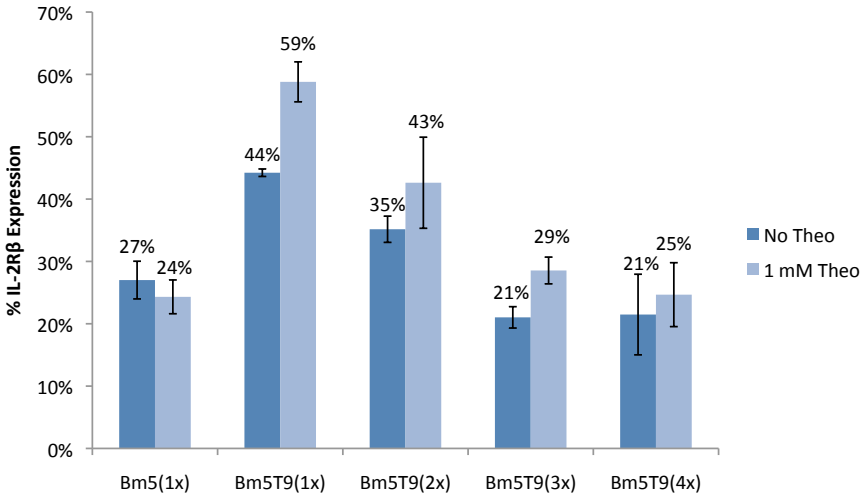

Figure 5.10. miRNA switches show tunable, theophylline-responsive knockdown of endogenous IL-2Rβ expression levels. IL-2Rβ-targeting miRNA constructs with and without a theophylline aptamer incorporated in the miRNA basal segment were transiently transfected in CTLL-2 cells and evaluated by surface antibody staining for IL-2Rβ in the presence and absence of theophylline. The non-switch construct, Bm5(1x), shows effective knockdown and no response to theophylline. Constructs expressing the Bm5 Theo9 (Bm5T9) switch in one to four copies show effective IL-2Rβ knockdown as well as theophylline-dependent ON switch activities. Normalization and background subtraction were performed as described in Figure 5.3, using control samples treated with the appropriate concentration of theophylline. Reported values are mean ± s.d. from two samples.

γ_c-Targeting miRNA Switches Demonstrate Tunable Knockdown Activities. The γ_c-targeting sequences in the miRNAs Gm1 and Gm8 were used to construct theophylline-responsive switches Gm1 Theo1 and Gm8 Theo1, respectively, with the same RNA structure as Bm5 Theo9. Multiple-copy constructs were tested by transient transfection, and results show similar behaviors as the Bm5 Theo9 switch. Specifically, knockdown efficiencies of miRNA switches are lower than those of non-switch miRNAs, but the efficiencies increase with copy number (Figure 5.11). As with non-switch miRNAs, switch constructs carrying the Gm1 target sequence have stronger knockdown activities than those carrying the Gm8 target sequence. However, it appears that the Gm8 Theo1 design can still benefit from additional miRNA switches beyond the third copy, whereas the Gm1 Theo1 construct may have reached its maximum knockdown efficiency at two copies (Figure 5.11).

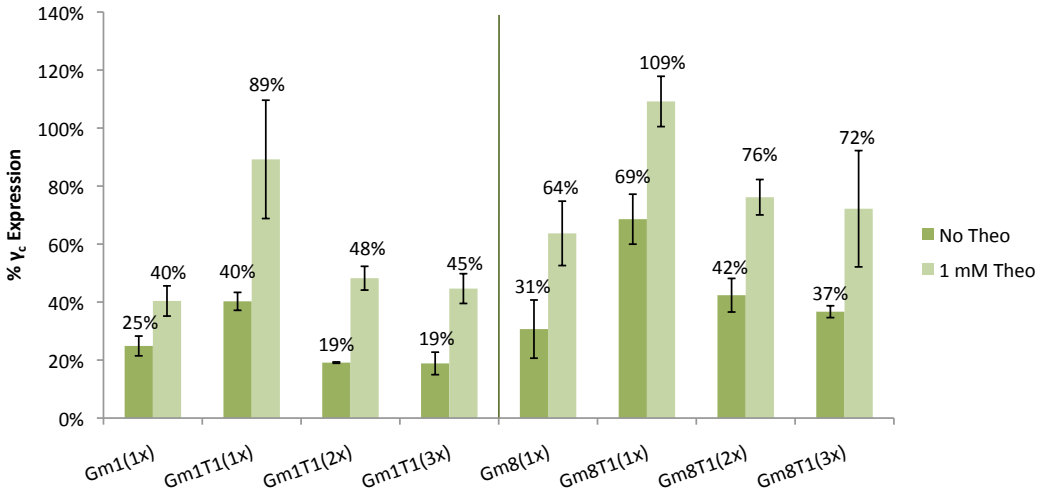

Figure 5.11. miRNA switches show tunable knockdown of endogenous γ_c expression levels. γ_c-targeting miRNA constructs with two distinct target sequences (Gm1 and Gm8) were transiently transfected in CTLL-2 cells and evaluated by surface antibody staining for γ_c. Both non-switch and switch constructs show effective γ_c knockdown, with increasing miRNA copy numbers corresponding to increasing knockdown efficiency. However, even the non-switch constructs Gm1 and Gm8 show ON switch behavior in response to theophylline, thus preventing accurate evaluation of the theophylline dependence of the switch constructs Gm1 Theo1 (Gm1T1) and Gm8 Theo1 (Gm8T1). Normalization and background subtraction were performed as described in Figure 5.10. Reported values are mean ± s.d. from two samples.

A critical difference between the IL-2Rβ- and γ_c-targeting switch constructs lies in their response to ligand input. As anticipated, the non-switch Bm5 miRNA does not respond to theophylline addition, indicating that the ON switch behavior exhibited by the Bm5 Theo9 construct is a ligand-specific response (Figure 5.10). However, the non-switch Gm1 and Gm8 constructs show ON switch behavior in the presence of theophylline (Figure 5.11). Repeated transfection experiments indicate that although the absolute expression levels of both IL-2Rβ and γ_c decrease with theophylline addition, the effect is smaller on IL-2Rβ than on γ_c (Supplementary Table 5.1). Furthermore, since the absolute intensity of γ_c is relatively low, minute changes in intensity—which can be caused by non-specific effects of theophylline, the trauma of electroporation, and small differences in transfection efficiency—significantly affect the calculated % γ_c expression level. As a result, theophylline-dependent switch activities of the Gm1 Theo1 and Gm8 Theo1 constructs cannot but accurately evaluated by surface antibody staining for the γ_c chain in transiently transfected samples.

More precise evaluation of γ_c silencing by the switch constructs may be achieved with stable integration of the miRNAs into the host genome, which would prevent the physical trauma caused by electroporation and allow the selection of cells that express the constructs of interest. However, in the absence of site-specific integration capabilities, stably integrated cells will vary in the target gene's basal expression levels due to differences in the construct insertion site and in the resultant miRNA expression levels. Nevertheless, a stably integrated system is likely to permit more accurate evaluation of the switch behavior of γ_c-targeting constructs in response to ligand addition, which is influenced by but not entirely dependent on the basal expression level.

Effects of IL-2Rβ and γ_c Modulation on T-Cell Proliferation are Dependent on the Type and Concentration of Cytokines Present in the Cell Culture. Although IL-2 and IL-15 share the IL-2Rβ and γ_c chains in their signaling pathways, it is unknown whether their abilities to promote T-cell proliferation are affected in the same manner by changes to the levels of IL-2Rβ and γ_c. An integrated control system that includes both ribozyme- and miRNA-based switches can regulate cytokine and receptor chain levels simultaneously and specify the cytokine molecule that drives T-cell proliferation. Therefore, understanding the difference between the two cytokines' responses to receptor-chain modulation will assist in designing the optimal combination of regulatory devices and genetic targets. Previous studies have reported T-cell growth inhibition by supplementing culture media with soluble monoclonal antibodies (mAbs) that specifically block IL-2Rβ and γ_c[22, 24]. In these experiments, CTLL-2 cells were cultured in the presence of exogenous IL-2, and results indicate that simultaneous blockage of IL-2Rβ and γ_c significantly reduces cell proliferation at IL-2 concentrations below 100 nM, confirming IL-2Rβ and γ_c as potent targets for T-cell proliferation control. However, similar studies have not been performed with cells cultured in IL-15.

To evaluate the relative impact of the two cytokines as regulatory targets for a T-cell proliferation control system, we examined the effects of IL-2Rβ- and γ_c-blocking mAbs on the growth of CTLL-2 cells treated with either IL-2 or IL-15. CTLL-2 cells were cultured with isotype control, IL-2Rβ-blocking, γ_c-blocking, or both IL-2Rβ- and γ_c-blocking mAbs in media supplemented with either IL-2 or IL-15 at various concentrations. To enable comparison between the two cytokines, we supplied IL-2 and IL-15 at concentrations known to support comparable levels of cell growth under regular

culturing conditions. Specifically, titration studies indicate that 100 U/ml of IL-2 is approximately equivalent to 0.5 ng/ml of IL-15 in its ability to sustain CTLL-2 survival and expansion (Supplementary Figure 5.4). Cell viability and total cell count were measured by flow cytometry after 48 hours of incubation with cytokine and mAb. Consistent with previous reports, proliferation of CTLL-2 cells cultured in IL-2 is significantly reduced only with simultaneous blockage of IL-2Rβ and γ_c (Figure 5.12A). In contrast, CTLL-2 cells cultured in IL-15 are sensitive to blockage of individual receptor chains, even though simultaneous blockage of both IL-2Rβ and γ_c results in more pronounced growth inhibition (Figure 5.12B). Furthermore, cultures require a larger input of IL-15 relative to IL-2 to overcome the growth-inhibitory effect of mAb treatment, indicating that CTLL-2 cells conditioned with IL-15 are more sensitive to fluctuations in the level of receptor chains available for cytokine binding and signaling. The increased sensitivity to receptor chain levels observed with IL-15 suggests this cytokine as the preferred target for incorporation into an integrated T-cell proliferation control system.

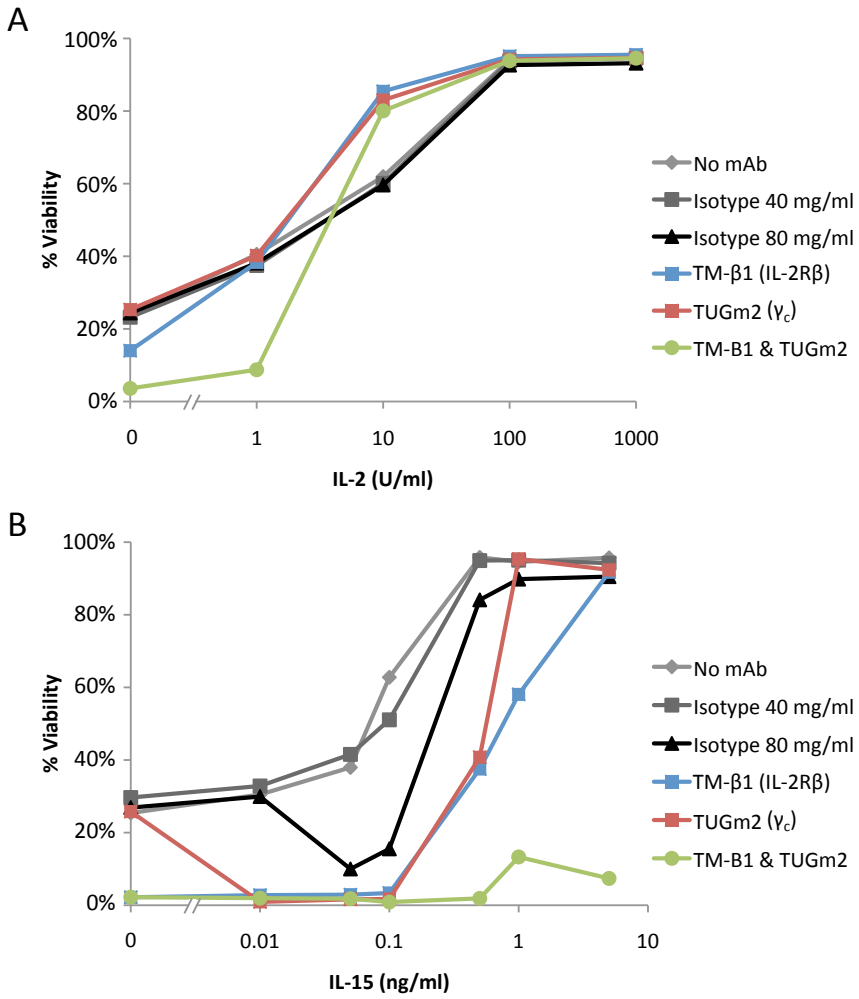

Figure 5.12. CTLL-2 cells cultured with IL-2 and IL-15 respond differently to treatments with IL-2Rβ- and γ_c-blocking antibodies. Monoclonal antibodies known to block either IL-2Rβ (clone TM-β1) or γ_c (clone TUGm2) were added to the culture media of untransfected CTLL-2 cells. Cultures were supplemented with a gradient concentration of either (A) IL-2 or (B) IL-15. Cells were treated with 7-AAD dead-cell stain and analyzed by flow cytometry for cell viability 48 hours after antibody and cytokine additions. CTLL-2 cells cultured in IL-15 are more sensitive to treatment with blocking antibodies, and a combination of IL-2Rβ- and γ_c-blocking antibodies is the most effective at inhibiting CTLL-2 proliferation.

miRNA Switches Show Drug-Responsive Regulation of Activities in the IL-15 Signaling Pathway. To evaluate the impact of IL-2Rβ- and γ_c-targeting miRNA switches on the functional output of the cytokine signaling pathway, we performed intracellular antibody staining for phosphorylated STAT5 (pSTAT5) in transiently transfected CTLL-2 cells. The phosporylation of STAT5 is an essential step in the IL-2/IL-15 signaling

cascades and in the induction of T-cell proliferation[3] (Figure 3.1). We chose to examine the IL-15 pathway based on this cytokine's sensitivity to receptor chain expression modulation. Cells were cultured in the absence of cytokine for 24 hours after transfection and stimulated with 1 ng/ml of IL-15 for 15 minutes prior to cell fixation and pSTAT5 staining. Results indicate that non-switch miRNA constructs are capable of pSTAT5 knockdown with minimal response to theophylline addition (Figure 5.13A). In contrast, γ_c-targeting miRNA switches demonstrate both pSTAT5 knockdown and theophylline-dependent ON switch activities, indicating drug-responsive regulation of functional outputs in the IL-15 signaling pathway (Gm1T1(1x) and Gm1T1(3x), Figure 5.13B).

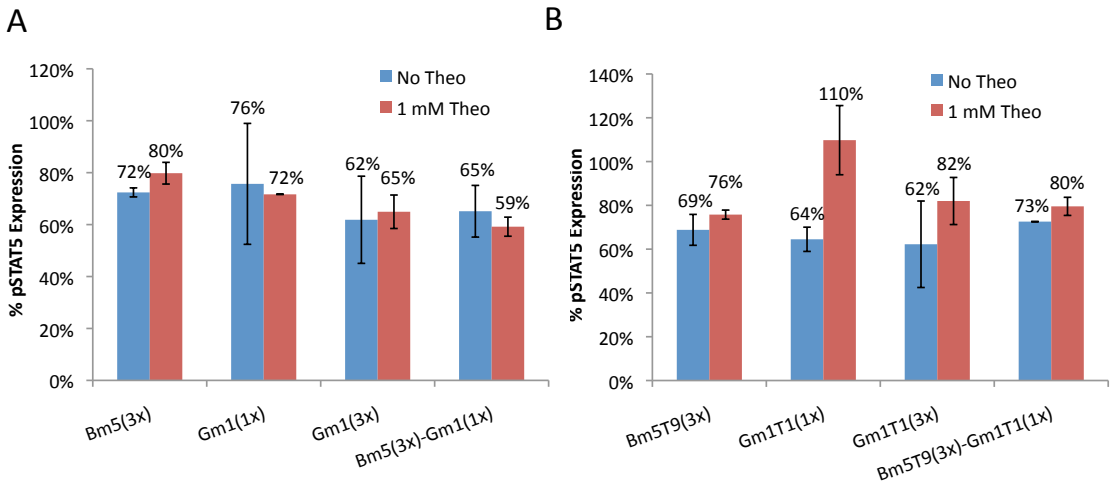

Figure 5.13. miRNA switches regulate functional outputs in the IL-15 signaling pathway. (A) Non-switch, IL-2Rβ- and γ_c-targeting miRNA constructs reduce intracellular pSTAT5 levels in transiently transfected CTLL-2 cells in a theophylline-independent manner. (B) γ_c-targeting miRNA switch constructs effectively reduce pSTAT5 levels and exhibit theophylline-dependent ON switch activity. However, IL-2Rβ-targeting switch constructs show minimal theophylline responsiveness. Normalization and background subtraction were performed as described in Figure 5.10. Reported values are mean ± s.d. from two samples.

Although the miRNA constructs exhibit several prescribed functions as discussed above, two unexpected outcomes were observed in the pSTAT5 intracellular staining experiments. First, the basal pSTAT5 expression levels are very similar in all the samples tested, regardless of the type and copy number of miRNAs in each construct. Although

surface antibody staining for the receptor chain indicates a two-fold difference in γ_c expression between the one-copy and three-copy constructs for both Gm1 (Figure 5.3) and Gm1 Theo1 (Figure 5.11), results from intracellular pSTAT5 staining suggest similar levels of signaling activity in the IL-15 pathway for all four constructs in the absence of theophylline (Figure 5.13). Furthermore, combinatorial constructs including both IL-2Rβ and γ_c-targeting miRNAs (Bm5(3x)-Gm1(1x) and Bm5T9(3x)-Gm1T1(1x), Figure 5.13) show no significant difference in their impact on pSTAT5 levels compared to single-target constructs with fewer miRNA copy numbers. These results suggest a potential limit to the extent of pSTAT5 regulation that can be achieved by modulating IL-2 receptor chains. Since IL-2/IL-15 signaling requires heterodimerization of the IL-2Rβ and γ_c chains, elimination of one of the chains is theoretically sufficient to inhibit signaling, and knockdown of both chains may not result in an additive effect on reducing pSTAT5 levels. Furthermore, STAT5 is involved in multiple signaling pathways and is activated in response to a variety of cytokines and tyrosine kinase receptors[25]. Therefore, STAT5 phosphorylation resulting from processes unrelated to IL-2/IL-15 signaling may have led to the relatively high pSTAT5 levels observed in this study. However, CTLL-2 cells cultured for 24 hours in the absence of cytokines exhibit <10% pSTAT5 relative to the same cell culture induced with IL-2 for fifteen minutes prior to pSTAT5 staining (Supplementary Figure 5.5), suggesting that the background pSTAT5 level in cytokine-starved cells is relatively low and that the high pSTAT5 levels observed in transient transfection experiments are a direct consequence of cytokine stimulation. Therefore, it is yet unclear whether the miRNA constructs tested have truly reached the maximum extent

of pSTAT5 regulation that can be achieved by modulating IL-2 receptor chain expression levels.

Second, although constructs containing IL-2Rβ-targeting miRNA switches exhibit theophylline-dependent control over IL-2Rβ expression levels (Figure 5.10), they show minimal response to theophylline in their effect on pSTAT5 levels (Bm5T9(3x) and Bm5T9(3x)-Gm1T1(1x), Figure 5.13B). One possible explanation is that the particular IL-2Rβ-targeting constructs tested here, which contain three and four copies of miRNAs, cause sufficiently strong IL-2 receptor chain knockdown to reach the lowest pSTAT5 levels possible even in the ON state. This hypothesis assumes that pSTAT5 levels are "buffered" by cellular mechanisms to maintain a minimum threshold, and this buffering activity can mask the ON switch behavior of the miRNA constructs. Further investigation, including the evaluation of lower-copy-number constructs and miRNA sequences with weaker knockdown activity, may shed light on the cause of the phenomena observed. More importantly, alternative measures of T-cell proliferation are necessary to accurately evaluate the impacts of IL-2Rβ and γ_c-targeting miRNAs.

We closely examined the percent viability of CTLL-2 cells transiently transfected with miRNA constructs, but the results show no viability impact by miRNAs that have clear knockdown activity toward IL-2Rβ and γ_c (Supplementary Figure 5.6A). Studies have shown that cell proliferation is dependent on the concentration of IL-2 and IL-15 present in the culture media. At sufficiently high cytokine concentrations, it is possible to achieve robust cell proliferation even when the cultures are treated with saturating amounts of IL-2Rβ- and γ_c- blocking antibodies[22, 24] (Figure 5.12). To address this possibility, we have evaluated the viability of CTLL-2 cells transiently transfected with

miRNA constructs and cultured at various IL-2 concentrations. However, the results show no significant miRNA-mediated viability knockdown at any of the IL-2 levels tested (Supplementary Figure 5.6B). It should be noted that viability measurements do not permit gating for transfection efficiency. Since dead cells are autofluorescent, it is impossible to separate transfected and untransfected populations (which are distinguished by the expression of the fluorophore mTagBFP encoded by the transfected plasmid) prior to viability measurements. Since the transfection efficiency for miRNA constructs in CTLL-2 cells is generally below 35% (based on the percent $mTagBFP^+$ population observed in transfected samples), the impact of miRNAs on the viability of transfected cells is necessarily obscured by the presence of large untransfected populations that do not express any miRNA. This is the main reason for our decision to evaluate the proliferative response by intracellular staining of pSTAT5, which permits gating for transfection efficiency.

We have also attempted intracellular labeling with carboxylfluorescein succinimidyl ester (CFSE) to monitor cell division in CTLL-2 cells[26]. However, CTLL-2 cells show a robust proliferative response to IL-2 and divide in a synchronous manner. As a result, only a single peak (instead of multiple peaks corresponding to different cell division numbers) is observed at any given time point (Supplementary Figure 5.7). Although CFSE dilution is observed over time, the decrease in dye intensity does not correspond to the increase in viable cell count, thereby precluding the use of CFSE labeling as a quantitative assay for CTLL-2 proliferation.

Discussion

The efficacy of adoptive T-cell therapy depends on a strong proliferative response of transferred T cells *in vivo*. However, the safety of this strategy depends, in part, on the ability to effectively inhibit T-cell proliferation at the conclusion of the treatment period. Earlier work has shown that a synthetic T-cell proliferation control system regulating the transgenic expression of a proliferative cytokine through ribozyme-based devices is capable of sustaining robust T-cell growth[2]. However, the application of engineered genetic control systems in human patients will benefit from additional layers of safety control that ensures stringent suppression of cell proliferation in the OFF state. Here, we expanded the control system to include RNAi-based regulatory devices that target endogenous cytokine receptor chains, which are necessary for the IL-2 and IL-15 signaling pathways critical to T-cell proliferation.

The targeting of endogenous genes requires *trans*-acting control devices that do not need to be physically linked to the target transcript. We adapted a previously described ligand-responsive miRNA switch system[13] to the control of common cytokine receptor chains. The miRNA switch platform is capable of titratable gene expression regulation in response to a specific ligand, similar to inducible promoter systems. Our studies demonstrate that the miRNA switches are capable of greater knockdown efficiency and comparable regulatory dynamic range relative to non-switch miRNAs expressed from the commonly used tet-inducible promoter system. Furthermore, the unique modularity of the miRNA switch platform allows for systematic programming of switch devices to respond to researcher-specified molecular inputs. This characteristic enables the construction of regulatory systems that respond to ligands with lower toxicity

than the inducer molecules required for commonly used promoter systems, such as tetracycline and doxycyline. Furthermore, it allows for the simultaneous implementation of multiple control devices that can regulate different genetic targets in response to different ligand inputs, thus enabling combinatorial control systems with greater versatility and regulatory stringency.

We constructed theophylline-responsive miRNA switches capable of effective regulation over the expression levels and signaling activities of the IL-2Rβ and γ_c receptor chains critical to T-cell proliferation. We generated optimized switch constructs through a systematic evaluation of structural and sequence requirements that maximize silencing efficiency and switch dynamic range. A large terminal loop, an internal bulge in the upper stem, and careful sequence optimization in the basal segment were shown to have significant impacts on both the knockdown activity and the ligand responsiveness of miRNA switches.

Although we demonstrated effective gene expression knockdown and theophylline-responsive ON switch behavior by IL-2Rβ- and γ_c-targeting miRNAs, we were unable to show miRNA-mediated impact on T-cell proliferation through direct measurements of cell viability and growth. This difficulty in characterizing the viability response of transiently transfected samples is partly due to mismatches in the timing and level of expression for the regulatory device (i.e., the miRNA), the regulatory target (i.e., IL-2Rβ or γ_c), and the proliferative signaling molecule (i.e., IL-2 or IL-15). In transient transfection studies, the miRNAs are expressed from plasmids for a relatively brief period, whereas the targeted receptor chains are expressed endogenously and are present both before and after the brief surge of miRNA expression. Pre-existing receptor chains

contribute to signaling and cell viability, and new receptor chains are continuously produced after the transient effects of plasmid-based miRNA expression, thus introducing two uncontrollable factors that can obscure the effects of miRNA-mediated receptor chain knockdown. Furthermore, cell proliferation is dependent on the concentration of IL-2 and IL-15 present in the culture media. Unlike the ribozyme-based control system discussed in Chapter 3, in which the regulatory device is co-expressed with the cytokine, the miRNA-based system interacts with exogenous cytokines whose concentrations are difficult to match precisely to the expression levels of the miRNA constructs in transiently transfected samples. As a result, the impact of miRNA constructs on cell viability is not as readily observable as that of ribozyme-based control devices.

Percent viability measurements provide a rough-grained evaluation of the cumulative effects of cell growth over time. That is, cell viability measured at 24 hours after transfection does not capture a snapshot view of the sample's proliferative capability at that moment. Instead, it reflects the cumulative effect of cellular events experienced by the sample up to the time of measurement. A more precise evaluation method may be the incorporation of ^{3}H-thymidine, which measures DNA production within a defined time period between ^{3}H-thymidine addition and cell harvest for radioactivity measurement. In addition, stable integration may be necessary for the accurate evaluation of miRNA-based regulatory systems. Unlike transiently transfected cells, stably integrated cell lines will express the regulatory device and its target at the same time and at more comparable levels, thus removing two important variables in the evaluation of knockdown activities. In addition, clonal cell lines will have narrower distributions in miRNA expression levels (see discussions in Chapter 2, Figure 2.4A), thus enabling more precise characterization

of each miRNA device. Ongoing efforts in the Smolke Laboratory aim to generate a Flp-In CTLL-2 host cell line, which will allow site-specific integration of RNA-based regulatory systems for long-term characterizations.

Despite the challenges in evaluating system performance based on cell viability, antibody staining results have clearly demonstrated the ability of miRNA switches to knockdown IL-2Rβ and γ_c expressions and regulate signaling activities in the IL-15 pathway. In addition to constructing individual miRNA switches capable of gene silencing, we demonstrated the ability to fine-tune the regulatory stringency of our system through combinatorial expression of miRNA switches. Multiple-copy expression improved silencing efficiency. Furthermore, synthetic miRNA clusters expressing miRNAs specific for different genes can achieve the simultaneous knockdown of multiple targets, thus generating a regulatory system that can more effectively specify a functional output by the concurrent regulation of multiple cellular components involved in the associated pathway.

An important feature of miRNA switches that has not been fully utilized in the current study is their ability to act both in *cis* and in *trans*. Since Drosha processing of the miRNA results in excision of the mature miRNA hairpin from its surrounding sequence, one could regulate gene expression in *cis* by inserting the miRNA switch in the 3' UTR of a target transgene. For example, an IL-2Rβ-targeting miRNA switch inserted in the 3' UTR of a transgene encoding for IL-2 or IL-15 can regulate both the cytokine and its receptor chain simultaneously. This compact, dual-function device can thus provide two layers of defense against undesired cell proliferation in the OFF state, which is of critical importance to the safety of cell-based therapeutic strategies. Alternatively, the miRNA

switches developed in this work can be combined with previously reported ribozyme-based devices to generate integrated control systems capable of simultaneous regulation of multiple targets essential to T-cell proliferation. We discovered that the IL-15-induced T-cell proliferation response is highly sensitive to changes in IL-2Rβ and γ_c expression levels. Therefore, a control system in which IL-15 expression is regulated by ribozyme switches while IL-2Rβ and γ_c expressions are modulated by miRNA switches can be constructed to exert stringent control over T-cell proliferation. In this system, the ribozyme and miRNA switches may be programmed to respond to the same molecular input, such that a single drug can both promote cytokine production and prevent receptor chain knockdown when administered to patients receiving adoptively transferred T cells. Conversely, termination of drug intake will simultaneously reduce cytokine production and receptor chain expression, thereby ensuring effective inhibition of T-cell expansion.

In addition to controlling growth-stimulatory targets such as cytokines and their receptor chains, regulatory devices targeting growth-inhibitory genes can also be incorporated into an expanded proliferation control system. For example, the transgenic expression of pro-apoptotic proteins such as caspase 3 and caspase 9 can be regulated by ribozyme or miRNA switches, and the endogenous expression of growth-inhibitory signaling receptors such as the tumor growth factor β receptor (TGF-βR)[27] and cytotoxic T-lymphocyte antigen 4 (CTLA4)[28] can be regulated by miRNA switches. The compact and modular nature of RNA-based regulatory devices enables the construction of multi-targeted systems in which switches regulating growth-stimulatory and growth-inhibitory signals are programmed to respond to different ligand inputs, such that different drug molecules can be sequentially administered to promote T-cell expansion during the

treatment period and induce T-cell death after the transferred T cells have achieved the therapeutic objective.

The development of RNAi-based devices that can control both transgenic and endogenous targets presents an important expansion in the capability of RNA-based regulatory designs. The RNAi-based regulatory systems discussed in this work, together with previously described ribozyme-based control systems, provide a practical demonstration of integrated regulatory systems that can exert stringent control over T-cell proliferation and improve the safety and efficacy of T-cell immunotherapy. The combinatorial strategies presented here can be applied to further extensions in T-cell proliferation control systems by incorporating additional control devices and genetic targets. More importantly, they illustrate a basic framework for the construction of integrated regulatory systems that can be adapted to diverse application areas, particularly those in health and medicine.

Materials and Methods

Plasmid construction. All plasmids were constructed using standard molecular biology techniques[29]. Plasmid maps are provided in Supplementary Figure 5.8. All miRNA and miRNA switch sequences are provided in Supplementary Text 5.3. All oligonucleotides were synthesized by Integrated DNA Technologies and all constructs were sequence verified by Elim Biopharmaceuticals. Cloning enzymes, including restriction enzymes and T4 DNA ligase, were obtained from New England Biolabs, and DNA polymerases were obtained from Stratagene.

The coding region of dsRed-Express was inserted into pcDNA3.1(+) (Invitrogen) via the KpnI and XhoI sites to construct pCS350. For inducible promoter studies, the tetO-CMV promoter was PCR amplified from pTRE-Tight (Clontech) and inserted into pCS350 via the BglII and NheI sites, thereby replacing the original CMV promoter to construct ptetO-DsRed. The wt miRNA was inserted into the XbaI and ApaI sites downstream of the dsRed-Express coding region in ptetO-DsRed to construct ptetO-wt.

For IL-2Rβ- and γ_c-targeting miRNA studies, mTagBFP was PCR amplified from pTagBFP-C (Evrogen) and inserted into pcDNA3.1(+)-CAT (Invitrogen) to construct pCS1919. miRNA and miRNA switches were subsequently inserted into the XhoI and ApaI sites downstream of the CAT coding region in pCS1919. Multiple-copy non-switch miRNA constructs were built by PCR amplifying the miRNA insert from the single-copy construct using forward and reverse primers AvrII-IL2R miR Fwd (5'AATACCTAGGCTGGAGGCTTGCTGAAGG) and XbaI-XhoI-IL2R Multi miR Rev (5'AATACTCGAGTATATCTAGAAAAGGACAGTGGGAGTGG), respectively. Inserts were digested by AvrII and XhoI and inserted into the XbaI and XhoI sites on the parent vector. Sticky ends from the AvrII site on the insert and the XbaI site on the vector were ligated together to form a scar, thereby freeing both sites to be used again for the cloning of subsequent miRNA copies. Multiple-copy miRNA switch constructs were built by PCR amplifying the miRNA switch insert from the single-copy construct using the forward primer AvrII-Chase IL2R miR Fwd (5'AATACCTAGGACGGGTCCTG ATACCAG) and the same reverse primer XbaI-XhoI-IL2R Multi miR Rev as before. Inserts and vectors were digested and ligated as described for non-switch miRNA constructs. Constructs shown in Supplementary Figures 5.1A and 5.1B were built by

inserting the miRNAs into the XhoI and ApaI sites downstream of the CAT coding region in pcDNA3.1(+)-CAT. Therefore, these constructs did not contain the mTagBFP transfection marker. Bm5 and Gm1 were subsequently recloned into pCS1919 as described above. Supplementary Text 5.3 lists sequences for these two miRNAs as they appear in the pCS1919-based constructs.

Mammalian cell culture maintenance. The HEK 293 cell line stably expressing EGFP was generated as described previously[13]. HEK 293 cells were cultured in D-MEM (Gibco) supplemented with 10% fetal bovine serum (FBS, Gibco) and 0.1 mg/ml G418 (Gibco). Cells were seeded at 0.02 x 10^6 cells/ml and passaged regularly. The mouse T-cell line CTLL-2 was obtained from ATCC and maintained in RPMI-1640 media (Lonza) supplemented with 10% heat-inactivated FBS (Hyclone), 2 mM sodium pyruvate (Gibco), and 4.5 g/L D-(-)-glucose (Sigma). Unless otherwise specified, CTLL-2 cells were fed 100 U/ml IL-2 every 48 hours and maintained between 0.05 x 10^6 and 0.50 x 10^6 cells/ml.

HEK 293 transient transfection and fluorescence quantification. All transient transfections of HEK 293 cells were performed using FuGENE 6 (Roche) following the manufacturer's protocol. Cells were seeded at 0.08 x 10^6 cells/ml, 500 μl/well, in 24-well plates 24 hours prior to transfection. All experiments were performed with triplicate samples for each condition. Unless otherwise noted, 10 ng of pCS350, 72 ng of ptetO-wt, and 168 ng of pTet-Off (Clontech) encoding the transcriptional activator (tTA) were mixed prior to incubation with the FuGENE6 transfection reagent. Doxycycline at the

specified concentration was added immediately after transfection. Cells were fed with fresh media supplemented with the appropriate concentration of doxycycline two days after transfection.

Three days after transfection, cells were trypsinized and analyzed using a Quanta Cell Lab Flow Cytometer equipped with a 488-nm laser (Beckman Coulter). EGFP and dsRed-Express were measured through 525/30-nm band-pass and 610-nm long-pass filters, respectively. Viability was gated based on side scatter and electronic volume, and only viable cells were included in fluorescence measurements. The median EGFP intensity of transfected ($DsRed^+$) cells was normalized to that of untransfected ($DsRed^-$) cells within each sample to adjust for well-to-well variations. The internally normalized EGFP intensity was subsequently normalized to that of a control sample transfected with the original ptetO plasmid, which does not contain any miRNA. This normalization method was used to enable direct comparison with data from Ref. 13, and the calculation was performed using the following equation:

$$\%GFP = \left(\frac{GFP_{sample}^{transfected}}{GFP_{sample}^{untransfected}} \right) \left(\frac{GFP_{no-miRNA\ control}^{untransfected}}{GFP_{no-miRNAcontrol}^{transfected}} \right).$$

CTLL-2 transient transfection and fluorescence quantification. All transient transfections of CTLL-2 cells were performed with an Amaxa Nucleofector II and the Mouse T Cell Nucleofector Kit (Amaxa) following the manufacturer's protocol. Electroporations were performed with 3 x 10^6 cells and 3 μg of plasmid DNA. In surface antibody staining experiments, transfected samples were resuspended in 4 ml of media and split into 4 wells in 24-well plates. In experiments testing switch response, theophylline was added to a final concentration of 1 mM in 2 of the wells. Cells were

harvested for surface staining 24 hours after transfection. Antibody staining was performed by washing each sample once with 500 μl HBSS (Gibco), incubating with PE-conjugated IL-2Rβ or γ_c antibody (BioLegend) diluted with HBSS in a total volume of 50 μl for 15 min at 4°C in the dark, washing twice with 500 μl HBSS, and resuspending in 250 μl of HBSS prior to flow cytometry analysis.

In intracellular antibody staining experiments, duplicate samples were transfected with each plasmid construct, and each sample was resuspended in 2 ml of media and split into 2 wells in 24-well plates. Theophylline was added to a final concentration of 1 mM in 1 well form each of the duplicate transfection samples. Cells were harvested for fixation and intracellular staining 24 hours after transfection. Cells were fixed with 1.5% formaldehyde at room temperature for 15 min and permeabilized with 500 μl of ice-cold methanol for 30 min. Fixed and permeabilized cells were washed twice with 500 μl PBS-FBS (1X PBS with 5% heat-inactivated FBS) and incubated with Alexa Fluor 488-conjugated pSTAT5 antibody (Cell Signaling) diluted with PBS-FBS in a total volume of 50 μl for 30 min at room temperature in the dark. Cells were washed twice more with 500 μl PBS-FBS and resuspended in 200 μl of PBS-FBS for flow cytometry analysis.

Fluorescence and cell viability data were obtained using a Quanta Cell Lab Flow Cytometer equipped with a 488-nm laser and an UV arc lamp. mTagBFP and PE, and 7-AAD were measured through 465/30-nm band-pass, 575/30-nm band-pass, and 610-nm long-pass filters, respectively. Viable population was gated based on side scatter and electronic volume as well as 7-AAD (when measuring percent viability), and only viable cells were included in fluorescence measurements. Viable cells were further gated for mTagBFP expression, which served as a transfection efficiency control, before PE

intensity values were collected. All fluorescence measurements were reported as the geometric mean intensity of the gated population. To control for toxicity and other possible non-specific effects of transfection and theophylline, cells transfected with a construct lacking any miRNA sequence and treated with the corresponding concentration of theophylline served as positive controls to which values from cells transfected with miRNAs were normalized. Background fluorescence levels were determined by staining with the appropriate isotype control antibody. The scale for percent receptor chain expression was adjusted such that the relative percent expression of the isotype control was set to 0% and that of the no-miRNA control was set to 100%. Normalization was performed using the following equations:

$$R_{sample} = \frac{FU_{sample}}{FU_{no-miRNA\ control}} \text{ and}$$

$$N_{sample} = \frac{R_{sample} - R_{isotype}}{100\% - R_{isotype}}, \text{ where}$$

R is the relative percent receptor chain expression normalized to no-miRNA control, and N is the normalized percent receptor chain expression. Transient transfection experiments were performed with two replicate samples, and reported error bars indicate one standard deviation from the mean normalized value.

CTLL-2 proliferation assay with IL-2Rβ- and γ_c-blocking monoclonal antibodies. CTLL-2 cells were seeded at 0.025 x 10^6 cells/ml, 200 μl/well, in 96-well round-bottom plates. Each well was supplemented with no cytokine, IL-2 (at 1, 10, 100, or 1000 U/ml) or IL-15 (at 0.01, 0.05, 0.1, 0.5, 1, or 5 ng/ml). One well at each cytokine concentration was supplemented with one of the following: no antibody, 40 μg/ml rat IgG2b κ isotype

control, 80 μg/ml rat IgG2b κ isotype control antibody, 40 μg/ml anti-IL-2Rβ (clone TM-β1) antibody, 40 μg/ml anti-γ_c (clone TUGm2) antibody, or both 40 μg/ml anti-IL-2Rβ antibody and 40 μg/ml anti-γ_c antibody. All antibodies were purchased from BioLegend. The plates were wrapped in foil to reduce evaporation and stored in a 37°C incubator. Each well was treated with 1 μg/ml of 7-AAD dead-cell stain and analyzed on a Quanta Cell Lab Flow Cytometer equipped with a 488-nm laser. 7-AAD was measured through a 610-nm long-pass filter. Viability was gated based on side scatter and electronic volume followed by 7-AAD fluorescence.

Acknowledgments

We thank Dr. Chase Beisel for advice on miRNA switch construction. This work was supported by the City of Hope's National Cancer Institute–Cancer Center Support Grant, the Alfred P. Sloan Foundation (fellowship to C.D.S.), and the National Institutes of Health (grant to C.D.S., RC1GM091298).

References

1. Kovanen, P.E. & Leonard, W.J. Cytokines and immunodeficiency diseases: critical roles of the gamma(c)-dependent cytokines interleukins 2, 4, 7, 9, 15, and 21, and their signaling pathways. *Immunol Rev* **202**, 67-83 (2004).
2. Chen, Y.Y., Jensen, M.C. & Smolke, C.D. Genetic control of mammalian T-cell proliferation with synthetic RNA regulatory systems. *Proc Natl Acad Sci U S A* **107**, 8531-8536 (2010).

3. Johnston, J.A. et al. Tyrosine phosphorylation and activation of STAT5, STAT3, and Janus kinases by interleukins 2 and 15. *Proc Natl Acad Sci U S A* **92**, 8705-8709 (1995).

4. Dubois, S., Mariner, J., Waldmann, T.A. & Tagaya, Y. IL-15Ralpha recycles and presents IL-15 In trans to neighboring cells. *Immunity* **17**, 537-547 (2002).

5. Malek, T.R. The biology of interleukin-2. *Annu Rev Immunol* **26**, 453-479 (2008).

6. Nelson, B.H. & Willerford, D.M. Biology of the interleukin-2 receptor. *Adv Immunol* **70**, 1-81 (1998).

7. Minami, Y., Kono, T., Miyazaki, T. & Taniguchi, T. The IL-2 receptor complex: its structure, function, and target genes. *Annu Rev Immunol* **11**, 245-268 (1993).

8. Stauber, D.J., Debler, E.W., Horton, P.A., Smith, K.A. & Wilson, I.A. Crystal structure of the IL-2 signaling complex: paradigm for a heterotrimeric cytokine receptor. *Proc Natl Acad Sci U S A* **103**, 2788-2793 (2006).

9. Wang, X., Rickert, M. & Garcia, K.C. Structure of the quaternary complex of interleukin-2 with its alpha, beta, and gammac receptors. *Science* **310**, 1159-1163 (2005).

10. Burkett, P.R. et al. Coordinate expression and trans presentation of interleukin (IL)-15Ralpha and IL-15 supports natural killer cell and memory CD8+ T cell homeostasis. *J Exp Med* **200**, 825-834 (2004).

11. He, L. & Hannon, G.J. MicroRNAs: small RNAs with a big role in gene regulation. *Nat Rev Genet* **5**, 522-531 (2004).

12. Siolas, D. et al. Synthetic shRNAs as potent RNAi triggers. *Nat Biotechnol* **23**, 227-231 (2005).

13. Beisel, C.L., Chen, Y.Y., Culler, S.J., Hoff, K.G. & Smolke, C.D. Design of small molecule-responsive microRNAs based on structural requirements for Drosha processing. *Nucleic Acids Res* (2010). doi: 10.1093/nar/gkq954.

14. Khvorova, A., Reynolds, A. & Jayasena, S.D. Functional siRNAs and miRNAs exhibit strand bias. *Cell* **115**, 209-216 (2003).

15. Kim, D.H. et al. Synthetic dsRNA Dicer substrates enhance RNAi potency and efficacy. *Nat Biotechnol* **23**, 222-226 (2005).

16. Han, J. et al. Molecular basis for the recognition of primary microRNAs by the Drosha-DGCR8 complex. *Cell* **125**, 887-901 (2006).

17. Zeng, Y., Yi, R. & Cullen, B.R. Recognition and cleavage of primary microRNA precursors by the nuclear processing enzyme Drosha. *EMBO J* **24**, 138-148 (2005).

18. Zhang, X. & Zeng, Y. The terminal loop region controls microRNA processing by Drosha and Dicer. *Nucleic Acids Res* (2010).

19. Schwarz, D.S. et al. Asymmetry in the assembly of the RNAi enzyme complex. *Cell* **115**, 199-208 (2003).

20. Amarzguioui, M. et al. Rational design and in vitro and in vivo delivery of Dicer substrate siRNA. *Nat Protoc* **1**, 508-517 (2006).

21. Heale, B.S., Soifer, H.S., Bowers, C. & Rossi, J.J. siRNA target site secondary structure predictions using local stable substructures. *Nucleic Acids Res* **33**, e30 (2005).

22. Kondo, M. et al. Sharing of the interleukin-2 (IL-2) receptor gamma chain between receptors for IL-2 and IL-4. *Science* **262**, 1874-1877 (1993).

23. Bartel, D.P. MicroRNAs: genomics, biogenesis, mechanism, and function. *Cell* **116**, 281-297 (2004).

24. Tanaka, T. et al. A novel monoclonal antibody against murine IL-2 receptor beta-chain. Characterization of receptor expression in normal lymphoid cells and EL-4 cells. *J Immunol* **147**, 2222-2228 (1991).

25. Ihle, J.N. The Stat family in cytokine signaling. *Curr Opin Cell Biol* **13**, 211-217 (2001).

26. Quah, B.J., Warren, H.S. & Parish, C.R. Monitoring lymphocyte proliferation in vitro and in vivo with the intracellular fluorescent dye carboxyfluorescein diacetate succinimidyl ester. *Nat Protoc* **2**, 2049-2056 (2007).

27. Wallace, A. et al. Transforming growth factor-beta receptor blockade augments the effectiveness of adoptive T-cell therapy of established solid cancers. *Clin Cancer Res* **14**, 3966-3974 (2008).

28. Curran, M.A., Montalvo, W., Yagita, H. & Allison, J.P. PD-1 and CTLA-4 combination blockade expands infiltrating T cells and reduces regulatory T and myeloid cells within B16 melanoma tumors. *Proc Natl Acad Sci U S A* **107**, 4275-4280 (2010).

29. Sambrook, J. & Russell, D.W. Molecular Cloning: A Laboratory Manual, Edn. 3. (Cold Spring Harbor Press, Cold Spring Harbor; 2001).

Supplementary Text 5.1

Parameter Optimization for Tet-OFF Promoter System. The Tet-OFF promoter system contains two plasmid components that must be co-transfected in characterization studies. The first plasmid, ptetO or its derivative, contains a transgene expressed from the tetO-CMV promoter. The second plasmid, pTet-Off, expresses the tet transcriptional activator (tTA) whose presence activates the tetO-CMV promoter. The ratio of the two plasmids must be optimized to achieve maximum transgene expression from the tetO-CMV promoter. To determine the optimum promoter-to-tTA ratio, transient transfections were performed in HEK 293 cells using different ratios of pTet-Off and ptetO-DsRed, a ptetO derivative that expresses dsRed-Express from the tetO-CMV promoter. The total plasmid input was fixed at 250 ng as recommended by the manufacturer's protocol, and results indicate that the 75:175, ptetO-DsRed:pTet-Off ratio yields the maximum transfection efficiency (as determined by the percentage of cells that are $DsRed^{+}$) and transgene expression (as determined by the dsRed-Express fluorescence intensity) (Supplementary Figure 5.9).

A second system parameter is the concentration of doxycycline that must be administered to fully suppress the tetO-CMV promoter. To optimize this parameter, transient transfections were performed in HEK 293 cells using 75 ng of ptetO-DsRed, 175 ng of pTet-Off, and doxycycline at a range of concentrations. pCS350, a plasmid that expresses dsRed-Express from a constitutive CMV promoter, was included as a positive control. Results indicate that expression from the tetO-CMV promoter is considerably weaker than that from the constitutive CMV promoter even at the fully activated state (i.e., no doxycycline) (Supplementary Figure 5.10). The lower expression levels observed

in the inducible system may be due to the tetO-CMV promoter being weaker than the constitutive CMV promoter, and may also be a result of the reduced input of ptetO-DsRed relative to pCS350 due to the need to co-transfect pTet-Off. Since co-transfection with pTet-Off is required for activity and increasing ptetO-DsRed input is therefore not a viable option, this reduced expression represents a fundamental limitation of the inducible promoter system. The transfection results also indicate that 100 ng/ml doxycycline is sufficient to fully suppress gene expression from the tetO-CMV promoter. Furthermore, results show that the tetO-CMV promoter has minimal leakiness, such that almost no dsRed-Express fluorescence is observed at doxycycline concentrations above 100 ng/ml. As a result, transfected and untransfected cells cannot be effectively distinguished at high doxycycline concentrations, thereby preventing accurate quantification in miRNA characterization studies.

To enable identification of transfected populations, we co-transfected pCS350 with pTet-Off and ptetO-wt, which expresses the wt miRNA in the 3' UTR of the dsRed-Express gene in ptetO-DsRed. The dsRed-Express encoded by pCS350 is expressed even when the tetO-CMV promoter in ptetO-wt is fully suppressed, thereby allowing for gating of transfected populations. We performed the three-plasmid transfection at various plasmid ratios in HEK 293 cells that stably express EGFP. Results show that 5 ng of pCS350 is sufficient to generate an observable $DsRed^{+}$ population in the OFF state with 100 ng/ml doxycycline (Supplementary Figure 5.11A). Furthermore, maximum EGFP knockdown and switch dynamic range in response to doxycycline addition can be observed at a minimum of 10 ng of pCS350 input (Supplementary Figure 5.11B). Therefore, all subsequent transfection experiments for inducible promoter system

characterization were performed using 10 ng of pCS350, 72 ng of ptetO-wt, and 168 ng of pTet-Off to allow for gating of transfected populations while maximizing miRNA expression from the tetO-CMV promoter in the ON state.

Supplementary Text 5.2

Secondary Structure Affects miRNA Knockdown Efficiency. Despite considerable effort directed to elucidating the structural requirements for efficient miRNA processing, no general consensus has been reached in the field to date on the optimal miRNA structure. In this study, we examined two main structures in our miRNA designs. Structure A (Supplementary Figure 5.3A) is the default structure used by the Invitrogen BLOCK-iT^{TM} RNAi Designer tool. This structure includes a large terminal loop and an internal bulge inside the mature miRNA stem, which contains the targeting sequence on the 5' side. A second structure, termed structure B (Supplementary Figure 5.3B), is based on the naturally occurring miRNA-30a and served as the base structure from which ligand-responsive miRNA switches were originally designed in earlier work[13]. This structure includes a 4-nt terminal loop and a 5-nt internal bulge immediately above the mature miRNA stem, which may contain the targeting sequence on either the 5' or the 3' side.

To evaluate the impact of different secondary structures on knockdown efficiency, we designed three miRNA structures that contain the same IL-2Rβ-targeting sequence. Bm1 is a structure B-based design that contains the targeting sequence on the 5' side of the mature miRNA stem (Supplementary Figure 5.12A). Bm2 is identical to Bm1 except the targeting sequence is moved to the 3' side of the mature miRNA stem

(Supplementary Figure 5.12B). Bm14 is a structure A-based design, which contains the targeting sequence on the 5' side of the mature miRNA stem (Supplementary Figure 5.12C). Transient transfection results indicate that, in structure B, having the targeting sequence on the 5' instead of 3' side of the mature miRNA stem leads to higher knockdown efficiency (Supplementary Figure 5.1C). It is possible that the 5' side is favorable because the target sequence was identified using the Invitrogen BLOCK-iT™ RNAi Designer tool, which designs miRNAs with the targeting sequence on the 5' side of the miRNA stem and may therefore be programmed to identify targets that are more efficiently silenced in this configuration. Further experiments with structure B-based miRNAs carrying target sequences identified through alternative algorithms would be necessary to confirm the results observed here. Nevertheless, our results show that structure A achieves significantly higher knockdown efficiency compared to either structure B-based designs (Supplementary Figure 5.1C). Therefore, structure A was used as the template for all other non-switch miRNAs constructed in this study.

Supplementary Text 5.3

miRNA sequences are listed below. Color schemes: Green, miRNA targeting (antisense) sequence; red, target (sense) sequence; blue, theophylline aptamer; underlined, restriction sites.

Ms IL2RB miRNA1 (Bm1)
5'TCTAGACTCGAGGTTTGACAGTGAGCGCGTTCTTGAAGAGACAGATAGGCA
GTGAAGCCACAGATGTGCCTATCTGTCTCTTCAAGAACTTGCCTACTGCCTCG
GACTGAATTCATAGGGCCC

Ms IL2RB miRNA2 (Bm2)
5’TCTAGACTCGAGGTTTGACAGTGAGCGCGCCTATCTGTCTCTTCAAGAATA
GTGAAGCCACAGATGTATTCTTGAAGAGACAGATAGGCATGCCTACTGCCTC
GGACTGAATTCATAGGGCCC

Ms IL2RB miRNA3 (Bm3)
5’TCTAGACTGGAGGCTTGCTGAAGGCTGTATGCTGTAATACGGATGCATCCT
CCCAGTTTTGGCCACTGACTGACTGGGAGGACATCCGTATTACAGGACACAA
GGCCT GTTACTAGCACTCACATGGAACAAATGGCCGGGCCC

Ms IL2RB miRNA4 (Bm4)
5’TCTAGACTGGAGGCTTGCTGAAGGCTGTATGCTGTTAGGTGGACTGAATCT
TGGGGTTTTGGCCACTGACTGACCCCAAGATAGTCCACCTAACAGGACACAA
GGCCTGTTACTAGCACTCACATGGAACAAATGGCCGGGCCC

Ms IL2RB miRNA5 (Bm5)
5’TCTAGAAATACTCGAGCTGGAGGCTTGCTGAAGGCTGTATGCTGTCAAGAG
ACCTCTTAAGCAGTGTTTTGGCCACTGACTGACACTGCTTAAGGTCTCTTGAC
AGGACACAAGGCCTGTTACTAGCACTCACATGGAACAAATGGCCGGGCCC

Ms IL2RB miRNA6 (Bm6)
5’TCTAGACTGGAGGCTTGCTGAAGGCTGTATGCTGTTATCAGGACCTCTTCGT
TTGGTTTTGGCCACTGACTGACCAAACGAAGGTCCTGATAACAGGACACAAG
GCCT GTTACTAGCACTCACATGGAACAAATGGCCGGGCCC

Ms IL2RB miRNA7 (Bm7)
5’TCTAGACTGGAGGCTTGCTGAAGGCTGTATGCTGCATAGAAGGAGCCCTCA
CTTCGTTTTGGCCACTGACTGACGAAGTGAGCTCCTTCTATGCAGGACACAAG
GCCT GTTACTAGCACTCACATGGAACAAATGGCCGGGCCC

Ms IL2RB miRNA8 (Bm8)
5’TCTAGACTCGAGCTGGAGGCTTGCTGAAGGCTGTATGCTGTCTGCTTGAGG
CTTAATACGGGTTTTGGCCACTGACTGACCCGTATTACCTCAAGCAGACAGG
ACACAAGGCCTGTTACTAGCACTCACATGGAACAAATGGCCGGGCCC

Ms IL2RB miRNA9 (Bm9)
5’TCTAGACTCGAGCTGGAGGCTTGCTGAAGGCTGTATGCTGTAAGCAGTCTT
CCTCAAGCCTGTTTTGGCCACTGACTGACAGGCTTGAAAGACTGCTTACAGG
ACACAAGGCCTGTTACTAGCACTCACATGGAACAAATGGCCGGGCCC

Ms IL2RB miRNA10 (Bm10)
5’TCTAGACTCGAGCTGGAGGCTTGCTGAAGGCTGTATGCTGTAAATGAGGAG
CAAGGTTATGGTTTTGGCCACTGACTGACCATAACCTCTCCTCATTTACAGGA
CACAAGGCCTGTTACTAGCACTCACATGGAACAAATGGCCGGGCCC

Ms IL2RB miRNA11 (Bm11)
5'TCTAGACTCGAGCTGGAGGCTTGCTGAAGGCTGTATGCTGTGTACAGCCAC
ATCACAACCTGTTTTGGCCACTGACTGACAGGTTGTGGTGGCTGTACACAGG
ACACAAGGCCTGTTACTAGCACTCACATGGAACAAATGGCCGGGCCC

Ms IL2RB miRNA12 (Bm12)
5'TCTAGACTCGAGCTGGAGGCTTGCTGAAGGCTGTATGCTGTCAACAGGCTG
CATTCAGTCTGTTTTGGCCACTGACTGACAGACTGAACAGCCTGTTGACAGGA
CACAAGGCCTGTTACTAGCACTCACATGGAACAAATGGCCGGGCCC

Ms IL2RB miRNA13 (Bm13)
5'TCTAGACTCGAGCTGGAGGCTTGCTGAAGGCTGTATGCTGCTCAGGTGATG
ACTGATGACCGTTTTGGCCACTGACTGACGGTCATCACATCACCTGAGCAGG
ACACAAGGCCTGTTACTAGCACTCACATGGAACAAATGGCCGGGCCC

Ms IL2RB miRNA14 (Bm14)
5'TCTAGACTCGAGCTGGAGGCTTGCTGAAGGCTGTATGCTGTTCTTGAAGAG
ACAGATAGGCGTTTTGGCCACTGACTGACGCCTATCTCTCTTCAAGAACAGG
ACACAAGGCCTGTTACTAGCACTCACATGGAACAAATGGCCGGGCCC

Ms IL2RG miRNA1 (Gm1)
TCTAGAAATACTCGAGCTGGAGGCTTGCTGAAGGCTGTATGCTGTCAGGATC
AAATCAGCTTTGAGTTTTGGCCACTGACTGACTCAAAGCTTTTGATCCTGACA
GGACACAAGGCCTGTTACTAGCACTCACATGGAACAAATGGCCGGGCCC

Ms IL2RG miRNA2 (Gm2)
TCTAGACTGGAGGCTTGCTGAAGGCTGTATGCTGAACAAATAGTGACTGCAC
TCCGTTTTGGCCACTGACTGACGGAGTGCACACTATTTGTTCAGGACACAAGG
CCTGTTACTAGCACTCACATGGAACAAATGGCCGGGCCC

Ms IL2RG miRNA3 (Gm3)
TCTAGACTGGAGGCTTGCTGAAGGCTGTATGCTGATTAGTTCCGTCCAGCTTC
GAGTTTTGGCCACTGACTGACTCGAAGCTACGGAACTAATCAGGACACAAGG
CCTGTTACTAGCACTCACATGGAACAAATGGCCGGGCCC

Ms IL2RG miRNA4 (Gm4)
TCTAGACTGGAGGCTTGCTGAAGGCTGTATGCTGTGGACAGGCTGGCTCCATT
TAGTTTTGGCCACTGACTGACTAAATGGACAGCCTGTCCACAGGACACAAGG
CCTGTTACTAGCACTCACATGGAACAAATGGCCGGGCCC

Ms IL2RG miRNA5 (Gm5)
TCTAGACTCGAGCTGGAGGCTTGCTGAAGGCTGTATGCTGTTGAGGTTCCATC
AAAGGATTGTTTTGGCCACTGACTGACAATCCTTTTGGAACCTCAACAGGAC
ACAAGGCCTGTTACTAGCACTCACATGGAACAAATGGCCGGGCCC

Ms IL2RG miRNA6 (Gm6)
TCTAGACTCGAGCTGGAGGCTTGCTGAAGGCTGTATGCTGATACCTTGTACCT
ATAGTGCAGTTTTGGCCACTGACTGACTGCACTATGTACAAGGTATCAGGAC
ACAAGGCCTGTTACTAGCACTCACATGGAACAAATGGCCGGGCCC

Ms IL2RG miRNA7 (Gm7)
TCTAGACTCGAGCTGGAGGCTTGCTGAAGGCTGTATGCTGTTAGCTTCTGTAC
AGCTCGCCGTTTTGGCCACTGACTGACGGCGAGCTACAGAAGCTAACAGGAC
ACAAGGCCTGTTACTAGCACTCACATGGAACAAATGGCCGGGCCC

Ms IL2RG miRNA8 (Gm8)
TCTAGACTCGAGCTGGAGGCTTGCTGAAGGCTGTATGCTGTTCACTATTAGTT
CCGTCCAGGTTTTGGCCACTGACTGACCTGGACGGCTAATAGTGAACAGGAC
ACAAGGCCTGTTACTAGCACTCACATGGAACAAATGGCCGGGCCC

Ms IL2RG miRNA9 (Gm9)
TCTAGACTCGAGCTGGAGGCTTGCTGAAGGCTGTATGCTGTAGGCAGGGAGA
ATCTAGGTTGTTTTGGCCACTGACTGACAACCTAGACTCCCTGCCTACAGGAC
ACAAGGCCTGTTACTAGCACTCACATGGAACAAATGGCCGGGCCC

Ms IL2RG miRNA10 (Gm10)
TCTAGACTCGAGCTGGAGGCTTGCTGAAGGCTGTATGCTGTTCCAGTGCAAA
CAAGGAAGGGTTTTGGCCACTGACTGACCCTTCCTTTTGCACTGGAACAGGA
CACAAGGCCTGTTACTAGCACTCACATGGAACAAATGGCCGGGCCC

Ms IL2RB miR5 Theo1 (Bm5 Theo1)
TCTAGAATTACTCGAGCTGGAGGCTGATACCAGCGCTGTATGCTGTCAAGAG
ACCTCTTAAGCAGTGTTTTGGCCACTGACTGACACTGCTTAAGGTCTCTTGAC
AGGACACAAGGCGCCCTTGGCAGCAGCACTCACATGGAACAAATGGCCGGG
CCC

Ms IL2RB miR5 Theo2 (Bm5 Theo2)
TCTAGAATTACTCGAGCTGGAGGCTTGCTGAAGGCTGATACCAGCGTCAAGA
GACCTCTTAAGCAGTGTTTTGGCCACTGACTGACACTGCTTAAGGTCTCTTGA
CGCCCTTGGCAGCAGCCTGTTACTAGCACTCACATGGAACAAATGGCCGGGC
CC

Ms IL2RB miR5 Theo3 (Bm5 Theo3)
TCTAGAATTACTCGAGACGGGTCCTGATACCAGCGTGAGCGAACTGCTTAAG
AGGTCTCTTGATAGTGAAGCCACAGATGTATCAAGAGACCTCTTAAGCAGTC
CGCCTACGCCCTTGGCAGCAGGGCCC

Ms IL2RB miR5 Theo4 (Bm5 Theo4)
TCTAGAATTACTCGAGACGGGTCCTGATACCAGCGTGAGCGACTCAAGAGAC
CTCTTAAGCAGTCGTGAAGCCACAGATGGACTGCTTAAGAGGTCTCTTGAGG
CGCCTACGCCCTTGGCAGCAGGGCCC

Ms IL2RB miR5 Theo5 (Bm5 Theo5)
TCTAGAATTACTCGAGCTGGAGGCTGATACCAGCGTATGCTGTCAAGAGACC
TCTTAAGCAGTGTTTTGGCCACTGACTGACACTGCTTAAGGTCTCTTGACAGG
ACACAAGCCCTTGGCAGCAGCACTCACATGGAACAAATGGCCGGGCCC

Ms IL2RB miR5 Theo6 (Bm5 Theo6)
TCTAGAATTACTCGAGCTGGAGGCTGATACCAGCGCTGTATGCTGTCAAGAG
ACCTCTTAAGCAGTGTTTTGGCCACTGACTGACACTGCTTAAGGTCTCTTGAC
AGGACAAGGCGCCCTTGGCAGCAGCACTCACATGGAACAAATGGCCGGGCC
C

Ms IL2RB miR5 Theo7 (Bm5 Theo7)
TCTAGAATTACTCGAGCTGGAGGCTGATACCAGCGCTGTATGCTGTCAAGAG
ACCTCTTAAGCAGTGTTTTGGCCACTGACTGACACTGCTTAAGGTCTCTTGAC
AGGACACAACGCCCTTGGCAGCAGCACTCACATGGAACAAATGGCCGGGCC
C

Ms IL2RB miR5 Theo8 (Bm5 Theo8)
TCTAGAATTACTCGAGCTGGAGGCTGATACCAGCGCTGTATGCTGTCAAGAG
ACCTCTTAAGCAGTGTTTTGGCCACTGACTGACACTGCTTAAGGTCTCTTGAC
AGGACACAAGGCCCTTGGCAGCAGCACTCACATGGAACAAATGGCCGGGCC
C

Ms IL2RB miR5 Theo9 (Bm5 Theo9)
TCTAGAATTACTCGAGACGGGTCCTGATACCAGCGTGAGCGACTCAAGAGAC
CTCTTAAGCAGTCTTTTGGCCACTGACTGAGACTGCTTAAGGTCTCTTGAGGC
GCCTACGCCCTTGGCAGCAGGGCCC

Ms IL2RB miR5 Theo10 (Bm5 Theo10)
TCTAGAATTACTCGAGACGGGTCCTGATACCAGCGTGAGCGACTCAAGAGAC
CTCTTAAGCAGTCTTTTGGCCACTGACTGAGACTGCTTAAGAGGTCTCTTGAG
GCGCCTACGCCCTTGGCAGCAGGGCCC

Ms IL2RB miR5 Theo11 (Bm5 Theo11)
TCTAGAATTACTCGAGACGGGTCCTGATACCAGCGTGAGCGACTCAAGAGAC
CTCTTAAGCAGTCGTGAAGCCACAGATGGACTGCTTAAGGTCTCTTGAGGCG
CCTACGCCCTTGGCAGCAGGGCCC

Ms IL2RG miR1 Theo1 (Gm1 Theo1)
TCTAGAATTACTCGAGACGGGTCCTGATACCAGCGTGAGCGCGTCAGGATCA
AATCAGCTTTGATTTTTGGCCACTGACTGAATCAAAGCTTTTGATCCTGACTC
GCCTACGCCCTTGGCAGCAGGGCCC

Ms IL2RG miR8 Theo1 (Gm8 Theo1)
TCTAGAATTACTCGAGACGGGTCCTGATACCAGCGTGAGCGAATTCACTATT
AGTTCCGTCCAGCTTTTGGCCACTGACTGAGCTGGACGGCTAATAGTGAATCC
GCCTACGCCCTTGGCAGCAGGGCCC

Supplementary Table 5.1. Effects of theophylline on IL-2Rβ and γ_c surface antibody staining intensities in transiently transfected CTLL-2 cells

		No Theophylline			1 mM Theophylline			No Theo vs. Theo
Antibody	**miRNA Construct**	**Geom Mean PE**	**Average**	**Standard Deviation**	**Geom Mean PE**	**Average**	**Standard Deviation**	**Fold Change in Avg PE**
IL-2Rβ	No miRNA	34.98	31.71	4.63	28.11	27.86	0.36	1.14
	pCS1934	13.56	14.17	0.86	11.26	11.67	0.58	1.21
	Bm5(1x)	18.96	19.08	0.17	18.56	19.05	0.69	1.00
	Bm5T9(1x)	16.07	16.49	0.60	14.48	15.59	1.56	1.06
	Bm5T9(2x)	12.12	12.47	0.49	12.25	12.58	0.46	0.99
	Bm5T9(3x)	11.29	12.59	1.84	10.97	11.75	1.10	1.07
	Bm5(3x)-Gm1-Gm8	12.48	12.68	0.28	11.87	11.12	1.06	1.14
	Bm5T9(3x)-Gm1T1	13.26	13.24	0.03	12.55	12.68	0.18	1.04
	Bm5T9(3x)-Gm1T1-Gm8T1	13.31	12.73	0.82	11.41	10.72	0.98	1.19
	No miRNA	28.43			27.60			
	pCS1934	14.78			12.08			
	Bm5(1x)	19.20			19.53			
	Bm5T9(1x)	16.92			16.69			
	Bm5T9(2x)	12.81			12.90			
	Bm5T9(3x)	13.90			12.52			
	Bm5(3x)-Gm1-Gm8	12.88			10.37			
	Bm5T9(3x)-Gm1T1	13.22			12.80			
	Bm5T9(3x)-Gm1T1-Gm8T1	12.15			10.03			
γ_c	No miRNA	31.27	34.26	4.22	16.12	19.36	4.58	1.77
	Gm1(1x)	12.29	12.98	0.97	10.42	10.05	0.53	1.29
	Gm1T1(1x)	16.71	17.33	0.88	16.49	15.02	2.08	1.15
	Gm1T1(2x)	11.39	11.35	0.06	10.55	10.85	0.42	1.05
	Gm1T1(3x)	10.49	11.27	1.10	10.11	10.48	0.52	1.08
	Gm8(1x)	16.63	14.62	2.84	11.62	12.42	1.13	1.18
	Gm8T1(1x)	23.63	25.36	2.44	16.43	17.06	0.88	1.49
	Gm8T1(2x)	19.09	17.93	1.64	14.13	13.69	0.62	1.31
	Gm8T1(3x)	16.73	16.32	0.58	14.73	13.29	2.04	1.23
	Bm5(3x)-Gm1-Gm8	12.90	14.51	2.28	10.52	10.86	0.49	1.34
	Bm5T9(3x)-Gm1T1	18.76	19.02	0.37	15.15	18.78	5.12	1.01
	Bm5T9(3x)-Gm1T1-Gm8T1	20.88	19.71	1.66	15.74	14.60	1.61	1.35
	Gm1(1x)-Gm8(1x)	11.86	10.84	1.44	9.05	8.67	0.54	1.25
	Gm1T1(1x)-Gm8T1(1x)	13.83	13.14	0.98	11.00	11.07	0.10	1.19
	Gm1T1(2x)-Gm8T1(2x)	11.51	12.16	0.92	10.96	9.97	1.40	1.22
	No miRNA	37.24			22.60			
	Gm1(1x)	13.66			9.67			
	Gm1T1(1x)	17.95			13.55			
	Gm1T1(2x)	11.30			11.14			
	Gm1T1(3x)	12.05			10.85			
	Gm8(1x)	12.61			13.22			
	Gm8T1(1x)	27.08			17.68			
	Gm8T1(2x)	16.77			13.25			
	Gm8T1(3x)	15.91			11.84			
	Bm5(3x)-Gm1-Gm8	16.12			11.21			
	Bm5T9(3x)-Gm1T1	19.28			22.40			
	Bm5T9(3x)-Gm1T1-Gm8T1	18.54			13.46			
	Gm1(1x)-Gm8(1x)	9.82			8.29			
	Gm1T1(1x)-Gm8T1(1x)	12.44			11.14			
	Gm1T1(2x)-Gm8T1(2x)	12.81			8.98			

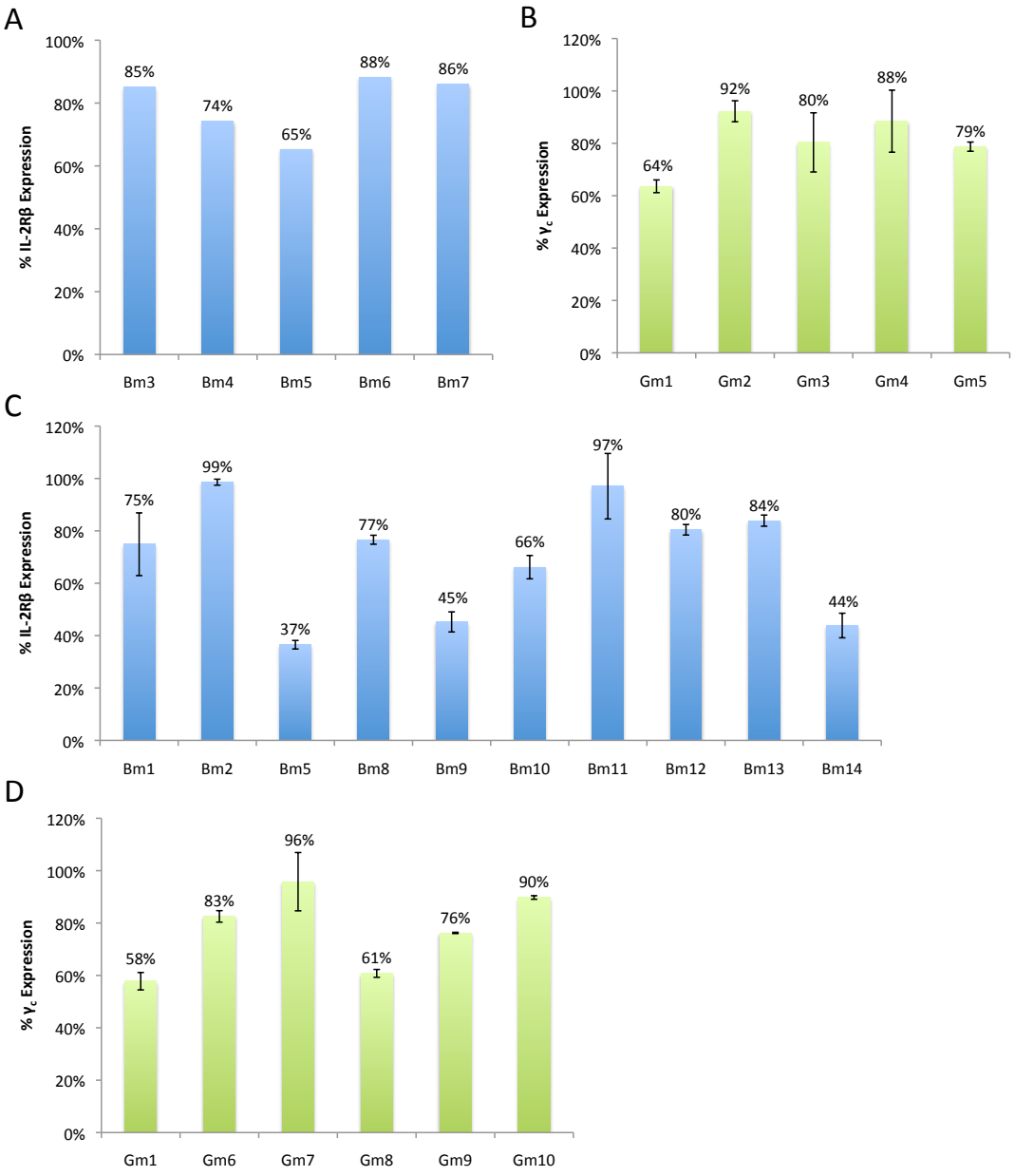

Supplementary Figure 5.1. miRNA sequences capable of effective knockdown of IL-2Rβ and γ_c are identified through screening by transient transfection in CTLL-2 cells. (A, C) IL-2Rβ- and (B, D) γ_c-targeting miRNA sequences were identified using the Invitrogen BLOCK-iT^{TM} RNAi Designer tool and inserted in the 3' UTR of the CAT gene expressed from a CMV promoter. Surface antibody staining was performed to evaluate the expression level of the relevant receptor chain. (A, B) Screening was initially performed using an expression vector lacking a transfection marker. Bm5 and Gm1 were identified to be the most effective IL-2Rβ- and γ_c-targeting sequences, respectively. (C, D) All subsequent characterizations were performed using a modified vector expressing mTagBFP from a SV40 promoter, and only mTagBFP$^+$ (i.e., transfected) cells were included for receptor chain expression level measurements. An additional γ_c-targeting sequence, Gm8, was identified from this second set of screening. Expression levels were normalized to those of control samples transfected with a construct lacking any miRNA sequence. Background expression levels were determined by isotype staining and set to 0% on the normalized scale (see Materials and Methods for details). Reported values in (B) through (D) are mean ± s.d. from two samples.

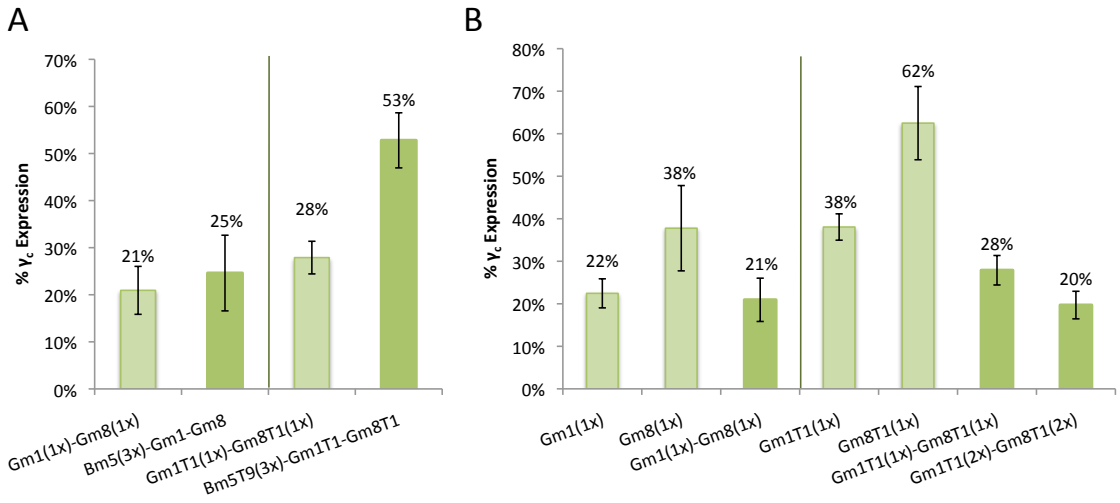

Supplementary Figure 5.2. Multiple-copy expression reduces gene silencing by individual miRNAs but increases overall knockdown activity toward a shared target gene. (A) Additional miRNAs that target a different gene reduces the knockdown efficiency of pre-existing miRNAs. CTLL-2 cells transiently transfected with two-copy miRNA constructs (Gm1-Gm8 and Gm1 Theo1-Gm8 Theo1 (Gm1T1-Gm8T1)) show greater γ_c knockdown compared to cells transiently transfected with five-copy miRNA constructs (Bm5(3x)-Gm1-Gm8 and Bm5T9(3x)-Gm1T1-Gm8T1, respectively). (B) Additional miRNAs that target the same gene increases the overall knockdown efficiency of a multiple-copy miRNA construct. The one-copy Gm1 and Gm8 miRNAs show weaker γ_c knockdown compared to the two-copy Gm1-Gm8 construct. Similarly, the one copy Gm1T1 and Gm8T1 miRNA switches show weaker γ_c knockdown compared to the two-copy Gm1T1-Gm8T1 construct, and the four-copy Gm1T1(2x)-Gm8T1(2x) shows the strongest γ_c knockdown among all the γ_c-targeting miRNA switches tested.

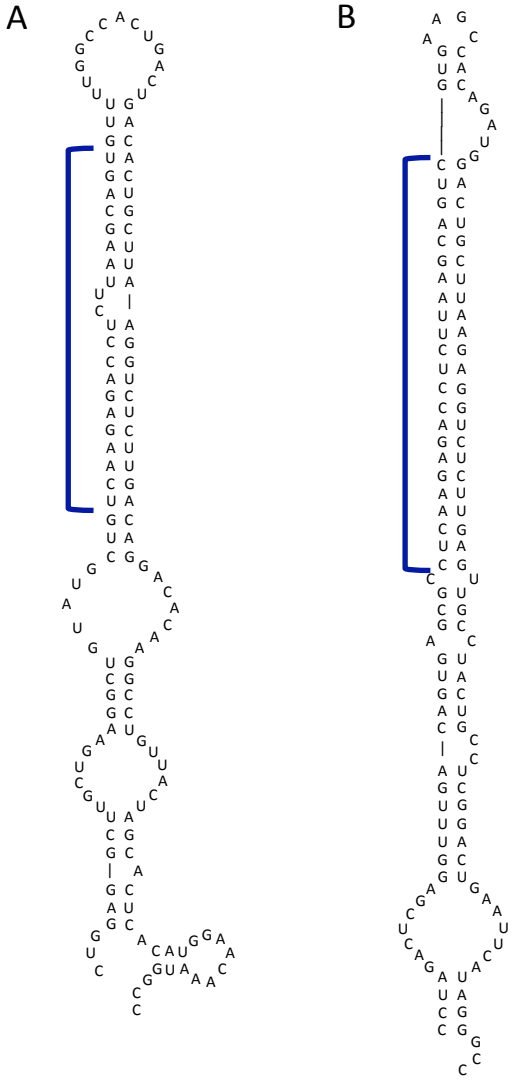

Supplementary Figure 5.3. Secondary structures for non-switch miRNAs. (A) miRNAs designed by the Invitrogen BLOCK-iT™ RNAi Designer tool contain a 13-nt terminal loop and a 2-nt internal bulge inside the mature miRNA stem. (B) miRNAs based on the naturally occurring miRNA-30a contain a 4-nt terminal loop and a 5-nt internal bulge immediately above the mature miRNA stem. Both structures contain multiple bulges in the basal segment of the stem-loop structure. Blue brackets indicate the miRNA targeting sequence that is complementary to the regulatory target.

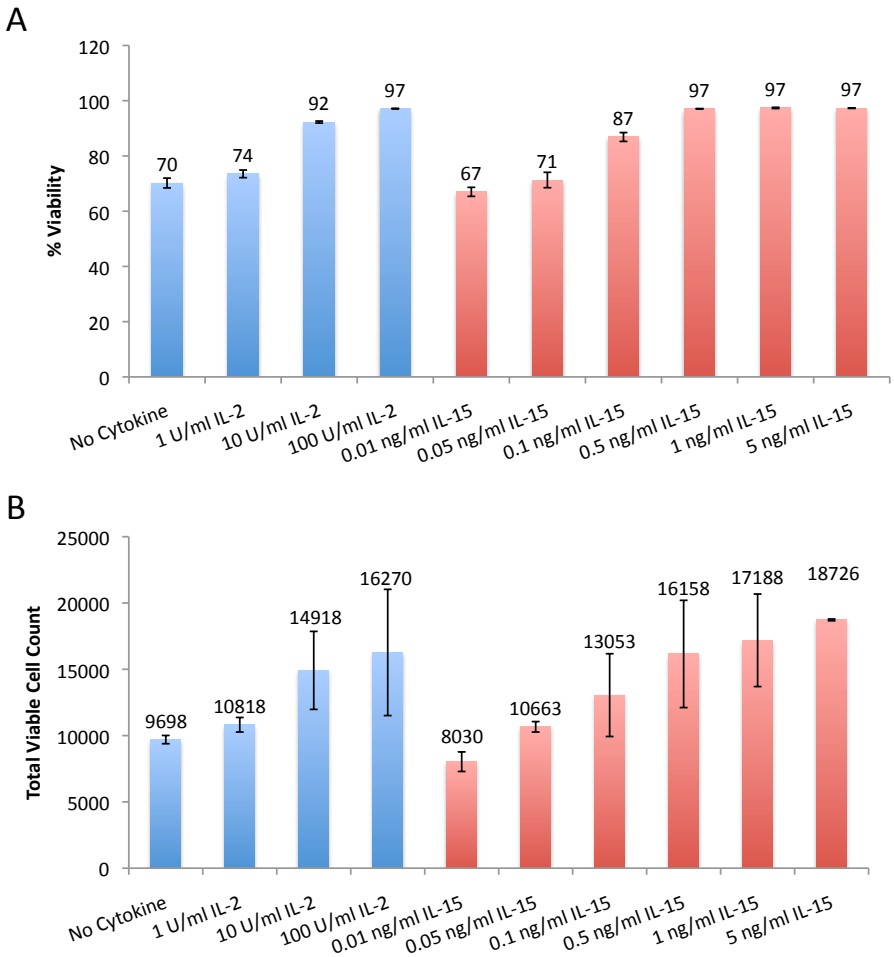

Supplementary Figure 5.4. IL-15 is capable of sustaining CTLL-2 cell growth at comparable levels as IL-2. CTLL-2 cells were cultured in media supplemented with either IL-2 or IL-15. Cells were treated with 7-AAD dead-cell stain and analyzed by flow cytometry for (A) % viability and (B) total viable cell count 48 hours after seeding and cytokine addition. Cultures supplemented with 0.5 ng/ml IL-15 show similar viability and growth as cultures supplemented with 100 U/ml IL-2, the typical culturing condition for CTLL-2 cells.

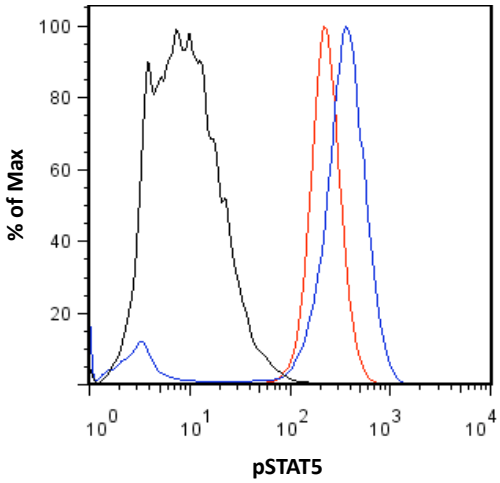

Supplementary Figure 5.5. pSTAT5 levels are dependent on cytokine stimulation. Untransfected CTLL-2 cells cultured for 24 hours in the presence of 100 U/ml IL-2 (red), in the absence of cytokines (black), or in the absence of cytokines for 24 hours followed by a 15-min incubation with 100 U/ml IL-2 (blue) were assayed for pSTAT5 levels by intracellular staining. Cytokine starvation results in low background pSTAT5 levels, whereas a brief stimulation by IL-2 induces rapid phosporylation of STAT5 in CTLL-2 cells. The small fraction of cytokine-starved cells that remains $pSTAT5^-$ after IL-2 stimulation is likely apoptotic or too sickly to activate the IL-2 signaling cascade.

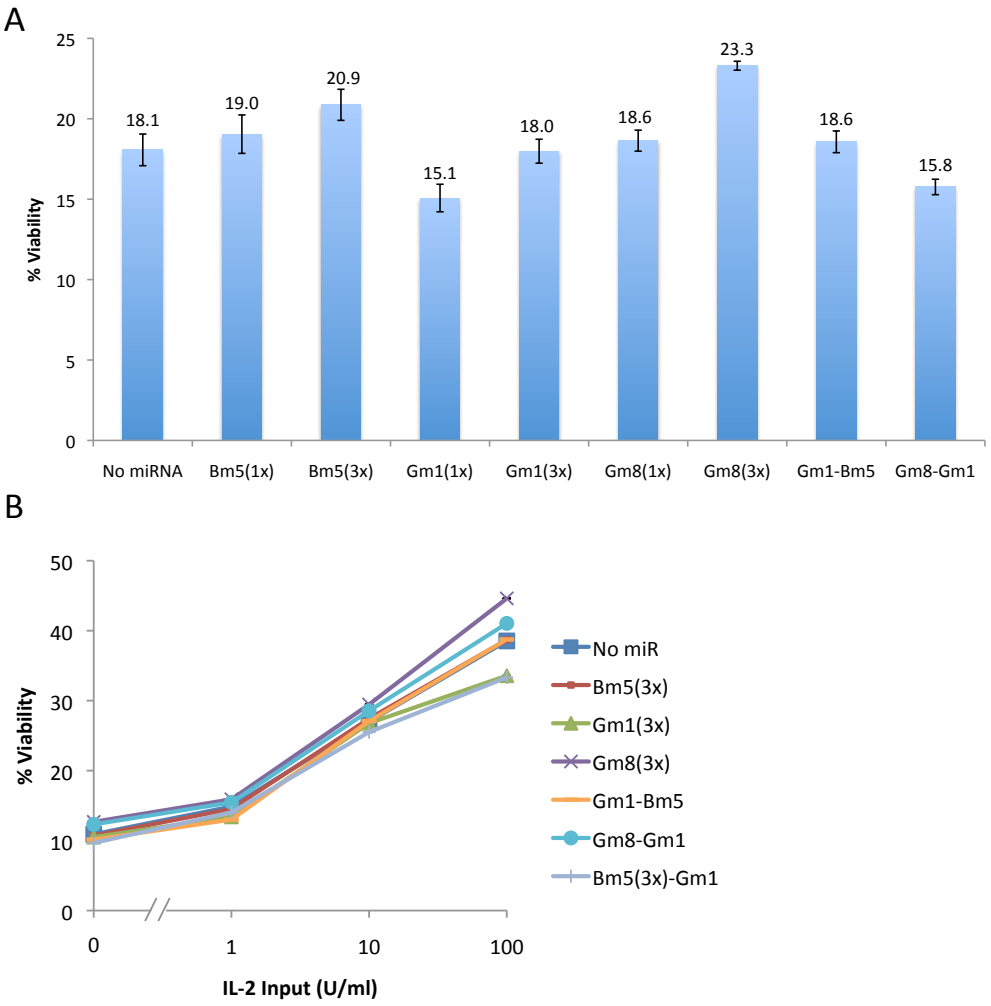

Supplementary Figure 5.6. The impact of IL-2Rβ- and γ_c-targeting miRNA constructs on CTLL-2 proliferation cannot be evaluated by overall percent viability. (A) Cell viability levels do not correspond to surface expression levels of IL-2Rβ and γ_c. The percent viability (i.e., viable cell count as a percent of total cell count) of transiently transfected CTLL-2 samples was measured by flow cytometry. Despite clear receptor chain knockdown activities (Figure 5.4), the miRNAs show no impact on overall percent viability. (B) IL-2 titration does not enhance the manifestation of viability impact by the miRNA constructs. Transiently transfected cells were cultured for 24 hours in media supplemented with IL-2 at various concentrations and assayed for percent viability by flow cytometry. Although viability increases with IL-2 input as expected, no significant difference is observed among the no-miRNA control and the various IL-2Rβ- and γ_c-targeting miRNA constructs tested.

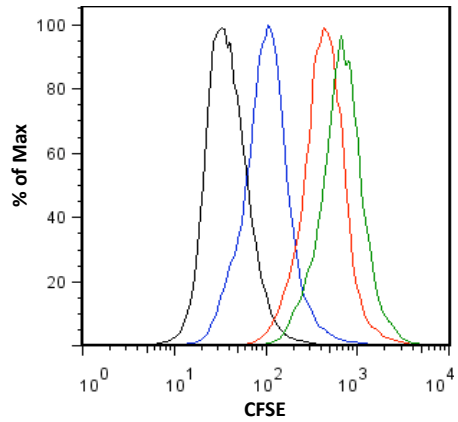

Supplementary Figure 5.7. CTLL-2 cell division cannot be quantitatively evaluated by CFSE staining. Untransfected CTLL-2 cells were labeled with 5 μM CFSE and assayed by flow cytometry after 18 (green), 24 (red), 42 (blue), and 69 hours (black) of incubation. Proliferation is indicated by CFSE signal dilution, but single peaks suggest synchronous cell division and preclude quantification of division numbers.

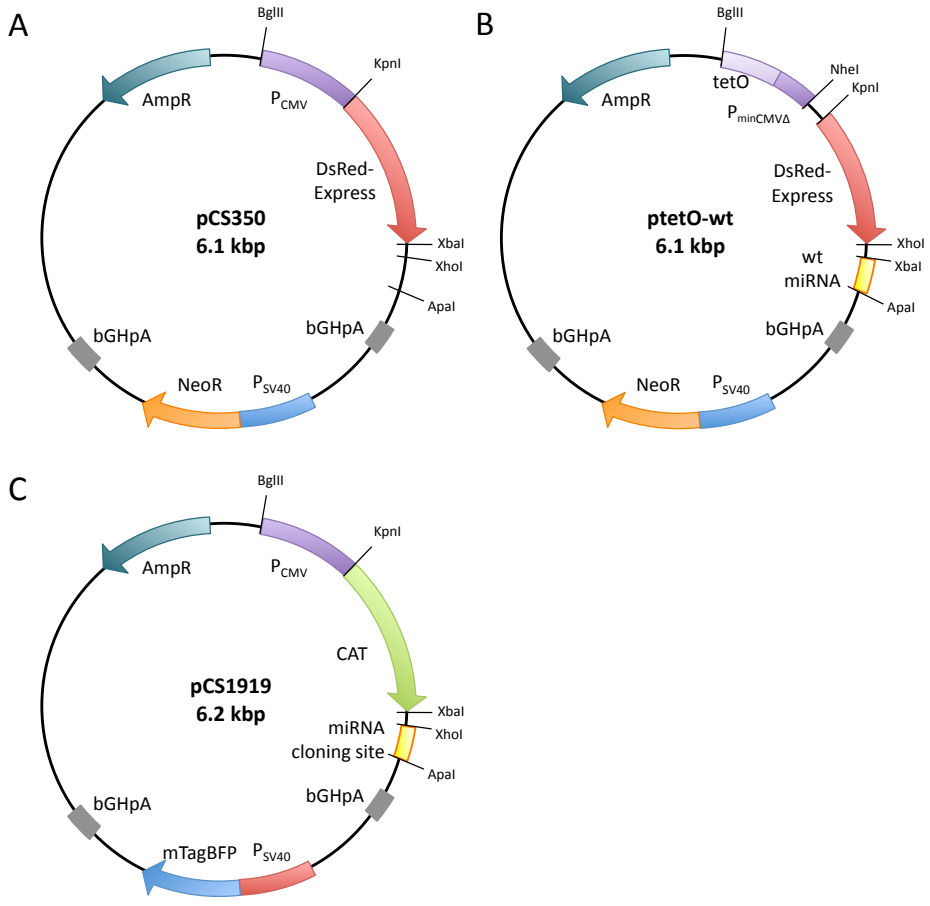

Supplementary Figure 5.8. Plasmid maps of miRNA constructs. (A) pCS350, which encodes for dsRed-Express from a CMV promoter, serves as a transfection marker in inducible promoter studies. (B) ptetO-wt encodes for the wt miRNA inserted in the 3' UTR of the CAT gene expressed form a Tet-OFF promoter system. (C) pCS1919 serves as the base expression vector into which miRNA and miRNA switches are inserted.

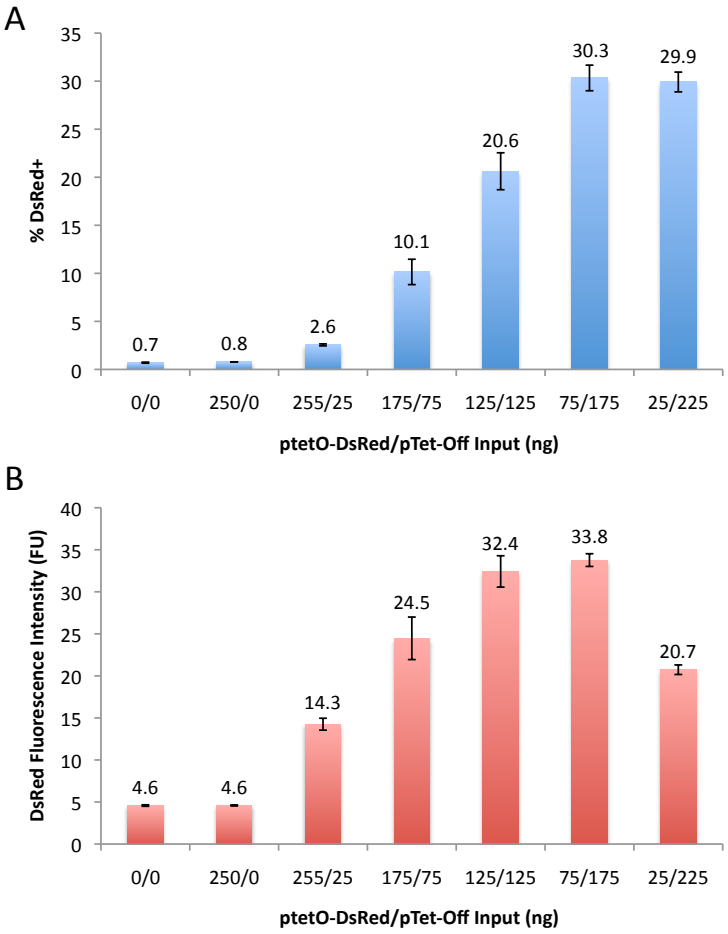

Supplementary Figure 5.9. Maximum transgene expression from the Tet-OFF promoter system requires an optimized input ratio between plasmids encoding for the tetO-CMV promoter and the tet transcriptional activator (tTA). Plasmids encoding for the tetO-CMV promoter expressing the fluorophore dsRed-Express (ptetO-DsRed) or the constitutive CMV promoter expressing tTA (pTet-Off) were co-transfected at various ratios into HEK 293 cells stably expressing EGFP. (A) An input of at least 175 ng of pTet-Off is necessary to reach maximum transfection efficiency. (B) The 75:175, ptetO-DsRed:pTet-Off, ratio is optimal for transgene expression from the tetO-CMV promoter. Reported values are mean ± s.d. from three independent samples.

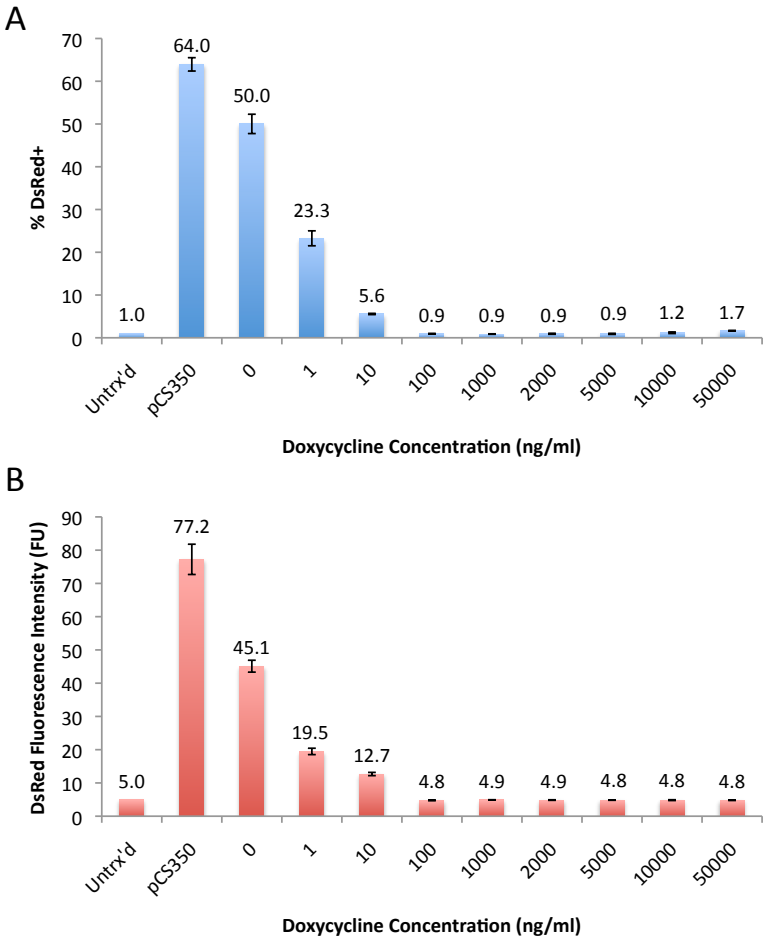

Supplementary Figure 5.10. The tetO-CMV promoter is tightly suppressed by the presence of doxycycline. ptetO-DsRed and pTet-Off were co-transfected at the optimized ratio (75 ng and 175 ng, respectively) into HEK 293 cells stably expressing EGFP. pCS350, a plasmid encoding for dsRed-Express expressed from a constitutive CMV promoter, was included as a positive control. Cells transfected with the Tet-OFF promoter system were treated with doxycycline at various concentrations. (A) Transfection efficiency as measured by the percentage of cells that are $DsRed^{+}$ and (B) transgene expression level as measured by dsRed-express fluorescence intensity both indicate that 100 ng/ml of doxycycline is sufficient to fully suppress the tetO-CMV promoter. Reported values are mean ± s.d. from three independent samples. Untrx'd, untransfected cells.

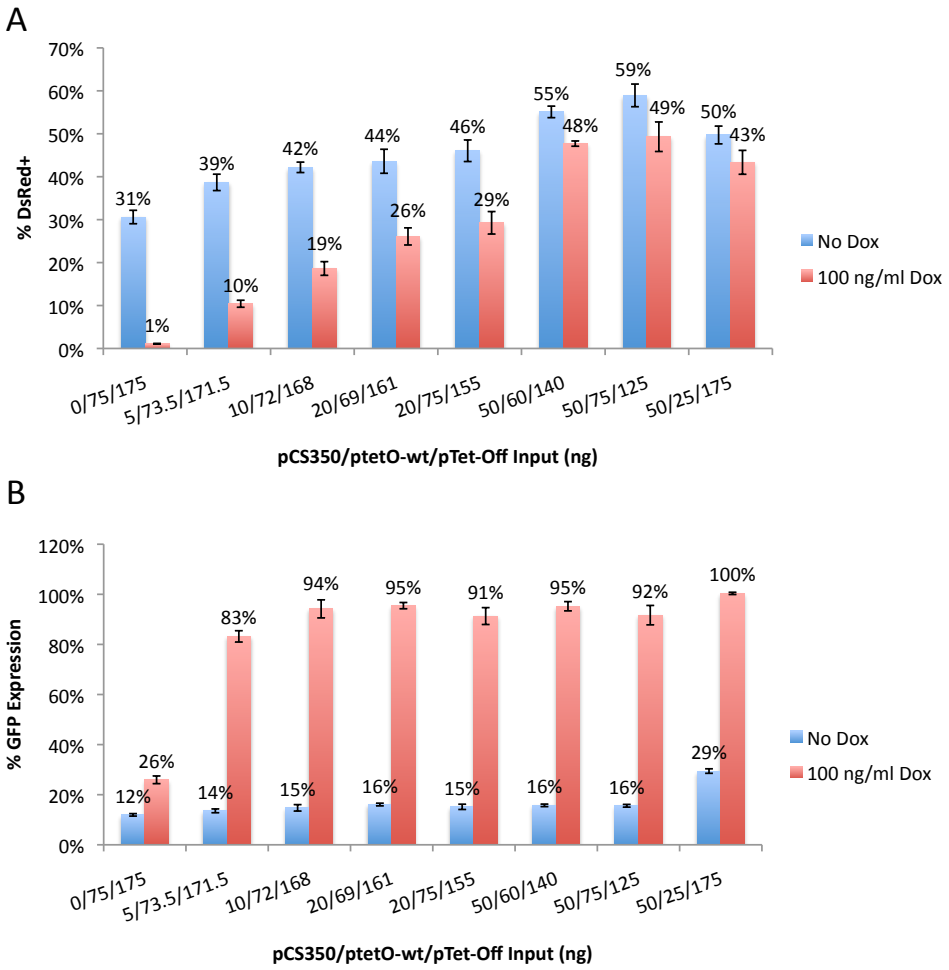

Supplementary Figure 5.11. A small input of pCS350 permits gating of transfected populations as well as maximum knockdown efficiency and switch activity by the ptetO-wt miRNA construct. pCS350, ptetO-wt, and pTet-Off were co-transfected at various ratios into HEK 293 cells stably expressing EGFP. Transfected cells were cultured in the absence or presence of 100 ng/ml of doxycycline. (A) dsRed-Express fluorescence increases with pCS350, with 5 ng being sufficient to generate an observable DsRed^{+} population even when the tetO-CMV promoter in ptetO-wt is fully suppressed. (B) Maximum knockdown efficiency and switch dynamic range from the ptetO-wt construct can be obtained with an input of 10 ng pCS350, which provides fluorescence signals for transfection-gating purposes. Reported values are mean ± s.d. from three independent samples.

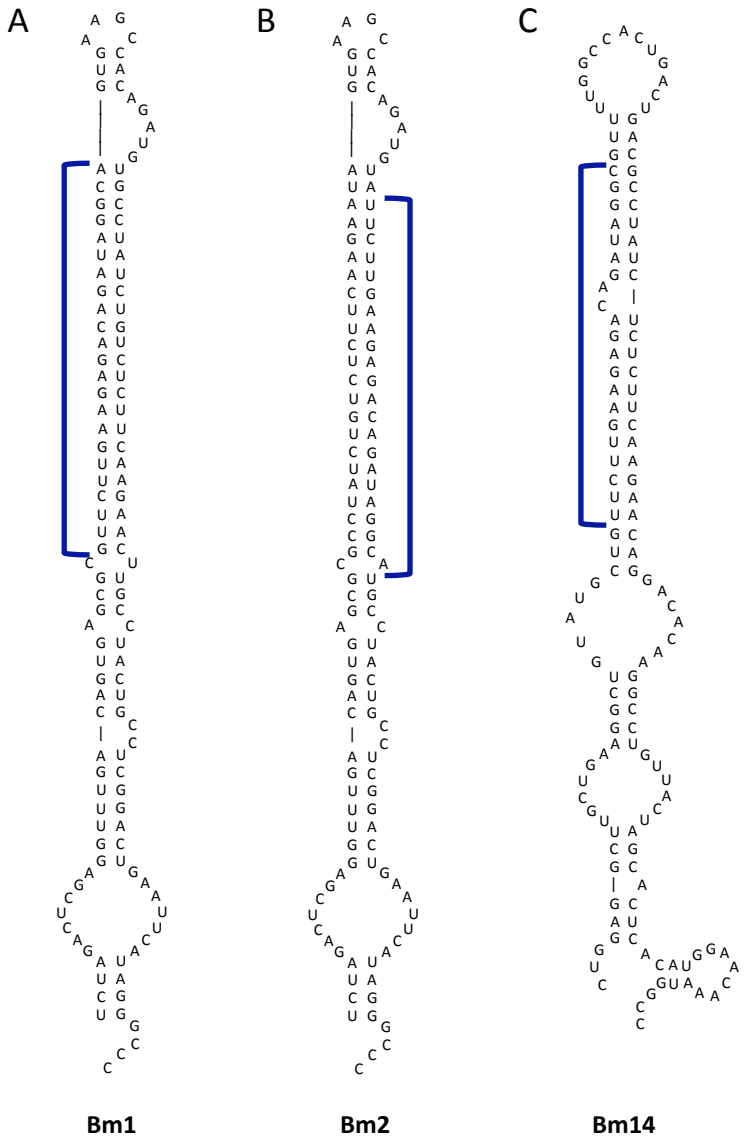

Supplementary Figure 5.12. Secondary structures for three miRNAs containing the same IL-2Rβ-targeting sequence. (A) The targeting sequence was inserted into the 5' side of the mature miRNA stem in structure B to construct Bm1. (B) The targeting sequence was inserted into the 3' side of the mature miRNA stem in structure B to construct Bm2. (C) The targeting sequence was inserted into the 5' side of the mature miRNA stem in structure A to construct Bm14.

Chapter 6

In Vitro Selection of RNA Aptamers to Clinically Applicable Small-Molecule Ligands

Abstract

Various platforms for constructing ligand-responsive RNA-based gene regulatory devices have been demonstrated. Although these devices utilize diverse architectures, most existing devices that can sense and respond to molecular inputs include sensor components consisting of RNA aptamers that bind to specific ligands of interest. In particular, well-characterized aptamers such as those responsive to the small molecules theophylline and tetracycline have been used in the majority of synthetic RNA control devices developed to date. Although theophylline and tetracycline have been invaluable in proof-of-concept studies, their use in practical applications such as metabolic engineering and cellular therapy is limited by their toxicity. *In vitro* selection procedures have been developed for the generation of new RNA aptamers, but few aptamers have been selected to clinically applicable small molecules that would be required for applications such as T-cell proliferation control in cellular immunotherapy. Here, we present three different *in vitro* aptamer selection procedures for the selection of aptamers to phenobarbital, vitamin B_{12}, and folinic acid. While ligand binding was observed in qualitative assays, we have been unable to quantitatively determine the binding affinities of aptamers obtained from these initial efforts. We discuss specific aspects of the selection processes—including partition efficiency evaluation for nitrocellulose membranes, format and timing of counter-selections, sequence and structural analyses of RNA pools, and techniques for characterizing putative aptamer sequences—that may contribute to the improvement of aptamer selection protocols.

Introduction

Ligand-responsive regulation over gene expression and cellular behavior has broad applicability in areas ranging from fundamental biomolecular investigation to metabolic engineering to health and medicine. However, the practicality of such regulatory schemes is dependent, in part, on the ability to tailor the input response of these control devices to each application. For example, control devices responsive to specific metabolite intermediates may be required for pathway engineering in biofuel production, whereas those responsive to pharmaceutical molecules are critical to the success of various therapeutic applications.

The RNA-based regulatory devices developed in the Smolke Laboratory and examined in the context of mammalian cell regulation in this thesis are composed of modular components, including sensor domains that can be systematically altered to program the desired input response specificity[1-3]. The aptamer sequence comprising the sensor domain specifies the input responsiveness of each regulatory device, independent of the actuator domain and the regulatory target. The work presented thus far on RNA-based regulatory systems has utilized molecular inputs such as theophylline and tetracycline, which are small molecules with well-characterized aptamer sequences. To fully realize the potential of these RNA-based regulatory devices for therapeutic applications, we investigate the generation of new RNA aptamers to clinically relevant input molecules. In particular, we focus on small-molecule ligands to avoid the use of heterologous proteins, which are prone to immunogenicity.

Although the Systematic Evolution of Ligands by EXponential enrichment (SELEX; see Chapter 1 for detailed description) has been successfully applied to the

selection of numerous ligand molecules, a number of challenges remain in generating aptamers to clinically relevant small molecules. The ability to effectively enrich ligand-binding sequences depends on efficient partition methods that can separate ligand-bound sequences from the unbound pool. In the case of protein ligands, filtration through nitrocellulose membranes, which are capable of separating proteins and protein-bound nucleic acids from free nucleic acid molecules, is the most commonly used separation method[4-8]. However, membrane filtration cannot be applied to the selection of aptamers to small-molecule ligands due to the inability of nitrocellulose membranes to retain small molecules. Instead, column chromatography, in which the small-molecule ligand is immobilized onto resin particles and ligand-bound nucleic acid sequences are specifically eluted, is the conventional separation method employed for the selection of aptamers to small-molecule ligands[9-11]. However, ligand conjugation to resin particles requires that the small molecules of interest possess suitable functional groups for the necessary chemistry. This is a requirement unmet by many clinically relevant small molecules, including phenobarbital and tamoxifen—two pharmaceutical molecules of particular interest to the development of T-cell proliferation control systems due to their known tolerance by human patients and potential for creating combinatorial regulatory systems utilizing both RNA-based switch devices and engineered cytokine receptor chains (M.C. Jensen, personal communication) that are responsive to these molecules.

To address this challenge, we examined the use of protein-conjugated small molecules for aptamer selection and developed alternative methods combining both membrane filtration and affinity elution to isolate aptamers specific for phenobarbital. Furthermore, we performed column-based SELEX to select aptamers specific for vitamin

B_{12} (cyanocobalamin) and folinic acid, two well-tolerated small molecules that are amenable to resin conjugation. While ligand binding was observed in qualitative assays, we have been unable to quantitatively determine the binding affinities of aptamers isolated from our efforts to date. Nevertheless, these early attempts led to a greater understanding of the selection procedure, which informs ongoing aptamer selection efforts in the Smolke Laboratory. Here, we present a summary of the procedures performed and discuss specific aspects of these selection processes—including evaluation of partition efficiency by nitrocellulose membranes, format and timing of negative selections, sequence and structural analyses of enriched RNA pools, and techniques for characterizing putative aptamer sequences—that contribute to the continuing improvement of aptamer selection protocols.

Results

Conventional Nitrocellulose Membrane-Based SELEX Has Low Partition Efficiency and Enriches for Nitrocellulose-Binding RNA Sequences. Phenobarbital is a barbiturate approved by the United States Food and Drug Administration for use as an anticonvulsant in human patients[12]. It is well tolerated by both mouse T cells (Appendix 1) and human natural killer cells (Appendix 2) in culture, and is a promising molecule for use in ligand-responsive RNA-based regulatory systems. As an aptamer to phenobarbital does not exist, we attempted to isolate a novel RNA aptamer to this molecule using SELEX. However, phenobarbital is a compact molecule with no appropriate functional group for conjugation to resin particles (Figure 6.1), thus precluding aptamer selection using column chromatography in the absence of chemical modification to the molecule.

Furthermore, nitrocellulose membranes cannot retain small molecules such as phenobarbital, thus eliminating the second conventional method for separating free and ligand-bound nucleic acids during SELEX. To address this challenge, we performed membrane-based selection of RNA aptamers toward phenobarbital conjugated to bovine serum albumin (phenobarbital-BSA). The BSA enables separation by nitrocellulose membranes, and rigorous negative selection against unconjugated BSA is expected to reduce enrichment of BSA-binding RNA sequences.

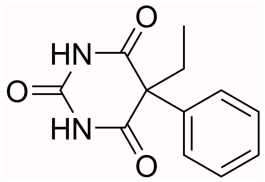

Figure 6.1. Chemical structure of phenobarbital. In the absence of chemical modification, phenobarbital contains no functional group suitable for resin conjugation chemistry.

An initial RNA library of approximately 1.2 x 10^{13} unique sequences, each containing a 30-nt randomized (N30) region, was subjected to 20 rounds of selection (Figure 6.2). Prior to the first selection cycle, the RNA library was filtered through a nitrocellulose membrane to remove membrane-binding sequences. In each selection cycle, RNA was incubated with phenobarbital-BSA (containing 12–15 phenobarbital molecules per BSA molecule) and filtered through a nitrocellulose membrane. The membrane was washed by filtering through selection buffer (20 mM Tris-HCl, pH7.5; 100 mM NaCl; 750 μM $MgCl_2$) and subsequently soaked in phenol-chloroform to elute the bound RNA. The eluted RNA was reverse transcribed to generate DNA templates for the subsequent selection cycle. Several selection conditions were gradually modified throughout the process to increase selection stringency. Specifically, the phenobarbital-to-RNA molar ratio and ligand-RNA incubation time were gradually reduced, whereas

the wash volume was gradually increased (see Materials and Methods for detailed protocol). In addition, negative selections against BSA were performed before positive selections for phenobarbital-BSA in cycles 11 to 13 and 15 to 20.

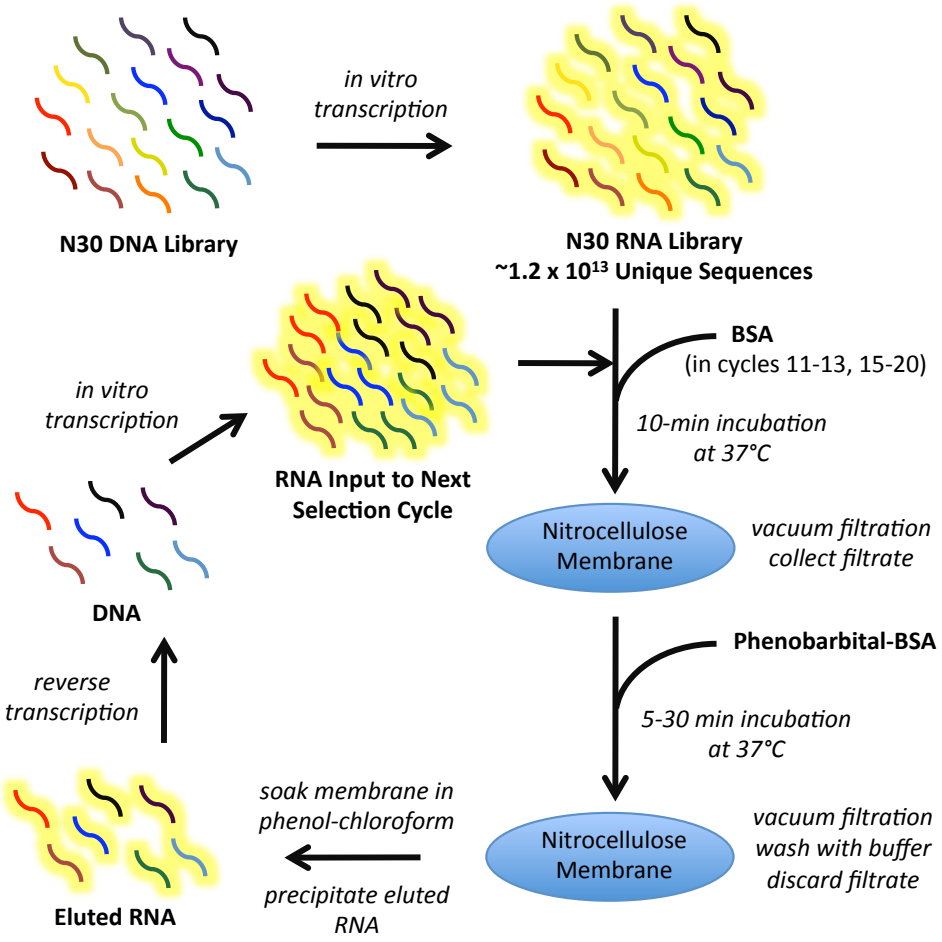

Figure 6.2. Schematic of conventional nitrocellulose membrane-based SELEX for RNA aptamer selection to BSA-conjugated phenobarbital. An RNA sequence library was generated by *in vitro* transcription and incubated with the target protein (phenobarbital-BSA). The binding mixture was filtered through a nitrocellulose membrane, which retains proteins and protein-bound RNA molecules. The membrane was washed with selection buffer to remove non-specifically or weakly binding RNA sequences. Protein-bound RNA sequences were eluted from the membrane by phenol-chloroform and reverse transcribed into cDNA, which served as the transcription template for the next selection cycle. In cycles 11-13 and 15-20, an additional negative selection step against BSA-binding sequences was inserted before the positive selection step with phenobarbital-BSA.

RNA pools obtained after cycles 15 and 20 of the selection were examined for ligand-binding specificity. ^{32}P-labeled RNA sequences were incubated with

phenobarbital-BSA, BSA (unconjugated), lysozyme, or no protein, and the binding mixture was filtered through nitrocellulose membranes as in regular selection cycles. The initial RNA flow-through was collected, and the membrane was washed with 1.8 ml of selection buffer. Radioactivity in the initial filtrates and on the washed membrane was quantified by scintillation counting to measure the extent of RNA binding to target proteins. RNA pools from both cycles show no specific binding to phenobarbital or to either of the proteins tested (Figure 6.3). Furthermore, the majority of RNA was retained on the membrane even in the absence of protein input, indicating strong affinity of the RNA library for the nitrocellulose membrane.

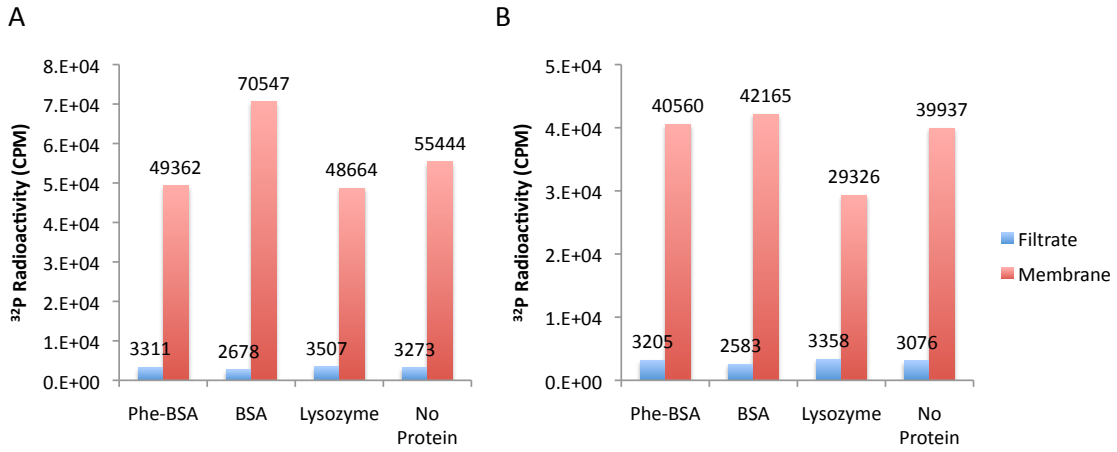

Figure 6.3. RNA sequence pools obtained after multiple selection cycles show strong affinity for nitrocellulose membranes and no specific binding for phenobarbital-BSA. Radiolabeled RNA was transcribed from cDNA obtained after (A) 12 and (B) 15 selection cycles and incubated with phenobarbital-BSA, BSA alone, lysozyme, or no protein. The binding solutions were filtered through nitrocellulose membranes, followed by washes with selection buffer. Radioactivity in the initial filtrates and on the washed membranes was quantified by scintillation counting. Regardless of the type of protein input, the majority of radioactivity is retained on the membrane, with a small fraction found in the initial filtrate, indicating strong binding to the nitrocellulose membrane.

To verify that RNA in general does not have non-specific affinity for nitrocellulose, we performed the radioactive binding assay on the initial N30 RNA library. The N30 RNA pool shows minimal retention by the membrane (Figure 6.4),

suggesting the membrane-binding activities observed in post–cycle 15 and post–cycle 20 RNA pools are specific to RNA sequences that have been enriched through multiple rounds of membrane-based separation.

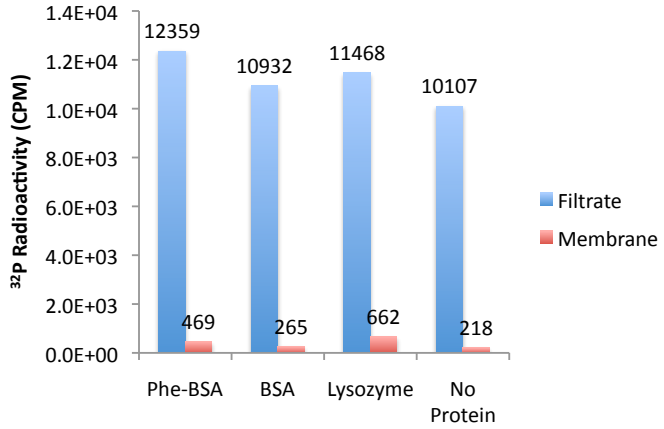

Figure 6.4. Randomized RNA sequence pool has minimal affinity for nitrocellulose membranes. Radiolabeled RNA was transcribed from randomized N30 DNA library and incubated with phenobarbital-BSA, BSA alone, lysozyme, or no protein. Filtration was performed as described in Figure 6.3. The majority of radioactivity is found in the initial filtrate, indicating low binding affinity for nitrocellulose membranes.

RNA pools obtained after cycles 1, 4, 8, 12, and 16 were analyzed using the radioactive binding assay without protein incubation to better understand the process by which nitrocellulose-binding sequences were enriched. Results indicate a noticeable increase in nitrocellulose binding starting in cycle 8, and affinity for nitrocellulose is prominent by cycle 12 (Figure 6.5). Although we did perform negative selection against the nitrocellulose membrane in cycle 1, these observations suggest that the negative selections should be continued in subsequent cycles to prevent the enrichment of nitrocellulose-binding sequences.

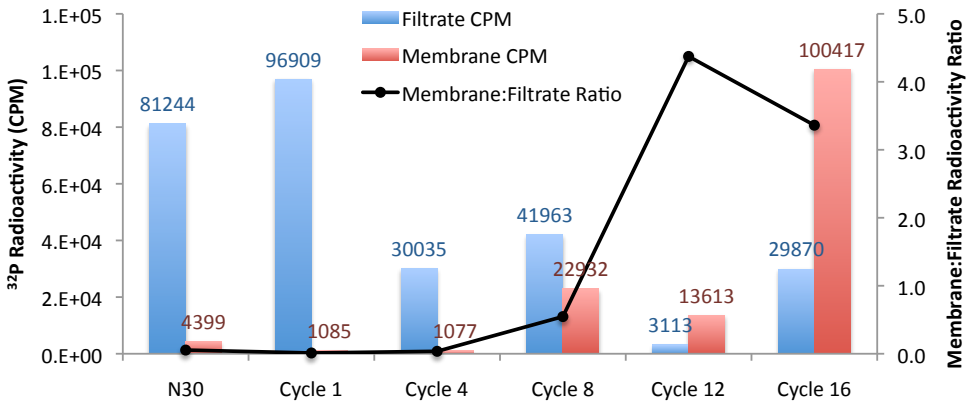

Figure 6.5. Nitrocellulose membrane-binding RNA sequences are enriched through selection cycles. Radiolabeled RNA was transcribed from either the randomized N30 DNA library or cDNA obtained after various selection cycles. The RNA was filtered through nitrocellulose membranes without prior incubation with protein targets, and radioactivity was measured as described in Figure 6.3. The black curve indicates the ratio of radioactivity on the membrane to radioactivity in the filtrate. Results reveal a significant increase in membrane-binding affinity in later selection cycles.

The enrichment of membrane-binding RNA sequences suggests a more detailed investigation on the performance characteristics of nitrocellulose membranes may be beneficial to subsequent endeavors in membrane-based SELEX. We first examined non-specific binding interactions between RNA and nitrocellulose membranes to determine the wash volume needed for complete removal of RNA from the membranes in the absence of protein components. A radioactive preparation of the N30 RNA library was filtered through a nitrocellulose membrane without prior protein binding, and the membrane was washed by filtering through five 1-ml aliquots of selection buffer. Radioactivity in the initial filtrate, each wash fraction, and the washed membrane was measured by scintillation counting. Results indicate that approximately 85% of all RNA passed through the membrane upon initial filtration, and the first 1-ml wash was sufficient to remove almost all residual RNA (Figure 6.6). Filtrates from subsequent wash steps and the washed membrane yielded minimal or undetectable levels of radioactivity, suggesting that RNA has low non-specific binding affinity for nitrocellulose membranes.

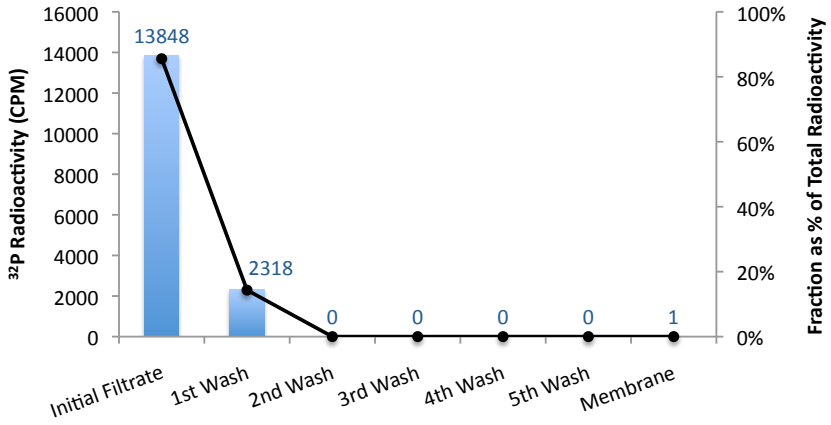

Figure 6.6. Removal of non-specifically bound RNA molecules from nitrocellulose membranes can be achieved with small wash volumes. Radiolabeled RNA was transcribed from randomized N30 DNA library and filtered through nitrocellulose membranes without prior binding incubation with protein targets. The membrane was washed with five 1-ml aliquots of selection buffer, and radioactivity in the initial filtrate, each 1-ml wash fraction, and the washed membrane was quantified by scintillation counting. The black curve indicates the percent of total measured radioactivity in each fraction.

We next examined the efficiency of nitrocellulose membranes in separating free and protein-bound RNA sequences by performing radioactive binding assays on known RNA aptamers incubated with either their cognate protein targets or with a mismatched protein (BSA). The lysozyme RNA aptamer, which has a K_D of 31 nM[13], was incubated with 300 nM of either lysozyme or BSA. The NF-κB RNA aptamer, which has a K_D of 5.4 nM[14], was incubated with 24 nM of either NF-κB or BSA. The binding solution was filtered through a nitrocellulose membrane, follow by washing with three 1-ml aliquots of selection buffer. Radioactivity in the initial filtrate, each wash fraction, and the washed membrane was measured by scintillation counting. The majority of RNA was found in the initial filtrate and never retained by the membrane, possibly due to a molar excess of RNA relative to protein targets (Figure 6.7). Incubating RNA aptamers with their cognate proteins did result in greater initial RNA retention on the nitrocellulose membrane compared to incubation with a mismatched protein, indicating protein-specific binding activity by the aptamers. However, the retained RNA was rapidly lost during the

subsequent wash steps, suggesting that the ligand-specific binding interaction is easily disrupted by buffer filtration.

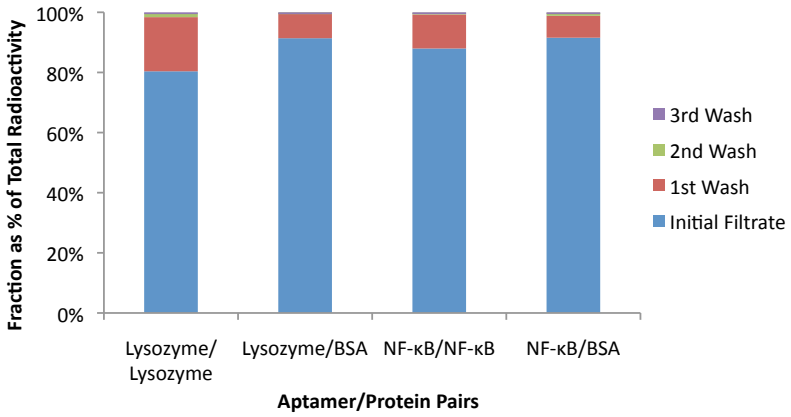

Figure 6.7. Nitrocellulose membranes show weak retention of RNA aptamers bound to their specific protein ligands. RNA aptamer sequences were incubated with either their cognate protein or a mismatched target (BSA) and filtered through nitrocellulose membranes. Incubation with cognate proteins results in greater RNA retention on the membrane in the initial filtration, but the retained RNA is easily removed by subsequent wash steps.

The observation that even pure RNA aptamer sequences with high affinities for their target proteins cannot withstand relatively gentle wash conditions suggests that the conventional membrane-based SELEX protocol—in which membranes are loaded with RNA, washed extensively with buffer, and eluted by soaking in solutions such as phenol-chloroform or urea—may not be the most efficient method for recovering and enriching protein-bound RNA sequences. Specifically, protein-bound RNA sequences initially retained on the membrane are likely to be lost during washing, while only strongly nitrocellulose-binding sequences are able to withstand the wash steps and be recovered in the elution step. In light of these observations, we modified the membrane-based selection procedure to incorporate an alternative elution strategy that is similar in principal to affinity elution in column chromatography.

RNA Recovery by Affinity Elution Prevents Enrichment of Nitrocellulose-Binding Sequences. In a second attempt to select for phenobarbital-binding RNA aptamers, we modified the nitrocellulose membrane-based SELEX procedure to perform ligand-specific elution by filtering concentrated phenobarbital solutions through the RNA-loaded membrane (Figure 6.8). Unlike the previous RNA recovery method, in which washed nitrocellulose membranes were soaked in phenol-chloroform to remove membrane-bound RNA molecules, the modified protocol is expected to release phenobarbital-specific RNA sequences from the membrane through competitive binding between free phenobarbital and phenobarbital-BSA molecules. RNA sequences released from the protein can flow through the membrane and be collected in the eluate fraction.

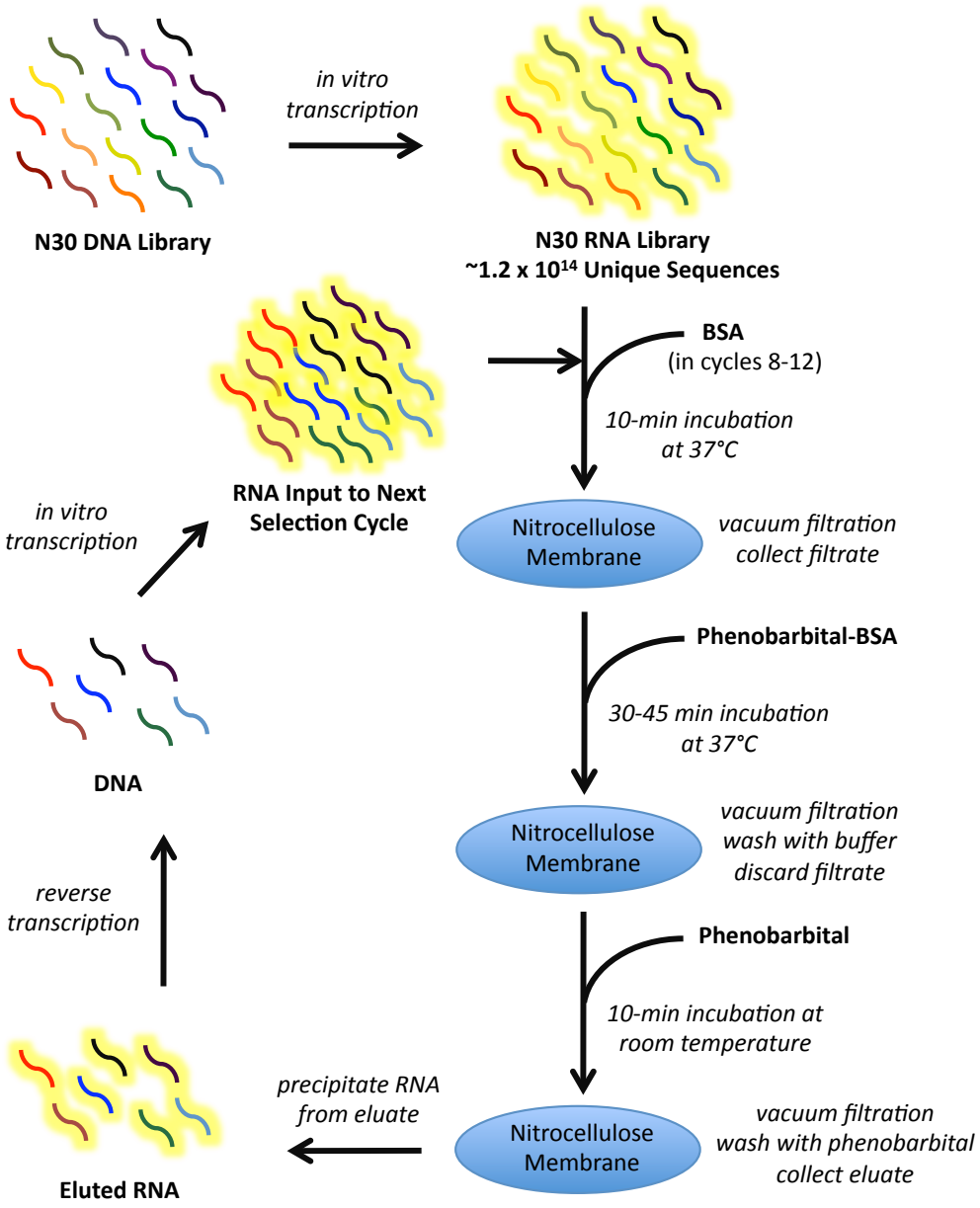

Figure 6.8. Schematic of nitrocellulose membrane-based SELEX with ligand-specific elution for the selection of RNA aptamers to BSA-conjugated phenobarbital. The selection procedure depicted in Figure 6.2 was modified such that ligand-bound RNA was specifically eluted by filtration with concentrated phenobarbital solutions rather than non-specific elution by soaking the membrane in phenol-chloroform.

An initial N30 RNA library containing approximately 1.2 x 10^{14} unique sequences (ten times more than the previous library) was employed to broaden the selection pool. Twelve selection cycles were performed, with the phenobarbital-to-RNA ratio fixed at 14:1 throughout the selection. The decision not to reduce the ligand-to-RNA ratio was

informed by the observation that even high-affinity RNA aptamer sequences incubated with their cognate proteins are easily lost during the filtration process (Figure 6.7), suggesting that a low ligand-to-RNA ratio may impose an unproductively stringent selection condition. The wash volume was maintained at 1 ml for cycles 1 through 9 and increased to 2 ml for cycles 10 through 12. Negative selection against BSA was performed before positive selection with phenobarbital-BSA in cycles 8 through 12.

RNA pools obtained after cycles 6 and 12 of the selection were examined for ligand-binding specificity, and the N30 RNA library was included as a control. ^{32}P-labeled RNA sequences were incubated with phenobarbital-BSA, BSA, or no protein, and the binding mixture was filtered through nitrocellulose membranes as in regular selection cycles. The initial RNA flow-through was collected, and the membrane was washed with 1.2 ml of selection buffer followed by elution with 200 μl of 1 mM phenobarbital and 800 μl of 5 mM phenobarbital. Radioactivity in the initial filtrate, wash fraction, combined eluate fraction, and the washed membrane was quantified by scintillation counting. In all three RNA pools tested, the presence and identity of protein have minimal impact on the binding and elution behavior of the RNA (Figure 6.9). Compared to the N30 library, RNA pools from cycles 6 and 12 show significantly more RNA retention by the membrane upon initial filtration, but the great majority of retained RNA is removed by the wash step. The small percentage of RNA found on the final washed membrane indicates that the modified protocol succeeded in preventing the enrichment of nitrocellulose-binding sequences. However, the minimal amount of RNA found in the eluate fraction also indicates that the RNA pool has not been sufficiently enriched for phenobarbital-binding species.

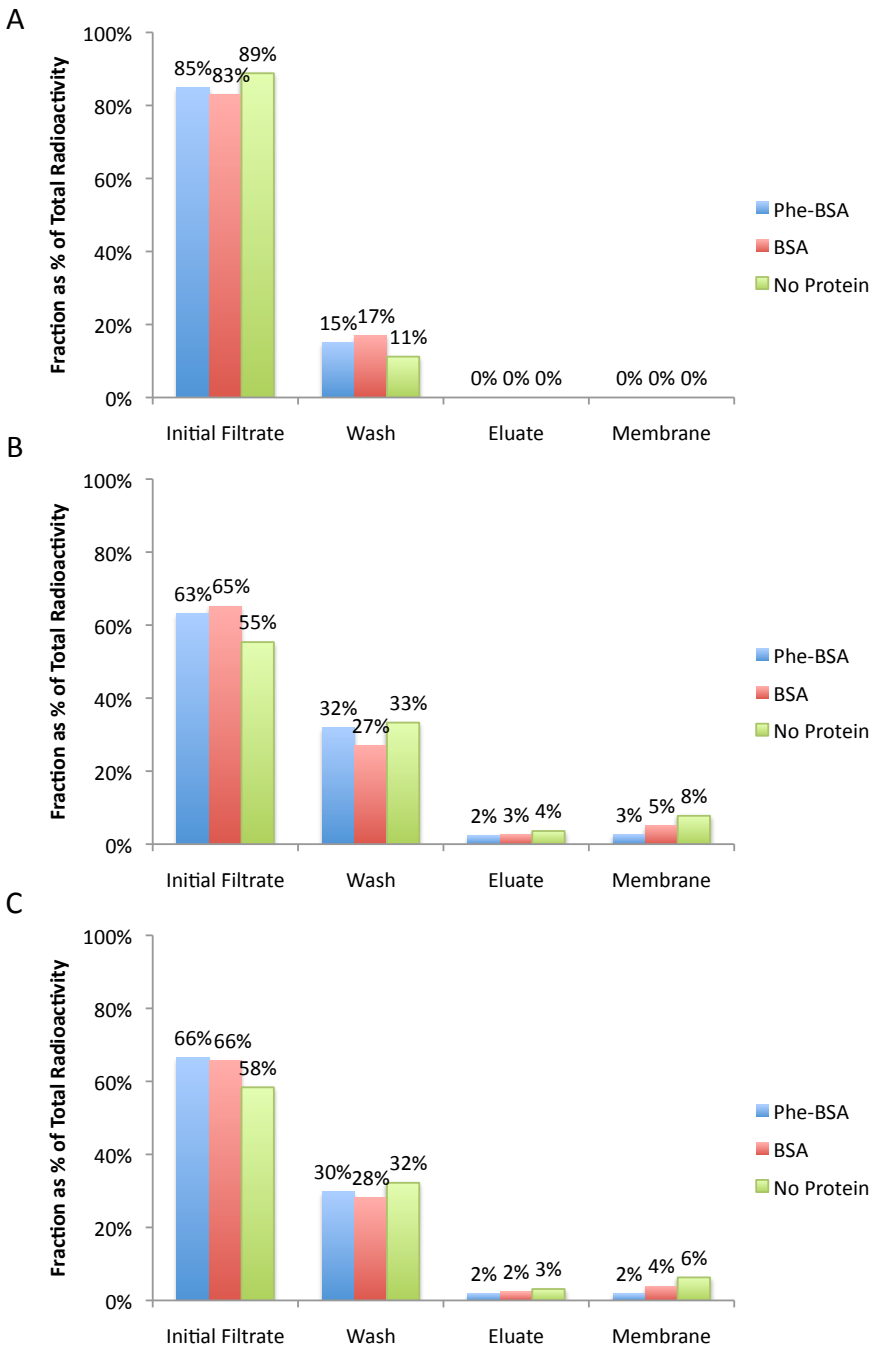

Figure 6.9. RNA sequence pools obtained after multiple selection cycles show no specific binding for phenobarbital-BSA (phe-BSA) or BSA alone. (A) The N30 DNA library and cDNA obtained after (B) six and (C) twelve selection cycles served as templates for the transcription of radiolabeled RNAs, which were incubated with phenobarbital-BSA, BSA alone, or no protein. Filtration was performed as described in Figure 6.3, with an added step of elution with phenobarbital after the wash step with selection buffer. Radioactivity in each fraction was analyzed by scintillation counting. Radioactivity found in each fraction is reported as the percent of total measured radioactivity. Sequence pools obtained after cycles 6 and 12 show increased retention by the membrane upon initial filtration, but the RNA-nitrocellulose binding interaction is sufficiently weak for the majority of retained RNA to be removed by the wash step. No increase in RNA retention is seen with either phenobarbital-BSA or BSA alone.

We sequenced the cycle 12 pool to better understand the extent of sequence enrichment at the end of the selection process. Surprisingly, only six unique and highly related sequences were found, with two-thirds (20 of 29) of the sequences being identical (Cycle 12 Sequence, Figure 6.10) We then sequenced pools from the initial N30 library and cycles 1, 4, 7, and 8 (the first cycle after negative selection began). Results from the N30 library confirm that the initial pool is diverse, with no repeats or detectable motifs found among 14 sequenced samples. However, the dominant sequence found in cycle 12 (SVC12.6) is already present in the cycle 1 pool. The cycle 4 pool is dominated by two sequences, including SVC12.6, and this sequence accounts for the great majority of sequences found in cycles 7 and 8.

ID	N30 Library Sequence	Frequency
N30.1	*AGCTAGCCAGG*AGCGCAGCGCGCAACACGGAGAGGTTGATC*GAGGCAAAGCTTCCG*	1 of 14
N30.2	*AGCTAGCCAGG*CAGTGTGATACGCACTGAGTTCCGATGGGGG*AGGCAAAGCTTCCG*	1 of 14
N30.6	*AGCTAGCCAGG*ATCTTAGGTTTACCCCTGGAGGTAGTATGGG*AGGCAAAGCTTCCG*	1 of 14
N30.10	*AGCTAGCCAGG*TGGGATACGGCCCATGAAGGCGGGCGGGAT*GAGGCAAAGCTTCCG*	1 of 14
N30.11	*AGCTAGCCAGG*ATCCTAGATTAGCGCAGGTAGCGTTAGTGGG*AGGCAAAGCTTCCG*	1 of 14
N30.13	*AGCTAGCCAGGGG*AGCAAAAGAGTCCCGGACTAATACAGGGG*AGGCAAAGCTTCCG*	1 of 14
N30.14	*AGCTAGCCAGG*TGTGCCGTCAGGAAAAGTGAATCACCTGTGG*AGGCAAAGCTTCCG*	1 of 14
N30.20	*AGCTAGCCAGGGG*TGGATCGTGGAATGTATCCGCACGACGG*GAGGCAAAGCTTCCG*	1 of 14
N30.31	*AGCTAGCCAGG*AAAACACCAAAAGGTGGCCAGCATCTACAG*GAGGCAAAGCTTCCG*	1 of 14
N30.32	*AGCTAGCCAGG*AGGCCGAAAGCGGAAGAAAACAAGTAGGAT*GAGGCAAAGCTTCCG*	1 of 14
N30.33	*AGCTAGCCAGG*CAAACCGGTTACGTATCGTCTACGTACGGG*GAGGCAAAGCTTCCG*	1 of 14
N30.191	*AGCTAGCCAGG*AACAGGCTGCGAAGGGGTATATGATTTAGA*GAGGCAAAGCTTCCG*	1 of 14
N30.192	*AGCTAGCCAGG*ATAGTTCGGGTTGTATGGTTAAGTGCTTGG*GAGGCAAAGCTTCCG*	1 of 14
N30.193	*AGCTAGCCAGG*AACAGAAGATCGAGGATCGATGAATCATG-*GAGGCAAAGCTTCCG*	1 of 14

ID	Cycle 1 Sequence	Frequency
SVC1.28	*AGCTAGCCAGG*CTGGGCGTCATCAGGAGTGTCGGGTCGGTG*GAGGCAAAGCTTCCG*	1 of 13
SVC1.30	*AGCTAGCCAGG*AATGGGGGACCCCAGATTAGTACCTGTGGGG*AGGCAAAGCTTCCG*	1 of 13
SVC1.34	*AGCTAGCCAGG*CATATCGGGGATCAAAGAATCGGTGGAGGG*GAGGCAAAGCTTCCG*	1 of 13
SVC1.36	*AGCTAGCCAGG*GCATTACCGAGCTACACTCAACGCCTCTGGG*AGGCAAAGCTTCCG*	1 of 13
SVC1.38	*AGCTAGCCAGG*AGTAAGTGGGAGGAGAACGTAGGGGTCTGGG*AGGCAAAGCTTCCG*	1 of 13
SVC1.40	***AGCTAGCCAGG*AAAGTGAGGAGGTGGTGAAGTACTGGTGTA*GAGGCAAAGCTTCCG***	1 of 13
SVC1.42	*AGCTAGCCAGG*CGCAAGCAGGAGGGATAACAGTACGGCGGG*GAGGCAAAGCTTCCG*	1 of 13
SVC1.44	*AGCTAGCCAGG*GCTTCGGATCGAATCTAATGCTTGATTGAT*GAGGCAAAGCTTCCG*	1 of 13
SVC1.46	***AGCTAGCCAGG*AAAGTGAGGAGGTGGTGAGGTACTGGTGTA*GAGGCAAAGCTTCCG***	1 of 13
SVC1.50	*AGCTAGCCAGG*AGGAATCATACGATGTATTCGTAAGGCATG*GAGGCAAAGCTTCCG*	1 of 13
SVC1.321	*AGCTAGCCAGG*TGGCGAACAGGAGAACTGAGCGGTGAGGGT*GAGGCAAAGCTTCCG*	1 of 13
SVC1.322	*AGCTAGCCAGG*CTGAAGATGCAAGTAGGTAGGCTATGTGTT*GAGGCAAAGCTTCCG*	1 of 13
SVC1.323	*AGCTAGCCAGG*GAAGCCGGGGTGGGCAAACCAGGTGCGTG*G-AGGCAAAGCTTCCG*	1 OF 13

ID	Cycle 4 Sequence	Frequency
SVC4.8	***AGCTAGCCAGG*AAAGTGAGGAGGTGGTGAAGTACTGGTGTA*GAGGCAAAGCTTCCG***	8 of 19
SVC4.11	*AGCTAGCCAGG*GAACGTGACAGGAAAACTGCGTCTCGGCTG*GAGGCAAAGCTTCCG*	1 of 19
SVC4.16	***AGCTAGCCAGG*TTGAAGGTGGAGGAGGAGTAATCTTGGTA*GAGGCAAAGCTTCCG***	8 of 19
SVC4.28	*AGCTAGCCAGG*CAATGTATTGACCTGGTATACGGGGTGGG-*GAGGCAAAGCTTCCG*	1 of 19
SVC4.242	*AGCTAGCCAGG*GTTGAAAGTGGACGAGGATTGTTGCGGGTA*GAGGCAAAGCTTCCG*	1 of 19

ID	Cycle 7 Sequence	Frequency
SVC7.27	***AGCTAGCCAGG*AAAGTGAGGAGGTGGTGAAGTACTGGTGTA*GAGGCAAAGCTTCCG***	10 of 13
SVC7.40	*AGCTAGCCAGG*AGAATCGTGGACTTGAGATCGTGCGCGTGG*GAGGCAAAGCTTCCG*	1 of 13
SVC7.45	*AGCTAGCCAGG*GTTGAAGGTGGAGGAGGAGTAATCTTGGTA*GAGGCAAAGCTTCCG*	1 of 13
SVC7.46	*AGCTAGCCAGG*GGCAAAAGCAATTCTTGTGTTGTTGCTGTT*GAGGCAAAGCTTCCG*	1 of 13

ID	Cycle 8 Sequence	Frequency
SVC8.2	***AGCTAGCCAGG*AAAGTGAGGAGGTGGTGAAGTACTGGTGTA*GAGGCAAAGCTTCCG***	13 of 14
SVC8.16	***AGCTAGCCAGG*AAAGTGAGGAGGAGGTGAAGTACTGGTGTA*GAGGCAAAGCTTCCG***	1 of 14

ID	Cycle 12 Sequence	Frequency
SVC12.6	***AGCTAGCCAGG*AAGTGAGGAGGTGGTGAAGTACTGGTGTA*GAGGCAAAGCTTCCG***	20 of 29
SVC12.53	*AGCTAGCCAGG*AAGTGAGGAGGAGGTGAAGTACTGGTGTA*GAGGCAAAGCTTCCG*	2 of 29
SVC12.60	*AGCTAGCCAGGG*CTTCGAGGGAGGAGGAGGAGTGAAGTGTT*GAGGCAAAGCTTCCG*	4 of 29
SVC12.70	***AGCTAGCCAGGG*TTGAAGGTGGAGGAGGAGTAATCTTGGTA*GAGGCAAAGCTTCCG***	1 of 29
SVC12.402	*AGCTAGCCAGG*AAGTGAGCAGGCGCTGAAGTACTCGTGTA*GAGGCAAAGCTTCCG*	1 of 29
SVC12.482	*AGCTAGCCAGG*ATTGAAGGTGGAGGAGGAGTAATCTTGGTA*GAGGCAAAGCTTCCG*	1 of 29

Figure 6.10. Sequences obtained after various selection cycles show a rapid decrease in sequence diversity and the early appearance of a dominant sequence. Italicized nucleotides constitute the constant regions. Bolded sequences of the same color are identical, except where blue highlights mark point mutations that distinguish the two red-colored sequences in cycles 1 and 8. Green and yellow highlights mark sequence motifs among sequences found in the cycle 12 pool.

These results indicate that the selection conditions rapidly eliminated sequence diversity from the RNA library. The sequence pool was nearly homogenous by the time negative selection against BSA commenced in cycle 8, likely rendering subsequent cycles ineffectual. However, it is curious that the SVC12.6 sequence accounts for 77% (10 of 13) of the sequenced cycle 7 pool and 93% (13 of 14) of the cycle 8 pool but only 69% (20 of 29) of the cycle 12 pool, suggesting a resurgence of less prevalent sequences during the later cycles. The six unique sequences found in the cycle 12 pool are all highly enriched in G and show conserved motifs. The AGG motif (alone or in repeats) was found in all sequences at similar positions, and the AAGT sequence was found in all but two (Figure 6.10). The 5' and 3' ends of all six sequences also show convergence upon similar bases. A purine occupies the first nucleotide after the 5' constant region in all six sequences, and KKGTA (K = G or T) is found immediately before the 3' constant region in all but one sequence (which has KKGTT). Such sequence similarities are typical of enriched aptamer pools, yet no ligand-binding activity was detected in radioactive binding assays performed on the final sequence pool (Figure 6.9C), suggesting that the binding characterization method may not be ideal. As an alternative method, capillary electrophoresis (CE) was employed for binding affinity evaluation.

Capillary Electrophoresis (CE) Assay Shows No Ligand-Binding Activity by Putative Phenobarbital Aptamers. CE is an automated process that separates mixture components based on differences in electrophoretic mobility, which is dependent on the size-to-charge (approximated by the mass-to-charge, or m/z) ratios of the various species within a mixture[15]. A capillary, which is typically made of fused silica and carries

negative charges on its surface, connects an inlet anode and an outlet cathode. As a run buffer containing background electrolytes passes through the capillary, an electroendoosmotic flow (EOF) toward the cathode is transmitted throughout the diameter of the capillary, creating a nearly perfect plug flow down the length of the tube. When a sample mixture is injected into the capillary, components are simultaneously separated by charge due to the EOF and by size due to frictional drag in accordance with Stoke's Law.

Since RNA molecules are highly negatively charged, a mixture of free protein, free RNA, and protein-RNA complexes can be separated by CE based on differences in their m/z ratios. Free protein molecules are eluted first, followed by protein-RNA complexes and finally the free RNA molecules. For the purpose of characterizing ligand-binding behavior of putative phenobarbital aptamers, RNA molecules were transcribed from single-sequence DNA templates and incubated with an equimolar amount of phenobarbital-BSA (5.24 μM each). The three most prevalent sequences from cycle 12 (SVC12.6, SVC12.60, and SVC12.70) were examined. The resulting elution profiles show clear peaks corresponding to free phenobarbital-BSA and free RNA but no detectable protein-RNA complex peak (Figure 6.11), indicating a lack of phenobarbital- and BSA-binding activities by the RNA sequences. Together with the radioactive binding assay results, these observations suggest that the selection process failed to enrich for phenobarbital-binding sequences, and alternative aptamer selection protocols or molecular targets need to be identified.

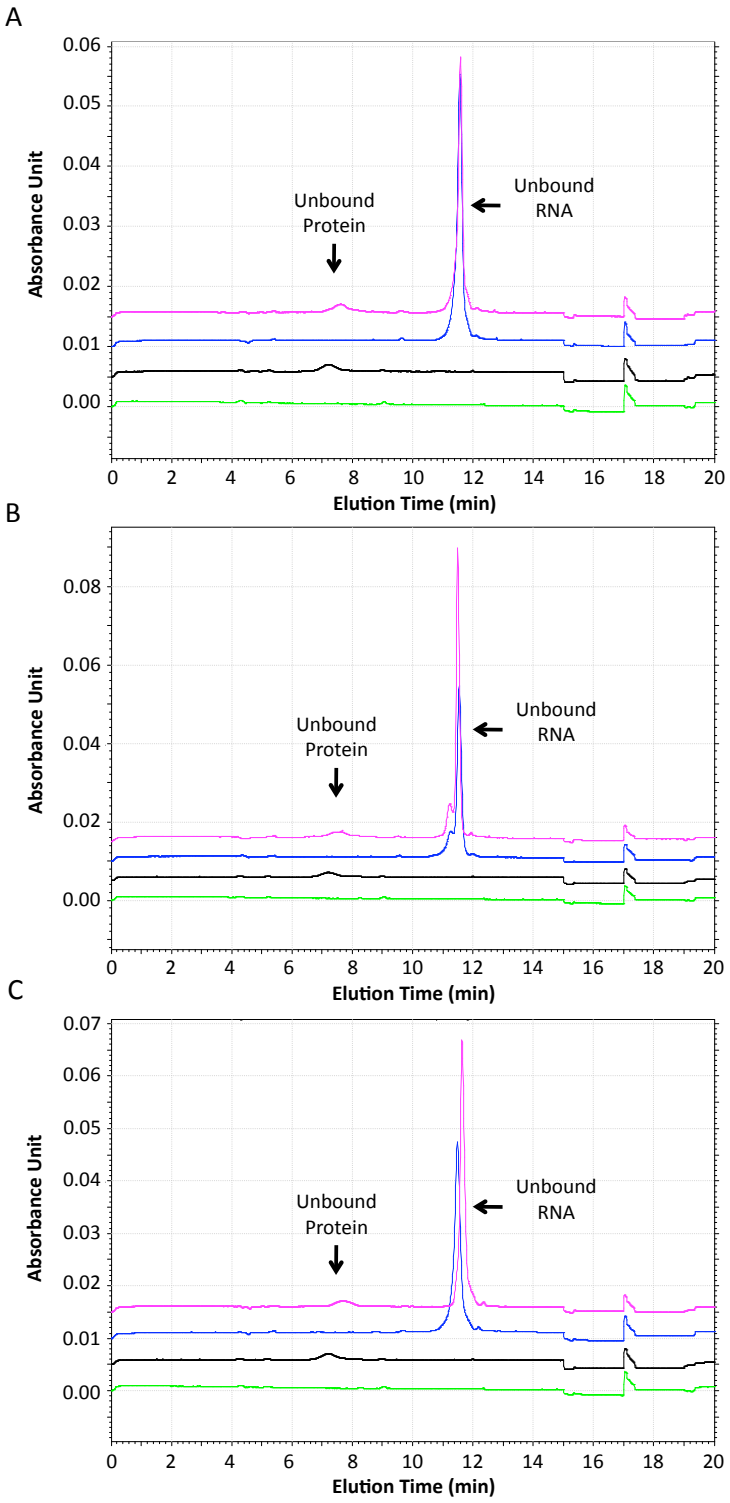

Figure 6.11. Capillary electrophoresis shows no evidence of ligand binding by putative phenobarbital aptamer sequences. Selection buffer alone (green), phenobarbital-BSA alone (black), RNA alone (blue), and a binding solution containing both RNA and phenobarbital-BSA (pink) were analyzed by CE. The RNA sequences (A) SVC12.6, (B) SVC12.60, and (C) SVC12.70 were characterized, with none showing specific binding to the phenobarbital-BSA molecule.

Column-Based SELEX for Vitamin B_{12} Fails to Enrich for Ligand-Binding RNA Sequences. Unlike nitrocellulose membrane–based separation, column chromatography allows for the selection of aptamers to small molecules without protein conjugation. However, phenobarbital does not possess appropriate functional groups for resin-conjugation chemistry and thus cannot be immobilized onto columns for nucleic acid separation. As a result, alternative small-molecule ligands were evaluated as SELEX candidates. Vitamin B_{12} (cyanocobalamin) and folinic acid are two small molecules commonly used as a nutritional supplement and an adjuvant in cancer chemotherapy[16], respectively (Figure 6.12). We have also demonstrated that these molecules have low or no toxicity toward mouse T cells (Appendix 1) and human natural killer cells (Appendix 2), and would be suitable input molecules for ligand-responsive RNA-based regulatory systems. Importantly, both vitamin B_{12} and folinic acid can be conjugated to agarose resin molecules through standard chemistry, thus enabling the use of column-based SELEX.

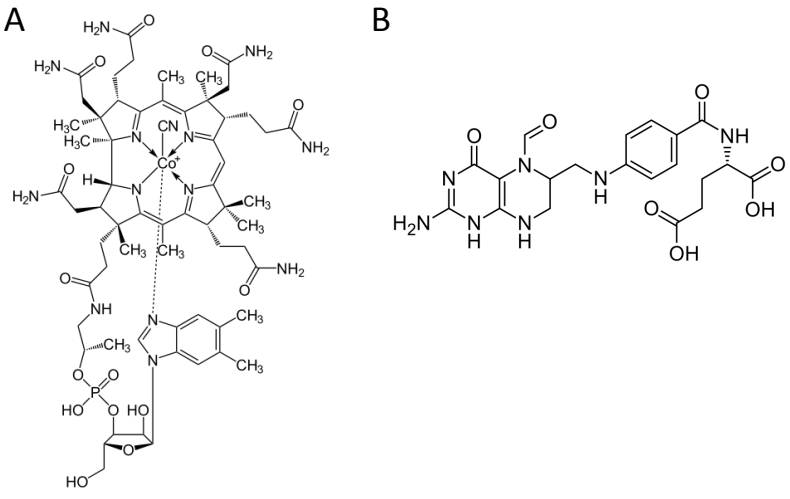

Figure 6.12. Chemical structures of (A) vitamin B_{12} (cyanocobalamin) and (B) folinic acid. Vitamin B_{12} can be conjugated to Sepharose 6B resin through its hydroxyl group. Folinic acid can be conjugated to EAH Sepharose 4B resin through its carboxyl groups.

An RNA aptamer for vitamin B_{12} had previously been isolated by column-based SELEX[17]. However, the binding activity of this aptamer is dependent on the presence of high concentrations of Li^+, making it unsuitable for *in vivo* applications. Furthermore, this aptamer has a complex tertiary structure, including pseudoknots required for ligand binding[18]. Such structural complexities render the incorporation of this aptamer into RNA-based regulatory devices difficult, if not impossible. Nevertheless, the previous example of vitamin B_{12} aptamer selection indicates that it is possible to isolate vitamin B_{12}–binding RNA sequences by column-based SELEX, and that the ion dependence of the isolated sequences is partially dictated by the composition of the selection buffer[17]. To generate a vitamin B_{12}–specific RNA aptamer capable of *in vivo* functionality, we performed a modified SELEX protocol in which the selection buffer contained a more physiological ion concentration (250 mM NaCl and 2.5 mM $MgCl_2$ in contrast to 1 M LiCl and 5 mM $MgCl_2$ in the published selection process). Furthermore, the randomized RNA library was designed to contain 5' and 3' constant regions that formed a stem at the base of all sequences to facilitate future integration into RNA-based regulatory devices (Figure 6.13).

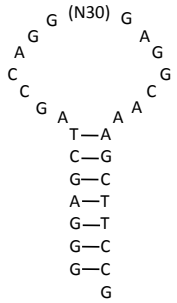

Figure 6.13. The randomized RNA library contains constant regions that form a stable basal stem. The 5' and 3' constant regions flanking the N30 sequence form a stable hairpin through Watson-Crick base pairing to ensure that aptamer sequences obtained from the selection process have structures appropriate for integration into RNA-based regulatory devices.

An initial RNA library containing approximately 2.4 x 10^{14} unique sequences was subjected to 15 cycles of selection (Figure 6.14). In each cycle, a column packed with commercially available vitamin B_{12}–conjugated agarose (same as used in Ref. 17) was equilibrated with selection buffer, loaded with RNA, washed with selection buffer, and eluted with 5 mM vitamin B_{12}. Eluted RNA was precipitated and reverse transcribed to produce DNA templates for the next selection cycle. Negative selection against an adipic acid dihydrazide agarose column was performed immediately before positive selection for vitamin B_{12} in cycles 1 through 3 to eliminate agarose-binding sequences. The wash volume was increased from 5 column volumes (CV) in cycle 1 to 10 CV in cycle 4. The volume was subsequently increased in 10-CV intervals from cycle 5 to cycle 10, then in 20-CV intervals from cycle 10 to cycle 15. Mutagenic PCR was performed after cycle 10 to diversify the selection pool.

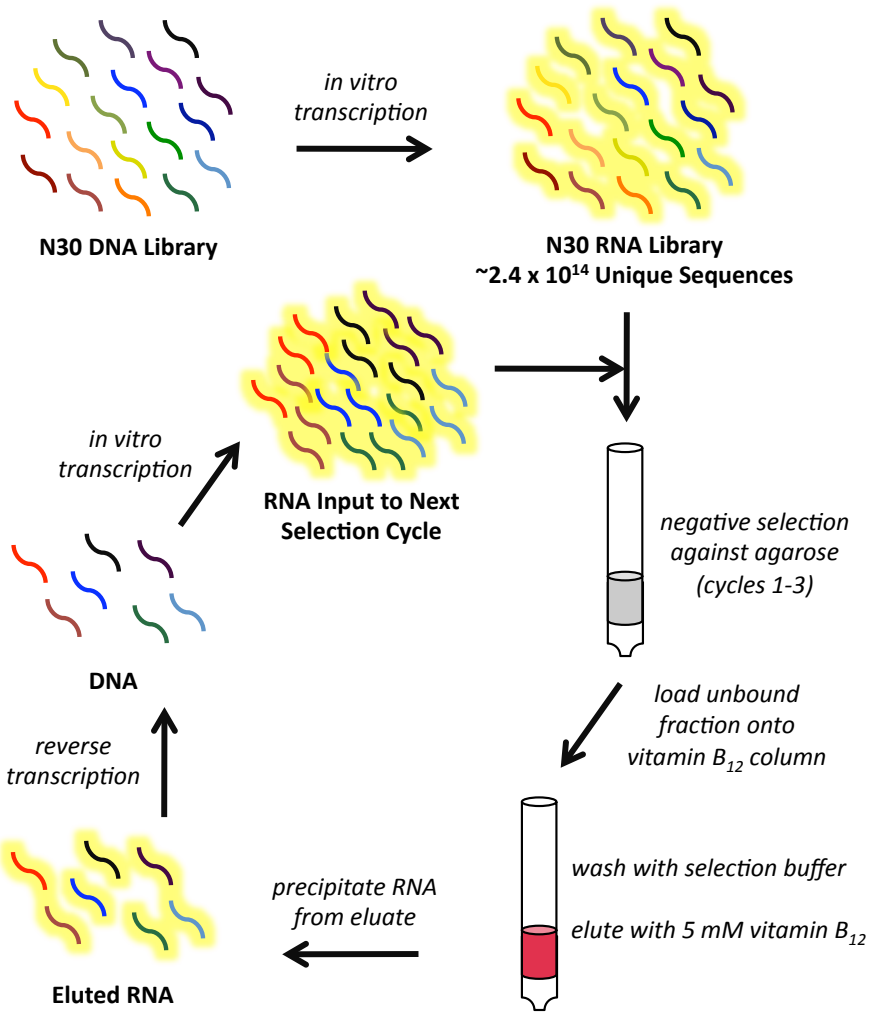

Figure 6.14. Schematic of column-based SELEX used to select for RNA aptamers to vitamin B_{12}. An RNA sequence library was generated by *in vitro* transcription and filtered through a vitamin B_{12}–conjugated agarose column. The column was washed with selection buffer, and specifically bound RNA was eluted with concentrated vitamin B_{12} solution. Eluted RNA was reverse transcribed into cDNA, which served as the transcription template for the next cycle's RNA pool. In cycles 1-3, an additional negative selection step against agarose resin was inserted before the positive selection step with vitamin B_{12}–conjugated agarose.

The RNA pool obtained after 15 selection cycles was sequenced, and no repeat was observed among 43 sequenced samples. Analyses were performed to investigate potential sequence and structural relationships among the sequences, and a number of conserved motifs were manually identified (Figure 6.15). Several sequences form stem-

loop structures, likely due to structural constraints imposed by the constant regions in the sequence library, but no single structure dominates the sequence pool.

A

B12-4
>AAGGATTCAATGCTAGTTTCCCGCCACCAT<
B12-44
>AGCTTAGGTGCTAGTTCTCCCGCTTCTGTAAAGGCAAAGCTTCCG

B12-2
>CAAATAGTCTGTGTAACCCGTTCCCGTGTT<
B12-23
>AGAGACTTGTCTGGCAATGTTCGTTCCCAT<

B12-6
>TGTTATTAGGCGAGTACTCCCGTCTCTGTA<
B12-10
>TTTATTAGGCGGTAGTTCCCCTCCGTAGAT<

B12-7
>ATCCTACCTCTGGCGCTTCCACGTCCTGTA<
B12-66
>CGAGCAGTATCCCACCTAGGCACTCCTGTA<

B12-15
>GTTCTTCCGGTTGGCGTACCCATGCACTAT<
B12-45
>TATTCTTGTGGTTAGCGCTTTCCATACTAT<
B12-11
>TATCATCTCTGGTTAGCGGTACCACTGTAT<

B12-19
>TATGTTAGCTCGCCATTCGTCTTCATGCAT<
B12-48
>TGCTAGTTCGATCCAGATCGCTCATGTGTT<
B12-71
>TTCTCGAGAATCTTAGTTTCGTCATGTGTA<

B12-1
>TGTCCGCGTTGGCTGGTTCCGTACCTTGTA<
B12-12
>TCCGACATCACTGGTGTGGTCCCTGCTGTA<
B12-49
>CCGATTGGGGTCGGGTAGTCCCATGCTGTA<

B

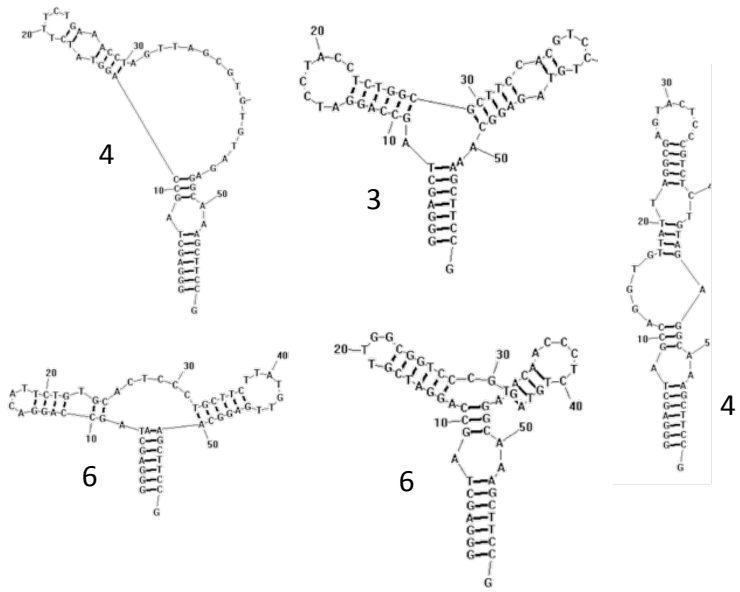

Figure 6.15. Vitamin B_{12} SELEX resulted in a diverse sequence pool with several sequence and structural motifs after 15 selection cycles. (A) No sequence appears more than once in the pool, but similar motifs can be found among the diverse sequences. Colored highlights mark motifs found within each group of sequences. (B) The secondary structures of sequenced samples were determined using the RNAstructure software[19], and structural motifs were identified. Structural elements including loop size, loop number, stem shape, and stem number were analyzed manually, and five structure groups were found to include multiple sequences. The number next to each structure denotes the number of sequences for which the shown structure is representative.

Several groups of similar sequences were identified (Figure 6.15A), and one sequence from each of three such groups was chosen for evaluation by radioactive binding assays. Radiolabeled RNA was loaded onto a vitamin B_{12}–conjugated agarose column, washed with three 500-μl aliquots of selection buffer, and eluted with six 500-μl aliquots of 5 mM vitamin B_{12}. Radioactive quantification of wash and eluate fractions shows weak specific elution by vitamin B_{12} (Figure 6.16A). More importantly, the overwhelming majority (>97%) of RNA remains bound to the column, indicating strong binding affinity toward resin particles. However, the same sequences tested on adipic acid dihydrazide agarose columns show minimal RNA retention on the column (Figure 6.16B), suggesting that the adipic acid dihydrazide agarose may not have been sufficiently similar to the vitamin B_{12}–conjugated agarose to serve as an effective negative selection target, even though dihydrazide agarose was used for this purpose in the previously published selection for vitamin B_{12} aptamers[17].

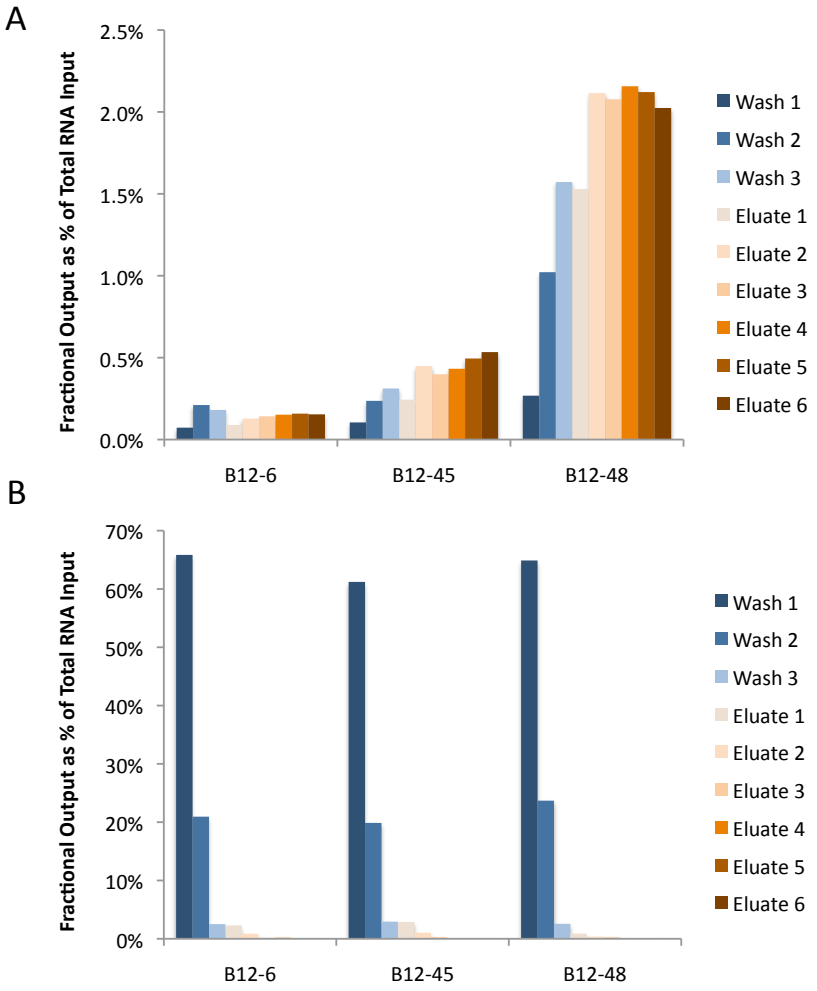

Figure 6.16. Putative vitamin B_{12} aptamer sequences show weak binding affinity for vitamin B_{12}, strong affinity for vitamin B_{12}–conjugated agarose, and no affinity for dihydrazide agarose. Radiolabeled, single-sequence RNAs were filtered through (A) vitamin B_{12}–conjugated or (B) adipic acid dihydrazide agarose columns. The columns were washed with selection buffer and eluted with 5 mM vitamin B_{12}. Each 500-µl aliquot of wash and eluate was collected and analyzed for radioactivity by scintillation counting. Values are reported as a percent of total radioactivity loaded onto each column. The B12-45 and B12-48 sequences show slight preferences for specific elution by vitamin B_{12} compared to selection buffer. All three sequences show strong binding affinity toward vitamin B_{12}–conjugated agarose as indicated by the small percentage of radioactivity removed from the B_{12}–conjugated column through wash and elution. The sequences show no affinity for dihydrazide agarose and are efficiently removed from those columns.

Eight additional sequences were evaluated by a modified radioactivity binding assay, in which alternate cycles of wash and elution steps were applied to vitamin B_{12}–conjugated agarose columns loaded with RNA. This alternating sequence was designed to rule out the possibility that any increase in RNA recovery during the elution steps was

simply due to non-specific removal by increased liquid volumes flowing through the column. None of the sequences evaluated by this method show specific elution by vitamin B_{12}, and all of them show strong binding affinity toward the column matrix (Table 6.1).

Table 6.1. Radioactive binding assay for putative vitamin B_{12} aptamer sequences with vitamin B_{12}–conjugated agarose columns

	% of Total RNA Input[a]							
Seq #	**2**	**4**	**7**	**12**	**15**	**19**	**23**	**44**
Wash 1[b]	0.06	0.08	0.24	0.05	0.09	0.91	0.18	0.12
Wash 2	0.20	0.22	0.67	0.22	0.22	N/A	0.39	0.34
Wash 3	0.17	0.20	1.20	0.22	0.23	1.30	0.72	0.40
Eluate 1	0.15	0.16	1.64	0.17	0.24	1.06	0.76	0.33
Eluate 2	0.14	0.14	2.07	0.15	0.26	0.80	0.87	0.32
Eluate 3	0.14	0.13	2.40	0.15	0.29	0.66	0.91	0.31
Wash 4	0.13	0.13	2.35	0.13	0.29	0.59	0.98	0.31
Wash 5	0.12	0.12	2.30	0.13	0.31	0.55	1.03	0.32
Eluate 4	0.13	0.13	2.40	0.13	0.36	0.51	1.12	0.34
Eluate 5	0.15	0.15	2.32	0.13	0.41	0.45	1.21	0.34
Total	**1.38**	**1.47**	**17.58**	**1.48**	**2.70**	**6.83**	**8.16**	**3.13**

[a]Value indicates the radioactivity of each wash or eluate fraction as a percentage of the total radioactivity loaded onto each column.
[b]Each wash and eluate fraction is 500 µl in volume.

Affinity toward agarose does not negate the potential usefulness of these putative aptamer sequences, provided they exhibit sufficient binding affinity for vitamin B_{12}. However, the minute amount of RNA recoverable from the vitamin B_{12}–conjugated agarose used in the selection process compromises the accuracy of these binding assays. To better characterize the isolated RNA sequences, we performed radioactive binding assays using an alternative separation medium—columns with Sepharose 6B resin particles that were either unmodified or conjugated to vitamin B_{12} through its hydroxyl group. The five unique sequences tested show varying degrees of non-specific binding to the Sepharose 6B resin, but all to a considerably lesser extent compared to the previous agarose resin (Table 6.2). However, the results also provide no evidence of specific

elution by vitamin B_{12}. These findings indicate that the SELEX procedure performed has failed to enrich for vitamin B_{12}–binding sequences.

Table 6.2. Radioactive binding assay for putative vitamin B_{12} aptamer sequences with Sepharose 6B columns

		% of Total RNA Input[a]	
RNA Sequence #	**Sample**	**Unmodified Sepharose 6B**	**Vitamin B_{12}–Conjugated Sepharose 6B**
5	**Wash**	77.92	66.79
	Eluate	0.35	0.28
6	**Wash**	67.74	54.96
	Eluate	0.20	0.20
9	**Wash**	78.04	67.09
	Eluate	0.17	0.27
45	**Wash**	50.92	45.85
	Eluate	0.13	0.16
48	**Wash**	69.57	66.81
	Eluate	0.13	0.13

[a]Value indicates the radioactivity of each wash or eluate fraction as a percentage of the total radioactivity loaded onto each column.

Column-Based SELEX Isolates Aptamer Sequences with Binding Affinity for Both Folinic Acid and Sepharose Matrix. We also performed column-based SELEX for RNA aptamers to folinic acid. Folinic acid is a 5-formyl derivative of folic acid and comprises 10%–20% of total cellular folates[20]. The 6S stereoisomer is biologically active and found in natural systems. Although not present in natural physiological environments, 6R–folinic acid is equally well tolerated *in vivo*, and racemic 6(R,S)–folinic acid is commonly used in cancer treatments either as an adjuvant in methotraxate therapy or in combination with 5-fluorouracil in the treatment of colorectal cancer and other neoplasms[20-22]. Pharmacokinetics studies have shown that 6R–folinic acid does not undergo metabolism and has a significantly longer serum half-life than 6S–folinic acid[23-25]. This combination of low toxicity, biological stability, and absence in natural systems makes 6R–folinic acid an ideal input signal for ligand-responsive regulatory systems.

Since racemic folinic acid is the most commonly used and thus widely available therapeutic agent, we began our aptamer selection process using the racemic mixture as the molecular target. Subsequent efforts to isolate aptamers specific to the 6R stereoisomer are described in a later section in this chapter.

The same selection procedure as described for vitamin B_{12} (Figure 6.14) was performed using racemic folinic acid as the target molecule. Folinic acid was conjugated through its carboxyl groups to EAH Sepharose 4B resin, and unmodified EAH Sepharose 4B resin was used for negative selection against the column matrix. The RNA pool obtained after 15 selection cycles was sequenced. In marked contrast to vitamin B_{12}, the folinic acid pool yielded only three unique sequences among 30 sequenced samples (Cycle 15 Sequence, Figure 6.17). One sequence (FA15.1) accounts for 93% (28 of 30) of the pool, and all three sequences share similar motifs. To better understand the sequence enrichment process, we sequenced RNA pools obtained after cycles 5, 10, and 11. Sequencing results indicate a diverse sequence pool after ten selection cycles, with no repeat observed among ten sequenced samples (Figure 6.17). Surprisingly, the dominant sequence makes its first appearance in cycle 11, after the mutagenic PCR step, accounting for two of ten sequenced samples. These results suggest that mutagenic PCR may have biased the sequence library, even though a similar effect was not observed in the vitamin B_{12} sequence pool.

ID	Cycle 5 Sequence	Frequency
FA5.30	*GGGAGCTAGCCAGG*CCTTCGGGTCTCGCCGGTCCCCTTCATCGT*GAGGCAAAGCTTCCG*	1 of 8
FA5.37	*GGGAGCTAGCCAGG*ATAATGGGATGGGGGCTCCGGTCGCTTGTT*GAGGCAAAGCTTCCG*	1 of 8
FA5.39	*GGGAGCTAGCCAGG*TCCACAAGGCTGTTTCCACTCTCGCGTGAT*GAGGCAAAGCTTCCG*	1 of 8
FA5.40	*GGGAGCTAGCCAGG*TGTACTGGCGTGGCTCGGCGGTTCTCGTGAT*GAGGCAAAGCTTCC G*	1 of 8
FA5.41	*GGGAGCTAGCCAGG*CGCCATAACCCAGCACCTCGGCTTACCCCT*GAGGCAAAGCTTCCG*	1 of 8
FA5.42	*GGGAGCTAGCCAGG*GTCTTGTTTAAGGACTTTCGGCTAGTTGTT*GAGGCAAAGCTTCCG*	1 of 8
FA5.43	*GGGAGCTAGCCAGG*CGAGATGCTTGCGCAGGCAACCACTTTGAT*GAGGCAAAGCTTCCG*	1 of 8
FA5.44	*GGGAGCTAGCCAGG*TTGAGCTGGCTAAACGATTGTGTAGGTGGT*GAGGCAAAGCTTCCG*	1 of 8

ID	Cycle 10 Sequence	Frequency
FA10.3	*GGGAGCTAGCCAGG*TTCCCTGACAGTTGCTTATAGTTCATTCTA*GAGGCAAAGCTTCCG*	1 of 10
FA10.5	*GGGAGCTAGCCAGG*CTCTCTGGTGCTTCCTTACTTGATTGTGAT*GAGGCAAAGCTTCCG*	1 of 10
FA10.6	*GGGAGCTAGC*----------TTGCATTAGAACTCGGTA*GAGGCAAAGCTTCCG*	1 of 10
FA10.7	*GGGAGCTAGCCAGG*ATGATGCTTGGGGAGCTCTGTCTCTGCTGT*GAGGCAAAGCTTCCG*	1 of 10
FA10.9	*GGGAGCTAGCCAGG*CTTCCTTAGTGCTTCGTGGATTTATGTGAT*GAGGCAAAGCTTCCG*	1 of 10
FA10.10	*GGGAGCTAGCCAGG*GTCTCTAGATTCTGTTACAGCGTTTATGTA*GAGGCAAAGCTTCCG*	1 of 10
FA10.11	*GGGAGCTAGCCAGG*TTGATACTCTAGCTCTTTAGTTGTCTTGAT*GAGGCAAAGCTTCCG*	1 of 10
FA10.12	*GGGAGCTAGCCAGG*TTACTAGTTAGCTCTGCGCTGAGATGTTAT*GAGGCAAAGCTTCCG*	1 of 10
FA10.13	*GGGAGCTAGCCAGG*TATTTAAGGGCTCCTTGTGTTCGTACATAT*GAGGCAAAGCTTCCG*	1 of 10
FA10.14	*GGGAGCTAGCCAGG*ATCTGGTCTTGGTGTTGCTCCACCTCGTGT*GAGGCAAAGCTTCCG*	1 of 10

ID	Cycle 11 Sequence	Frequency
FA11.3	***GGGAGCTAGCCAGG*AATGGTAGCTCGACTTCATGCTTCAGTGAT*GAGGCAAAGCTTCCG***	2 of 10
FA11.4	*GGGAGCTAGCCAGG*TGTTTCAGGCTAGATTCTTAACTCGTGCAT*GAGGCAAAGCTTCCG*	1 of 10
FA11.6	*GGGAGCTAGCCAGG*GCTCCGTCCTTTCCATTCTATTTTCGTGTA*GAGGCAAAGCTTCCG*	1 of 10
FA11.7	*GGGAGCTAGCCAGG*TTCCCGCTTCCACTCAGTCGATGTTGTGAT*GAGGCAAAGCTTCCG*	1 of 10
FA11.8	*GGGAGCTAGCCAGG*TTGGTGCAGGCTCCGTCCTTTGTCGGCTA*GAGGCAAAGCTTCCG*	1 of 10
FA11.16	*GGGAGCTAGCCAGG*AGACTGGTTAGACTCGTCCAACCCGTTGTA*GAGGCAAAGCTTCCG*	1 of 10
FA11.17	*GGGAGCTAGCCAGG*TATGGTTCTAGCTTCGGCTTCTGGATTGTA*GAGGCAAAGCTTCCG*	1 of 10
FA11.18	*GGGAGCTAGCCAGG*ACTTGGTTAGCGTCATAGTTTGCTGTAGTA*GAGGCAAAGCTTCCG*	1 of 10
FA11.21	*GGGAGCTAGCCAGG*TGTCGCACCTGCTAATCCCACTTGCTGCAT*GAGGCAAAGCTTCCG*	1 of 10

ID	Cycle 15 Sequence	Frequency
FA15.1	***GGGAGCTAGCCAGG*AATGGTAGCTCGACTTCATGCTTCAGTGAT*GAGGCAAAGCTTCCG***	28 of 30
FA15.5	*GGGAGCTAGCCAGG*AATTTGATAGCTCCGTTGGTGTTCTCATAT*GAGGCAAAGCTTCCG*	1 of 30
FA15.35	*GGGAGCTAGCCAGG*TTTCTGGTACTCCGTGTTCATGTCTCGTGT*GAGGCAAAGCTTCCG*	1 of 30

Figure 6.17. Sequence diversity in folinic acid SELEX is dramatically reduced after mutagenic PCR. RNA pools obtained after various selection cycles were cloned and sequenced. The sequence pools remained diverse through cycle 10, but one sequence, FA15.1 (red and bolded), began to emerge in cycle 11 and eventually dominated the pool after 15 cycles. Italicized nucleotides constitute the constant regions. The yellow and green highlights mark conserved motifs among the three sequences found in the cycle 15 pool.

A radioactive binding assay was performed to evaluate the binding affinity of the dominant FA15.1 sequence for both racemic and stereospecific isomers of folinic acid. Columns packed with EAH Sepharose 4B resin conjugated to racemic folinic acid were loaded with radiolabeled FA15.1 RNA and treated with alternate cycles of wash with selection buffer and elution with 5 mM racemic folinic acid, 6R–folinic acid, or 6S–folinic acid. Radioactivity measurement of each wash and eluate fraction indicates specific elution by folinic acid, with no preference for either stereoisomer (Figure 6.18).

Importantly, the sequence has a strong affinity for the Sepharose 4B resin, as more than 90% of the RNA input remain bound to the column after extensive wash and elution steps.

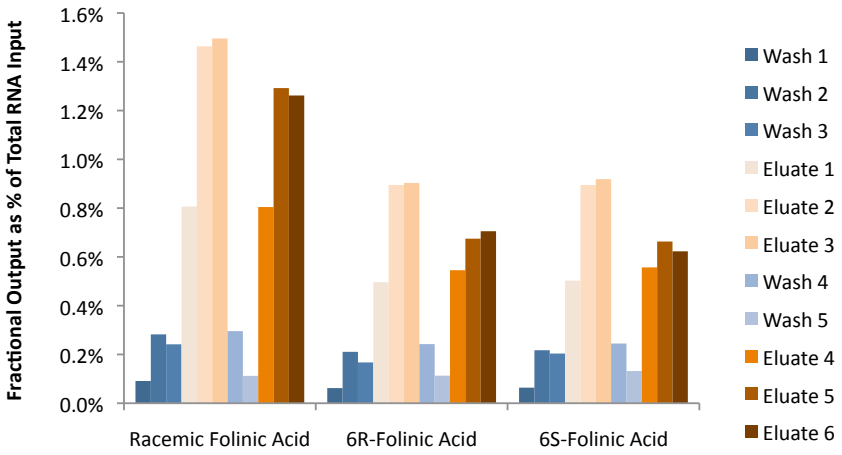

Figure 6.18. The putative folinic acid aptamer sequence shows folinic acid–specific binding, no stereospecific binding preference, and strong affinity for the column resin. The FA15.1 RNA sequence was loaded onto columns packed with resin conjugated to racemic folinic acid and washed with selection buffer. RNA elution was performed with 5 mM solutions of racemic folinic acid, 6R–folinic acid, or 6S–folinic acid. Radioactivity in each 500-µl aliquot of wash or eluate fraction was quantified by scintillation counting. Values are reported as a percent of total radioactivity loaded onto each column. The RNA sequence shows specific elution with all three ligands, with no preference for either stereoisomer. The great majority of RNAs remain bound to the column despite the large wash and elution volumes applied.

To circumvent challenges posed by the RNA sequence's affinity for Sepharose resin, we repeated the radioactivity binding assay using a vitamin B_{12}–conjugated agarose column. Over 98% of the RNA loaded onto the column remains bound after washing with three 500-µl aliquots of selection buffer, suggesting that the sequence also has non-specific affinity for the agarose resin (Figure 6.19). However, over 60% of the RNA is eluted from the column with three 500-µl aliquots of racemic folinic acid, indicating a significantly stronger affinity for folinic acid than for the column matrix. This difference in RNA elution is observed again in the second round of wash and elution steps,

confirming that elution with folinic acid is ligand-specific and not simply due to RNA being removed from the column by additional flow-through volumes.

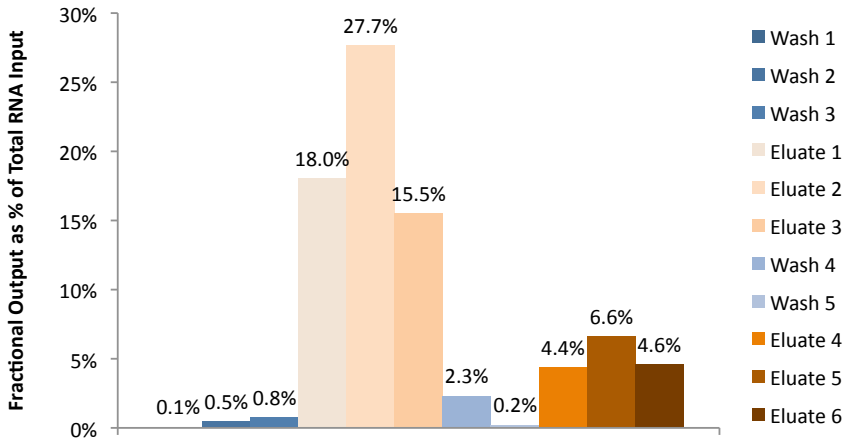

Figure 6.19. The putative folinic acid aptamer shows ligand-specific elution. The FA15.1 RNA sequence was loaded onto a vitamin B_{12}–conjugated agarose column and washed with selection buffer. RNA elution was performed with 5 mM racemic folinic acid, and radioactivity in each 500-µl aliquot of wash or eluate fraction was quantified by scintillation counting. Values are reported as a percent of total radioactivity loaded onto each column. The RNA shows specific elution with folinic acid and only weak affinity for the vitamin B_{12}–conjugated agarose resin.

The two remaining sequences found in the cycle 12 sequence pool were also characterized by the radioactive binding assay using Sepharose resin conjugated to racemic folinic acid. Results indicate that both sequences have strong affinity for the resin, and only one of the sequences (FA15.5) shows specific elution by folinic acid (Table 6.3). Since the dominant FA15.1 sequence shows greater elution by folinic acid and a slightly weaker affinity for the Sepharose resin compared to FA15.5, subsequent characterization efforts were focused on FA15.1.

Table 6.3. Radioactive binding assay for putative folinic acid aptamer sequences with folinic acid–conjugated and unmodified Sepharose 6B columns

	% of Total RNA Input[a]			
Sequence #	**FA15.5**		**FA15.35**	
Column	**Folinic Acid**	**Unmodified**	**Folinic Acid**	**Unmodified**
Wash 1[b]	0.03	0.00	0.00	0.03
Wash 2	0.09	0.00	0.01	0.09
Wash 3	0.11	0.01	0.03	0.10
Eluate 1	0.56	0.03	0.05	0.13
Wash 4	0.28	0.03	0.04	0.08
Wash 5	0.18	0.02	0.02	0.06
Wash 6	0.18	0.01	0.02	0.06
Wash 7	0.18	0.01	0.02	0.06
Eluate 2	1.06	0.03	0.05	0.12
Eluate 3	1.44	0.05	0.06	0.16
Eluate 4	1.40	0.04	0.05	0.15
Total	**5.51**	**0.24**	**0.35**	**1.04**

[a]Value indicates the radioactivity of each wash or eluate fraction as a percentage of the total radioactivity loaded onto each column.
[b]Each wash and eluate fraction is 500 µl in volume.

LC-MS Provides Qualitative Evaluation of Ligand-Binding Activity by Putative Aptamer Sequences. In light of the substantial affinity toward column resins exhibited by the putative aptamer sequences described above, binding assays utilizing alternative separation methods are desired. Various affinity assays have been devised for the evaluation of aptamers to small-molecule ligands[9, 11, 17, 26], but quantitative measurements of dissociation constants have generally been obtained through either surface plasmon resonance (SPR) analysis or methods employing radiolabeled ligand molecules. We have examined the use of SPR analysis in our efforts to characterize RNA aptamers. However, the protocol is still in the optimization stage as of this writing, and the results will be presented in later work. An alternative "equilibrium filtration" method that is simple and potentially effective in aptamer evaluation was presented by Jenison and colleagues in the characterization of the theophylline aptamer[9]. In this assay, known concentrations of aptamer RNA and radiolabeled theophylline are co-incubated and filtered through a

membrane-based size-exclusion column. Free theophylline is sufficiently small to pass through the membrane while RNA-bound theophylline is retained. Theophylline concentrations in the filtrate and the retentate are measured by scintillation counting, and their difference represents the concentration of RNA-bound theophylline. The K_D value is obtained by finding the RNA concentration at which 50% of the theophylline is bound.

Radiolabeled folinic acid and vitamin B_{12} are not commercially available, thus preventing the evaluation of putative aptamers to these ligands by the method described above. However, a slightly altered protocol may be performed using liquid chromatography (LC) combined with mass spectrometry (MS). LC-MS is a powerful tool for the quantitative analysis of chemical mixtures, and we applied this analytical tool to the evaluation of aptamer sequences. In this protocol, aptamer RNA is incubated with unlabeled ligand molecules at a known concentration and filtered through a size-exclusion column. Ligand concentration in the filtrate, which is the final free-ligand concentration, is quantified by LC-MS. The percentage of ligand bound is calculated from the known initial and measured final free-ligand concentrations. A range of RNA input concentrations is tested with a fixed folinic acid input concentration to generate a binding curve, from which the K_D value can be obtained by finding the RNA concentration at which 50% of the ligand molecules are bound.

This characterization method was first demonstrated using theophylline and its RNA aptamer, which has a reported K_D value of 0.1 μM[9]. RNA at concentrations ranging from 1.25 μM to 10 μM was incubated with 5 μM theophylline and processed as described above. Ligand concentration in the filtrate was calculated based on the intensity of the theophylline peak in the extracted ion chromatogram, which was calibrated to a

standard curve generated with pure theophylline solutions at known concentrations. The resulting binding curve is incomplete in that ligand binding does not reach saturation even at the highest RNA input concentration tested (Figure 6.20). However, the results show a clear ligand-RNA binding response, with approximately 50% of theophylline bound at RNA input concentrations between 1.5 μM and 2.5 μM. These observations suggest that the LC-MS method is able to reveal aptamer-binding activity, even though accurate quantification of the K_D value remains challenging.

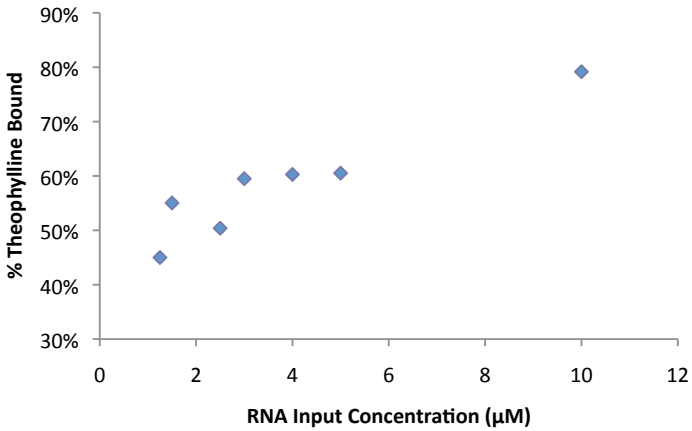

Figure 6.20. LC-MS and size-exclusion columns can be used to verify binding interactions between RNA aptamers and their cognate small-molecule ligands. The theophylline RNA aptamer was incubated with 5 μM theophylline and filtered through a size-exclusion column. Theophylline concentration in the filtrate was measured by LC-MS, and the percent of theophylline bound to RNA (and thus retained by the membrane) was calculated based on a one-to-one theophylline-to-RNA binding assumption.

We next examined the FA15.1 RNA sequence for binding affinity toward racemic folinic acid. RNA at concentrations ranging from 0 μM to 90 μM was incubated with 5 μM folinic acid and processed as described above. The resulting binding curve shows clear concentration-dependent binding between folinic acid and the RNA sequence, suggesting the FA15.1 sequence may have specific binding toward folinic acid (Figure 6.21). However, only 33% of the folinic acid was bound at the maximum RNA input concentration tested. Higher RNA input concentrations could not be achieved due to

limitations in *in vitro* transcription efficiency and RNA solubility, thus preventing accurate quantification of the K_D value by this method.

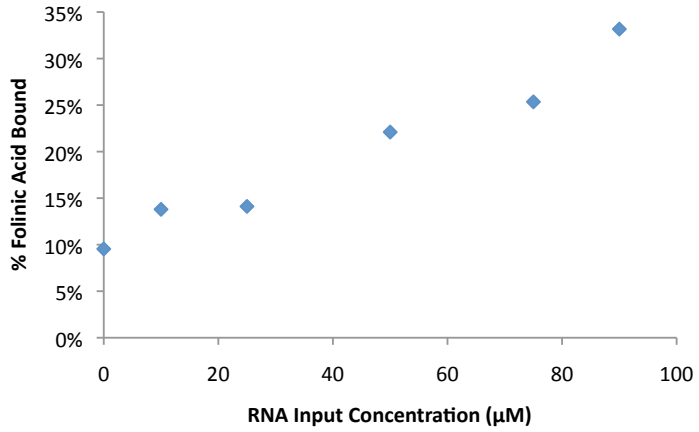

Figure 6.21. The putative folinic acid aptamer shows ligand-specific binding by LC-MS analysis. The FA15.1 RNA sequence was incubated with 5 μM racemic folinic acid, and the sample was processed and analyzed as described in Figure 6.20. Increasing RNA input concentration corresponds to increasing percent of folinic acid bound, indicating specific ligand-RNA binding interaction.

The observation that almost 10% of folinic acid was missing from the filtrate even in the absence of RNA input (Figure 6.21) suggests that the size-exclusion column retains some free folinic acid despite the molecule's being well below the molecular weight cutoff of the column membrane. One possible explanation is that the ligand concentration is above the carrying capacity of the membrane and causes membrane fouling. This hypothesis is supported at high folinic acid concentrations by the observation that yellow residues are retained on the column membrane for solutions at 500 mM and above. In addition, standard curves generated with folinic acid that has been filtered through the column in the absence of RNA deviate from linearity at concentrations beyond 100 μM (Figure 6.22A). In comparison, standard curves generated with unfiltered folinic acid remain linear up to 400 μM (Figure 6.22B). Even unfiltered folinic acid deviates from the linear trend line beyond 400 μM, indicating a limited concentration range that can be

accurately quantified by the LC-MS system. This constraint in the LC-MS detection range can be circumvented by careful sample dilution. However, limits in the folinic acid concentration that can be properly filtered by column membrane undermines the feasibility of an alternative binding assay in which a fixed RNA input concentration is paired with varying folinic acid input concentrations.

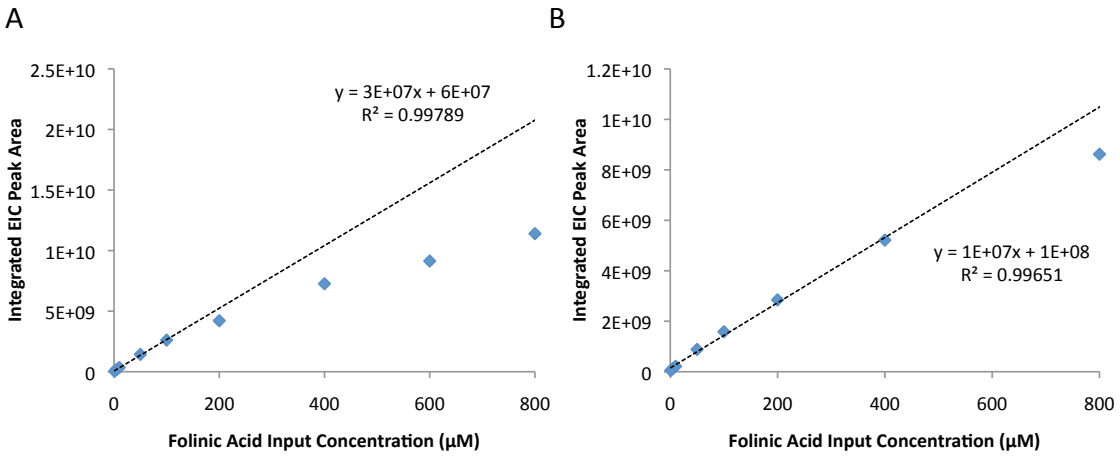

Figure 6.22. LC-MS binding assays cannot be performed at high folinic acid concentrations due to errors associated with inefficient membrane filtration. LC-MS analysis was performed on racemic folinic acid solutions that are either (A) filtered through size-exclusion columns or (B) unfiltered. The integrated peak areas of extracted ion chromatograms at a molecular weight of 474 are shown. Filtered samples with concentrations above 100 μM deviate from a linear relationship between detected signal strength and folinic acid input concentration, whereas unfiltered samples remain linear through 400 μM. The difference between filtered and unfiltered samples indicates errors introduced by the membrane filtration step.

Although the binding curve shown in Figure 6.21 suggests ligand-specific binding by the putative folinic acid aptamer, it does not rule out non-specific binding between folinic acid and RNA in general. To evaluate this possibility, the binding assay was repeated using the theophylline RNA aptamer instead of the FA15.1 RNA. Results indicate that there is nonspecific loss of folinic acid from the filtrate with increasing RNA input concentration (Theo Aptamer, Figure 6.23), either due to non-specific RNA-folinic acid interaction or due to concentrated RNA contributing to membrane fouling. Nevertheless, the extent of folinic acid "binding" observed with the theophylline aptamer

is significantly less than that with the FA15.1 RNA, suggesting that the FA15.1 sequence has specific affinity for folinic acid.

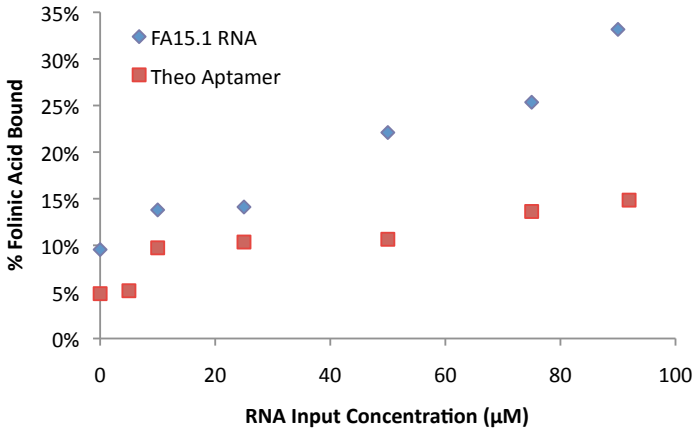

Figure 6.23. Folinic acid binding to the putative folinic acid aptamer is specific to the RNA sequence. The FA15.1 RNA sequence and the theophylline RNA aptamer were each incubated with 5 μM racemic folinic acid, and the samples were processed and analyzed as described in Figure 6.20. Folinic acid shows weak non-specific binding to the theophylline aptamer, but at noticeably lower levels than to the FA15.1 RNA, suggesting that the latter binding interaction is sequence specific.

Selection for Stereoisomer-Specific Folinic Acid Aptamer Results in Diverse Sequence Pool. As described previously, 6R–folinic acid is an unnatural stereoisomer of folinic acid whose low toxicity, relatively long serum half-life, and absence in natural systems make it an ideal molecular input for ligand-responsive gene regulatory systems. To isolate RNA aptamers with binding specificity for 6R–folinic acid, we used the RNA pool obtained after cycle 10 of the racemic folinic acid aptamer selection as the starting material. This choice was made for two reasons. First, negative selection against chemically similar ligands are typically performed after several cycles of positive selection in order to prevent premature elimination of sequence diversity prior to enrichment of ligand-binding sequences. Therefore, cycle 10 is a reasonable point to begin stereospecific selection for the 6R isoform of folinic acid. Second, sequencing results from the racemic folinic acid aptamer selection suggest that the mutagenic PCR

step performed after cycle 10 in that selection process may have biased the sequence pool. Therefore, it is of interest to repeat the selection without the mutagenic PCR step to determine whether sequence diversity would follow the same pattern as observed in the previous selection. In light of the observation that all isolated sequences from the previous selection show significant binding affinity toward the Sepharose 4B matrix, we performed negative selection against unmodified Sepharose 4B resins in every cycle prior to positive selection using a 6R–folinic acid–conjugated Sepharose 4B column.

In this selection process, RNA was filtered through an unmodified Sepharose column and the unbound fraction was collected and loaded onto a 6R–folinic acid–conjugated column. The column was washed with 4 CV of selection buffer followed by 5 CV of 5 mM 6S–folinic acid and another 10 CV of buffer to select against the natural stereoisomer. The column was eluted with 7 CV of 5 mM 6R–folinic acid, and the eluted RNA was prepared as previously described for the next selection cycle. We performed five rounds of selection and sequenced the RNA pool obtained after the last cycle. Results indicate a diverse sequence pool with no repeats found among 21 sequenced samples (Figure 6.24A). FA15.1, the dominant sequence isolated from the racemic folinic acid selection, is present in the 6R–folinic acid pool (as 6RFA15.55) but shows no obvious relation with the remaining sequences in the pool. Short sequence motifs were identified among the sequenced samples, but most contain slight variations among sequences and none are truly conserved in more than two sequences (Figure 6.24B). As of this writing, characterization of these isolated sequences awaits results from ongoing efforts in the development of more accurate, high-throughput assays for ligand-RNA binding affinity.

A

ID	Cycle 15 Sequence	Frequency
6RFA15.1	*GGGAGCTAGCCAGG*CTCCGCACAAATGTATCCTTACATCGTGTA*GAGGCAAAGCTTCCG*	1 of 21
6RFA15.45	*GGGAGCTAGCCAGGG*TTAGCTTCAGTGAGTTTCTTATTGTTGTC*GAGGCAAAGCTTCCG*	1 of 21
6RFA15.48	*GGGAGCTAGCCAGG*CTTCCCTGCTAACTGTATCTCTCCGGTATA*GAGGCAAAGCTTCCG*	1 of 21
6RFA15.49	*GGGAGCTAGCCAGG*CTCCTCCTGTTGACTGTTCATTCAGTTGGC*GAGGCAAAGCTTCCG*	1 of 21
6RFA15.50	*GGGAGCTAGCCAGG*CTCTTGCTAGTTCCGCGCTATCTTGTGGTT*GAGGCAAAGCTTCCG*	1 of 21
6RFA15.52	*GGGAGCTAGCCAGG*ATTATCCCGGTGTCTCCTATCTTGCGTTAT*GAGGCAAAGCTTCCG*	1 of 21
6RFA15.53	*GGGAGCTAGCCAGGG*CGCATAAAATTTTAATCGCAAACTTATAT*GAGGCAAAGCTTCCG*	1 of 21
6RFA15.55	***GGGAGCTAGCCAGGAATGGTAGCTCGACTTCATGCTTCAGTGAT*GAGGCAAAGCTTCCG**	1 of 21
6RFA15.57	*GGGAGCTAGCCAGG*ATTTGCTTGGCGAACCCCGATACCTTTGTA*GAGGCAAAGCTTCCG*	1 of 21
6RFA15.66	*GGGAGCTAGCCAGG*TCCGGCAACAGGCCCTGGCCTAAATTCGAT*GAGGCAAAGCTTCCG*	1 of 21
6RFA15.67	*GGGAGCTAGCCAGG*TATTCCTCTTGGCTAACCCGTTGTCTCTAT*GAGGCAAAGCTTCCG*	1 of 21
6RFA15.68	*GGGAGCTAGCCAGG*TTGGACAAGCCCCAACGATTAATCTAGGAA*GAGGCAAAGCTTCCG*	1 of 21
6RFA15.69	*GGGAGCTAGCCAGG*TTGTGCTGTAGCTCACCACTCAACATGTAT*GAGGCAAAGCTTCCG*	1 of 21
6RFA15.70	*GGGAGCTAGCCAGG*TGTTGTTGCTGCTCCGATGTCGTACTTCAT*GAGGCAAAGCTTCCG*	1 of 21
6RFA15.72	*GGGAGCTAGCCAGG*CTCCGTGAGTGCTTTTACAAGTGGTTGTGT*GAGGCAAAGCTTCCG*	1 of 21
6RFA15.74	*GGGAGCTAGCCAGG*TAAAAGGTTACGGACACGCCGAGGGTCAGG*GAGGCAAAGCTTCCG*	1 of 21
6RFA15.77	*GGGAGCTAGCCAGG*TCTTTGGCGGCTCGCGAGTGTCTTCTAGGT*GAGGCAAAGCTTCCG*	1 of 21
6RFA15.80	*GGGAGCTAGCCAGG*TATGGCTAGGGGCTCTCGGTCTCTGAGTAT*GAGGCAAAGCTTCCG*	1 of 21
6RFA15.84	*GGGAGCTAGCCAGG*CTACTCACGATAACTGGTTCGCAACCTTGT*GAGGCAAAGCTTCCG*	1 of 21
6RFA15.85	*GGGAGCTAGCCAGG*CTCCTCATATTTGGCTTTCAGATGTGTA*GAGGCAAAGCTTCCG*	1 of 21
6RFA15.88	GGGAGCTAGCGAACGCCAGTTTCAGTTGTGTT*GAGGCAAAGCTTCCG*	1 of 21

B

6RFA15.84
>CTACTCACGATAACTGGTTCGCAACCTTGT<
6RFA15.53
>GCGCATAAAATTTTAATCGCAAACTTATAT<
6RFA15.1
>CTCCGCACAAATGTATCCTTACATCGTGTA<

6RFA15.48
>CTTCCCTGCTAACTGTATCTCTCCGGTATA<
6RFA15.67
>TATTCCTCTTGGCTAACCCGTTGTCTCTAT<

6RFA15.1
>CTCCGCACAAATGTATCCTTACATCGTGTA<
6RFA15.72
>CTCCGTGAGTGCTTTTACAAGTGGTTGTGT<
6RFA15.49
>CTCCTCCTGTTGACTGTTCATTCAGTTGGC<
6RFA15.45
>GTTAGCTTCAGTGAGTTTCTTATTGTTGTC<

Figure 6.24. 6R–folinic acid SELEX yields a diverse sequence pool with conserved motifs. (A) The sequence pool remains diverse after 10 selection cycles toward racemic folinic acid and 5 subsequent cycles toward 6R–folinic acid. The RNA pool was cloned and sequenced. Results indicate a diverse sequence pool, even though the dominant sequence found in the racemic folinic acid selection (FA15.1) also appears in the 6R–folinic acid pool (6RFA15.55, red and bolded). (B) No sequence appears more than once in the pool, but similar motifs can be found among the diverse sequences. Italicized nucleotides constitute the constant regions. Colored highlights mark motifs found within each group of sequences.

Discussion

RNA aptamers constitute the sensor domain of most existing ligand-responsive RNA-based regulatory devices, including the switch systems presented in this thesis. Our efforts in selecting new RNA aptamers toward therapeutically applicable small molecules have met with several challenges, leading to a close examination of different selection protocols and the potential pitfalls associated with each separation method. Studies

detailed in this chapter show that nitrocellulose membranes, though widely used for aptamer selection to protein targets, have surprisingly low partition efficiencies. Specifically, nitrocellulose membranes cannot effectively retain even high-affinity RNA aptamers in the presence of their cognate protein targets, thus undermining the usefulness of nitrocellulose membranes as a separation method in aptamer selection.

An alternative selection method employs column chromatography, which requires target immobilization on resin particles. However, many small molecules suitable for clinical applications lack appropriate functional groups for resin conjugation. Although synthetic chemistry has been used to generate modified small molecules for resin conjugation in some instances[9, 27], such modifications are not always possible and may affect the binding specificity of the aptamer sequences isolated from such selection processes. In collaboration with the Chemistry Core Facility at City of Hope, we have examined the possibility of chemically modifying phenobarbital for resin conjugation, but our efforts were unsuccessful due to phenobarbital's compact structure. Furthermore, any modification to phenobarbital would have represented a significant change to its chemical makeup, and aptamer sequences isolated for such modified molecules may not have the same binding affinity for the intended target.

Another challenge associated with both membrane- and column-based selections is the enrichment of sequences with high affinity for the solid support itself. We repeatedly isolated sequences that bind strongly to either nitrocellulose or the column resin used for separation. These findings indicate that stringent negative selections against the solid support must be applied throughout the selection process. Combining affinity elution with membrane filtration was effective in preventing the enrichment of

membrane-binding sequences, but it is unclear whether the hybrid method is effective for aptamer selection. The ability to use more than one separation method in a selection process (e.g., alternating between membrane- and column-based selection for each cycle) would shift the selection bias away from sequences with strong binding affinity for a specific solid support. Alternative selection methods that do not require solid supports, including the use of capillary electrophoresis[28-30] and direct ribozyme switch isolation through *in vitro* and *in vivo* screening, are also being explored in the Smolke Laboratory.

Our aptamer selection efforts yielded diverse pools of potential aptamers for vitamin B_{12} and 6R–folinic acid. The binding characterization assays developed thus far—including radioactive binding assays and LC-MS analyses—have been qualitative and low throughput, making them unsuitable for screening through large sequence pools. Development of more quantitative and higher throughput methods, including the use of SPR-based technology such as Biacore (GE Healthcare), is ongoing and will be applied to the sequence pools obtained from these selection processes.

The racemic folinic acid selection yielded a dominant sequence that shows specific binding to its intended target by both radioactive binding assays and LC-MS analyses. However, initial characterizations by Biacore have shown no quantitative evidence for binding between the putative aptamer and racemic folinic acid (J. C. Liang, personal communication). The putative aptamer sequence has been integrated into the ribozyme switch platform and tested both by *in vitro* cleavage assays and in yeast cultures, but no functional switch construct has been developed thus far (J. C. Liang and M. N. Win, personal communication). The ribozyme switches may be improved by randomizing the transmitter domain and performing a library screen for effective switch

activity. Furthermore, the putative aptamer sequence will have to be characterized in greater detail as more quantitative evaluation methods become available.

SELEX technology was first developed in 1990 and has been used widely for the *de novo* generation of diverse DNA and RNA aptamer sequences. However, no aptamer with *in vivo* activity and specificity for clinically suitable ligand molecules has been isolated thus far. Our attempts at selecting novel RNA aptamers toward small-molecule targets have generated mixed results but also provided insights into the optimization of various selection parameters. Informed by past challenges, ongoing efforts in the Smolke Laboratory continue to explore the intricacies of aptamer selection, with the aim of developing more efficient and reliable methods for the isolation of new aptamers.

Materials and Methods

Nitrocellulose membrane-based SELEX for phenobarbital aptamer. A N30 DNA library was generated by PCR using forward primer N30 Fwd (5'TTC*TAATACGACTCA CTATA*GGGAGCTAGCCAGG), reverse primer N30 Rev (5'CGGAAGCTTTGCCTC), and the N30 Template (5' TTCTAATACGACTCACTATAGGGAGCTAGCCAGG (N30) GAGGCAAAGCTTCCG), where the italicized sequence denotes the T7 promoter and underlined sequences denote the restriction sites NheI and HindIII used for cloning. All oligonucleotides were synthesized by Integrated DNA Technologies. The initial PCR amplification was performed with 20 pmol of the N30 Template, corresponding to approximately 1.2×10^{13} unique sequences, assuming complete randomization in the oligonucleotide synthesis process. A N30 RNA library was generated by *in vitro* transcription using the N30 DNA library as template. The reaction was performed with

40 mM Tris-HCl, pH 7.9, 16 mM $MgCl_2$, 10 mM dithiothreitol (DTT), 2 mM spermidine, 3 mM of ATP, CTP, and UTP (Epicentre), 300 μM of GTP (Invitrogen), 10 μCi of [α-^{32}P]-GTP (GE Healthcare), 50 U of T7 RNA polymerase (New England Biolabs), and 40 U of RNaseOUT ribonuclease inhibitor (Invitrogen) and incubated at 37°C overnight. The transcription product was treated with 2 U of DNaseI (New England Biolabs) at 37°C for 15 min and purified with a NucAway column (Ambion) hydrated with selection buffer (20 mM Tris-HCl, pH 7.5, 100 mM NaCl, 750 μM $MgCl_2$). RNA was denatured by heating to 75°C for 3 min and allowed to renature at room temperature for 30 min.

Membrane filtration was performed using a Multiscreen$_{HTS}$ Vacuum Manifold (Millipore) with a 96-well Multiscreen$_{HTS}$-HA filter plate (Millipore). In all filtration steps, the membrane wells were pre-wetted by incubation with 100 μl of selection buffer for 1 min before buffer removal by vacuum filtration at a pressure of 5 in. Hg. In cycle 1, the N30 RNA library was filtered through a membrane well and the filtrates were collected for incubation with 75 pmol of phenobarbital-BSA (Meridian Life Science) at 37°C for 30 min. The binding reaction was filtered through a new membrane well, and the membrane was washed with 800 μl of selection buffer. The membrane was removed from the plate and soaked in 600 μl of Tris-buffered phenol-chloroform, pH 7.9, at room temperature for 30 min. RNA was extracted by adding 200 μl of RNase-free water and collecting the aqueous layer. A second extraction step was performed with phenol-chloroform before RNA precipitation with 2 volumes of 95% ethanol, 0.1 volumes of 3 M sodium acetate, and 0.1 mg/ml glycogen (Ambion) followed by a wash step with 500 μl of 70% ethanol. Reverse transcription and cDNA amplification was performed in a single step with a 50-μl RT-PCR reaction containing 20 mM Tris-HCl, pH8.4, 50 mM

KCl, 5 mM DTT, 200 μM dNTP, 0.2 μM each of the N30 Fwd and N30 Rev primers, 40 U of RNaseOUT, 200 U of SuperScriptIII reverse transcriptase (Invitrogen), and 5 U of *Taq* DNA polymerase. The reaction was incubated at 55°C for 35 min (for reverse transcription) and immediately subjected to 15 cycles of PCR amplification. The cDNA product was used for transcription in the next selection cycle.

The process was repeated as described for 20 selection cycles with the following changes. First, negative selection against nitrocellulose membrane was not performed beyond cycle 1. Second, starting in cycle 3, transcriptions were performed with 3 mM of each rNTP with no radioactivity, and the reaction was allowed to proceed at 37°C for 2 hours. RNA concentration was quantified using a Nanodrop spectrophotometer, and the amount of phenobarbital-BSA added to the binding reaction was adjusted accordingly to achieve the desired ligand-to-RNA ratio. The phenobarbital-BSA stock used contains 12–15 phenobarbital molecules per BSA molecule, and the BSA:RNA ratio used in each cycle is summarized in the table shown on the following page. Third, the ligand-RNA incubation time was gradually decreased and the volume of selection buffer filtered through the membrane during the wash step gradually increased through the selection cycles to increase selection stringency (see table on next page). Fourth, negative selection against unconjugated BSA was performed prior to positive selection with phenobarbital-BSA in cycles 11-13 and 15-20. In these negative selections, renatured RNA was first incubated with unconjugated BSA (New England Biolabs) at a BSA:RNA ratio of 1:10 at 37°C for 10 min. The binding mixture was filtered through a membrane well, and the filtrate was collected for incubation with phenobarbital-BSA as in a typical selection cycle.

Cycle #	Negative Selection	BSA:RNA Ratio (for positive selection)[a]	Binding Incubation Time (min)	Wash Volume (ml)
1	Nitrocellulose	1:1	30	0.8
2	None	1:1	30	0.8
3	None	1:1	30	0.8
4	None	1:10	30	0.8
5	None	1:1	30	0.8
6	None	1:10	15	1.2
7	None	1:10	15	1.6
8	None	1:20	15	2.0
9	None	1:50	15	2.0
10	None	1:100	15	2.0
11	BSA	1:10	15	2.0
12	BSA	1:10	15	2.0
13	BSA	1:10	15	2.0
14	None	1:100	10	2.0
15	BSA	1:100	10	2.0
16	BSA	1:133	5	4.0
17	BSA	1:100	5	4.0
18	BSA	1:100	5	4.0
19	BSA	1:100	5	4.0
20	BSA	1:100	5	4.0

Nitrocellulose membrane-based SELEX for phenobarbital aptamer with ligand-specific elution. A N30 DNA library was generated by PCR as described above using 200 pmol of template input for a total of approximately 1.2 x 10^{14} unique sequences. Overnight radioactive RNA transcription was performed for cycle 1 as described previously, and all subsequent transcriptions were performed at 37°C for 2 hours without radiolabeling. The selection buffer composition was changed to 20 mM Tris-HCl, Ph7.5, 100 mM NaCl, and 1 mM $MgCl_2$ for this selection process. Twelve selection cycles were performed as described using phenobarbital-BSA, with the BSA:RNA ratio fixed at 11:1 throughout the selection. The binding reaction was performed at 37°C for 45 min in cycles 1–5 and for 30 min in cycles 6–12. Wash volume was maintained at 1 ml for cycles 1–9 and increased to 2 ml for cycles 10–12. Negative selection against BSA was

performed with a BSA:RNA ratio of 1:1 before positive selection with phenobarbital-BSA in cycles 8–12. No explicit negative selection against nitrocellulose was performed.

Nitrocellulose membrane-based radioactive binding assay. Radioactive RNA was transcribed, purified, denatured, and renatured as described above. Radiolabeled RNA was incubated with either no protein or the specified protein target at 37°C for 10 min. The binding mixture was filtered through a membrane well as described above, and the membrane was washed with selection buffer or eluted with concentrated ligand solutions as specified by the experiment. Collected samples (either liquid filtrate or washed nitrocellulose membrane) were added to 5 ml of Safety-Solve scintillation liquid (Research Products International) and analyzed using a liquid scintillation counter (Beckman Coulter).

Column-based SELEX for vitamin B_{12}. Chromatography matrices were prepared by packing 850 μl of vitamin B_{12}–agarose (Sigma) or adipic acid dihydrazide-agarose (Sigma) into columns with a column volume (CV) of approximate 500 μl following manufacturer's protocol (Pierce). The packed columns were washed with 25 ml of RNase-free water and 10 ml of selection buffer and wrapped in foil (to prevent photo-degradation of vitamin B_{12}) prior to use. A N30 DNA library was generated by PCR as described above using 400 pmol of template input for a total of approximately 2.4×10^{14} unique sequences. The initial N30 RNA library was generated by a ten 100-μl transcription reactions each containing 40 mM Tris-HCl, pH 7.9, 16 mM $MgCl_2$, 10 mM DTT, 2 mM spermidine, 25 mM of each rNTP, 200 U of T7 RNA polymerase, and 120 U

of RNaseOUT ribonuclease inhibitor and incubated at 37°C for 2 hours. Each 100 μl of transcription product was treated with 4 U of DNaseI at 37°C for 1 hour and purified with a NucAway column hydrated with selection buffer (20 mM Tris-HCl, pH7.5, 250 mM NaCl, 2.5 mM $MgCl_2$).

The resulting RNA was split into two equal aliquots: one for vitamin B_{12} selection and the other for folinic acid selection. The RNA was loaded onto the adipic acid dihydrazide-agarose column, incubated for 20 min, and eluted with selection buffer. This negative selection against unmodified column matrix was performed in cycles 1 through 3. The unbound fraction was subsequently loaded onto the vitamin B_{12}–agarose column, incubated for 20 min, and washed with 5 CV of selection buffer. The column was incubated with 5 mM vitamin B_{12} (Sigma) dissolved in selection buffer for 30 min and the RNA was eluted in a total of 7 CV of 5 mM vitamin B_{12}. The entire column chromatography procedure was performed at room temperature. Eluted RNA was precipitated with 2 volumes of 95% ethanol, 0.1 volumes of 3 M sodium acetate, and 10 μg/ml of glycogen followed by a wash step with 500 μl of 70% ethanol. Reverse transcription and cDNA amplification was performed in a single step with a 100-μl RT-PCR reaction containing 20 mM Tris-HCl, pH8.4, 50 mM KCl, 0.1 M DTT, 200 μM dNTP, 0.2 μM each of the N30 Fwd and N30 Rev primers, 80 U of RNaseOUT, 400 U of SuperScriptIII reverse transcriptase, and 10 U of *Taq* DNA polymerase. The reaction was incubated at 55°C for 35 min (for reverse transcription) and immediately subjected to 10 cycles of PCR amplification. Transcription for subsequent cycles was performed as described but in one 50-μl reaction for each cycle using cDNA from the previous cycle as template.

Fifteen selection cycles were performed, with the wash volume increasing from 5 CV to 10 CV in cycle 4. The wash volume was subsequently increased in 10-CV intervals from cycle 5 to cycle 10, then in 20-CV intervals from cycle 10 to cycle 15. The cDNA obtained after cycle 10 served as template for a 15-cycle, 100-μl mutagenic PCR reaction containing 10 mM Tris-HCl, pH8.3, 50 mM KCl, 7 mM $MgCl_2$, 0.5 mM $MnCl_2$, 0.4 μM each of the N30 Fwd and N30 Rev primers, 0.2 mM of dATP and dGTP, 1 mM of dTTP and dCTP, and 10 U of *Taq* DNA polymerase. This PCR product was used as the template for RNA transcription in cycle 11 of the selection process.

Column-based SELEX for racemic folinic acid. EAH Sepharose 4B resin (GE Healthcare) washed with water at pH 4.5 and 0.5 M NaCl before overnight incubation with 0.1 M EDAC (Invitrogen) and 5 mM racemic folinic acid (Sigma) at room temperature in the dark on a rotating rack. Unreacted functional groups on the resin were blocked by incubation with 1 M glacial acetic acid at room temperature for 3 hours. The ligand-conjugated resin was packed into columns with a column volume of approximate 500 μl following manufacturer's instructions. Three wash cycles each consisting of 10 CV of low pH salt solution (0.1 M sodium acetate, pH 4.0, 0.5 M NaCl) followed by 10 CV of high pH salt solution (0.1 M Tris-HCl, pH 8.3, 0.5 M NaCl) were performed on the packed columns to remove unconjugated folinic acid that may have remained in the column through weak ionic interactions. Columns were then washed with 20 CV of selection buffer and wrapped in foil (to prevent photo-degradation of folinic acid) prior to use. Unmodified EAH Sepharose 4B resin was washed with water and NaCl as described above and used to pack unmodified columns used for negative selections. Packed

columns were washed only with selection buffer prior to use. The selection process was performed exactly as described for vitamin B_{12}, except racemic folinic acid was used instead of vitamin B_{12}.

Column-based SELEX for 6R–folinic acid. EAH Sepharose 4B resin was conjugated to 5 mM 6R–folinic acid (Schircks Laboratories) and used to pack columns as described for racemic folinic acid. cDNA obtained after cycle 10 of the racemic folinic acid aptamer selection was used as template for *in vitro* transcription to generate the starting RNA pool for this selection. In each of 5 selection cycles, RNA was first loaded unto an unmodified Sepharose 4B column, incubated for 20 min, and eluted with selection buffer. The unbound fraction was subsequently loaded onto the 6R–folinic acid column, incubated for 20 min, and washed with 5 CV of selection buffer followed by 5 CV of 5 mM 6S–folinic acid (Schircks Laboratories) and another 10 CV of selection buffer. The column was incubated with 5 mM 6R–folinic acid dissolved in selection buffer for 30 min and the RNA was eluted in a total of 7 CV of 5 mM 6R–folinic acid. The entire column chromatography procedure was performed at room temperature, and the eluted RNA was precipitated and reverse transcribed as described for the vitamin B_{12} selection process.

Column-based radioactive binding assay. RNA was transcribed in a 20-μl reaction using the AmpliScribe T7 High Yield Transcription Kit (Epicentre) following manufacturer's protocol, except only 750 μM of GTP was used and 10 μCi of [α-^{32}P]-GTP was added to generate radiolabeled RNA. The transcription product was treated with 2 U of DNaseI at 37°C for 1 hour and purified with a NucAway column hydrated

with selection buffer. RNA was loaded onto the appropriate column as specified by the experiment, incubated at room temperature for 20 min, and the unbound fraction was collected. The column was subsequently washed with selection buffer or eluted with dissolved ligand as specified by the experiment. Collected samples were added to 5 ml of Safety-Solve scintillation liquid and analyzed using a liquid scintillation counter.

Sequence and structural analyses. RNA pools from the specified selection cycles were reverse transcribed into cDNA and amplified by PCR as described. The PCR products were digested with the NheI and HindIII restriction enzymes and cloned into pcDNA3.1(+) (Invitrogen) for sequencing. Sequence results were aligned with the Clustal X software (University College Dublin) to assist with identifying sequence motifs. RNA folding was determined using the RNAstructure software (University of Rochester Medical Center), and structural motifs were identified by manual sorting.

Capillary electrophoresis binding assay. DNA templates encoding the SV12.6, SVC12.60, and SVC12.70 sequences were synthesized by Integrated DNA Technologies and PCR amplified using the N30 Fwd and N30 Rev primers. RNA transcription was performed in 20-μl reactions using the AmpliScribe T7 High Yield Transcription Kit following manufacturer's protocol. The transcription product was treated with 2 U of DNaseI at 37°C for 1 hour and purified with a NucAway column hydrated with RNase-free water. For RNA-only samples, RNA was diluted to 100 ng/μl (5.24 μM) with selection buffer (20 mM Tris-HCl, Ph7.5, 100 mM NaCl, 1 mM $MgCl_2$). For ligand-binding reactions, 2 μg of RNA was diluted to a total volume of 17.72 μl with selection

buffer, denatured in a PCR block at 75°C for 3 min, renatured by cooling to 25°C at 0.3°C/sec, and added to 2.28 μl of 45.81 μM phenobarbital-BSA to produce a 20-μl mixture with a final concentration of 5.24 μM RNA and 5.24 μM phenobarbital-BSA (molar concentration for BSA).

Capillary electrophoresis was performed with a P/ACE MDQ Capillary Electrophoresis System (Beckman Coulter) using a photodiode array (PDA) detector. For each run, 110 nl of sample was injected at 2 psi over 8 sec, and separation was performed at 22.5 kV over 14 min. The capillary was filled with run buffer (25 mM sodium tetraborate, pH 9.1) prior to each sample injection. Capillary regeneration was performed by rinsing with 0.1 M HCl, followed by 0.1 M NaOH, water, and finally the run buffer. Each rinse step was performed for 2 min at 20 psi. Elution profiles were analyzed using the 32Karat software (Beckman Coulter).

LC-MS binding assay. RNA was transcribed in five 100-μl reactions using the AmpliScribe T7 High Yield Transcription Kit following manufacturer's protocol. Each 100-μl transcription product was treated with 20 U of DNaseI at 37°C for 1 hour and purified with a NucAway column hydrated with RNase-Free water. The eluted RNA was extracted with phenol-chloroform and precipitated with 2 volumes of 95% ethanol and 0.1 volume of 3 M sodium acetate followed by a wash step with 500 μl of 70% ethanol. The precipitated RNA was resuspended in 100 μl of selection buffer (20 mM Tris-HCl, pH7.5, 250 mM NaCl, 2.5 mM $MgCl_2$), denatured at 75°C for 3 min, and renatured at room temperature for 30 min. Binding reactions were set up with the RNA and ligand (folinic acid or theophylline) concentration specified by the experiment. The binding

mixture was incubated at 37°C for 30 min and loaded onto a Microcon YM-10 column (Millipore). The column was centrifuged at maximum speed for 30 min, and the filtrate was analyzed by LC-MS. Standard curves for concentration calculation were generated with pure ligand solutions prepared at known concentrations (16 μM to 1 μM in two-fold dilutions for typical binding assays) and filtered in the same way as the RNA-ligand binding mixtures.

LC-MS analysis was performed with an Agilent 6320 Ion Trap LC/MS system using either an Agilent ZORBAX SB-Aq, 3.0 x 250 mm, 5 μm column (for folinic acid) or an Agilent ZORBAX Eclipse XDB-C18, 2.1 x 50 mm, 3.5 μm column (for theophylline). The method for analyzing folinic acid is shown below, where solvent A is 0.1% acetic acid and 0.1% methanol in water, solvent B is 0.1% acetic acid in methanol, and solvents A and B always sum to 100% of the liquid flux.

Time (min)	% Solvent B	Flow Rate (ml/min)
0.00	45	0.500
6.00	45	0.500
6.50	60	0.500
7.00	75	0.500
7.50	100	0.500
13.00	100	0.500
13.50	45	0.500
38.00	Method Ends	Method Ends

The method for analyzing theophylline is shown on the following page, where the solvent setups are as described for the folinic acid protocol.

Time (min)	% Solvent B	Flow Rate (ml/min)
0.00	15	0.350
2.50	15	0.350
3.00	100	1.000
4.50	100	1.000
5.00	15	1.000
6.50	15	1.000
6.60	15	0.350
7.00	Method Ends	Method Ends

Acknowledgments

The column-based selection for vitamin B_{12} and racemic folinic acid was performed with J.C. Liang. We thank A. Brown and M. Greenwood-Goodwin for assistance with capillary electrophoresis, M.N. Win for advice on column-based SELEX, and M. Siddiqui and J. Michener for assistance with LC-MS. This work was supported by the City of Hope's National Cancer Institute–Cancer Center Support Grant, the National Science Foundation (fellowship to Y.Y.C.), the Alfred P. Sloan Foundation (fellowship to C.D.S.), and the National Institutes of Health (grant to C.D.S., RC1GM091298).

References

1. Win, M.N. & Smolke, C.D. A modular and extensible RNA-based gene-regulatory platform for engineering cellular function. *Proc Natl Acad Sci U S A* **104**, 14283-14288 (2007).
2. Beisel, C.L., Bayer, T.S., Hoff, K.G. & Smolke, C.D. Model-guided design of ligand-regulated RNAi for programmable control of gene expression. *Mol Syst Biol* **4**, 224 (2008).

3. Beisel, C.L., Chen, Y.Y., Culler, S.J., Hoff, K.G. & Smolke, C.D. Design of small molecule-responsive microRNAs based on structural requirements for Drosha processing. *Nucleic Acids Res* (2010). doi: 10.1093/nar/gkq954.

4. Conrad, R.C., Giver, L., Tian, Y. & Ellington, A.D. In vitro selection of nucleic acid aptamers that bind proteins. *Methods Enzymol* **267**, 336-367 (1996).

5. Giver, L., Bartel, D.P., Zapp, M.L., Green, M.R. & Ellington, A.D. Selection and design of high-affinity RNA ligands for HIV-1 Rev. *Gene* **137**, 19-24 (1993).

6. Kubik, M.F., Stephens, A.W., Schneider, D., Marlar, R.A. & Tasset, D. High-affinity RNA ligands to human alpha-thrombin. *Nucleic Acids Res* **22**, 2619-2626 (1994).

7. Hirao, I., Spingola, M., Peabody, D. & Ellington, A.D. The limits of specificity: an experimental analysis with RNA aptamers to MS2 coat protein variants. *Mol Divers* **4**, 75-89 (1998).

8. Lebruska, L.L. & Maher, L.J., 3rd Selection and characterization of an RNA decoy for transcription factor NF-kappa B. *Biochemistry* **38**, 3168-3174 (1999).

9. Jenison, R.D., Gill, S.C., Pardi, A. & Polisky, B. High-resolution molecular discrimination by RNA. *Science* **263**, 1425-1429 (1994).

10. Berens, C., Thain, A. & Schroeder, R. A tetracycline-binding RNA aptamer. *Bioorg Med Chem* **9**, 2549-2556 (2001).

11. Win, M.N., Klein, J.S. & Smolke, C.D. Codeine-binding RNA aptamers and rapid determination of their binding constants using a direct coupling surface plasmon resonance assay. *Nucleic Acids Res* **34**, 5670-5682 (2006).

12. http://www.ncbi.nlm.nih.gov/pubmedhealth/PMH0000542. *U.S. National Library of Medicine, National Institutes of Health* (2008).

13. Cox, J.C. & Ellington, A.D. Automated selection of anti-protein aptamers. *Bioorg Med Chem* **9**, 2525-2531 (2001).

14. Huang, D.B. et al. Crystal structure of NF-kappaB (p50)2 complexed to a high-affinity RNA aptamer. *Proc Natl Acad Sci U S A* **100**, 9268-9273 (2003).

15. Weinberger, R. Practical Capillary Electrophoresis, Edn. 2nd. (Academic Press, San Diego; 2000).

16. Bleyer, W.A. New vistas for leucovorin in cancer chemotherapy. *Cancer* **63**, 995-1007 (1989).

17. Lorsch, J.R. & Szostak, J.W. In vitro selection of RNA aptamers specific for cyanocobalamin. *Biochemistry* **33**, 973-982 (1994).

18. Sussman, D., Nix, J.C. & Wilson, C. The structural basis for molecular recognition by the vitamin B 12 RNA aptamer. *Nat Struct Biol* **7**, 53-57 (2000).

19. Mathews, D.H. et al. Incorporating chemical modification constraints into a dynamic programming algorithm for prediction of RNA secondary structure. *Proc Natl Acad Sci U S A* **101**, 7287-7292 (2004).

20. Keshava, C., Keshava, N., Whong, W.Z., Nath, J. & Ong, T.M. Inhibition of methotrexate-induced chromosomal damage by folinic acid in V79 cells. *Mutat Res* **397**, 221-228 (1998).

21. Mini, E., Trave, F., Rustum, Y.M. & Bertino, J.R. Enhancement of the antitumor effects of 5-fluorouracil by folinic acid. *Pharmacol Ther* **47**, 1-19 (1990).

22. Etienne, M.C., Thyss, A., Bertrand, Y., Rubie, H. & Milano, G. [l-folinic acid versus racemic folinic acid in the treatment of leukemia in children with high dose of methotrexate]. *Bull Cancer* **80**, 357-363 (1993).

23. Etienne, M.C., Speziale, N. & Milano, G. HPLC of folinic acid diastereoisomers and 5-methyltetrahydrofolate in plasma. *Clin Chem* **39**, 82-86 (1993).

24. Newman, E.M., Straw, J.A. & Doroshow, J.H. Pharmacokinetics of diastereoisomers of (6R,S)-folinic acid (leucovorin) in humans during constant high-dose intravenous infusion. *Cancer Res* **49**, 5755-5760 (1989).

25. Schilsky, R.L. et al. Clinical pharmacology of the stereoisomers of leucovorin during repeated oral dosing. *Cancer* **63**, 1018-1021 (1989).

26. Ellington, A.D. & Szostak, J.W. In vitro selection of RNA molecules that bind specific ligands. *Nature* **346**, 818-822 (1990).

27. Sinha, J., Reyes, S.J. & Gallivan, J.P. Reprogramming bacteria to seek and destroy an herbicide. *Nat Chem Biol* **6**, 464-470 (2010).

28. Mendonsa, S.D. & Bowser, M.T. In vitro selection of high-affinity DNA ligands for human IgE using capillary electrophoresis. *Anal Chem* **76**, 5387-5392 (2004).

29. Berezovski, M. et al. Nonequilibrium capillary electrophoresis of equilibrium mixtures: a universal tool for development of aptamers. *J Am Chem Soc* **127**, 3165-3171 (2005).

30. Drabovich, A., Berezovski, M. & Krylov, S.N. Selection of smart aptamers by equilibrium capillary electrophoresis of equilibrium mixtures (ECEEM). *J Am Chem Soc* **127**, 11224-11225 (2005).

Chapter 7

Conclusions

The development of cell-based therapies ranging from well-established practices such as bone marrow transplant to next-generation strategies such as adoptive T-cell therapy represents exciting progress in medical technology. The ability to harness the complex functionalities and adaptive responses of living cells as therapeutic agents promises to address critical diseases that have so far eluded effective treatment. However, with the intricate capabilities of living cells come myriad system parameters that must be fine-tuned and stringently controlled to achieve safe and effective therapies. To address this challenge, we have developed rationally designed, RNA-based regulatory systems capable of genetic control over functional outputs in mammalian lymphocytes.

We constructed ligand-responsive regulatory systems that employ *cis*-acting ribozyme switches and *trans*-acting miRNA constructs for the effective regulation of T-cell proliferation in primary human cell culture and in mouse models. We demonstrated unique properties of these synthetic control systems—including modular composition, tunable regulatory stringency, and rapid response to ligand input—that are critical for translations to clinical applications. This work provides a foundation upon which further system developments may be achieved, particularly in the incorporation of additional regulatory targets, the generation of novel sensor components to clinically suitable molecular inputs, and the development of engineered T cells with enhanced tumor-targeting capabilities for cancer treatment.

Immediate Challenges for the Clinical Translation of RNA-Based T-Cell Proliferation Control Systems

The regulatory systems developed in this work modulate the expression of upstream signaling molecules in the growth-stimulatory Interleukin (IL)-2/IL-15 cytokine signaling pathways. Although the autocrine signaling processes mediated by the cytokines and receptor chains that are the focus of our current system designs are critical to T-cell proliferation, several additional factors have profound impacts on the survival and expansion of T cells *in vivo*. For example, the tumor microenvironment is known to be immunosuppressive due to the presence of potent T-cell growth-inhibitory molecules such as tumor growth factor β (TGF-β)[1] and receptor programmed death ligand 1 (PD-L1)[2]. Furthermore, receptors such as the cytotoxic T-lymphocyte antigen 4 (CTLA4) on T-cell surfaces interact with ligands present in the tumor microenvironment to inactivate tumor-infiltrating lymphocytes[3]. Future regulatory system designs can incorporate the TGF-β receptor, PD-1 (the receptor to PD-L1), and CTLA4 as regulatory targets to mediate these intercellular, growth-inhibitory signaling events.

A second area of potential improvement is the generation of new RNA aptamers that will enable the construction of regulatory devices responsive to more clinically suitable molecular inputs. The constructs developed in this work have relied on well-characterized aptamers to theophylline and tetracycline, neither of which can be administered to human patients at the dosages required for regulatory system function due to cytotoxicity concerns. Our efforts in generating new RNA aptamers to better tolerated molecules such as folinic acid and vitamin B_{12} have not resulted in high-affinity aptamer sequences. The selection of aptamers to small-molecule ligands is particularly challenging due to a frequent lack of functional groups suitable for chemical conjugation to solid supports, which are required for the aptamer selection process. Furthermore,

clinical applications pose the additional requirements of low toxicity, high bioavailability, and efficient cell permeability for the target molecules. Ongoing efforts in the Smolke Laboratory aim to develop alternative aptamer selection methods—including *in vivo* selection and *in vitro* protocols utilizing alternative separation techniques such as capillary electrophoresis that do not require the use of solid supports—to facilitate the selection of new RNA aptamers. The experiences presented in this work suggest that not all small-molecule ligands are equally well suited to RNA aptamer selections. Therefore, the effective generation of novel aptamers will require the identification of a broad range of clinically applicable molecules and the development of high-throughput protocols that enable the simultaneous selection of aptamers toward a large panel of target molecules, a subset of which may yield high-affinity aptamer sequences.

The goal of T-cell proliferation control is to improve the safety and efficacy of adoptive T-cell therapy for cancer. Therefore, it is of great scientific interest to verify that effective control over T-cell growth *in vivo* can enhance the tumor-fighting capability of engineered T cells. Tumor-targeting T cells stably expressing RNA-based regulatory systems should be tested in tumor xenograft models to examine not only T-cell proliferation, but also the impact on tumor regression and eradication. Since relevant models for therapeutic applications will require systemic injections of input ligands, which must be well tolerated by the host organism, this investigation will be more effectively performed after the development of RNA aptamers to clinically suitable molecules. Beyond these immediate steps toward the development of a more complete and versatile T-cell proliferation control system, several areas of investigation have the

potential to further improve the functionalities of RNA-based regulatory systems and broaden their applications in health and medicine.

Future Directions for the Development of RNA-Based Regulatory Systems for Clinical Applications

Stringent control of the fates and functions of cells in therapeutic applications will likely require the simultaneous regulation of multiple targets in response to various molecular inputs. The regulatory systems developed in this work are adaptable to diverse input molecules and genetic targets, have compact footprints, do not require exogenous and potentially immunogenic protein components, and support the construction of integrated control networks incorporating both ribozyme- and miRNA-based regulatory mechanisms. However, several critical challenges remain in the development of RNA-based regulatory systems for clinical applications and present interesting opportunities for future investigations.

First, compared to alternative regulatory strategies such as inducible promoter systems, RNA-based control devices have relatively high basal expression levels or "leakiness" in target-gene expression. Although we have demonstrated that miRNA switch systems are capable of greater gene expression knockdown compared to non-switch miRNAs expressed from inducible promoters (Chapter 5), neither miRNA switches nor ribozyme-based devices can completely suppress gene expression, as would be possible with transgenes placed directly under the control of inducible promoters. Patient safety demands that T-cell proliferation be fully and reliably terminated in the OFF state, and even a low level of leakiness in proliferative cytokine or cytokine receptor

chain expression may prove unacceptable for therapeutic applications. In addition to the various performance tuning strategies presented in this work, the regulatory stringency of RNA-based control systems may be improved by utilizing alternative ribozymes with optimal cleavage activities in mammalian hosts, by placing critical target genes under the simultaneous control of multiple types of control devices, and by carefully specifying the strengths of constitutive promoters from which transgenes such as proliferative cytokines and regulatory devices such as ribozyme and miRNA switches are expressed.

Second, the switch dynamic ranges of the RNA-based control devices presented in this work are relatively modest and leave significant room for improvement. We have demonstrated that by targeting upstream signaling events and taking advantage of signal amplification cascades, even systems with modest switch dynamic ranges can meaningfully regulate functional outputs in both mouse and human T cells. However, such signal amplification effects may not be available in all applications of interest, and the ability to generate a large output range in response to a defined input gradient will greatly enhance the applicability of RNA-based regulatory systems. Ligand toxicity has been an important constraint on the dynamic ranges of devices presented in this work. Specifically, the maximum ON-state expression level is often inaccessible due to the inability to administer ligand molecules at high concentrations, which frequently compromise cell survival. This challenge would be addressed by continuing efforts to generate high-affinity RNA aptamers to molecules with low toxicity and high cell permeability. Furthermore, the maximum dynamic range of RNA-based regulatory devices is subject to intrinsic thermodynamic and kinetic limitations[4]. Theoretical modeling and empirical studies have revealed several tuning strategies—including the

modulation of the rates of transcription, translation, and protein decay; the introduction of transcriptional pause sites to bias transcriptional folding; and the design of switch sequences to favor disrupted-aptamer conformations—that can be applied to increase the dynamic ranges of RNA-based control devices[4].

Third, the RNA-based regulatory systems presented here have been designed to generate gene-regulatory outputs in response to exogenously administered molecular inputs and have not been examined for their ability to respond to endogenous signals. The versatility of these control systems, particularly in the context of cancer treatment, can greatly benefit from the ability to detect endogenous molecular inputs. For example, a T-cell proliferation control system that promotes T-cell growth in the presence of a soluble tumor antigen would enable autonomous disease detections that lead to a therapeutic response. Alternatively, a system that detects changes in endogenous T-cell markers (e.g., surface receptors that indicate the transformation of a regulatory T cell into an effector T cell or vice versa) and subsequently eliminates the transformed cells would provide critical safeguards against unintended and potentially detrimental alterations in T-cell populations after their adoptive transfer to cancer patients. An RNA-based regulatory system capable of regulating alternative splicing patterns in response to endogenous signaling pathways and protein targets was recently reported[5], providing a novel example of RNA-based genetic control over critical cellular processes in response to endogenous input signals.

Finally, the stable integration of RNA-based regulatory systems into cellular hosts intended for therapeutic applications will likely require additional development and optimization. Although RNA-based regulatory systems have the distinct advantage of a

compact footprint compared to protein-based systems, genetically modifying cellular hosts such as primary human T cells to express any transgenic control system remains a non-trivial challenge. Safety considerations require that the cells used for immunotherapy be of sufficient genotypic and phenotypic consistency for adoptive transfer into human patients. Conversely, the race against tumor expansion and metastasis demands that such therapeutic cell populations be generated in a timely manner, possibly without allowance for a careful selection procedure to isolate optimally performing clones. We have demonstrated that the RNA-based regulatory systems presented in this work are sufficiently robust to produce the prescribed functional output without population refinement after stable integration into primary human T cells. Nevertheless, additional developments on efficient genetic modification techniques, such as site-specific gene insertions into mammalian genomes using engineered viral vectors, will greatly enhance the applicability of genetic control strategies in clinical settings.

The work presented here demonstrates the ability of RNA-based regulatory systems to control both gene expression and functional outputs in mammalian cells, and highlights the potential of synthetic biological designs to carry out complex functions with programmed precision. The continuing development of rationally designed biological systems promises to bring forth novel capabilities with diverse applications, particularly in the advancement of next-generation technologies in health and medicine.

References

1. Wallace, A. et al. Transforming growth factor-beta receptor blockade augments the effectiveness of adoptive T-cell therapy of established solid cancers. *Clin Cancer Res* **14**, 3966-3974 (2008).

2. Curran, M.A., Montalvo, W., Yagita, H. & Allison, J.P. PD-1 and CTLA-4 combination blockade expands infiltrating T cells and reduces regulatory T and myeloid cells within B16 melanoma tumors. *Proc Natl Acad Sci U S A* **107**, 4275-4280 (2010).

3. Peggs, K.S., Quezada, S.A. & Allison, J.P. Cell intrinsic mechanisms of T-cell inhibition and application to cancer therapy. *Immunol Rev* **224**, 141-165 (2008).

4. Beisel, C.L. & Smolke, C.D. Design principles for riboswitch function. *PLoS Comput Biol* **5**, e1000363 (2009).

5. Culler, S.J., Hoff, K.G. & Smolke, C.D. Reprogramming cellular behavior with RNA controllers responsive to endogenous proteins. *Science* **330**, 1251-1255 (2010).

Appendix 1

Small-Molecule Toxicity Curves in CTLL-2 Cells

Introduction

The toxicities of various small molecules to CTLL-2 cells were measured to determine the optimal ligand input concentration for regulatory device evaluations and to determine whether certain small molecules of interest are sufficiently non-toxic to be useful candidates for aptamer selection. Specifically, theophylline, tetracycline, and doxycycline toxicities were measured to determine the maximum concentration that could be tolerated for characterization studies on theophylline- and tetracycline-responsive RNA switch devices. Phenobarbital, tamoxifen, folinic acid, and vitamin B_{12} (cyanocobalamin) are pharmaceuticals approved for clinical use by the United States Food and Drug Administration. Therefore, they are potentially suitable molecular inputs for RNA-based regulatory systems in therapeutic applications. The toxicity levels of these molecules were measured to assist in the choice of target ligands for the aptamer selection processes described in Chapter 6.

Results and Discussion

Theophylline at concentrations between 5 μM and 250 μM shows moderate toxicity to CTLL-2 cells (Appendix Figure 1.1). Toxicity increases significantly at 500 μM and above, but cells could still sustain growth at the highest concentration tested (1 mM) during the 5-day study. Based and these results, we determined 1 mM to be an appropriate concentration for use in transient transfection experiments, and 500 μM was chosen for long-term studies of cell lines stably integrated with RNA regulatory systems. Tetracycline causes severe toxicity even at low micromolar levels (Appendix Figure 1.2), and doxycycline shows very similar toxicity profiles (Appendix Figure 1.3). Although the

tetracycline aptamer has a reported K_D value of 0.8 nM[1], the concentration needed to trigger ribozyme switches may be higher, and the intracellular tetracycline concentration is likely to be significantly lower than the extracellular concentration. These conflicting constraints imposed by tetracycline toxicity and aptamer affinity preclude the determination of a specific input concentration for characterization studies. Therefore, transient transfection experiments were performed with a range of tetracycline input concentrations (Figure 3.3). T-cell growth regulation was impossible due to tetracycline's strong toxicity, thus tetracycline-responsive switches were not chosen for stable integration and subsequent characterizations.

Folinic acid is essentially nontoxic to CTLL-2 cells, and both phenobarbital and vitamin B_{12} can be administered to 1 mM or above without causing severe growth inhibition (Appendix Figures 1.4-1.6). Therefore, these small-molecule pharmaceuticals were chosen for aptamer selection studies (Chapter 6). In contrast, tamoxifen was found to be extremely toxic to CTLL-2 cells (Appendix Figure 1.7) and soluble only in organic solvents such as methanol, which also causes modest toxicity (Appendix Figure 1.8). As a result, tamoxifen was eliminated from the list of candidates for aptamer selection.

Materials and Methods

Theophylline toxicity curve. CTLL-2 cells stably expressing firefly luciferase (CffLuc cells) were cultured as described in Chapter 3. On Day 0, nine T25 tissue culture flasks were each seeded with 5 ml of cells at 0.15 x 10^6 cells/ml. A 40 mM stock of theophylline anhydrous (Sigma) dissolved in sterile water and filtered through a 0.22-μm syringe filter was used to bring each flask to the appropriate final theophylline

concentration. A 4 mM diluted stock was used to supplement the 5-μM sample well in order to avoid pipetting volumes less than 1 μl. Cell count in each sample was manually obtained every 24 hours using Trypan Blue stain (Gibco) and a hemocytometer. Cultures were fed 100 U/ml IL-2 every 48 hours and split as necessary to maintain cell densities between 0.15 x 10^6 cells/ml and 1.50 x 10^6 cells/ml. The relatively high cell density was chosen to allow more accurate manual cell count with a hemocytometer.

Tetracycline and doxycycline toxicity curves. CffLuc cells were cultured as described in Chapter 3. On Day 0, 24-well plates were seeded with cells at 0.03 x 10^6 cells/ml, 1 ml/well, 1 well for each ligand concentration tested. A 20 mM tetracycline hydrochloride (Sigma) stock and an 80 mM doxycycline hyclate (Sigma) stock were prepared by dissolving in sterile water and filtering through 0.22-μm syringe filters. Stocks were further diluted with water as necessary so a volume between 1 μl and 7.5 μl of dissolved ligand was added to each well to bring cultures to the appropriate final ligand concentrations. Starting on Day 1, 100 μl of each well was sampled every 24 hours for cell density measurements using a Quanta Cell Lab Flow Cytometer (Beckman Coulter). Viable populations were gated based on side scatter and electronic volume, and cell density was determined by viable cell count divided by total volume of sample analyzed on the flow cytometer. Cultures were fed 100 U/ml IL-2 every 48 hours, and samples with a measured density above 0.1 x 10^6 cells/ml on Day 4 were split ten-fold on Day 5 using media containing the appropriate ligand concentration.

Phenobarbital toxicity curve. CffLuc cells were cultured as described in Chapter 3. On Day 0, 24-well plates were seeded with cells at 0.02 x 10^6 cells/ml, 1 ml/well, 1 well for each ligand concentration tested. A 2 mM stock of phenobarbital (Sigma) was prepared by dissolving in RPMI-1640 media. Since a more concentrated stock could not be made due to phenobarbital's low solubility, large volumes of the dissolved ligand had to be added to samples at the high concentration points. Extensive dilution with water could have adverse effects on cell physiology, thus the phenobarbital stock was prepared in media. The stock was further diluted with media as necessary so >1 μl of dissolved phenobarbital was added to each well to bring cultures to the appropriate final concentrations. All wells were fed 100 U/ml IL-2 every 48 hours and split ten-fold on Days 3 and 5 using media containing the appropriate ligand concentration. Cell density was measured as described for tetracycline and doxycycline toxicity curves.

Folinic acid and vitamin B_{12} toxicity curves. CffLuc cells were cultured as described in Chapter 3. On Day 0, 24-well plates were seeded with cells at 0.05 x 10^6 cells/ml, 1 ml/well, 1 well for each ligand concentration tested. A 40 mM folinic acid calcium salt hydrate (Sigma) stock was prepared by dissolving in sterile water and filtering through 0.22-μm syringe filters. A 10 mM stock of vitamin B_{12} (cyanocobalamin, Sigma) was prepared by dissolving in RPMI-1640 media (see phenobarbital toxicity curve methods for the use of media instead of water). Stocks were further diluted as necessary so >0.5 μl of dissolved ligand was added to each well to bring the culture to the appropriate final ligand concentration. Cultures were fed 100 U/ml IL-2 every 48 hours, and all wells were split 6-fold on Day 2. The 2 mM folinic acid culture was found with bacterial

contamination on Day 3 and discarded. All remaining wells were subsequently supplemented with 50 U/ml penicillin:streptomycin. On Day 4, all folinic acid cultures were split ten-fold and all vitamin B_{12} cultures were split six-fold using media containing the appropriate ligand concentration. Cell density was measured as described for tetracycline and doxycycline toxicity curves.

Tamoxifen and methanol toxicity curves. CffLuc cells were cultured as described in Chapter 3. On Day 0, 24-well plates were seeded with cells at 0.03 x 10^6 cells/ml, 1 ml/well, 1 well for each ligand concentration tested. Tamoxifen has extremely low solubility in aqueous solutions. Therefore, an 1 mM stock of tamoxifen citrate salt (Sigma) was prepared by dissolving in methanol with heating in a 37°C water bath and filtering through a 0.22-μm syringe filter. The stock was further diluted with methanol as necessary so a volume between 1 μl and 5 μl of dissolved ligand was added to each well to bring cultures to the appropriate final ligand concentrations. For the methanol toxicity curve, 100% methanol was used to supplement each cell culture to the appropriate final methanol concentration. Cultures were fed 100 U/ml IL-2 every 48 hours. All wells for the tamoxifen toxicity curve were split 11-fold on Days 2 and 4 using media containing the appropriate ligand concentration. Cultures for the methanol toxicity curve were never split. Cell density was measured as described for tetracycline and doxycycline toxicity curves.

Reference

1. Weigand, J.E. & Suess, B. Tetracycline aptamer-controlled regulation of pre-mRNA splicing in yeast. *Nucleic Acids Res* **35**, 4179-4185 (2007).

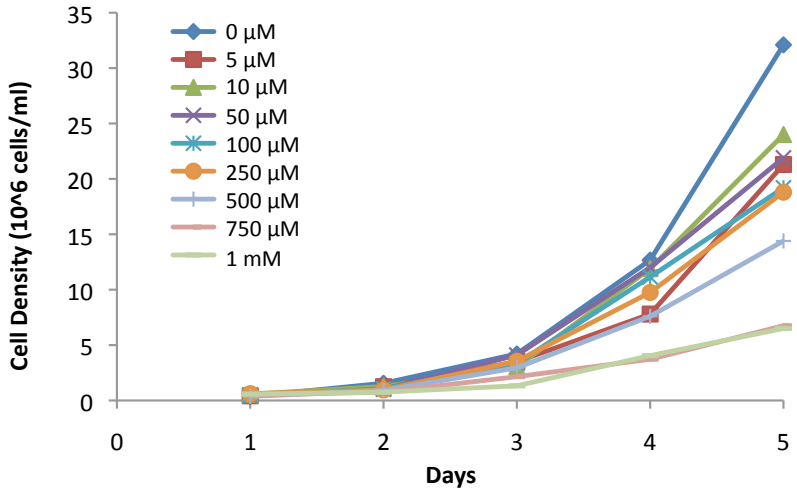

Appendix Figure 1.1. Theophylline toxicity curve in CTLL-2 cells.

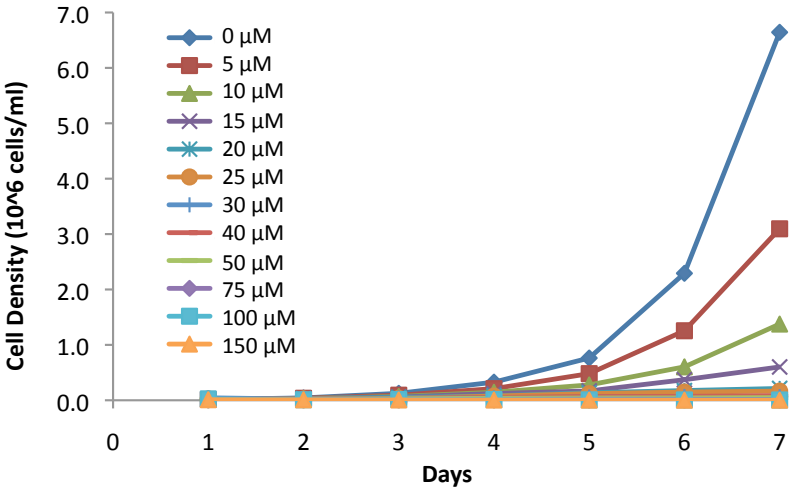

Appendix Figure 1.2. Tetracycline toxicity curve in CTLL-2 cells.

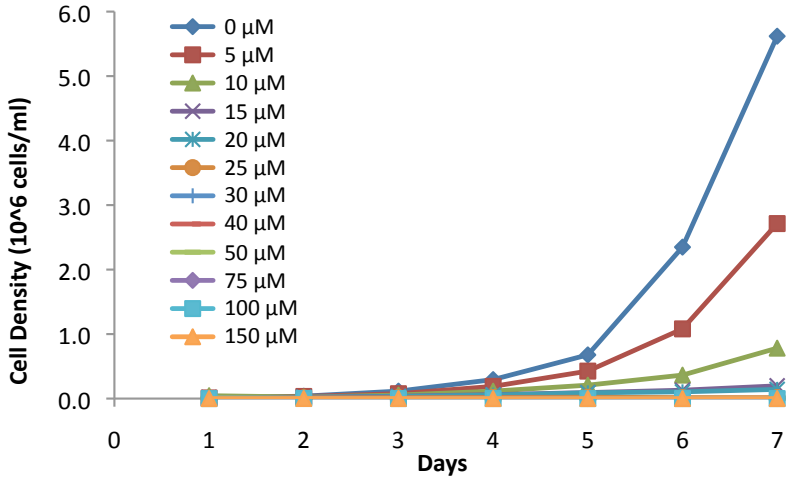

Appendix Figure 1.3. Doxycycline toxicity curve in CTLL-2 cells.

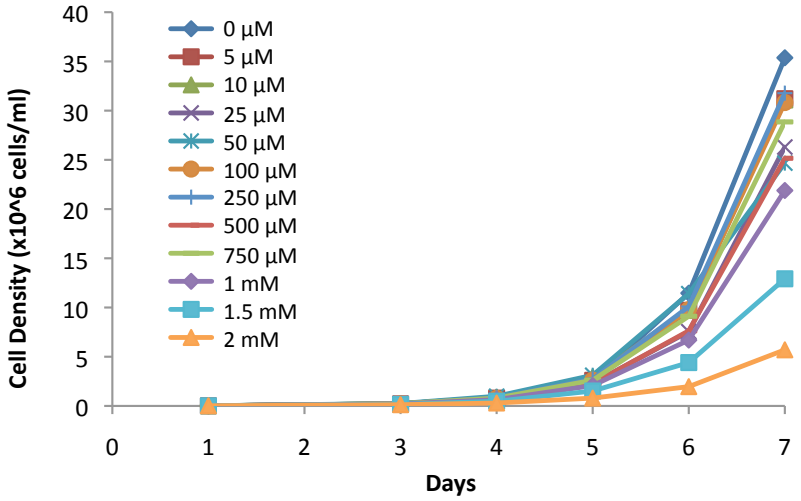

Appendix Figure 1.4. Phenobarbital toxicity curve in CTLL-2 cells.

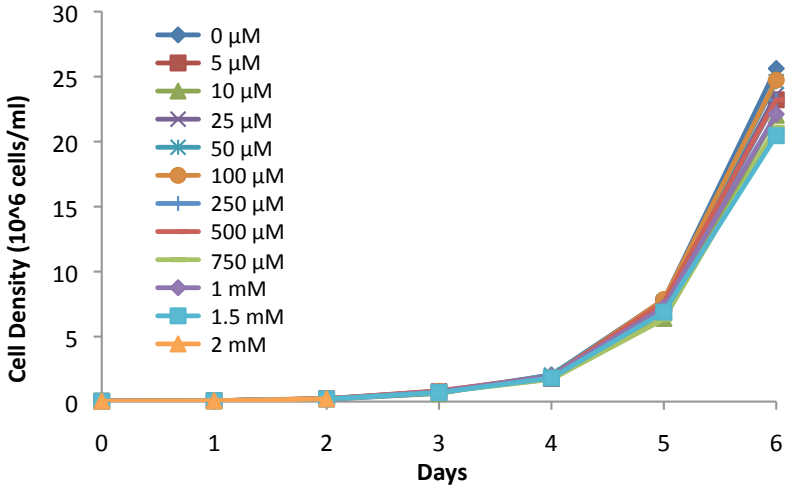

Appendix Figure 1.5. Folinic acid toxicity curve in CTLL-2 cells.

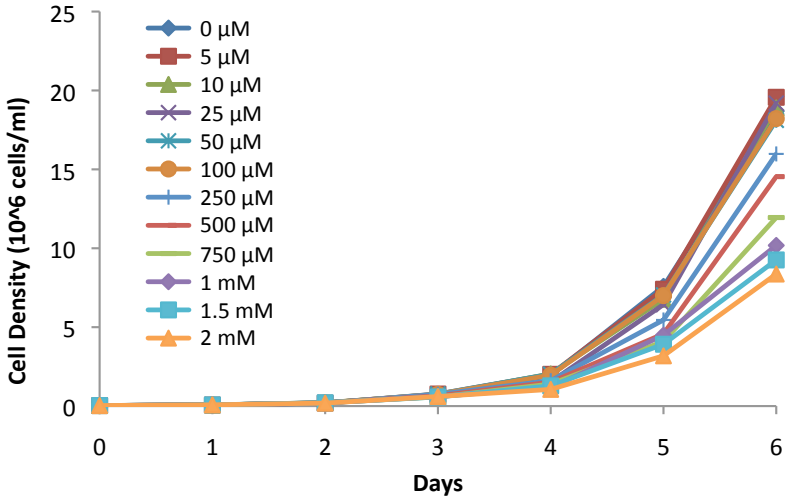

Appendix Figure 1.6. Vitamin B_{12} toxicity curve in CTLL-2 cells.

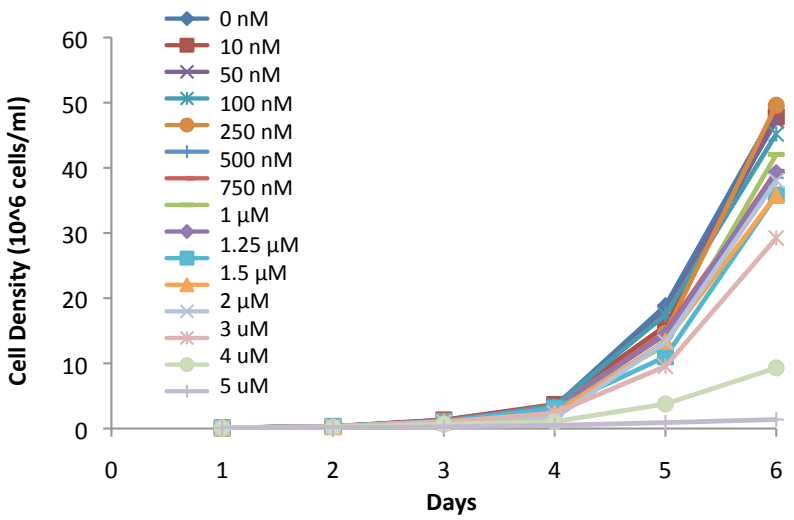

Appendix Figure 1.7. Tamoxifen toxicity curve in CTLL-2 cells.

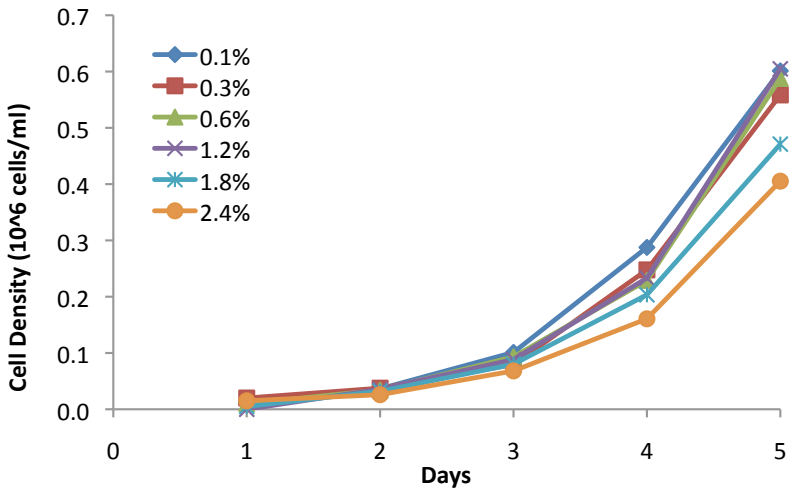

Appendix Figure 1.8. Methanol toxicity curve in CTLL-2 cells.

Appendix 2

Small-Molecule Toxicity Curves in NK-92 Cells

Introduction

The toxicity of various small molecules to NK-92 cells was measured to determine the optimal ligand input concentration for regulatory device evaluations and to determine whether certain small molecules of interest are sufficiently nontoxic to be useful candidates for aptamer selection. Molecules were chosen for toxicity measurements for the reasons described in Appendix 1.

Results and Discussion

Compared to CTLL-2 cells, NK-92 cells are slightly more robust when cultured in the presence of theophylline (Appendix Figures 1.1, 2.1) and significantly more viable in the presence of tetracycline (Appendix Figures 1.2, 2.2). Therefore, the concentrations used for characterization studies in CTLL-2 cells were considered acceptable and adopted for use in NK-92 cells. Vitamin B_{12} is essentially non-toxic to NK-92 cells (Appendix Figure 2.3), and phenobarbital can be administered to 1 mM without significant toxicity (Appendix Figure 2.4), thus confirming these small molecules as desirable candidates for apatmer selection. Interestingly, folinic acid shows significant toxicity to NK-92 cells at 50 μM and above (Appendix Figure 2.5). Visual inspection of cultures containing 2 mM or more of folinic acid reveals fine precipitates, suggesting concentrated folinic acid could have non-specific interactions with the X-VIVO 20 media used to culture NK-92 cells but not with the RPMI-1640 media used to culture CTLL-2 cells.

Materials and Methods

NK-92 cells stably expressing the *cd19-tk-t2a-il15* transgene were cultured in X-VIVO 20 media (Lonza) without exogenous cytokines or antibiotics. On Day 0, 12-well plates were seeded with cells at 0.08 x 10^6 cells/ml, 3 ml/well, 3 wells for each ligand concentration tested. The following small-molecule stocks were prepared by dissolving in X-VIVO 20 media and used without sterile filtration: 6 mM theophylline anhydrous (Sigma), 1 mM tetracycline hydrochloride (Sigma), 4 mM phenobarbital (Sigma), 10 mM folinic acid calcium salt (Sigma), and 10 mM vitamin B_{12} (cyanocobalamin, Sigma). Stocks were further diluted with media as necessary so that >3 μl of dissolved small molecule was added to each well to bring cultures to the appropriate final ligand concentrations. Culture plates were wrapped in foil to prevent excessive evaporation and stored in a 37°C incubator. All wells were split two-fold (phenobarbital and folinic acid samples) or three-fold (all remaining samples) using media containing the appropriate ligand concentration on Day 3. Starting on Day 1, 200 μl of each well was sampled every 24 hours for cell density measurements using a Quanta Cell Lab Flow Cytometer (Beckman Coulter). Viable populations were gated based on side scatter and electronic volume, and cell density was determined by viable cell count divided by total volume of sample analyzed on the flow cytometer. Reported values are the mean of triplicate samples ± s.d.

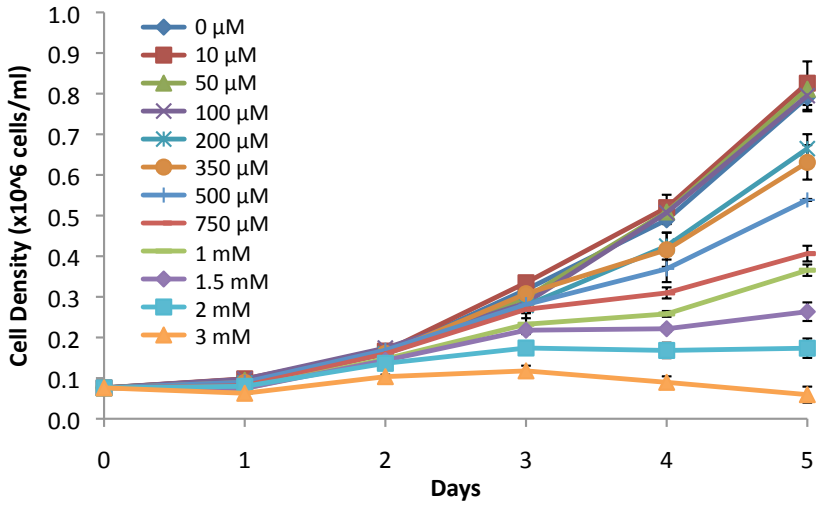

Appendix Figure 2.1. Theophylline toxicity curve in NK-92 cells.

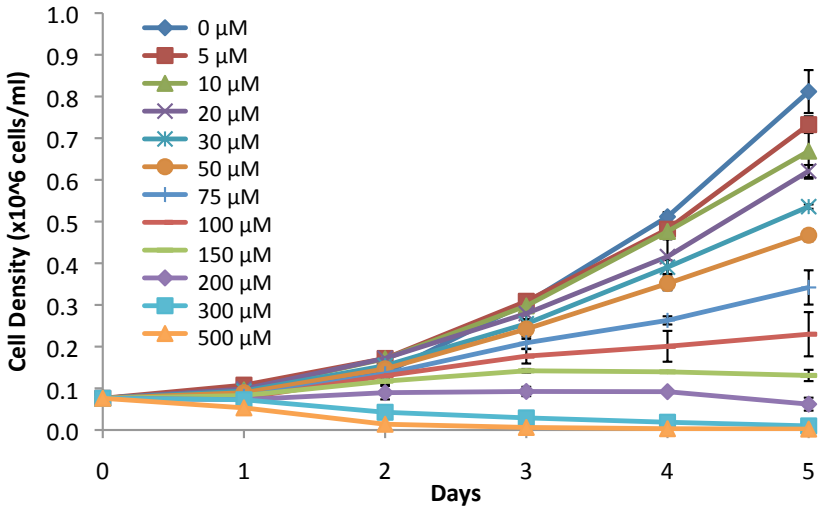

Appendix Figure 2.2. Tetracycline toxicity curve in NK-92 cells.

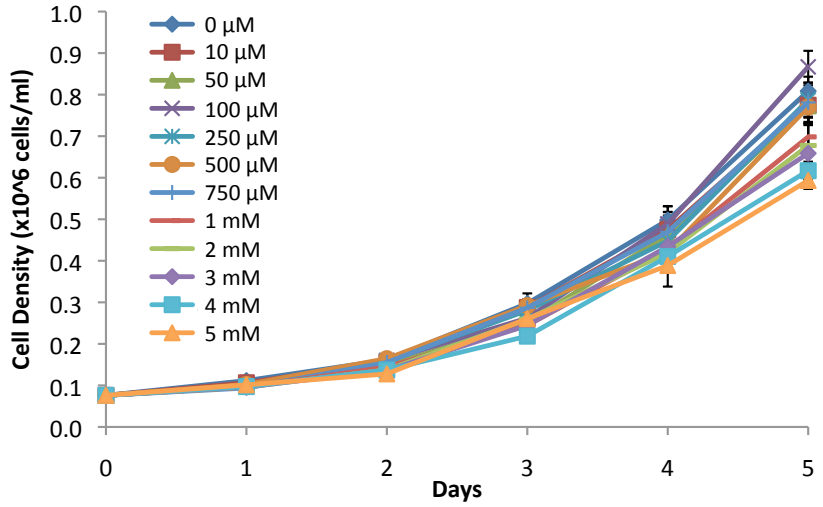

Appendix Figure 2.3. Vitamin B_{12} toxicity curve in NK-92 cells.

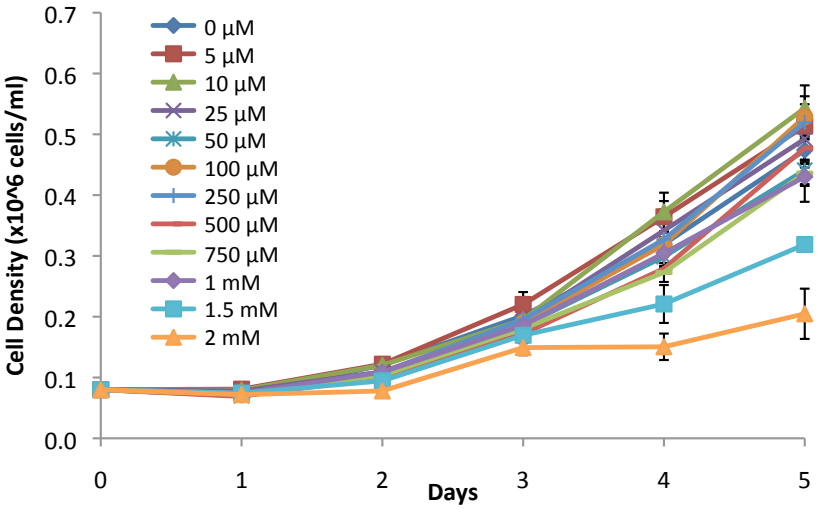

Appendix Figure 2.4. Phenobarbital toxicity curve in NK-92 cells.

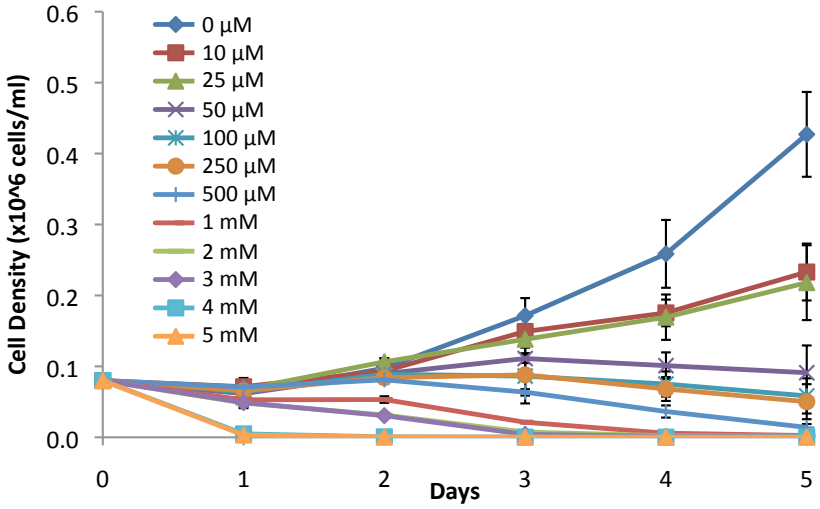

Appendix Figure 2.5. Folinic Acid toxicity curve in NK-92 cells.